2011

Petrology, geochemistry, U-Pb Zircon ages and structure of the Yiddah Porphyry Cu-(Au-Mo) prospect of the Late Macquarie Arc, NSW

Eva Goesch
University of Wollongong

Petrology, geochemistry, U-Pb Zircon ages and structure of the Yiddah Porphyry Cu-(Au-Mo) prospect of the Late Macquarie Arc, NSW

Abstract

The Yiddah porphyry Cu-(Au-Mo) system of central-southern New South Wales is contained within the Ordovician-Silurian Goonumbla-Trangie Volcanic Belt of the Macquarie Arc, 12km north of the village of Barmedman and 2 km east of the Gilmore Fault Zone. It is one of several small and poorly understood porphyry-related systems contained within a ~ 40 km north-northwest striking region known as the Rain Hill district. Petrography (microscopy, XRD, ion microprobe), whole rock geochemistry (XRF, ICP-MS), geophysical imagery and geochronology (U-Pb SHRIMP zircon dating) have been used to describe the geology and produce a petrogenetic model of the Yiddah system. This study shows that emplacement of the Yiddah porphyry Cu-(Au-Mo) system occurred during the early Silurian (433.8 ± 6.4 Ma) with the intrusion of a number of oxidised amphibole-feldspar porphyritic stocks of previously unrecognised primary monzodiorite shoshonitic affinity. These mineralised stocks evolved from a contemporaneous (439.2 ± 6.4 Ma) and genetically related sub-equigranular monzodiorite granitoid located to the west and beneath the mineralised zone. Geophysical, petrographic and geochemical findings indicate that this granitoid represents the northern extension of the Rain Hill Monzodiorite identified in the southern Gidginbung Volcanics. Mineralised stocks were intruded into two steeply eastward dipping volcaniclastic units; a low-K calc-alkaline basaltic volcaniclastic and a high-K calc-alkaline andesitic volcaniclastic.

The Yiddah porphyry system has an early, central chlorite-magnetite alteration zone containing disseminated and quartz-seam hosted chalcopyrite and molybdenite, a similarlymineralised overlying chlorite-sericite zone and a further overlying lesser-mineralised sericitic zone. Beneath the chlorite-magnetite zone, propylitic style alteration is developed within the basaltic volcaniclastics and the Rain Hill Monzodiorite, neither of which are significantly mineralised. Post-emplacement deformation relating to movement of the Gilmore Fault Zone generated sub-greenschist facies metamorphism at temperatures of ~ 300°C as constrained by chlorite geothermometry. The shear zone-related deformation manifests itself as a strong north-northwest trending foliation, a pervasive ‘regional-propylitic’ overprint and the minor mobilisation of chalcopyrite. All of the intrusive samples analysed possess trace element signatures consistent with subduction-related tectonic settings with a possible crustal component (moderate LIL/HFS element ratios and Ta-Nb depletion). Shoshonitic magmatism is therefore interpreted to be the result of either; (1) latest Macquarie Arc activity, whereby incorporation of an increased flux of Gondwanan-derived subducted sediment occurred, or (2) post-collisional collapse immediately following accretion of the arc onto eastern Gondwana, analogous to the configuration currently observed in the Northern Taiwan Volcanic Zone (Luzon Arc). The recognition of late Macquarie Arc shoshonitic affinity magmatism within the Gidginbung Volcanics is significant as it provides a genetic link between the Rain Hill Cu-(Au-Mo) porphyry systems and the world class Cadia and Goonumbla porphyry districts; thus improving prospectivity in this relatively under-explored portion of the Macquarie Arc.

Degree Type

Thesis

Degree Name

Bachelor of Science (Honours)

Department

School of Earth & Environmental Sciences

Keywords
XRD, XRF, Gilmoure Fault, volcanic

PETROLOGY, GEOCHEMISTRY, U-Pb ZIRCON AGES AND STRUCTURE OF THE YIDDAH PORPHYRY Cu-(Au-Mo) PROSPECT OF THE LATE MACQUARIE ARC, NSW

By Eva Goesch

A thesis submitted in part fulfilment of the requirements of the Honours degree of Bachelor of Science in the School of Earth and Environmental Science

University of Wollongong, 2011

The information in this thesis is entirely the result of investigations conducted by the author unless otherwise acknowledged, and has not been submitted in part, or otherwise, for any other degree or qualification.

Eva Goesch
12/10/2011

ABSTRACT

The Yiddah porphyry Cu-(Au-Mo) system of central-southern New South Wales is contained within the Ordovician-Silurian Goonumbla-Trangie Volcanic Belt of the Macquarie Arc, 12 km north of the village of Barmedman and 2 km east of the Gilmore Fault Zone. It is one of several small and poorly understood porphyry-related systems contained within a ~ 40 km north-northwest striking region known as the Rain Hill district. Petrography (microscopy, XRD, ion microprobe), whole rock geochemistry (XRF, ICP-MS), geophysical imagery and geochronology (U-Pb SHRIMP zircon dating) have been used to describe the geology and produce a petrogenetic model of the Yiddah system. This study shows that emplacement of the Yiddah porphyry Cu-(Au-Mo) system occurred during the early Silurian (433.8 ± 6.4 Ma) with the intrusion of a number of oxidised amphibole-feldspar porphyritic stocks of previously unrecognised primary monzodiorite shoshonitic affinity. These mineralised stocks evolved from a contemporaneous (439.2 ± 6.4 Ma) and genetically related sub-equigranular monzodiorite granitoid located to the west and beneath the mineralised zone. Geophysical, petrographic and geochemical findings indicate that this granitoid represents the northern extension of the Rain Hill Monzodiorite identified in the southern Gidginbung Volcanics. Mineralised stocks were intruded into two steeply eastward dipping volcaniclastic units; a low-K calc-alkaline basaltic volcaniclastic and a high-K calc-alkaline andesitic volcaniclastic. The Yiddah porphyry system has an early, central chlorite-magnetite alteration zone containing disseminated and quartz-seam hosted chalcopyrite and molybdenite, a similarly-mineralised overlying chlorite-sericite zone and a further overlying lesser-mineralised sericitic zone. Beneath the chlorite-magnetite zone, propylitic style alteration is developed within the basaltic volcaniclastics and the Rain Hill Monzodiorite, neither of which are significantly mineralised. Post-emplacement deformation relating to movement of the Gilmore Fault Zone generated sub-greenschist facies metamorphism at temperatures of ~ 300ºC as constrained by chlorite geothermometry. The shear zone-related deformation manifests itself as a strong north-northwest trending foliation, a pervasive ‘regional-propylitic’ overprint and the minor mobilisation of chalcopyrite. All of the intrusive samples analysed possess trace element signatures consistent with subduction-related tectonic settings with a possible crustal component (moderate LIL/HFS element ratios and Ta-Nb depletion). Shoshonitic magmatism is therefore interpreted to be the result of either; (1) latest Macquarie Arc activity, whereby incorporation of an increased flux of Gondwanan-derived subducted sediment occurred, or (2) post-collisional collapse immediately following accretion of the arc onto eastern Gondwana, analogous to the configuration currently observed in the Northern Taiwan Volcanic Zone (Luzon Arc). The recognition of late Macquarie Arc shoshonitic affinity magmatism within the Gidginbung Volcanics is significant as it provides a genetic link between the Rain Hill Cu-(Au-Mo) porphyry systems and the world class Cadia and Goonumbla porphyry districts; thus improving prospectivity in this relatively under-explored portion of the Macquarie Arc.

TABLE OF CONTENTS

LIST OF FIGURES

LIST OF TABLES

ACKNOWLEDGMENTS

I would like to thank my supervisors Dr. Solomon Buckman and Ass. Prof. Chris Fergusson for their advice, encouragement and reviews throughout the year. Your knowledge and expertise over a variety of fields has enabled me to tackle a diverse range of topics which has expanded my geological knowledge immeasurably. I would also like to thank Ass. Prof. Allen Nutman for providing practical and theoretical assistance and advice throughout the year regarding the zircon dating. Working on the SHRIMP at Geoscience Australia was an amazing experience and I am extremely grateful for the opportunity.

To Prof. Neil Williams, thank you for your consistent interest, encouragement, advice and the many long conversations regarding both the science at hand and the broader picture. Thank you for your thorough chapter reviews undertaken amidst a busy schedule.

My thanks go to Scott Munro, Dougal Munro, Malissa Washburn and all at Goldminco Corporation for providing me with the opportunity and financial backing to undertake this project. Thank you also for your guidance and support during my vacation employment.

Thank you to Ass. Prof. Paul Carr and Ass. Prof. Brian Jones for assistance and advice with undertaking and interpreting XRF and XRD analyses, and to José Abrantes for the preparation of thin sections and assistance in the laboratory. I would also like to thank Norm Pearson at GEMOC for the use of the electron microprobe, Alan Whitaker at Geoscience Australia for discussions regarding the geophysics and Prof. Bruce Chappell and Ekaterina Kiseeva of the Australian National University for their hospitality during Canberra trips.

To all of the academic and support the staff in the School of Earth and Environmental Science, thanks for making the past few years interesting and enjoyable. To my friends in the honours room, thanks for sharing the experience. To my housemates and other friends in Wollongong, thank you for the fun times– and also for putting up with me this year.

To my family, particularly my parents– thank you for the ongoing encouragement and support you have provided me with, and for always helping me keep things in perspective.

Lastly to Alex, for everything– thanks.

CHAPTER ONE
INTRODUCTION

1.1. LOCATION AND BACKGROUND

The Yiddah porphyry Cu-(Au-Mo) system is located 11 km northwest of Barmedman in central-southern New South Wales, 20 km southeast of West Wyalong and approximately 360 km west of Sydney (Figure 1.1). The prospect is situated in the southern portion of the Goonumbla-Trangie (formerly Junee-Narromine) Volcanic Belt, within the Ordovician Macquarie Arc of the Lachlan Orogen. Its maiden inferred resource (2008) totalled 61 Mt at 0.35 % Cu, 0.13 g/t Au and 38 g/t Mo.

Copper (predominantly as chalcopyrite), gold and molybdenum mineralisation are hosted in veins and as disseminations within heavily altered andesitic volcaniclastics of the Late Ordovician Gidginbung Volcanics and intruding intermediate porphyritic bodies. In addition to intense hydrothermal alteration, the deposit has been heavily sheared, with the Gilmore Fault Zone located ~ 2 km from its western margin.

The Yiddah prospect does not outcrop; at the surface, a north-northwest trending topographic rise composed of strongly weathered subcrop grades into flat, extensive plains covered by a clay veneer (Figure 1.2). Vegetation cover is primarily remnant native vegetation and cleared agricultural land.

The prospect is contained within the New South Wales Department of Industry and Investment Exploration Licence 6845, currently held by Goldminco Corporation, a subsidiary of Straits Resources Ltd.

1.2. MINING AND EXPLORATION HISTORY

1.2.1. Regional mining history

Gold mineralisation in the Temora – West Wyalong region occurs in a number of styles and is historically linked to European settlement. In the Temora region, structurally controlled vein-hosted and alluvial gold was first discovered in 1869, both associated with the

Figure 1.1: Location of the Yiddah Cu-Au system and surrounds. Aerial imagery: ESRI ArcMap 10 database.

Figure 1.2: Surface expression at Yiddah. Photographed eastward from 147º20’07”E; 34º02’42”S.

Mother Shipton Monzodiorite which intrudes the Ordovician Temora Volcanics (Downes et al. 2004). These workings produced over 4.6 t of gold (Suppel et al. 1986). At Reefton, 22 km north of Temora; 192.6 kg of gold was won from quartz veins thought to be related to remobilisation of gold from the nearby Gidginbung Volcanics during the Early to Middle Devonian Tabberabberan Orogeny (Downes et al. 2004). At West Wyalong, around 14 t of gold was produced from quartz veins occupying sheared zones of the Wyalong Granodiorite; whilst at Barmedman, three main quartz reef complexes produced at least 0.9 t of gold from 1872. An additional 917 g of gold was produced from pits located to the west of the present Yiddah prospect during 1895 (Suppel et al. 1986; MacCorquodale 1997).

In more recent times, the Gidginbung Au-Ag opencut mine (operational 1987-1996), located 16 km north-northwest of Temora, produced 21.07 t of gold with an average grade of 2.06 g/t Au (Downes et al. 2004). Located at the southern extent of the Gidginbung Volcanics, the deposit consists of a deformed silica-clay-pyrite hosted ore-body, considered to be either a high sulphidation epithermal system where mineralisation predates regional deformation (e.g. Lawrie et al. 1997); or a shear-hosted deposit cross-cutting peripheral older porphyry-style mineralisation, developed by the circulation of magmatic hydrothermal fluids synchronously with deformation to produce mineralised advanced argillic alteration (Allibone et al. 1995).

In addition to these deposit styles, the Temora – West Wyalong region is recognised to host a number of porphyry Cu-Au systems, situated along strike to the Gilmore Fault Zone. This province is termed the Rain Hill district (Mowat & Smith 2006). Porphyry prospects in this district include The Dam, Rain Hill, Monza, Culingerai, Mandamah, Kangaroo Hill, Bull Plain and Yiddah (Downes et al. 2004; Mowat & Smith 2006). These systems are variable in size and economic prosperity, with Yiddah being the largest in terms of potential tonnes contained ore. The region as a whole possesses a total resource at a 0.25% Cu equivalent cut-off of 21.1 Mt at 0.35% Cu, 0.5 g/t Au and 34 ppm Mo (indicated) and 121.1 Mt at 0.32% Cu, 0.25 g/t Au and 31 ppm Mo (inferred) (Goldminco Corporation 2010).

1.2.2. Exploration history of Yiddah

The Yiddah porphyry system was discovered by Le Nickel Exploration Pty Ltd in the mid 1970's in previous EL1563 using geological mapping, soil geochemistry and ground magnetic surveys. Since this time, the prospect has been re-examined by a number of

companies. From 1981 to 1983, Endeavour Resources and Base Resources mapped, reverse circulation drill sampled, performed geophysical induced polarisation (IP) and magnetic surveys and drilled limited percussion and diamond drill holes. Similar methodologies were again used by Seltrust Gold and Base Resources (1983 – 1985), Paragon Gold and Base Resources (1985 – 1986), Paragon Gold and Central Murchison Gold joint venture (1986 – 1990), Peko Wallsend and Paragon Gold joint venture (1990 – 1994), Gold Mines of Australia and North Mining joint venture (1994-1996) and Cyprus Gold Australia (1997 – 2000). In 2000, Goldfields Exploration (later renamed Aurion Gold Exploration) was granted a new tenement (EL5737). Goldminco Corporation purchased EL5737 in 2004, and grouped it with other Temora tenements to create a new single exploration license (EL6845) in 2007.

Despite these numerous exploration programs, and drilling of over 30 reverse circulation and 20 diamond core holes, the Yiddah porphyry system remains poorly understood. Host lithologies lack formal description and little research has been undertaken to determine the genesis of the system. A limiting factor has been the intense nature of deformation related to its shear zone setting, which has resulted in a dismembered deposit differing wholly from traditional descriptions of zoned porphyry copper systems. The most significant description of Yiddah to date was provided by MacCorquodale (1997) of Gold Mines of Australia, who compiled a summary of previous exploration work and additionally commissioned a petrology report (Mason 1996) describing ten rock samples from drill hole PY12.

1.3. **AIMS AND OBJECTIVES**

This study aims to better describe and define the Yiddah porphyry system and its host lithologies, with particular emphasis on outlining the geochemical and geochronological relationships of mineralised and non-mineralised intrusive units; the nature and spatial distribution of alteration assemblages and mineralisation styles within the system; and the regional geological setting of the deposit, as observed through analysis of structural features and geophysical imagery.

Another important outcome will be new petrographic, geochronological and geochemical knowledge of the highly prospective Gidginbung Volcanics, a unit almost entirely obscured by cover. In particular, the large intrusive unit present at the western margin of the deposit

will be compared to the Rain Hill Monzodiorite, located ~ 20 km SSE of Yiddah, with the aim of determining if the two are distinct or represent a continuous intrusive unit.

The culmination of results will be (1) a paragenetic model of formation for the Yiddah porphyry system and (2) the comparison of Yiddah to other porphyry deposits located within the Macquarie Arc, as well as those predicted by global porphyry models.

As this work represents the first comprehensive study of the Yiddah porphyry system, outcomes have the potential to impart further direction to exploration efforts within the Yiddah prospect, the Rain Hill district and the Macquarie Arc system; with a view to also contribute to knowledge regarding the formation and deformation of the Lachlan Orogen, a complex and much debated topic in the broader literature.

1.4. **METHODOLOGY**

1.4.1. Sample Collection

All samples of the Yiddah system used in the current study were sourced from diamond drill holes, stored at Goldminco Corporation's core yard at Orange, NSW (Appendix A). Three key holes identified from company logging were targeted for sampling. Each hole (TYHD003: 530190E 6232850N AMG66 Zone55, 514.75 m; TYHD004: 530430E 6232720N, 609.70 m and TYHD005: 530216E 6233397N, 648.80 m), was summary logged on the criteria of primary rock type, texture, alteration mineralogy, alteration intensity, vein mineralogy and mineralisation (Appendix B; see Figure 2.7 for spatial configuration of drill holes). Representative lithologies, alteration assemblages, contacts, structures, veins and other notable features were described and photographed on site, with a suite of samples collected for further analysis. Assay data attained for each metre of diamond core was provided by Goldminco Corporation and incorporated into statistical analysis. A further sample was obtained of the Rain Hill Monzodiorite (sample RHM) sourced from reverse circulation drill hole MHRC537 located ~ 20 km south-southeast of Yiddah (535080E 6211745N AMG66 Zone55, 174.00 m; see Figure 2.6).

1.4.2. Standard and polished thin sections

Sixteen standard thin sections were prepared at the University of Wollongong; 20 standard and 14 polished thin sections were prepared at the University of New England, Armidale. Sections were analysed on a Leica DM2500 petrological microscope to identify and quantify primary mineralogy, alteration mineralogy, textures and ore/mineral associations (Appendix C). Photomicrographs were taken using a Leica DFC400 camera at the University of Wollongong. Hand specimen photographs were taken in the field on a Canon PowerShot SX100 IS digital camera or at the University of Wollongong on a Leica MZ16A stereomicroscope fitted with a Leica DFC320 camera mount.

1.4.3. X-ray diffraction

Mineral phases from 15 samples of representative alteration assemblages and two vein samples were identified using X-ray diffraction (XRD) at the University of Wollongong. Samples were powdered in a chromium ring mill, and analysed using a Philips 1150 PW Bragg-Brentano diffractometer using CuK_{α} radiation. Diffraction peaks were identified using TRACES 4 software and quantified using SIROQUANT software (Appendix D).

1.4.4. Electron microprobe analysis

Seven polished thin sections were analysed by electron microprobe analysis at the ARC National Key Centre for Geochemical Evolution and Metallogeny of Continents (GEMOC) at Macquarie University, Sydney. Analysis was carried out by a CAMECA SX100 Electron Microprobe Analyser Spectrometer with operating conditions of 15keV accelerating voltage and 20nA beam current. Calibration was performed at the commencement of each session using a number of standards. A suite of 32 chlorite measurements were acquired from six samples to calculate formation temperatures as outlined by Cathelineau & Nieva (1985), Cathelineau (1988) and Jowett (1991). Additional spot analyses were acquired to confirm various oxide and sulphide mineral phases observed in thin section (Appendix E).

1.4.5. Geochemical analysis

Thirty eight samples were analysed for whole rock geochemistry using a SPECTRO XEPOS energy dispersive polarization X-ray fluorescence spectrometer (XRF) at the University of Wollongong (Appendix F). Samples were crushed in a chromium steel ring mill, with pressed pellets prepared for trace element analysis by mixing 5 g of sample with a PolyVinyl Acetate (PVA) binder and pressing to 2500 psi into an aluminium cup. Pellets were dried in a 65ºC oven for 24 hours. Glass buttons were fused for major element analysis using a pure metaborate flux for high silica (> 65% SiO_2) samples and a 12:22 tetraborate metaborate flux for mafic (45 – 65% SiO_2) samples. 400 mg of sample (high silica) and 300 mg of sample (mafic) was added to 2.4 g of each flux. Samples were blended in platinum crucibles and heated from 600ºC to 970ºC over a period of one hour, with a NH_4I pellet added to reduce viscosity prior to pouring and pressing on a graphite disc. Samples with > 1000 ppm sulphur or 400 ppm Cu as determined from trace element analysis were oxidised prior to fusing through the addition of 5 ml of $LiNO_3$ and drying overnight at 65ºC, then heating at 100ºC for one hour, then to 600ºC by increasing 50ºC in 20 minute increments. Deconvolution of the spectra and conversion of X-ray intensities was performed using Ametex Materials-Analysis Division proprietary software. Accuracy was controlled by calibration of the instrument against a wide range of natural rock standards and synthetic materials. Loss on ignition was calculated by firing 1 g of powdered sample in a ceramic crucible at 1050ºC for two hours. Samples were weighed after slight cooling with the difference in baked and initial weight converted to weight percent loss on ignition.

Rare earth elements were determined for each sample powder by Inductively Coupled Plasma Mass Spectrometry (ICP-MS) following lithium borate fusion and dissolution of the melt by ALS Laboratory Group Analytical Chemistry and Testing Services Mineral Division in Stafford, Queensland.

1.4.6. Geochronology

Absolute age dates were obtained via the $^{206}Pb/^{238}U$ zircon dating method performed using the sensitive high resolution ion microprobe (SHRIMP IIe) at Geoscience Australia, Canberra. Zircons were extracted via mechanical grinding, heavy liquid separation and barrier magnetic separation by Shane Paxton at the Australian National University, with

individual grains manually selected through binocular microscopy at the University of Wollongong. Approximately 175 grains of two unknowns were mounted in an epoxy resin along with ~ 65 grains of the TEMORA-2 standard (417 Ma; Black et al. 2004). The block was ground down to expose a cross section of the majority of zircon grains, and polished using diamond paste. Reflected light, transmitted light and cathodoluminescence images were taken at the University of Wollongong and the Australian National University to aid targeting and interpretation.

1.4.7. Structure and geophysics

Orientated core measurements consisting of bedding, foliation, contacts and vein features collected by Goldminco Corporation during routine core processing were incorporated into a structural overview of the Yiddah prospect and regional geological context. These measurements are referenced to true north using the grid reference AGD1966 AMG Zone55. All maps at the regional to deposit scale are similarly georeferenced. Stereoplots and other calculations performed for mapping were generated by GEOrient and GeoCalculator software. Gravity plan images at 500 m spacing (regional) and 200 m spacing (detailed) along with 100 m spaced east-west cross section gravity images were provided by Goldminco Corporation, generated from a gravity survey collected and processed in 2010 by GeoDiscovery Group, Brisbane. A regional aeromagnetic survey collected in 1995 by Gold Mines of Australia was also provided along with ground magnetics completed in 2010 by Precision Field Services at 50 m line spacing, also processed by GeoDiscovery Group. Magnetic imagery presented is in the format of total magnetic intensity, reduced to the pole to eliminate asymmetry due to inclination of the Earth's magnetic field. Total magnetic intensity images publically available from Geoscience Australia were also utilised during interpretation of commercial surveys.

CHAPTER TWO

REGIONAL GEOLOGY

2.1. THE LACHLAN OROGEN

The Yiddah porphyry system is located within the Lachlan Orogen (Glen 1995) or Lachlan Fold Belt (Scheibner 1973), which together with the Delamerian, Thomson and New England orogenic complexes comprises the Palaeozoic Tasmanides of eastern Australia (Gray & Foster 2004). Spanning 700 km in width and 1200 km in length, the Lachlan Orogen covers much of Victoria, New South Wales and extends into Tasmania (Fergusson & Coney 1992; Figure 2.1). The Lachlan Orogen is host to a number of eastern Australia's most significant ore deposits; which occur in a variety of styles, including orogenic gold (e.g. Bendigo, Ballarat), porphyry and porphyry related Cu-Au (e.g. Cadia, Goonumbla), volcanic-hosted massive sulphide (e.g. Woodlawn), sediment-hosted Cu-Au/Pb-Zn (Cobar style) and granite related Sn (e.g. Ardlethan) (Jaques et al. 2002).

The Lachlan Orogen is composed of deep-marine quartz-rich turbidites, cherts, black shales, shallow-marine sedimentary rocks, mafic and silicic volcanic rocks and intrusive igneous bodies (Gray et al. 1997). On the basis of the current configuration of these lithologies, along with ages and structural features, the orogen has been partitioned into three sub-provinces: the western Lachlan Orogen (accreted 450 – 420 Ma), central Lachlan Orogen (440 – 420 Ma), and eastern Lachlan Orogen (430 – 340 Ma) (Hough et al. 2007). The eastern sub-province contains the Ordovician Macquarie Arc of which Yiddah is a component, and is separated from the central Lachlan Orogen by the Gilmore Fault Zone. Yiddah lies approximately 2 km east of this contact.

Evolution of the Lachlan Orogen occurred from Cambrian to Carboniferous times through stepwise accretion, deformation and metamorphism off eastern Gondwana, where at least one long lived subduction zone was present (Gray et al. 1997; Gray & Foster 1998; Figure 2.2). Its formation originated following cessation of collisional activity and accretion of the Delamerian Orogen in the Late Cambrian, when it is considered that the subduction zone jumped hundreds to thousands of kilometres to the east, instigating formation of an oceanic

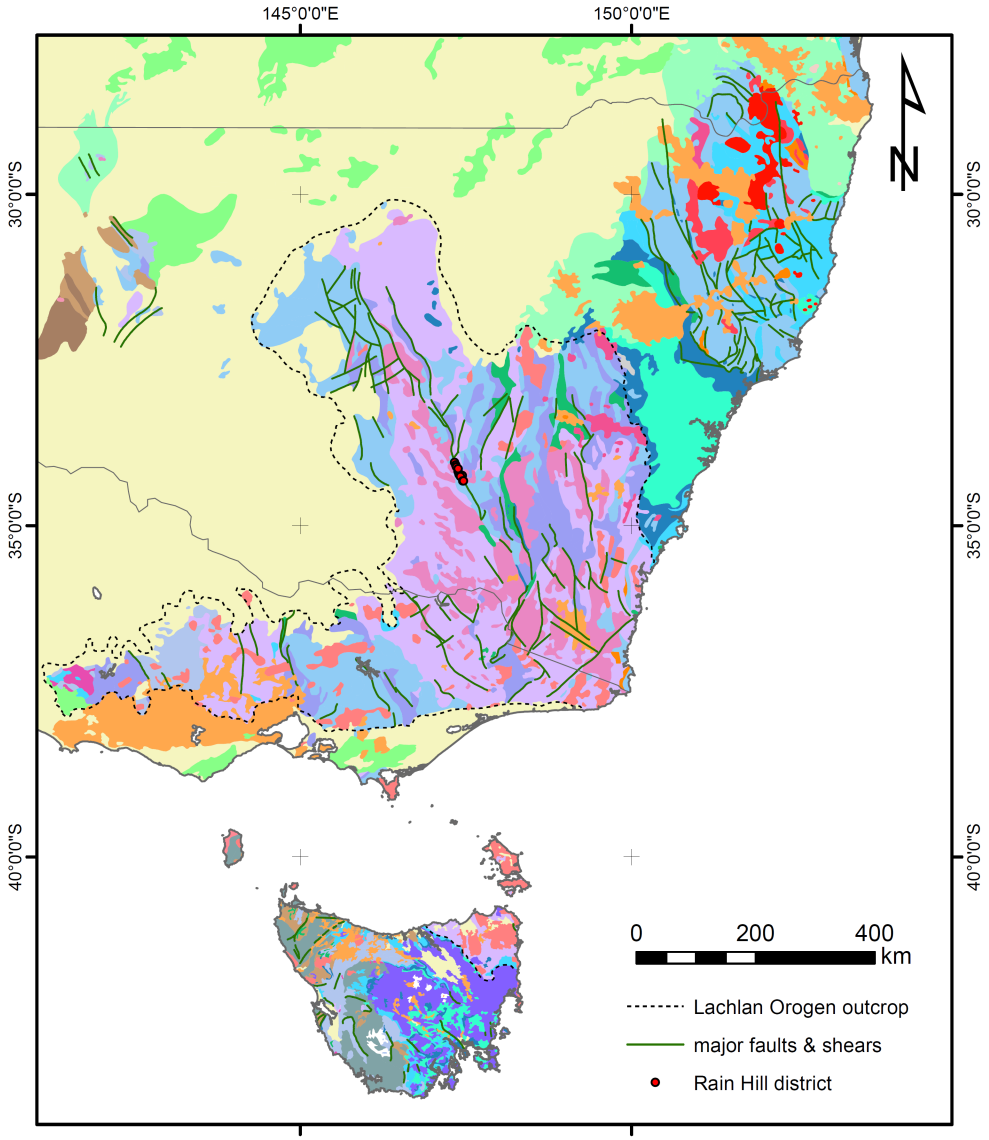

Figure 2.1: Location of the Palaeozoic Lachlan Orogen of eastern Australia. Modified after: Surface geology of Australia 1:2 500 000 scale, 2010 ed. [Digital Dataset] Geoscience Australia.

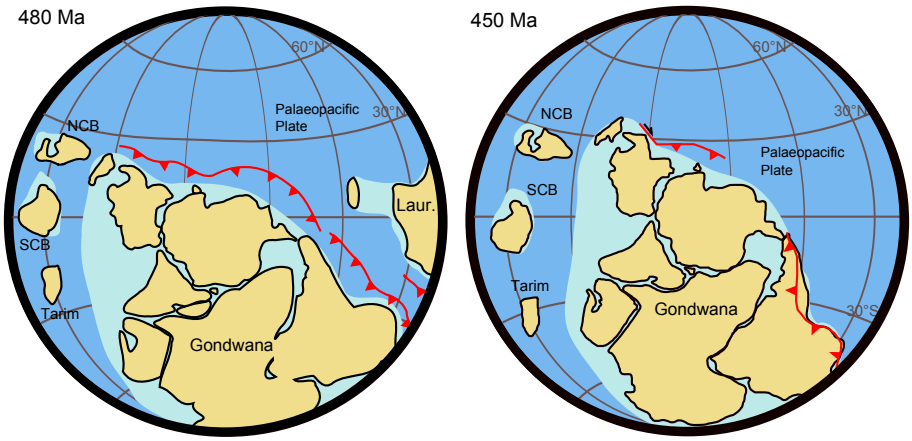

Figure 2.2: Palaeo-reconstruction of Gondwana at ca 480 Ma and ca 4550 Ma. A large subduction zone is evident flanking present day eastern Australia. NCB = North China Block, SCB = South China Block, Laur. = Laurentia. Redrawn from: Li & Powell (2001).

volcanic island-arc from *ca* 485 Ma (the Macquarie Arc) and an associated back-arc basin (the Wagga Marginal Sea) (Glen et al. 1998; Fergusson 2003).

Linear belts of calc-alkalic to shoshonitic mafic volcanic/volcaniclastic rocks of the Macquarie Arc formed from this configuration. Pb, Sr and Nd isotopic compositions are consistent with a mantle source, with limited crustal mixing (Carr et al. 1995; Cooke et al. 2007). Contemporaneously, deposition of deep-marine sediments onto an oceanic to quasi-continental basement began in the extensive back-arc region (Coney 1992). Initially, sediments chiefly consisted of chert and voluminous quartz-rich turbidites sourced from the Delamerian Orogen located to the west (Fergusson & Tye 1999). By the Late Ordovician however, lithic sandstones and mudstones derived from the island-arc were a major sediment component (Colquhoun et al. 1999; Fergusson & Tye 1999).

While the presence of a long-lived oceanic subduction zone off the eastern margin of Gondwana is generally accepted (Hough et al. 2007), debate exists surrounding the structural configuration and mechanisms of deformation in the region between the Macquarie Arc and the Gondwanan continental margin.

One school of thought suggests that widespread deformation and thrusting recognised within the Lachlan Orogen occurred in an intra-plate setting, the result of outboard subduction causing convergence in the back-arc region and adjacent Australian passive margin (Fergusson & Coney 1992). VandenBerg (1999) suggested that microcontinental fragment(s) (possibly Tasmania) existed in the back-arc region. Braun and Pauselli (2004) used a coupled thermo-mechanical finite element model to support this hypothesis, suggesting the entire deformation of the Lachlan Orogen was driven by a single, long lived, relatively fixed subduction zone.

In a second school of thought, multiple subduction zones are proposed to account for the observed thrust systems of the Lachlan Orogen (Gray et al. 1997; Bierlein et al. 2002; Fergusson 2003). This view is based on the presence of a number of interpreted accretionary complexes, such as those present in western Victoria (Stawell and Bendigo Zones), eastern Victoria (Tabberabbera Zone), and along the coastline of southeastern Australia (Narooma Subduction Complex) (Fergusson 2003).

Alternatively, it has also been suggested that the observed features were generated not through subduction related processes but through rifting, heating and possibly sinking of the lithospheric mantle, based on the "overwhelmingly shoshonitic" geochemical affinity of the Macquarie Arc (Wyborn 1992). More recently however, authors such as Blevin (1998; 2002) have emphasised the dominantly calc-alkaline mafic nature of the Macquarie Arc volcanic rocks, a chemistry essentially restricted to convergent settings (Winter 2001), reaffirming the intra-oceanic island-arc setting.

Deformation within the Lachlan Orogen occurred within a number of distinct orogenic periods, beginning with the Benambran Orogeny at *ca* 450 – 430 Ma (Foster & Gray 2000). Ickert & Williams (2011) have suggested that the large volume of S-type granites that intruded at *ca* 432 Ma constrains the timing of the 'late' Benambran event that affected the eastern Lachlan Orogen (Gray & Foster 2004). The intrusion of the S-type granites coincides with the cessation of *ca* 37 Ma of Macquarie Arc magmatism (Percival & Glen 2007; Glen et al. 2011) and closure of the Wagga Marginal Sea (Gray & Foster 2004). Major periods of deformation followed, including the Bindian/Bowning (*ca* Silurian – Devonian boundary), Tabberabberan (Early to Middle Devonian) and Kanimblan (Early Carboniferous) Orogenies (VandenBerg 1999). Terminal deformation of the orogenic system progressed from west to east, with concentrated deformation of the eastern sub-province continuing until the Early Carboniferous (Gray & Foster 2004; Hough et al. 2007), when the Lachlan Orogen became fully cratonised at *ca* 330 Ma (Gray & Foster 2004).

Despite overall shortening of at least 60% (Fergusson & Coney 1992), there is abundant evidence of significant extensional activity throughout the evolution of the Lachlan Orogen. Collins (2002) argued that tectonic evolution was characterised by protracted periods of extension driven by slab roll-back, which were punctuated by short (~ 10 Ma) periods of orogenesis. A large number of north-south striking extensional basins are evident, particularly within the central and eastern sub-provinces (e.g. Tumut, Cobar, Cowra and Hill End basins). The last stage of extension and magmatism has been likened to the Basin and Range Province of western North America (Glen 1992; Gray & Foster 2004).

Cycling of contractional and extensional regimes also produced widespread syn- and post-tectonic, granitoid emplacement. The most intensive phase occurred in the eastern sub-province during the Early Silurian to early Middle Devonian. Here, regional north-south

orientations of granitoids, along strike to bounding shear zones suggests emplacement to be predominantly syn-tectonic (Gray et al. 1997).

2.2. THE MACQUARIE ARC

The Macquarie Arc consists of linear belts of mafic to intermediate volcanic rocks, volcaniclastic rocks, limestones and chert. It evolved from the Ordovician to Early Silurian (480 – 430 Ma; Walshe et al. 1995), through volcanic activity of a series of subduction zone generated intra-oceanic volcanic centres which erupted onto an abyssal plain of probable Cambrian age (Fergusson & Coney 1992, Glen et al. 1998, Gray & Foster 2004). It is preserved as four north-south trending linear belts located in the eastern subprovince: the Goonumbla–Trangie (Fergusson 2009, formerly Junee–Narromine), Molong, Rockley–Gulgong and Kiandra Volcanic Belts (Glen et al. 2002). Yiddah is located in the southern portion of the Goonumbla–Trangie Volcanic Belt. Ordovician turbidites are present to the west of the Goonumbla–Trangie Volcanic Belt, between the Goonumbla–Trangie and Molong Volcanic Belts, and south of the Molong and Rockley–Gulgong Volcanic Belts (Figure 2.3).

Interpretation of these lithologies as subduction-zone-generated is supported by the widespread presence of low- to medium-K calc-alkaline volcanic rocks, characteristic of arc settings. Shoshonitic magmatism; often associated with Cu-Au mineralisation in the Macquarie Arc may be generated from a number of tectonic configurations, including temporally late arc evolution (Muller & Groves 1993) and syn- or post-collisional extension, as is the case of the Northern Taiwan Volcanic Zone (Wang et al. 1999).

Whilst a subduction related tectonic setting of formation is generally accepted, the polarity of subduction is subject to debate. Most authors associate arc volcanism with west-dipping subduction (Glen et al. 1998; Figure 2.4), while an east-dipping subduction zone has been argued by Fergusson (2009). This argument is based on a prominent limestone plateau situated in the western Molong Volcanic Belt that grades eastward into deep marine sediments, which is analogous to a frontal ridge, as observed at Guam in the western Pacific Ocean. The presence of deep marine, quartz-turbidite, chert, mudstone sequences to the east and west of the mafic volcanic belts is used as evidence that multiple subduction zones may have been present on either side of the Macquarie Arc (Gray et al. 1997; Fergusson, 2003).

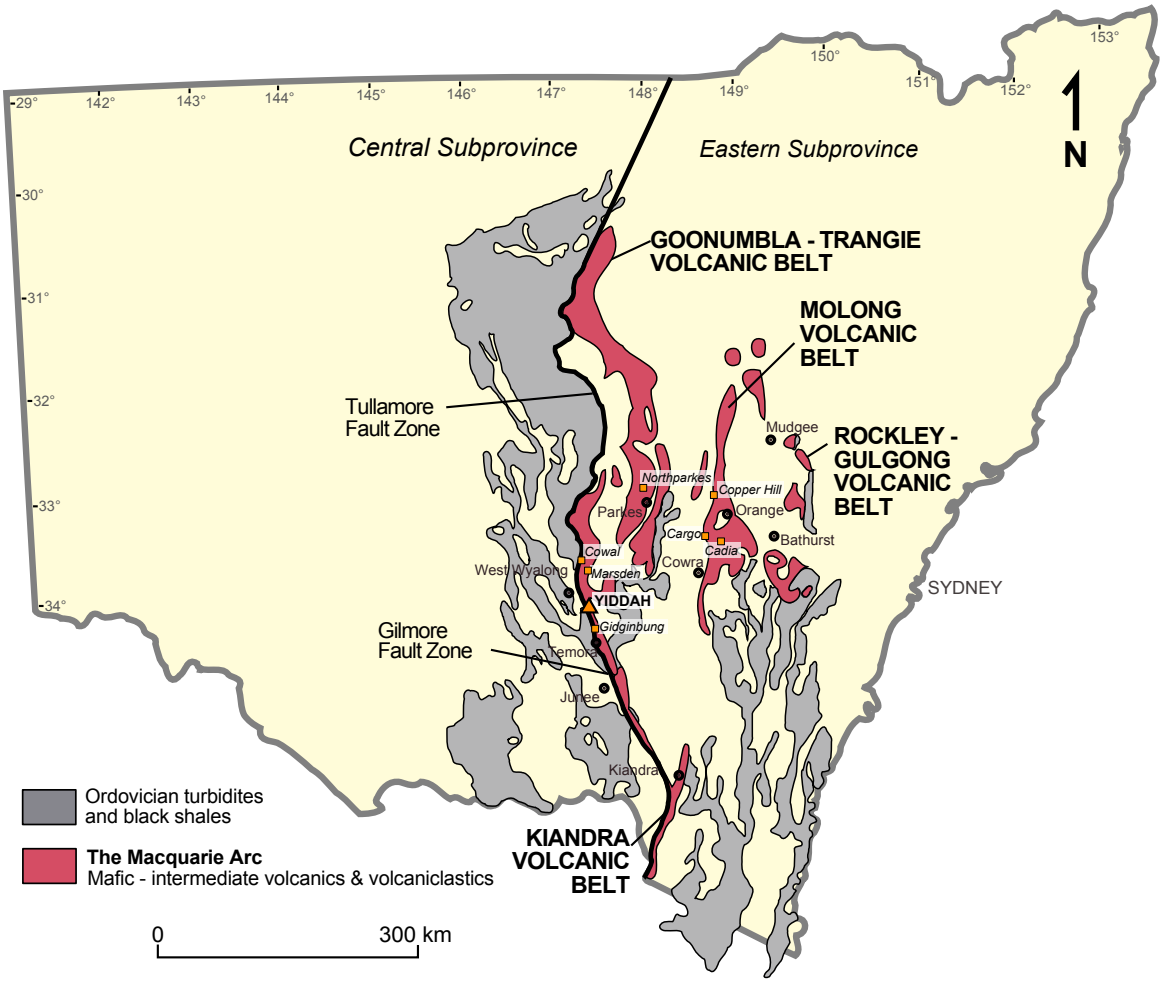

Figure 2.3: Ordovician units of the Lachlan Orogen in New South Wales. Quartz-rich turbidites and black shales surround the four elongate bodies of the Macquarie Arc: the Goonumbla-Trangie Volcanic Belt, the Molong Volcanic Belt, the Rockley-Gulgong Volcanic Belt and the Kiandra Volcanic Belt. Adapted after Glen et al. (2002).

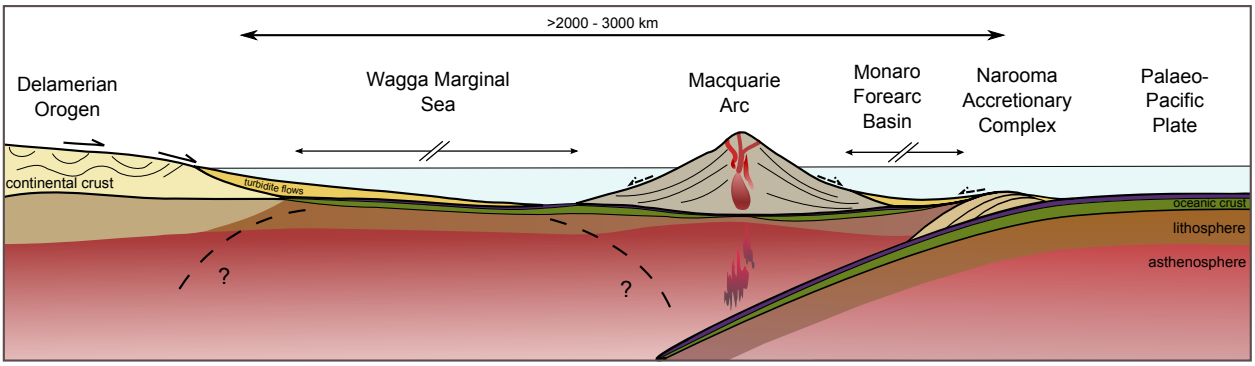

Figure 2.4: Key elements and tectonic configuration of the Macquarie Arc at *ca* Middle Ordovician. ? = possible subduction zones (Gray et al. 1997; Fergusson 2003). Not to scale (vertically exagerated). Adapted from Foster & Gray (2000) and Fergusson & Fanning (2002).

Debate also exists as to whether the four volcanic belts formed as separate linear features, or if they originally constituted a single arc which has been pulled apart. The latter is favoured due to the lack of inter-fingering between turbidite and volcanic material and recognition of faulted contacts at major turbidite/volcanic boundaries (Meffre et al. 2007). Fergusson (2009) has proposed this displacement occurred through anticlockwise rotation of an initial east-west continuous arc, which was fragmented by strike-slip displacement during rotation.

Crawford et al. (2007a), Glen et al. (2007a) and Percival & Glen (2007) have attempted to link the geochemistry and chronology of Macquarie Arc volcanism through a four phase model spanning the Ordovician to early Silurian (Figure 2.5). Their model does not include any intrusive bodies south of the Cowal Igneous Complex in the Goonumbla – Trangie Volcanic Belt. Although constrained by limited sampling, it is a significant initial step to outlining key magmatic events.

Phase 1 (*ca* 490 to *ca* 475 Ma) is characterised by high-K calc-alkaline to shoshonitic basaltic to andesitic lavas in the Molong and Goonumbla–Trangie Volcanic Belts. Relatively evolved (low MgO) monzodiorites, dated at 481 Ma are present in the Nelungaloo Formation of the Goonumbla–Trangie Volcanic Belt. These indicate that the arc had been active for some time at this stage, and possibly commenced as early as the late Cambrian (*ca* 490 Ma) (Glen et al. 2007a). Phase 1 concluded with a magmatic hiatus in the Middle Ordovician in the range 475 – 466 Ma associated with significant uplift and erosion (Glen et al. 2007a; Percival & Glen 2007).

Phase 2 magmatism occurred from the Middle to Late Ordovician (*ca* 466 – 450 Ma) in all Macquarie Arc volcanic belts. Magmatic compositions vary from medium- to high-K calc-alkaline (Cargo Block, Lower Fairbridge Volcanics), high-K calc-alkaline (Goonumbla, Blayney and Upper Fairbridge Volcanics) and shoshonitic (upper Blayney and Byng Volcanics) compositions (Crawford et al. 2007a). A distinct hiatus, signified by thick limestone deposition follows Phase 2 at *ca* 455 – 450 Ma in the western Molong Volcanic Belt, while only thin limestone beds occur in the hiatus in the eastern Molong Volcanic Belt (Percival & Glen 2007).

Phases 3 and 4 are less distinct, and possess greater variability in chronology and geochemical character than Phases 1 and 2 (Fergusson 2009). Phase 3, consisting only of intrusive bodies occurred at *ca* 456 – 443 Ma, largely within the widespread hiatus which terminated Phase 2. Some Phase 3 intrusives may be somewhat younger however (Glen et al. 2007a), with further work required to more tightly constrain this phase. It is thought that emplacement occurred during regional uplift, erosion and crustal thickening of the Macquarie Arc (Glen et al. 2007a; Percival & Glen 2007). Porphyritic intrusions in this phase include the medium-K calc-alkaline Copper Hill Suite and the shoshonitic monzonitic intrusive complex at Ridgeway (Glen et al. 2007a).

Phase 4 represented the final phase of magmatism in the Macquarie Arc before cessation in the early Silurian. This voluminous phase was dominantly shoshonitic, occurring between *ca* 458 and 437 Ma (Crawford et al. 2007a). Phase 4 magmas typically reflect greater crustal interaction than early phases, which is explained by the preceding Phase 3 crustal thickening, which also allowed for greater cooling and consequently greater fractionation of Phase 4 magmas. In the latter half of Phase 4 magmatism, the highly mineralised porphyry systems of Goonumbla (444 – 436 Ma) and Cadia (439 – 437 Ma) were emplaced (Percival & Glen 2007; Glen et al. 2007a).

2.3. THE GILMORE FAULT ZONE

The Gilmore Fault Zone is a major north-northwest trending structure of the Lachlan Orogen, separating the Wagga-Omeo Metamorphic Belt (central sub-province) and Tumut Synclinorial Zone (eastern sub-province) (see Figure 2.3). Despite relatively poor outcrop, the imbricate fault zone is well-defined by aeromagnetic and gravity patterns, which delineate the structure from near Cabramurra in the south to an area east of Cobar in the north with a maximum width of ~ 6 km (Suppel et al. 1986; Stuart-Smith 1991; Warren et al. 1995). Stuart-Smith (1991) interpreted the Gilmore Fault Zone as a westward dipping reactivated basement fault corresponding to an older terrane boundary; while in a seismic profile acquired immediately south of Barmedman it was interpreted by Glen et al. (2002) as a small east-dipping thrust (to *ca* 1 km), soling off a major west-dipping floor fault interpreted to be the Wagga Belt thrust over the Goonumbla-Trangie Belt.

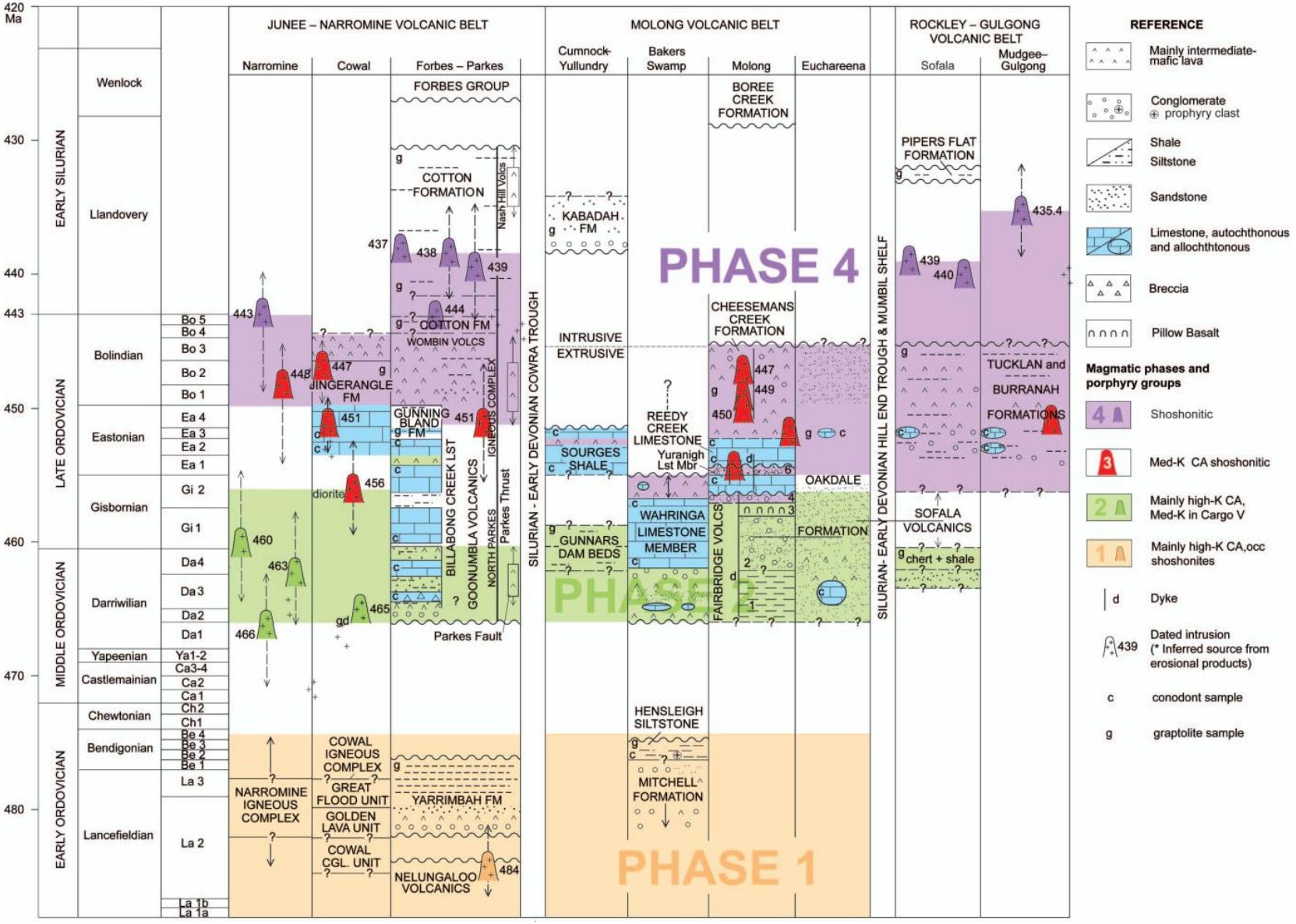

Figure 2.5: Lithostratigraphic column of the Macquarie Arc summarising the four phase model (Glen et al. 2007a).

Stuart-Smith (1991) noted that earliest observed structures were consistent with folding of Ordovician-Silurian rocks during the Bindian/Bowning Orogeny at the Siluro-Devonian boundary, but considered that the zone was probably active during the Benambran Orogeny. Dextral strike-slip movement was suggested at this time. Scheibner (1989, cited in Walshe et al. 1995) conversely suggests that the *en echelon* array of late Silurian to Early Devonian granites of the Wagga-Omeo Metamorphic Belt implies sinistral transtensional movement during the Bowning. Stuart-Smith (1991) further noted that sinistral transpression was the dominant movement along the Gilmore Fault Zone in the period following until at least the Carboniferous.

2.4. **THE GIDGINBUNG VOLCANICS**

2.4.1. Regional context

Yiddah is hosted within the Late Ordovician – early Silurian Gidginbung Volcanics; a narrow (< ~ 7 km), fault-bounded package extending from south of the Gidginbung Mine in the northwest of the Cootamundra 1:250,000 map sheet approximately 60 km north-northwest to West Wyalong in the south of the Forbes 1:250,000 map sheet (MacCorquodale 1997). In the Yiddah region, subcrop of the Gidginbung Volcanics based on aeromagnetic imagery is approximately 2.5 km in width (Figure 2.6).

To the west of the Gidginbung Volcanics is the Gilmore Fault Zone, which separates this unit from the Ordovician turbiditic metasedimentary rocks and Silurian S-type granitoids of the Wagga-Omeo Metamorphic Belt. The feature also separates the eastern and central sub-provinces of the Lachlan Orogen in this region.

The sedimentary Silurian Yiddah Formation lies to the east of the Gidginbung Volcanics, with the nature of this contact unknown. The Yiddah Formation and the more extensive adjoining Combaning Formation are components of the Tumut Synclinorial Zone; consisting of siltstone, phyllite, sandstone, conglomerate, carbonaceous siltstone and chert (Warren et al. 1995). Also contained in the Combaning formation are slivers of Ordovician volcanic units akin to the Gidginbung Volcanics, including the Belimebung and Boonabah Volcanics.

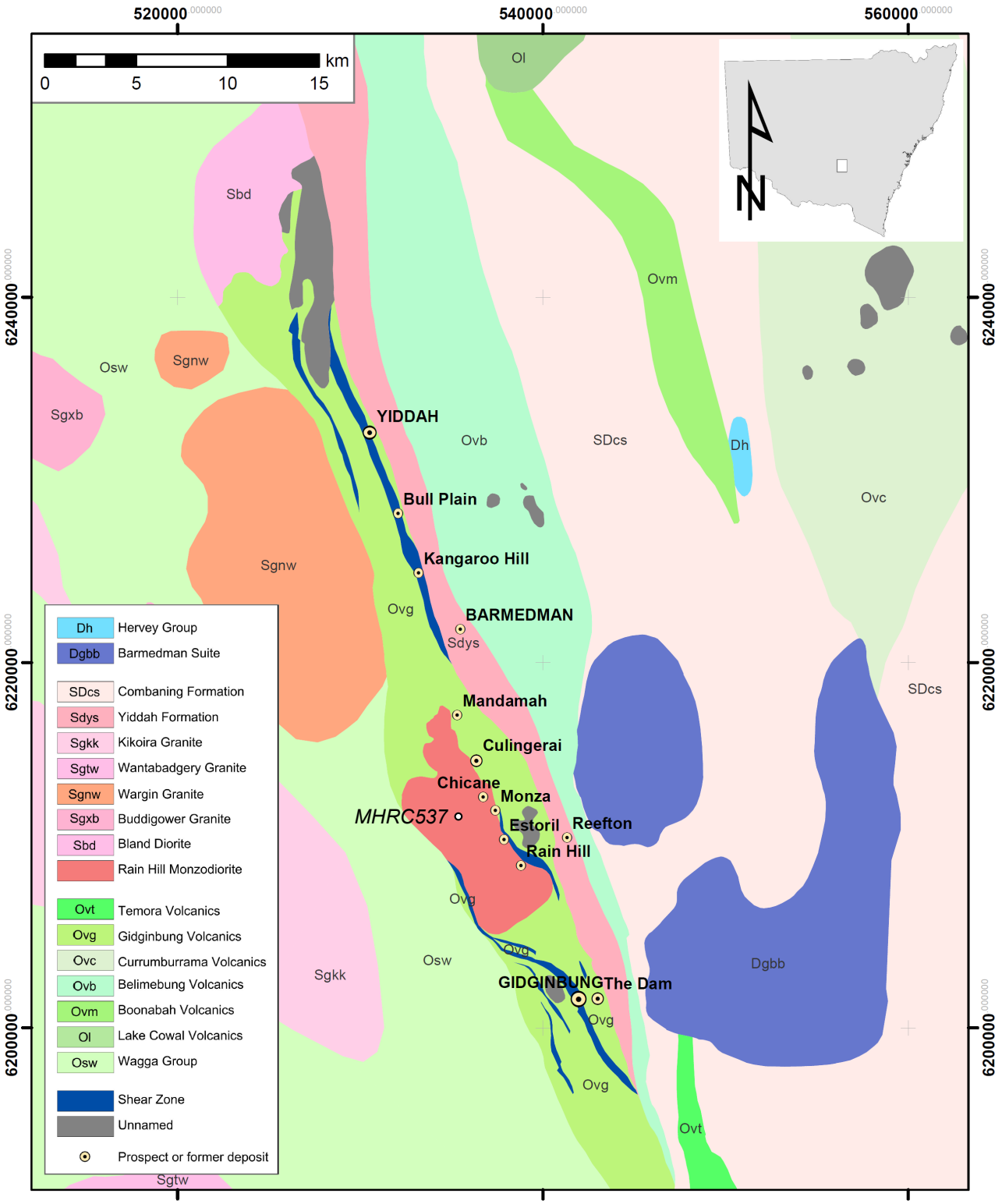

Figure 2.6: Interpreted regional bedrock geology of the Rain Hill district, highlighting the dominant north-northwest sheared nature of the Gidginbung Volcanics and adjacent units. The Rain Hill Monzodiorite (not formally named) is evident south of Barmedman, and is thought to extend north depth in the Gidginbung Volcanics to the Yiddah prospect. Interpreted from the Cootamundra 1:250,000 map sheet, aeromagnetic images and company data. Spatially referenced to AGD_1966_AMG_Zone55. 'MHRC537' indicates the collar location of the reverse circulation hole from which sample 'RHM' was sourced.

Intruding the Combaning Formation is the I-type Barmedman granite (364 ± 2.0 Ma, Warren et al. 1995; 370 ± 2.4 Ma, Fu et al. 2009), the Narraburra Suite and the I-type Middledale Gabbroic Diorite, from which the zircon standards Temora-1 (416.75 ± 0.24 Ma) and Temora-2 (418.1 ± 1.6 Ma) were sourced (Black et al. 2003; Black et al. 2004; Fu et al. 2009).

2.4.2. Geology and geochronology

Outcrop of the Gidginbung Volcanics is very poor due to thick Quaternary cover. As a consequence, its extent has largely been inferred from aeromagnetic data; where it represents a strong linear north-northwest striking belt of high magnetic intensity. Spatially limited outcrop is heavily altered, such that the nature of original lithologies is generally completely obscured (Warren et al. 1995). Exploration drilling however has enabled description of units, as summarised by Warren et al. (1995) to comprise plagioclase-amphibole andesites with lesser trachytic to dacitic flows/shallow intrusions and fine- to pebble-sized pyroclastics interbedded locally with siltstone, sandstone and conglomerate of volcanic origin. Limited petrography has been carried out on these units, with shearing and hydrothermal alteration representing major restricting factors.

Perkins et al. (1995) obtained a maximum $^{40}Ar/^{39}Ar$ age of 461.5 ± 1.1 Ma for illite from the Gidginbung open pit, suggesting deposition of the Gidginbung Volcanics occurred from at least the Middle to Late Ordovician. Zircons contained in an andesite flow at the Gidginbung open pit have been dated at 435 ± 2.5 Ma by SHRIMP 1 (Perkins et al. 1990), implying magmatic activity occurred around the early Silurian. This pattern appears broadly similar to that observed for the shoshonitic Goonumbla system.

The Gidginbung Volcanics are intruded by diorite, granodiorite, quartz monzodiorite and quartz monzonite granitoids, many in the form of sills and stocks which have resulted in moderate to intense hydrothermal alteration of volcanic units (Warren et al. 1995). The ‘Gidgingidginbung Quartz Monzodiorite’, (Wormald 1993) or ‘Rain Hill Quartz Monzonite’ (Downes et al. 2004) or ‘Rain Hill Monzodiorite’ (this study) is the most significant intrusive body; possessing a relatively large spatial extent immediately south of Barmedman, with a possible northern extent to the Yiddah prospect. Hornblende of the Rain Hill Monzodiorite was dated using the Ar-Ar method at 434.9 ± 2.3 Ma (C. Perkins cited by Wormald 1993).

Apart from this work, very little is known about this unit and its relationship with other intrusive units in the region. The proximity of absolute dates obtained for the late andesitic flow of the Gidginbung Volcanics and the Rain Hill Monzodiorite intrusive unit suggests emplacement of the latter was either coeval or occurred immediately following volcanism.

All units are overprinted by a strongly developed cleavage, considered to be the product of the proximal Gilmore Fault Zone (Warren et al. 1995). Evidence for timing of significant deformation has been proposed by Perkins et al. (1995) from illite K-Ar ages at 413 ± 4 Ma and 423 ± 5 Ma, around the Silurian – Devonian boundary. This age is considered to possibly constrain the timing of deformation related (remobilised) mineralisation of the Gidginbung deposit (Allibone et al. 1995).

2.5. **YIDDAH PROSPECT**

The Yiddah deposit is located in the north of the Gidginbung Volcanics, situated over an approximate 3.5 km north-northwest strike, broadly parallel to the regional strike of the Gidginbung Volcanics and Gilmore Fault Zone (Suppel et al. 1986; Goldminco Corporation 2010; Figure 2.6). At present, drilling remains relatively wide spaced and scope remains for along strike continuation of mineralisation (Munro 2010).

Early accounts describe Yiddah as a strongly deformed, intensively hydrothermally altered porphyry related system, with mineralisation associated with shallow intrusion related early quartz–sulphide veining and K-silicate alteration (Mason 1996). Suppel et al. (1986) described alteration as comprising a central zone of quartz-sericite-kaolinite-pyrite surrounded by propylitically altered rocks (chlorite-carbonate-epidote).

More recent exploration work (Munro 2010) has described the prospect's geology as a coarsening upward intermediate volcaniclastic sequence (basal siltstone, middle sandstone and upper crystal tuff) intruded by a series of diorite to monzodiorite sills and small stocks of probable high-K calc-alkaline affinity in addition to a large intrusive unit located on the western margin of mineralisation, informally named the 'Yiddah Monzodiorite' or 'Rain Hill Monzodiorite' (Figure 2.7).

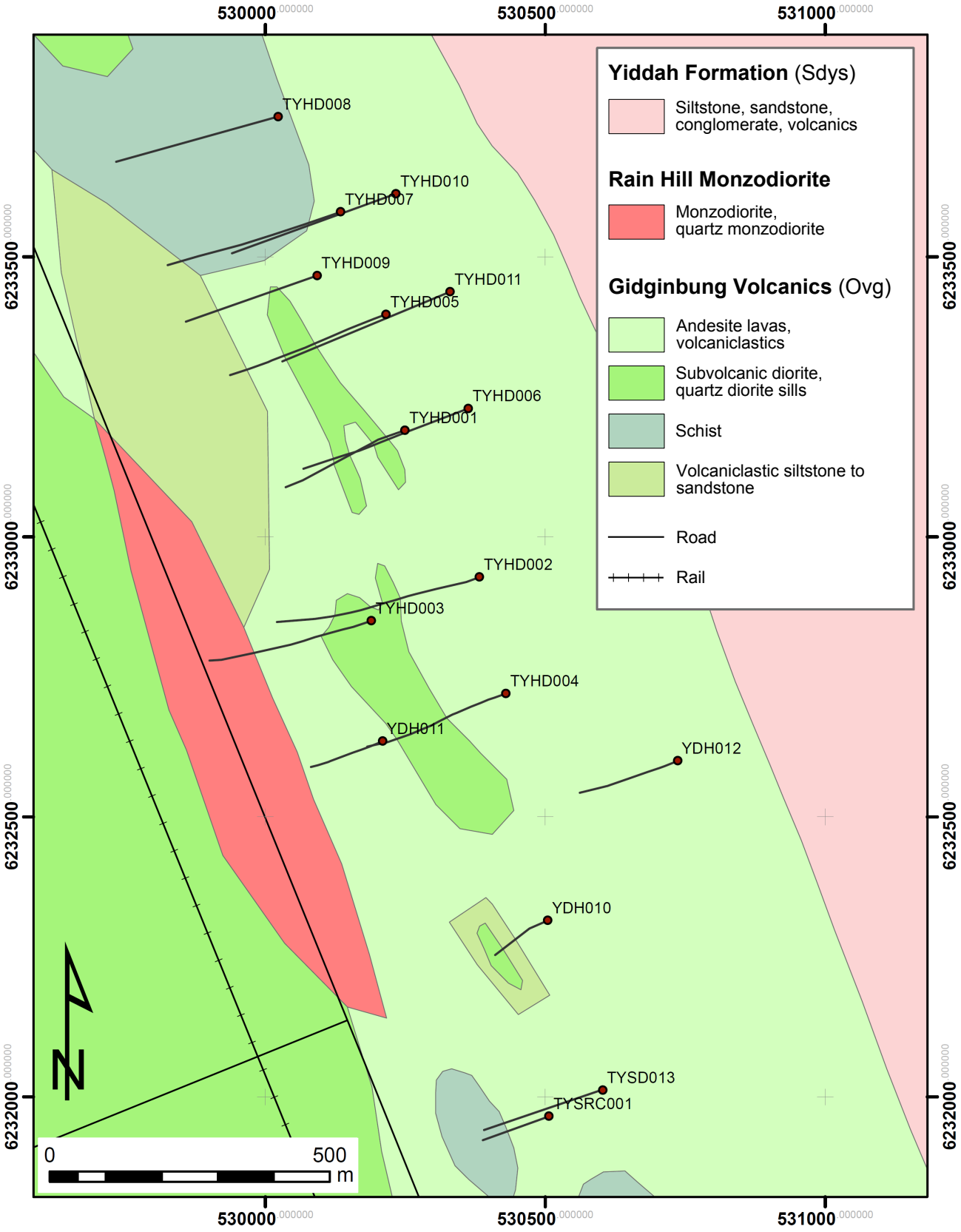

Figure 2.7: Deposit scale geology (Goldminco Corporation). Collars and traces of diamond drill holes used in the present study are marked, including TYHD003, TYHD004 and TYHD005 from which samples were taken. Spatially referenced to AGD_1966_AMG_Zone55.

The volcaniclastic units are reported to dip steeply east, with mineralised intrusive stocks/sills and foliation broadly sub-parallel (Goldminco Corporation 2010). Alteration has been summarised as comprising three key styles; extensive propylitic (chlorite, epidote, calcite, pyrite ± leucoxene), pervasive to patchy mineralised chlorite-magnetite ± sericite and an intense cross-cutting phyllic-argillic assemblage. Chalcopyrite and molybdenite mineralisation occurs as disseminations, along fracture surfaces and within seam quartz ± magnetite veins (Munro 2010).

2.6. **TEMPORAL RELATIONSHIPS**

The timing of depositional, intrusive, mineralising and deformational events related to the Gidginbung Volcanics is concordant with the general pattern observed across the Lachlan Orogen; demonstrated through a summary time-space diagram (Figure 2.8). Of particular significance is the 'mineralisation epoch' evident at ~ 440 Ma, which the Yiddah prospect appears to be a component (discussed further Section 3.4).

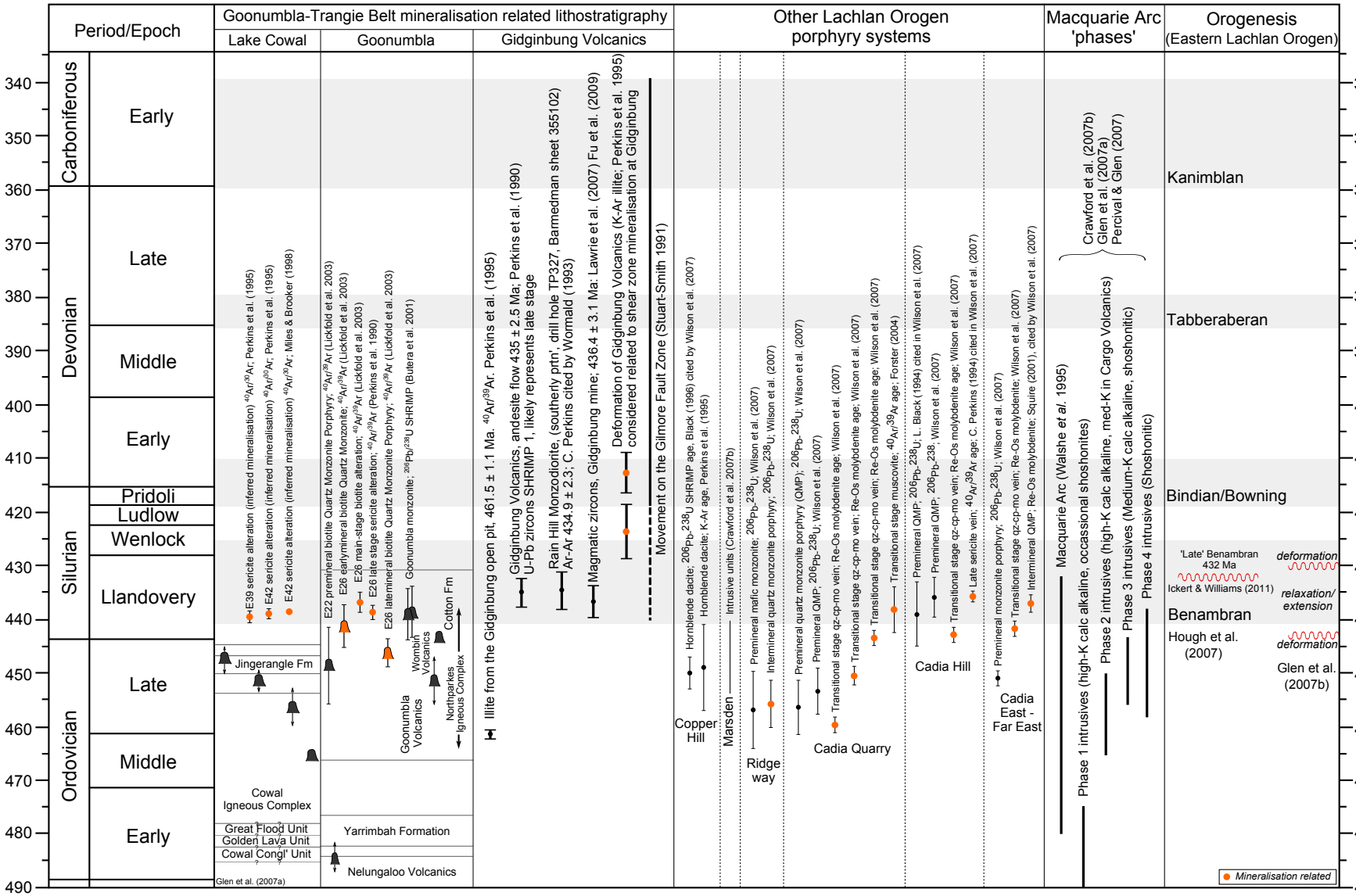

Figure 2.8: Time-space diagram containing significant depositional and intrusive dates within the Goonumbla-Trangie Volcanic Belt (including the Gidginbung Volcanics), Macquarie Arc intrusive 'phases' (Glen et al. 2007a), porphyry mineralisation events within the Lachlan Orogen and deformational events of the eastern Lachlan Orogen. References contained within. Boundaries based on the timescale by Gradstein et al. (2004).

CHAPTER THREE
PORPHYRY COPPER SYSTEMS

3.1. INTRODUCTION

3.1.1. Overview

Porphyry Cu-(Au-Mo) systems are large tonnage (10 – 100+ km^3), low grade (0.5–1.5% Cu, 0–1.5 g/t Au) ore bodies consisting of hydrothermally altered rocks centred on vertically elongate intrusive stocks which generally display porphyritic textures. Other common features include vein stockworks and hydrothermal breccias (Cooke et al. 2005; Sillitoe 2010). Other deposits associated with porphyry copper systems include epithermal (high to intermediate sulphidation), carbonate replacement sediment hosted and skarns (Sillitoe 2010). Porphyry and porphyry related deposits presently comprise a significant supply of the world's Cu (75%), Mo (50%), Au (~20%), Re and minor amounts of Ag, Pd, Te, Se, Bi, Zn and Pb (Richards 2003; Sillitoe 2010).

The vast majority of porphyry systems are formed at convergent plate boundaries in subduction zone settings of both oceanic and continental (Andean) nature, with continental porphyries tending to be more Mo rich and Au poor than their oceanic counterparts. This tectonic setting of formation is supported by their general occurrence in extensive linear and commonly trench or orogen parallel belts (Sillitoe 2010). Nonetheless, major isolated examples do occur (e.g. Butte and Bingham of the USA). At a regional scale, deposits often occur in clusters (e.g. Cadia and Goonumbla regions of New South Wales) (Mowat & Smith 2006). The prevailing stress regime of a deposit is dependent on plate conversion factors such as trench advance, slab rollback and oblique subduction.

Despite the recognition of porphyry formation dating since the Precambrian (e.g. Sukhoi Log, Siberia; Meso to Neoproterozoic and Haib, Namibia; Paleo to Mesoproterozoic, Porter 1998), most porphyries are relatively young (<100 Ma; Seedorff et al. 2005). As such, many recognised systems are situated along the active Pacific Rim (Figure 3.1). It is generally held that the greater prominence of younger systems is the result of their shorter erosional histories (Sillitoe 2010). Even so, numerous older deposits have been recognised in ancient fold belts

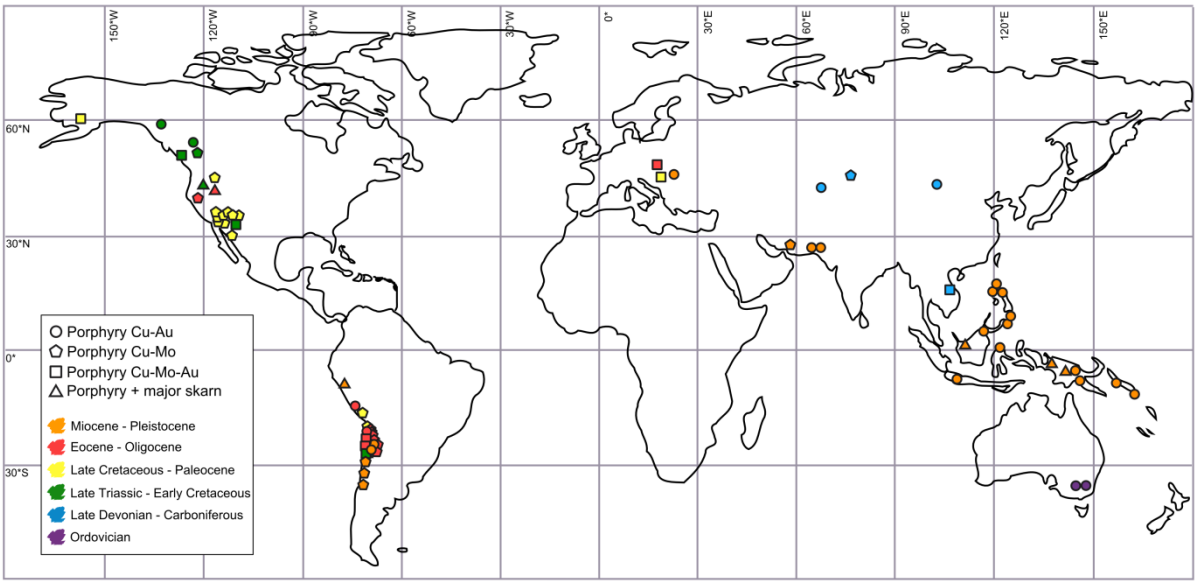

Figure 3.1: Global location, deposit types and ages of large and significant porphyry deposits. Clustering on the Pacific Rim is evident. Adapted from: Sillitoe (2010).

of suitable character (Cooke et al. 2005), with the Cadia system of the Ordovician Macquarie Arc being a particularly noteworthy example.

3.1.2. Early porphyry models

While major low-grade bulk tonnage mining operations have exploited porphyry deposits since the early twentieth century, it has only been in the last half century that sophisticated genetic concepts regarding their evolution have been developed (Hunt 1991). This development largely occurred in the Americas, building on the observations of a number of workers who had identified the involvement of hydrothermal fluids and consistent zonation patterns in many ore deposits (e.g. Emmons 1924; Lindgren 1933). Major advances to follow were predominantly industry driven. In 1941, Anaconda Copper Mining Company (ACMC) established a geologic research laboratory at Butte, Montana, where Sales and Meyer (1948) quantitatively determined and described alteration assemblages within the ore body over the following two decades.

In 1961, ACMC commissioned its second research laboratory at El Salvador, Chile. This highly detailed work was summarised by Gustafson and Hunt (1971, 1975), who described the hypogene evolution of El Salvador in two key phases, spanning no more than one million years (Figure 3.2). The first stage involved the intrusion of two early porphyries into Cretaceous andesites, with accompanying magmatic solutions of relatively high salinity,

oxidation level and temperature (600 – 1000°C). These solutions deposited disseminated sulphide assemblages (anhydrite, bornite, chalcopyrite, quartz) and produced K-feldspar and biotite (potassic/K silicate) alteration. Contemporaneously, overlying and outlying andesites were chloritised and epidotised (propylitic alteration). A transitional period of cooling to around 300°C subsequently occurred, where inrush of meteoric waters deposited the bulk of molybdenum within the deposit. Continued cooling and inrush of meteoric water produced predominantly radial and concentric fracture-hosted mineralisation and lead to the inward collapse of upper and peripheral sericitisation, replacing much of the earlier formed potassic and propylitic alteration.

At around the same time, J. D. Lowell used alteration zonation patterns to successfully predict the downfaulted other half of the San Manuel deposit, Arizona (Kalamazoo) (Hunt 1991). This was achieved through identifying the asymmetry of the San Manuel orebody and through recognition that the low-grade region exposed in the footwall of the San Manuel Fault was in fact the potassic core of the system, rather than the fringe or margin as previously thought. This subsequently lead to Lowell and Guilbert's (1970) widely reproduced version of the 'typical' alteration and mineralisation patterns of porphyry systems, modelled on the San Manuel-Kalamazoo deposit and other porphyries of the southwestern United States (Figure 3.3).

Later in the decade, the work of Kesler (1973) Kesler et al. (1975), Titley (1975), Gustafson (1978) and others sought to apply these models to the porphyries of island-arcs, chiefly focusing on the major examples contained in the southwestern Pacific. They reported that these systems were more Au than Mo rich, more mafic, and generally poorer in K-feldspar than their continental counterparts. Here, lithologies consist most typically of quartz diorites intruding andesitic volcanic rocks, commonly in a telescoped nature (Kesler et al. 1975). Sillitoe and Gappe (1984) later presented a 'Philippine Model', describing alteration in these settings as zoned; with potassic, sericite-chlorite-clay, propylitic, sheeted advanced argillic and patchily superimposed intense sericitic alteration assemblages.

Building upon these chiefly descriptive early models, more recent work (e.g. Sillitoe 1993; Figure 3.4) has attempted to incorporate time-space relationships, with the recognition that virtually all porphyry systems display high evolutionary complexity through time (Hunt 1991). The following sections synthesise these efforts to the current level of understanding

from tectonic to deposit scales, with the recognition that whilst some generalities can be drawn, every system is different with no single model applying to all.

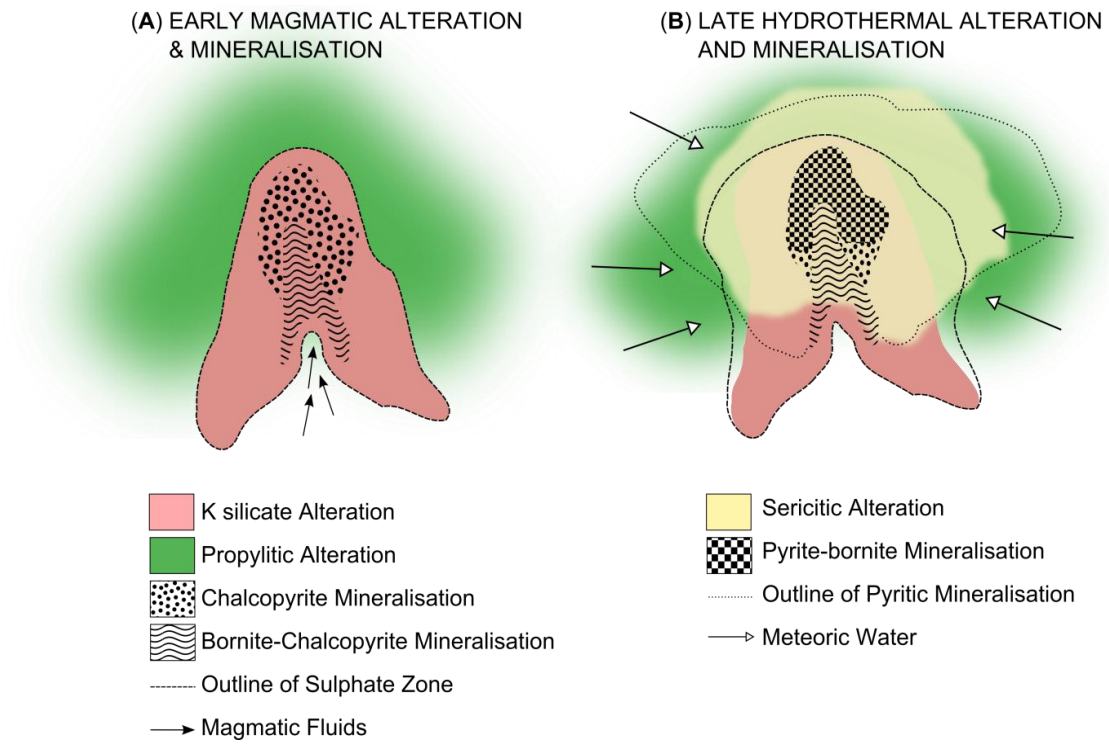

Figure 3.2: Diagrammatic cross sections of Gustafson and Hunt (1971, 1975), summarising the evolution of the El Salvador orebody, Chile.

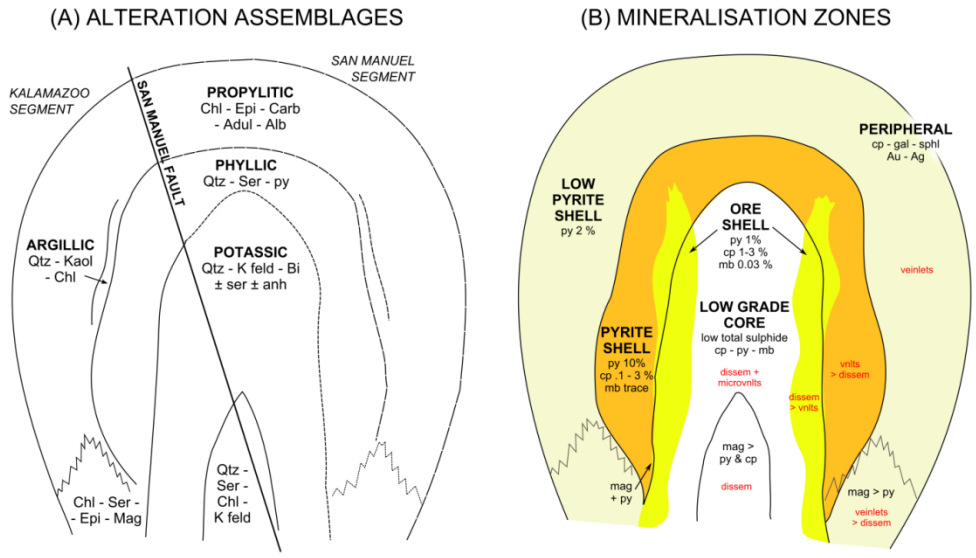

Figure 3.3: Alteration assemblages and mineralisation zones proposed by Lowell and Guilbert (1970) for their 'type' porphyry copper deposit, the San Manuel – Kalamazoo porphyry, Arizona.

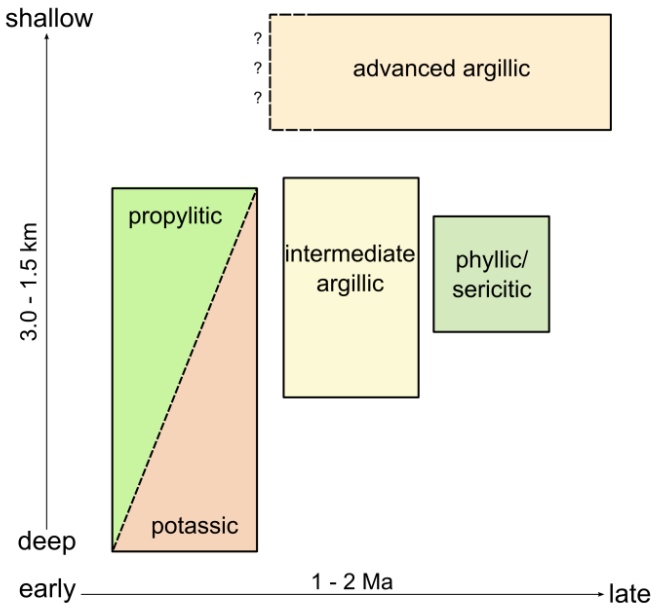

Figure 3.4: Schematic time-depth relations of principal alteration types in porphyry copper systems. After: Sillitoe (1993).

3.2. TECTONO-SCALE GENETIC PROCESSES

3.2.1. Magma genesis

Arc magmas originate above subducting oceanic crust via metasomatism of the overriding asthenospheric mantle wedge (Richards 2003; Kearey et al. 2009). This occurs due to dehydration of crustal material from ~ 65 km depth, which releases a solute-rich aqueous fluid which has three key implications. Firstly, addition of water acts as a flux, decreasing the solidus temperature of the peridotitic asthenosphere permitting melting. Secondly, it introduces fluid mobile components such as Cl, B, Sb, S, Bi, Pb and large ion lithophile elements (LILEs; e.g. Rb, K, Cs, Ba, Sr), whilst not introducing Ti, Nb and Ta. The enrichment of Cl and S in particular are essential to the later development of endowed porphyry systems (discussed further in Section 3.3.1) (Richards 2003; Candela & Piccoli 2005). Lastly, addition of water to the melt allows for the later formation of hydrous minerals including amphiboles and micas (Richards 2003).

The distance from the trench and/or depth at which such mantle melting occurs is considered to strongly influence the overall geochemical character of the supra-subduction volcanism. This theory is supported by the fact that in many arc systems, including the Japanese island-

arc, a compositional trend is observed from tholeiitic (low $Na_2O + K_2O$, high Fe), through calc-alkaline (low to moderate $Na_2O + K_2O$) to alkaline (high $Na_2O + K_2O$) magma series with increasing distance from the trench (Kearey et al. 2009). Tholeiitic rocks, located closest to the trench are interpreted to have formed from relatively primitive mantle melts at shallow depths (65 – 100 km). Calc-alkaline and alkaline magma series rocks however are considered to have originated at greater depths, following blueschist-eclogite transition at ~ 100 km. The $Na_2O + K_2O$ enrichment in the more distal alkali series magmas is attributed to either the dehydration of phlogopite at depth and/or a lower degree of partial melting in the wedge, which may be the result of decreased crustal fluid addition at depth (Richards 2003; Kearey et al. 2009). Of these series, calc-alkaline rocks comprise the most common and important variety of porphyry deposit, with high-K varieties common to gold-rich systems (Sillitoe 1997). Alkaline systems are less common but can also be significant contributors (e.g. Cadia-Ridgeway) (Winter 2001; Cooke et al. 2007).

Following melt generation in the wedge, a mechanism of extraction and transport is required to emplace magmas to suitable crustal levels for porphyry formation. It is evident from chemical and isotopic signatures that this process is complex and multistage (Tosdal & Richards 2001). Hildreth and Moorbath (1988) have presented a genetic model consisting of Melting, Assimilation of continental crust, Storage at the base of the crust and Homogenisation of the resultant magma (MASH). Fundamental to this model is that ascending mafic magmas derived from the wedge are of greater density than the continental crust, and therefore will pool, or underplate at the base of the crust. From this stage, the process of fractional crystallisation creates a progressively more evolved, incompatible enriched melt whilst releasing heat. This heat release leads to partial melting and assimilation of the lower continental crust, which homogenises over time to form a melt of basaltic andesitic to dacitic (intermediate) composition (Hildreth & Moorbath 1988).

Another important characteristic for the successful generation of a porphyry copper system is a relatively high oxygen fugacity (Richards 2003). This feature is typical of I-type, Fe-rich (magnetite series) magmas, of which comprise approximately half of the Lachlan Orogen granites (*s.l.* Ishihara 1981; Blevin & Chappell 1995; Figure 3.5). In oxidised melts, dissolved sulphur is contained as sulphate, which inhibits chalcophile elements (e.g. Cu, Au) from forming sulphide complexes and crystallising from the melt. This ensures these elements are retained and enriched with fractionation during the MASH process and ascent (Richards

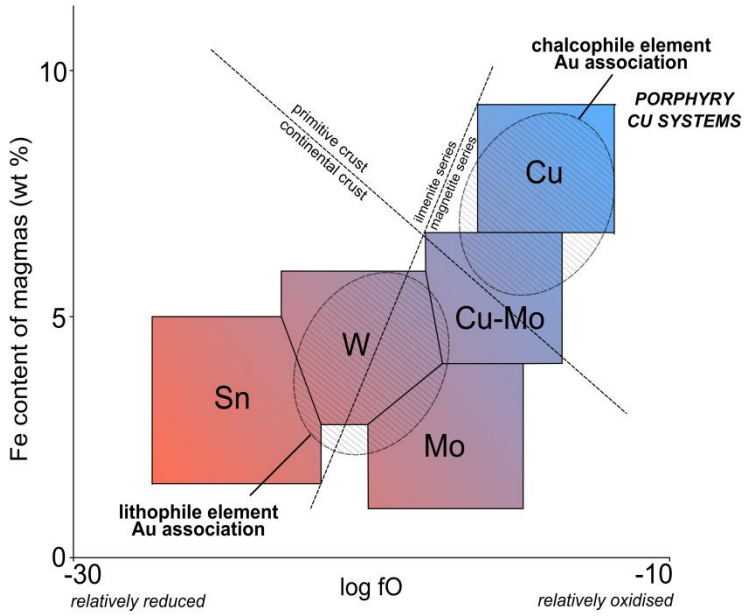

Figure 3.5: Relationship between fractionation level (higher with lower magmatic Fe content) and oxidation state (fO) for magmas associated with different metal assemblages. Adapted after Lang & Baker (2001).

2003). The metals themselves are probably derived from a combination of sources, including the wedge, lower crust and subducted lithosphere (Candela & Piccoli 2005).

3.2.2. Tectonic controls on magma transport

While it is likely that early magmatic ascent occurs via buoyancy driven expulsion, it is generally considered that structural conditions play the chief role in controlling crustal ascent and eventual magmatic emplacement (Clemens & Mawer 1992). As porphyry system formation is inextricably linked to convergent margin tectonic settings, such structural conditions must be viewed within the context of a differential stress field, governed by factors including convergence rate, convergence angle, slab dip and buoyancy. The net result of these factors may be a stress regime of compressional, extensional and/or transverse nature. Extensional stresses are the result of slab rollback of old, cold and therefore dense subducting slab, which has the effect of drawing the upper plate toward the trench (Royden 1993). Shear stress components result from oblique subduction, as convergence angles are rarely orthogonal (Richards 2003). Elements of strike-slip tension thus generally co-exist within overall shortening and/or extensional conditions, resulting in transtensional or transpressional regimes. These stress conditions are not fixed but rather vary over time, often quite rapidly, as evidenced by shifts in direction and speed of plate migration deduced from hot-spot island chains (Tosdal & Richards 2001).

A number of frequently observed characteristics of porphyry copper systems; including their common spatial concentrations within narrow, margin parallel belts, associations with major arc-parallel and transverse structures and emplacement during relatively limited time ranges, have led to the notion that unique structural conditions are related to optimum formational conditions. Glazner (1991) has suggested that emplacement occurs within dilational zones created by strike-slip motion due to an element of oblique subduction in dominantly compressional settings. Tosdal & Richards (2001) however argue that an overall compressional regime is unsuitable for porphyry formation, as volcanism is dominantly explosive, due to its high pressure ascent via tightly locked structures (Figure 3.6A). They also suggest that dominantly extensional settings are unsuitable, as magmas are able to ascend directly to the surface forgoing the MASH (enrichment) process (Hildreth & Moorbath 1988) (Figure 3.6B). Instead, they propose periods of transition between compressional and extensional conditions to be responsible (Figure 3.6C, D). These conditions are characterised by a long period of enrichment at the base of the lithosphere, followed by a steady ascent with fault relaxation to emplacement levels conducive to

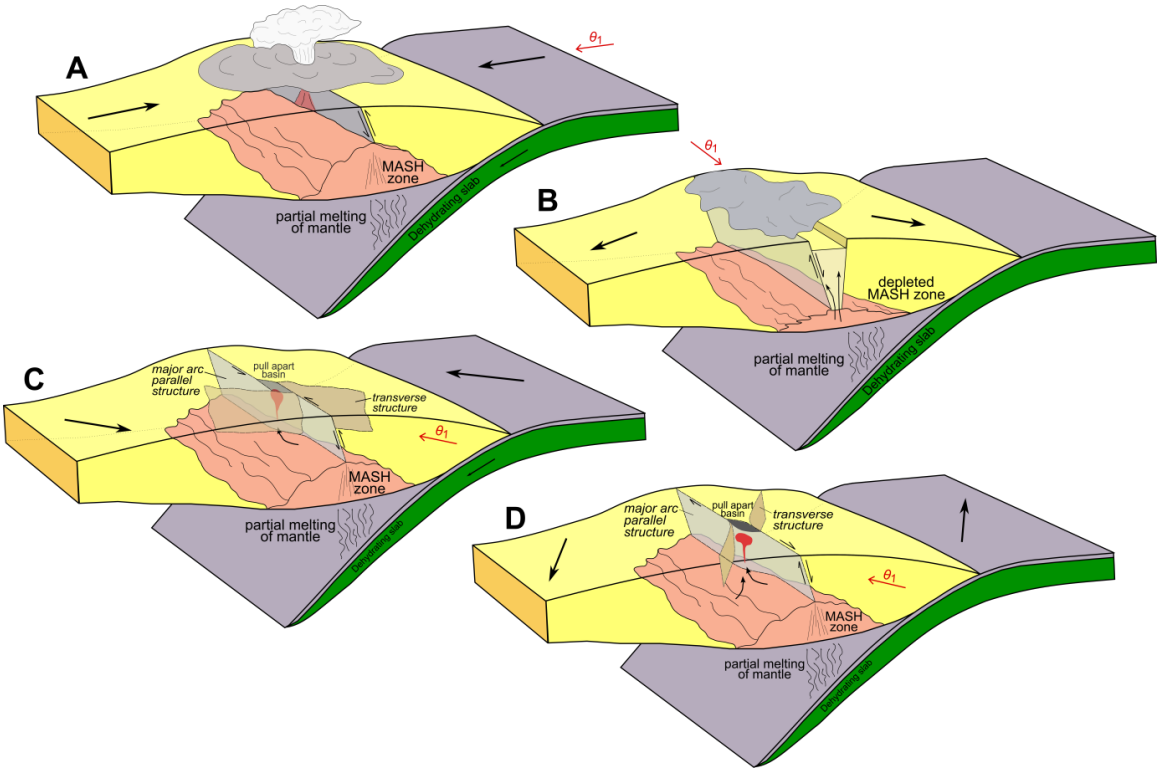

Figure 3.6: Alternative tectonic regimes present at convergent margins and their potential for porphyry copper system formation. (a) Compressional regime; little potential due to explosive nature of volcanism. (b) Extensional regime: little potential due to magmas ready access to the surface bypassing significant evolution and enrichment. (c) Transpressional regime: moderate potential due to prolonged MASH (enrichment) period and intermediate permeability of the crust provided by intersection of major and transverse structures. (d) Transtensional regime: maximum potential due to significant MASH (enrichment) period and high crustal permeability at fault intersections. Adapted from Tosdal & Richards (2001).

porphyry formation. Like Glazner (1991), they suggest that low-pressure zones such as those created by pull-apart basins at intersections of major structures and transverse shears are optimum targets for magma emplacement. The Lachlan Transverse Zone, containing the world class deposits of Cadia-Ridgeway and Goonumbla has been suggested to represent such a structure (Glen & Wyborn 1997; Glen & Walshe 1999). Many authors (e.g. Cooke et al. 2005) attribute transition from compressional to extensional conditions to the subduction of aseismic ridges, seamount chains and/or oceanic plateaus, events which promote subduction stalling. In the Lachlan Orogen, the major mineralisation period at *ca* 440 Ma (see Section 3.4) has been attributed to subduction zone lock-up following arc collision at *ca* 445 Ma (Squire & Miller 2003).

3.2.3. Parental/precursor plutons

If tectonic conditions facilitate successful transport of oxidised, endowed magmas to relatively high crustal levels (5-15 km), a porphyry Cu-(Au-Mo) system may result. In this case the pluton is termed the 'parental' or 'precursor' pluton. Emplacement at upper crustal levels is required to produce the necessary hydrofracturing, fluid exsolution and circulation of hydrothermal fluids for porphyry formation. Precursor plutons are typically multiphase, equigranular diorites to granites with volumes ranging from ~ 50 km^3 up to 500 km^3 for giant systems (Sillitoe 1973; 2010). Larger volume plutons may be associated with a number of porphyry deposits, leading to commonly observed patterns of regional clustering or alignment (Sillitoe 2010).

In addition to tectonic controlling factors and buoyancy of the melt, the level at which a pluton is emplaced is largely dependent on its magmatic water content (Burnham 1979). Magmas with high water contents undergo fluid exsolution or 'second boiling' at deep-seated levels, resulting from saturation of the melt with progressive crystallisation of dominantly anhydrous minerals. Water exsolution leads to crystallisation (e.g. Whitney 1975), which stalls magma ascent. Following Burnham (1979), an intermediate melt of greater than ~ 8 % contained water will generally not rise above 15 km depth. Magmatic water content also governs the behaviour of Cu in the system. The lack of substantial crystallisation occurring prior to high-level emplacement in relatively dry magmas enables significant concentrations of the compatible metal to be retained in the melt, available at later stages (Robb 2007). Therefore, whilst relatively high water contents in the melt are necessary at late stages to

exsolve fluids and generate a hydrothermal system, very high initial magmatic water concentrations are not conducive to the formation of porphyry copper systems.

3.2.4. Country rocks

Owing to their subduction zone settings, porphyry systems are often associated with co-magmatic alkaline to calc-alkaline volcanic rocks of intermediate to felsic composition, typically erupted subaerially 0.5 to 3 m.y. prior to mineralising stock intrusion (Sillitoe 2010). These rocks are often in a considerably degraded state due to the process of erosional unroofing of the porphyry, particularly in older systems such as the Macquarie Arc (Sillitoe 1973). Country rocks may also be comprised of older, igneous, sedimentary or metamorphic rocks. The chemical and physical characteristics of these rocks can greatly influence mineralisation. Carbonate rocks, common in volcanic arc sequences may result in skarn, carbonate replacement or sediment-hosted mineralisation, whilst the porosity and degree of fracturing within the country rocks will determine the effectiveness of fluid circulation and therefore impact upon the grade and geometry of the resultant orebody (Sillitoe 2010).

3.3. **DEPOSIT SCALE PROCESSES AND PRODUCTS**

3.3.1. Sill/stock evolution and fluid exsolution

In the 1 to 2 Ma following high level emplacement of the parental/precursor pluton, the evolution of a porphyry copper system is characterised by the multiphase intrusion of a number of porphyritic sills/stocks within the upper 5 km of the crust (e.g. as described for the Highland Valley porphyry, British Columbia, Casselman et al. 1995; the Rio Blanco porphyry, central Chile, Deckart et al. 2005; and the Chuquicamata Porphyry, northern Chile, Campbell et al. 2006). The composition of sills/stocks ranges from diorite to quartz diorite, monzodiorite, quartz monzodiorite, granodiorite, monzonite, quartz monzonite and uncommonly syenite (Seedorff et al. 2005). Geometries are typically vertically elongate but may also be circular or irregular (Seedorff et al. 2005; Sillitoe 2010).

It is these sills/stocks that exsolve the mineralised hydrothermal fluids necessary to generate a porphyry deposit. This fluid is sourced from underlying precursor plutons, with the sills/stocks acting as fluid conduits (Sillitoe 2010). Exsolution of fluids may occur following

fluid saturation ('second boiling') or more commonly, due to the sudden drop in pressure associated with high level emplacement ('first boiling') (Robb 2007). It is this rapid increase in crystallisation rate that results in the characteristic porphyritic texture of sills/stocks. The exsolved fluid typically consists of either a single phase liquid (high temperatures) or two immiscible phases which are exsolved directly or form as the single-phase liquid cools. The two phase fluid includes a small fraction of hypersaline liquid (brine) and a much larger volume of low density vapour. Fluid inclusion studies have shown the brine is enriched in Na, K and Fe chlorides at 35 – 70 wt% NaCl equivalent along with Zn, Rb, Cs, Ag, Sn, Pb, and Tl chlorides; whilst the vapour phase contains acidic volatiles such as SO_2, H_2S, CO_2, HCl and HF, along with Cu, As and Au probably as HS complexes (Heinrich et al. 1999).

The significance of these compounds is that many form effective coordination complexes with metals contained in the melt and thus enable their introduction to hydrothermal systems. This has been supported experimentally by workers including Holland (1972) who found a strong correlation between the solubilities of Zn, Mn and Pb with fluid Cl^- concentration and Candela and Holland (1984) who confirmed this relationship with Cu. This suggests that as boiling occurs, in order for large quantities of Cu to partition from the silicate melt to the fluid phase, it must be scavenged by a volatile such as Cl^- with which it can form a coordination complex and of which effectively partitions into the fluid phase itself ($Cl^-_{(melt)} + OH^-_{(melt)} \rightarrow HCl_{(fluid)} + O^{2-}_{(melt)}$) (Kilinc & Burnham 1972). It has also been demonstrated that S ligands (H_2S and SO_2) can act as major Cu and Au transporting agents (Sillitoe 2010); while the incompatible Mo may partition via Mo-oxochloride complexes, or less effectively without ligand complexing (Candela & Holland 1984; Candela & Holland 1986; Robb 2007).

The intrusion/fluid exsolution process of sills/stocks does not occur in one single event but rather in multiple phases, ranging from immediately before, to during and after alteration and mineralisation events (Gustafson 1978). In most deposits, early stocks and their contiguous host rocks contain the highest grade mineralisation, with late and post-mineralisation phases becoming progressively more barren. Consequently, early mineralised intrusions are often split by late, non-mineralised intrusions (Gustafson 1978; Sillitoe 2010). The release of fluid is also accompanied by a release of mechanical energy, as the exsolved fluid and dehydrated melt are of greater volume per unit mass than the equivalent fluid saturated magma. Fluid exsolution may therefore result in overpressuring of the chamber and brittle failure of

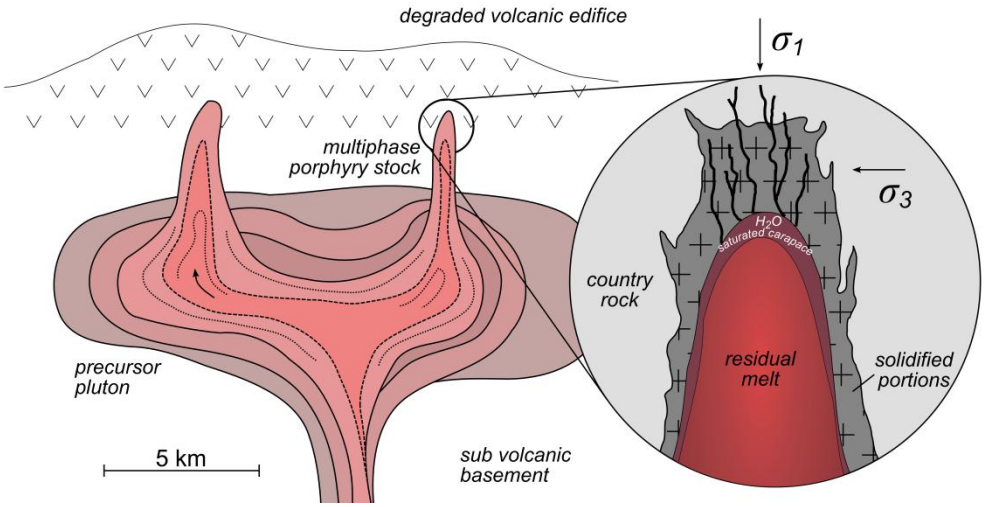

Figure 3.7: Spatial relationship of the underlying precursor pluton, porphyritic stocks and overlying comagmatic volcanic rocks. The precursor pluton is multiphase, with the innermost chamber considered the 'parental' pluton. Inset demonstrates the mechanical effects of fluid exsolution from stocks. Adapted from Robb (2007) figure 2.7 and Sillitoe (2010) Figure 4.

surrounding rocks (hydrofracturing), which may produce significantly mineralised high-angle fractures and/or breccias overlying the porphyry (Burnham 1979; Figure 3.7).

3.3.2. Alteration-mineralisation assemblages

As emphasised by early models; consistent, broad-scale patterns of hydrothermal alteration typically affecting several cubic kilometres of rock are hallmark features of porphyry copper systems (Lowell & Guilbert 1970). The characteristic properties and spatial arrangement of these assemblages are outlined in Table 3.1 and Figure 3.8. Although patterns of alteration in individual deposits may vary considerably, assemblages can be broadly summarised as (bottom to top); sodic-calcic, potassic, chlorite-sericite, sericitic (phyllic), advanced argillic and propylitic (marginally). Also uniquely associated with each assemblage are vein/veinlet sequences (fluid conduits) and mineralisation assemblages. The latter relationship results due to the significant influence of solution pH on both sulphidation state and alteration assemblage (Seedorff et al. 2005). Specific vein/veinlet sequences are tightly associated with the temporal evolution of the potassic, and later assemblages. As such, the occurrence of early, relatively insoluble veinlets (e.g. quartz) in overprinted rocks enables the earlier presence of potassic alteration to be inferred. Mineralisation sequences in contrast are highly spatially zoned. This zonation typically consists of a chalcopyrite-bornite core (the

centre of which may be barren) transitioning to a chalcopyrite-pyrite annulus which grades outward with increasing sulphide contents into pyrite haloes ± sphalerite and galena anomalies in the distal propylitically altered rocks (Sillitoe 2010).

Table 3.1: Typical characteristics of the dominant porphyry copper system alteration assemblages. Adapted from Seedorff et al. (2005) and Sillitoe (2010).

Alteration Assemblage	*Position*	*Key minerals*	*Principle sulphides*	*Contemporaneous veins*	*Economic potential*
Sodic-calcic	deep	albite/oligoclase, actinolite, magnetite	absent	magnetite, ± actinolite (M)	low
Potassic	core	biotite (more mafic), k-feldspar (felsic)	py-cp, cp, ± bn, ± chalcocite	biotite, k-feldspar, qz-sulphides ± magnetite (A), qz seam (moly ±py±cp) (B)	main contributor
Chlorite-sericite	upper core	chlorite, sericite/ illite, hematite	py-cp	chlorite, ± sericite, ± sulphides	common contributor
Sericitic (phyllic)	above chl-ser	quartz/sericite	py, ± cp	qz-py ± other sulphides (D)	low
Advanced argillic	above porphyry	qz (residual/vuggy), alunite, kaolinite	py-enargite py- chalcocite py-covellite	qz-sericite	can be significant
Propylitic	marginal	chlorite, epidote, albite, carbonate	py, (± sphal, galena)	py-enargite, ± Cu sulphides	minor (veins)

chl = chlorite, ser = sericite, qz = quartz, py = pyrite, cp = chalcopyrite, sphal = sphalerite, moly = molybdenite.

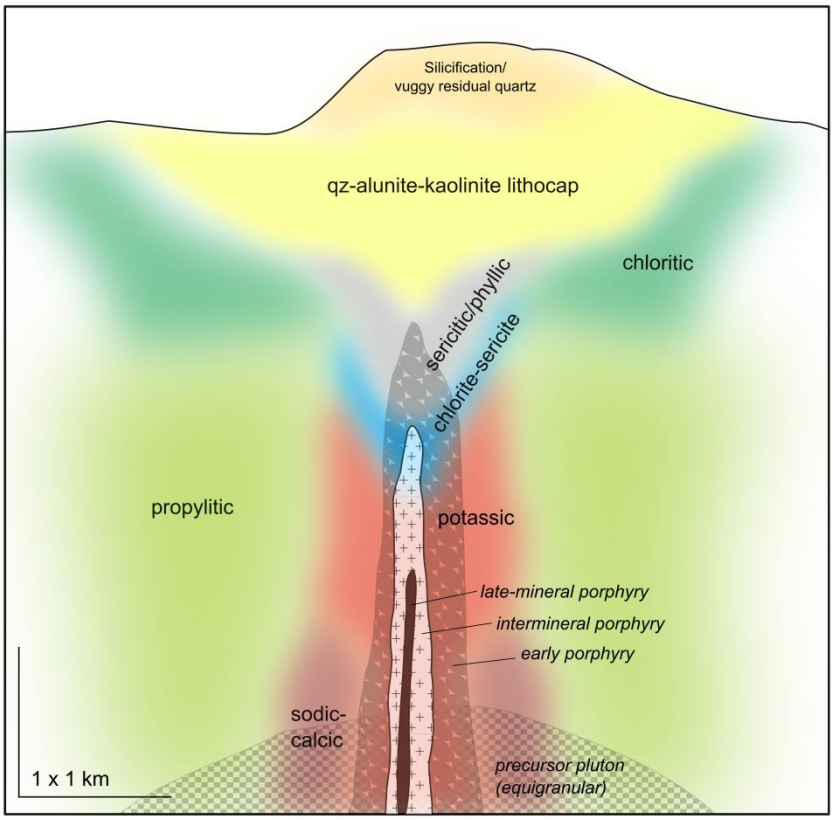

Figure 3.8: Spatial relationships of general alteration-mineralisation zoning patterns for a telescoped porphyry Cu deposit. Constant overprinting of deeper alteration assemblages is evident. Modified after Sillitoe (2010).

The consistency of alteration assemblage zonation is related to the conditions which produce contrasting mineral products; summarised by Reed (1997) as temperature, pressure, host rock composition, fluid composition and the fluid/rock ratio. Temperature and pressure largely dictate the stabilities of certain minerals, whilst the host rock influences the assemblage of elements available for forming new minerals. Fluid composition, along with temperature strongly influences the solubility of host rocks and minerals introduced by the fluid. The fluid/rock ratio, which varies significantly over the spatial extent of a porphyry system, is considered to be particularly influential as it dictates the extent to which alteration reactions will move to completion and thus the resultant mineral assemblage (Figure 3.9). For example, in proximal areas with high fluid/rock ratios or reinjections of fluid the common igneous mineral K-feldspar would be progressively altered via the following (Beane 1982):

$$\underset{\text{(K-feldspar)}}{3KAlSi_3O_8} + 2H^+ \leftrightarrow \underset{\text{(muscovite)}}{KAl_3Si_3O_{10}(OH)_2} + \underset{\text{(quartz)}}{6SiO_2} + 2K^+$$

and

$$\underset{\text{(muscovite)}}{2KAl_3Si_3O_{10}(OH)_2} + 2H^+ + H_2O \leftrightarrow \underset{\text{(kaolinite)}}{Al_2SiO_5(OH)_4} + 4SiO_2 + 2K^+$$

In distal areas however, a lesser amount of progressively neutralised fluid is available to perform alteration, therefore the resultant assemblage would be dominated by muscovite.

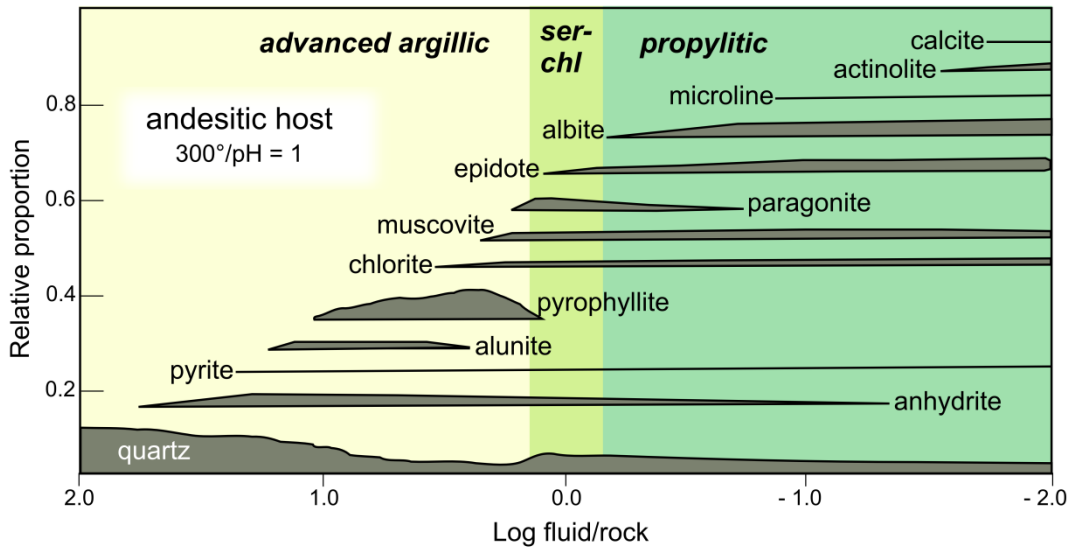

Figure 3.9: The relationship between principal alteration minerals and fluid/rock ratio for a relatively oxidised aqueous solution (magmatic fluid at 300ºC and initial pH =1) reacting with an andesitic rock. Alteration assemblage groupings are also shown. Adapted from Reed (1997).

Porphyry systems also evolve over time in response to changes in temperature and pressure conditions. Early potassic alteration involves the addition of K^+ ions to the core of the system as it cools through 700 to 550ºC (Sillitoe 2010). Extensive hydraulic fracturing and expansion of the ductile rock resulting from chamber overpressure acts to focus magmatic fluid ascent through pervasive stockwork veining (Burnham 1979). The resultant upward decompression leads to decreased solubility of vapour phase metals, which enables wholesale precipitation of sulphides in stockworks, porphyritic stocks and country rocks. Potassic alteration is therefore generally associated with the main ore body. Typical veinlet sequences consist of actinolite and/or magnetite ('M' type); biotite or sinuous to planar quartz ('A' type); or banded quartz (quartz seam) veins ± chalcopyrite, magnetite and molybdenite ('B' type) (Seedorff et al. 2005).

At deeper levels, commonly in the country rock immediately adjoining stock intrusions, sodic-calcic alteration may occur contemporaneously to, or in some deposits, as an alternative to potassic alteration. This alteration type is commonly magnetite bearing, but is typically poorly mineralised. It is characterised by abundant albite, epidote and actinolite and hence can commonly be confused with propylitic alteration; which occurs both later as an overprint, and distally during potassic alteration events (Robb 2007; Sillitoe 2010).

Propylitic alteration (chlorite, epidote ± lesser albite and calcite; essentially akin to regional greenschist metamorphism) is produced as a result of H^+ metasomatism at low fluid/rock ratios and relatively low temperatures (200 – 300 ºC) (Beane 1982; Beane & Bodnar 1995). It is generally not associated with significant mineralisation. $^{18}O/^{16}O$ and D/H analyses suggest that hydrothermal fluids in these distal areas are sourced from meteoric ± connate waters, which circulate within long-lived hydrothermal convection systems heated by intrusive bodies. The degree and extent of alteration here is chiefly controlled by the permeability of country rocks (Meyer & Hemley 1967; Taylor 1974; Taylor 1997).

Early stage porphyry system evolution also typically consists of advanced argillic lithocap formation, resulting from fault aided upward propagation of the voluminous low density magmatic derived vapour, which condenses to form a low pH fluid due to its high HCl and SO_2 (H_2SO_4 & H_2S) concentrations (Meyer & Hemley, 1967). The resultant assemblage consists of vuggy residual quartz and secondary clays (e.g. kaolinite, dickite, andalusite, pyrophyllite) (Seedorff et al. 2005). These minerals make this alteration type very susceptible

to erosion and as such it is commonly absent, particularly in older porphyries. Significant mineralisation is generally absent, a feature ascribed to the much decreased solubility of Cl^- at the low pressures of shallow depths (Kilinc & Burnham 1972).

As the parental chamber progressively solidifies, the supply of both heat and magmatic fluids to the overlying porphyry system significantly decreases (Sillitoe 2010). This reduces the exsolution rate of magmatic fluids, which leads to the production of a single-phase fluid rather than the two-phase fluid responsible for early potassic alteration. Cooling of the system also results in drawdown of the pressure boundary that had formerly separated inner magmatic fluids from the outer convective system, such that meteoric and magmatic fluids may mix (Taylor 1997). This involvement of meteoric fluids in sericitic/phyllic alteration was recognised early in the literature through stable isotope studies of predominantly North American deposits (e.g. Taylor 1974). Importantly however, examples where sericitic/phyllic alteration is largely or exclusively related to magmatic fluids are also well documented (e.g. at Endeavour 26 North, Northparkes; Harris & Golding 2002).

The resultant magmatic/meteoric or magmatic fluid is of much lower salinity (5 – 20 wt% NaCl equiv.) and temperature (250 – 350ºC) than earlier fluid generations. It ascends via pre-existing quartz veinlet stockworks, faults and contacts to form chlorite-sericite (chlorite, sericite/illite, hematite, ± carbonate ± epidote) and sericitic/phyllic (quartz/sericite ± carbonate ± pyrophyllite) alteration assemblages overlying and often overprinting potassic sequences (Seedorff et al. 2005; Sillitoe 2010). The former is a common contributor (and/or remobiliser) of mineralisation, whilst the latter typically will destroy earlier mineralisation, contributing only pyritic sulphides. Veins associated with these assemblages are typically chlorite ± sericite ± sulphides with chlorite and/or sericitic selvedges (chlorite-sericite alteration) and quartz-pyrite ± other sulphides with quartz-sericite selvedges (sericite/phyllic alteration) (‘D’ type veins; Sillitoe 2010).

3.4. PORPHYRY COPPER DEPOSITS OF THE LACHLAN OROGEN

3.4.1. Overview

Porphyry deposits of the Lachlan Orogen conform to the general model of formation at convergent plate boundaries during or immediately following subduction, possibly

associated with periods of extension (Bierlein et al. 2002). Thirty five known porphyry or porphyry related systems occur within the Early Ordovician to early Silurian Macquarie Arc of the eastern sub-province (see Mowat & Smith 2006 for full list). Their distribution is highly clustered, with four key districts containing the majority of systems (Cadia, Northparkes, Cowal and Rain Hill districts; Smith et al. 2004). Mineralisation ages of many of these deposits are proximal to 440 Ma, which has been suggested to be a 'mineralisation epoch', associated with upwelling in extensional conditions generated from subduction zone lock-up following arc collision at *ca* 455 Ma (Squire & Miller 2003).

Deposits are characterised by predominately andesitic to trachytic composition volcanic and intrusive rocks, which as a whole are slightly more felsic than the overall Macquarie Arc. These rocks commonly possess a pink to red colour due to hematite dusting (Mowat & Smith 2006). Pb isotope signatures indicate that parental magmas have a bimodal source, consisting of a depleted mantle reservoir and a more enriched, high μ (U/Pb) mantle reservoir, the latter of which appears to have an increasing contribution with decreasing deposit age (Carr et al. 1995). Mineralisation occurs both temporospatially related to its host volcanic complexes (Goonumbla, Cadia) and with no, or an uncertain temporal relationship to its host volcanic sequences (Lake Cowal, possibly Copper Hill).

The relatively ancient nature of these systems and the numerous orogenic cycles to which they have been subjected has led to varying degrees of deformation. Most systems display at least lower greenschist facies metamorphism (Bierlein et al. 2002), while some are considered to be structurally controlled (e.g. Cowal, Miles & Brooker 1998; Gidginbung, Allibone et al. 1995). As such, it is important to note that porphyry systems of the Lachlan Orogen generally do not possess the paradigmatic alteration and mineralisation patterns as described in traditional porphyry models based predominantly on Cenozoic examples.

Individual deposits can be subdivided into those of calc-alkaline chemistry (Marsden, Copper Hill, Cargo, Cowal) and those of alkalic (shoshonitic) chemistry (Cadia and Goonumbla). The shoshonitic deposits are overwhelmingly the most economically significant, which has led some authors to suggest that K-enrichment is associated with mineralisation potential in the Lachlan Orogen (e.g. Holliday et al. 2002; Blevin 2002).

3.4.2. Calc-alkaline systems

Calc-alkaline systems of the Lachlan Orogen were emplaced throughout Macquarie Arc volcanism and in the period immediately following its cessation (Glen et al. 2007b). The Copper Hill system (105 Mt at 0.33 g/t Au, 0.33 % Cu) is the most comprehensively studied, consisting of a medium-K affinity dacite (446 ± 6 Ma), hornblende tonalite (450 ± 6 Ma) and quartz diorite (447 ± 5 Ma) complex (Chivas & Nutter 1975; Cooke et al. 2007). Mineralisation/alteration consists of early quartz-magnetite-Fe-rich chlorite alteration associated with quartz veining, followed by quartz-sericite-pyrite alteration (minor chalcopyrite and molybdenite) and sericite-Mg/Fe chlorite-calcite-clay alteration containing quartz-pyrite-chalcopyrite-calcite veins which form the bulk of the high-grade ore (Cooke et al. 2007).

Mineralisation at Cowal is related to a diorite-granodiorite porphyritic suite emplaced in a number of phases (Crawford et al. 2007b). In the south of the complex, porphyry copper-style mineralisation (Endeavour 39, 35) dated at 439.6 ± 1.1 Ma is related to granodiorite emplaced significantly earlier (465.7 ± 1 Ma; Miles & Brooker 1998). To the north, mineralisation is thought to be low-sulphidation epithermal, progressing from Cu-Au (E40), Au-Cu (E41), Au-Zn (E42) to Zn-Au (E46) (Miles & Brooker 1998). At the largest deposit, E42 (63.5 Mt at 1.22 g/t Au; Cooke et al. 2007), a volcano-sedimentary package including a high-K calc-alkaline trachyandesitic lava/breccia is intruded by the high-K Muddy Lake Diorite (456 ± 5 Ma) and later basaltic to basaltic-andesitic porphyritic to aphanitic dykes. This activity generated four facies of alteration. Only the final Fe-rich chlorite-carbonate-pyrite assemblage was associated with mineralisation, which occurred at 439 ± 1 Ma as discrete and fracture infill quartz-carbonate-sulphide and carbonate-sulphide ± quartz veins (Perkins et al. 1995; Miles & Brooker 1998; Glen et al. 2007c).

Marsden, the third major calc-alkaline system of the Lachlan Orogen is less well studied, due to its truncation at depth by a major Carboniferous thrust fault limiting its resource potential (115 Mt at 0.3 g/t Au, 0.51 % Cu). It occurs on the western margin of the Cowal Igneous Complex and was emplaced at 447 ± 7 Ma (Crawford et al. 2007b).

3.4.3. Alkaline (shoshonitic) systems

Two world-class porphyry systems associated with shoshonitic magmatism occur within the Lachlan Orogen. They are the Cadia district, the sixth largest gold rich porphyry system in the world (1310 Mt at 0.74 g/t Au, 0.31 % Cu; Cooke et al. 2005; Cooke et al. 2007) and the Northparkes (Goonumbla) district (153 Mt at 0.46 g/t Au, 1.03 % Cu; Cooke et al. 2007). These deposits occur within the Lachlan Transverse Zone, a suggested west-northwest-trending transverse structure representing a long-lived cratonic structural weakness that propagated the upper crust during the Neoproterozoic to Palaeozoic, providing a locus for shoshonitic intrusion and porphyry formation in regions intersecting earlier Macquarie Arc volcanic rocks (Glen and Walshe 1999).

The Cadia Igneous complex consists of seriate to porphyritic textured K-feldspar, plagioclase, amphibole-biotite-titanite-apatite-magnetite quartz monzonite pipes, dykes and stocks; cumulate gabbro, monzodiorite, and minor syenogranitic aplite to pegmatitic dyklets (Blevin 2002; Cooke et al. 2007). Mineralisation occurs in two stages, with the Ridgeway deposit related to a monzonitic intrusive complex of early Late Ordovician age (456–454 Ma) and the Cadia Quarry, Cadia Hill and Cadia East orebodies related to early Silurian aged quartz monzonite porphyry stocks and dykes (Wilson et al. 2007) dated at 437.1 ± 3.5 Ma by the U-Pb zircon method (Squire and Crawford 2007).

Mineralisation styles of the latter stage range from sheeted and stockwork quartz-sulphide veins to broadly stratabound disseminations along a 5 km northwest trending corridor, with bornite dominated cores grading outward to chalcopyrite dominated zones (Holliday et al. 2002). A number of hydrothermally altered zones are recognised, occurring predominantly within a few hundreds of metres from monzonite complexes. The main ore-bearing potassic alteration stage varies from pervasive actinolite-biotite-magnetite-apatite (calc-potassic) to magnetite-orthoclase at Ridgeway; orthoclase-actinolite mineralised sheeted vein selvedges at Cadia Quarry, Cadia Hill, Cadia East and Cadia Far East and pervasive biotite alteration at Cadia East (Holliday et al. 2002; Wilson et al. 2003). Cadia East additionally possesses a peripheral quartz-albite-sericite-pyrite ± tourmaline zone characterised by low Cu-Au grades. Late fault controlled sericite-carbonate-pyrite alteration occurs in all deposits, as does propylitic alteration (epidote, chlorite, calcite, albite, prehnite, laumontite, pyrite, fluorite), both proximally and peripherally (Smith et al. 2004; Cooke et al. 2007).

The Northparkes (Goonumbla) district contains four economic porphyry systems (Endeavour 22, 26, 27 and 48) consisting of narrow, pipe-like quartz monzonite complexes (445 – 437 Ma; Lickfold et al. 2007) that intrude intermediate volcanosedimentary rocks (the Goonumbla and Wombin Volcanics) of the Ordovician Goonumbla Volcanic Complex (Lickfold et al. 2003). Mineralisation in the form of quartz stockwork veining grades outward in annular sheaths from bornite ± chalcocite-covellite cores to chalcopyrite dominated zones (Smith et al. 2004). Associated white mica has been dated at 439.2 ± 1.2 Ma via the $^{40}Ar/^{39}Ar$ method (Perkins et al. 1990) while $^{40}Ar/^{39}Ar$ analysis of biotite and hornblende by Lickfold et al. (2003) indicate that mineralisation and related alteration occurred between 446 and 437 Ma. Alteration is broadly similar to that at Cadia, consisting of a weakly mineralised early magnetite, biotite ± albite stage, which occurs in veins and fractures or as patchy to pervasive alteration (Heithersay & Walshe 1995); ore related potassic alteration in the form of pervasive (E26) to restricted (E22, E27, E44) magnetite destructive orthoclase ± actinolite-biotite alteration; central sericite-quartz ± alunite alteration associated with high grade mineralisation at E26 and E48; proximal sericite-bornite-hematite alteration at E48; peripheral quartz-albite-sericite-pyrite ± tourmaline alteration at E26; outboard epidote-calcite-chlorite-prehnite-laumontite-albite-pyrite-chalcopyrite propylitic style alteration and fault controlled pervasive carbonate-pyrite ± gypsum/anhydrite vein alteration that occurred during the waning stages of mineralisation (Smith et al. 2004).

CHAPTER FOUR

PETROLOGY OF HOST UNITS

4.1 INTRODUCTION

The Yiddah porphyry Cu-(Au-Mo) system consists of intermediate to felsic intrusions contained within fine to medium-grained highly altered mafic to intermediate volcanic to volcaniclastic material. These units have generally experienced intense deformation due to the proximity of the nearby Gilmore Fault Zone and major periods of deformation experienced during subsequent orogenies. In conjunction with the lack of outcrop, this feature has led to significant ambiguity regarding the spatio-temporal and evolutionary relationships of host lithologies; and their associations with alteration and mineralisation.

Previous descriptions of Yiddah have recognised three volcanosedimentary units: a basal volcanic siltstone, middle volcaniclastic sandstone and upper coarse crystal tuff (Munro 2010). The crystal tuff unit was not observed in the three drill holes sampled in the present work. These units strike north-northwesterly and dip moderately to steeply east. Intruding the volcaniclastic package is a monzodiorite granitoid unit and multiple sills/stocks of porphyritic texture. Considerable evidence acquired in this study suggests that the monzodiorite granitoid is spatially and genetically linked to the monzodiorite unit intersected in drilling south of Barmedman, informally named the Rain Hill Monzodiorite (see Figure 2.6). Therefore, the monzodiorite unit at Yiddah will hereafter be referred to as the Rain Hill Monzodiorite, with evidence for this relationship presented in relevant sections to follow.

While the Rain Hill Monzodiorite remains reasonably intact; intense alteration, contact metamorphism and post-emplacement deformation of the sills/stocks and volcaniclastic units has largely obscured their primary mineralogy. The following chapter comprises an integrated geochemical-petrographic classification and description of host units, in which both primary and secondary rock types are considered. Unit specific alteration processes and products are also considered, due to their integral link to underlying mineralogy.

4.2 PRIMARY ROCK NOMENCLATURE

A number of geochemical classification systems utilising whole-rock geochemical

data have been developed for igneous rocks. The IUGS Total Alkali versus Silica (TAS) diagram and CIPW normalised classifications are the most commonly used methods, however these techniques are not suitable for rocks which have undergone metamorphism, alteration and/or weathering (Winchester & Floyd 1977). As all volcanic and intrusive units at Yiddah display some level of alteration, this study alternatively implements immobile element proxies to derive information regarding primary rock compositions. This approach is necessary in all mineralised rocks where hydrothermal fluids are important to the process of metal concentration. Immobile elements are those which are considered to remain stable during metamorphism and alteration events. They include elements belonging to the high field strength (HFS) element group (REE, Sc, Y, Th, Zr, Hf, Ti, Nb, Ta and P) in addition to Co, Ni, V and Cr; whilst not including incompatible elements of the low field strength (LFS) group (Cs, Sr, K, Rb, Ba), which are mobile during these processes (Rollinson 1993).

The classification diagram of Pearce (1996), modified after Winchester & Floyd (1977) plots Nb/Y versus Zr/Ti; where Zr/Ti increases from mafic to felsic rocks and Nb/Y increases with alkalinity. Under this classification, the basal fine-grained and upper fine to coarse-grained volcaniclastic units plot as sub-alkaline basalt and sub-alkaline andesite respectively (Figure 4.1). This classification carries the assumption that each unit was derived from a single igneous source, which cannot be stated for certain, particularly for the fine-grained volcaniclastic unit. The Macquarie Arc is however dominated by mafic to intermediate island-arc volcanism with little or no interfingering, supporting a relatively *in situ* setting. The resultant fields are also consistent with whole rock SiO_2, Fe_2O_3+MgO and other accounts of the Gidginbung Volcanics, which describe the package as primarily intermediate in composition, with lesser basaltic andesite to latitic units (Warren et al. 1995; Fu et al. 2009).

Intrusive rocks sampled at Yiddah include the Rain Hill Monzodiorite and related decimetre to metre wide equigranular dykes intersected at the base of TYHD003 and TYHD004; and mineralisation related porphyritic textured sills/stocks which intrude volcaniclastics broadly parallel to the Rain Hill Monzodiorite margin and bedding orientations. All of these samples plot within the trachy-andesite field on the Pearce (1996) diagram, the extrusive equivalent of alkali-monzodiorite (Figure 4.1). A magmatic trend is evident for the Rain Hill Monzodiorite and its related late dykes, which provides a vector for the process of fractional crystallisation. Porphyritic sills/stocks plot as slightly more felsic than the Rain Hill Monzodiorite, but not as evolved as the majority of equigranular dykes and dyklets.

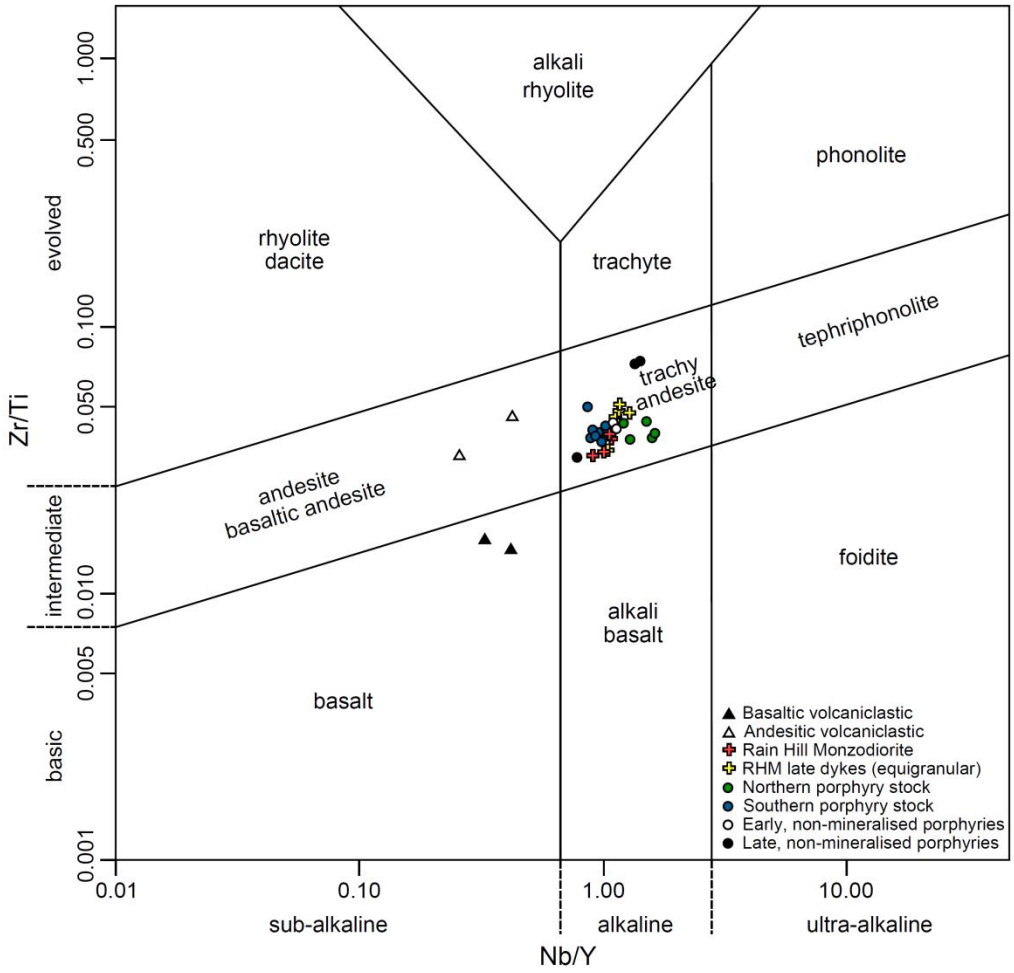

Figure 4.1: Immobile element classification diagram for units contained within the Yiddah prospect. Values plotted are from XRF (Ti) and ICP-MS (Nb,Y,Zr). After Pearce (1996).

4.3 VOLCANICLASTIC UNITS

4.3.1 Petrography

Fine-grained basaltic volcaniclastics

In hand specimen, this unit consists of a dark greenish to grey, uniformly fine-grained rock with indistinct banding or layering, defined by slightly darker and lighter bands (Figure 4.2a). Fine wispy yellowish epidote veins are relatively abundant, cross-cut by thicker tension gashes predominantly containing calcite. Thin section and X-ray diffraction analysis indicates a mineralogy assemblage comprising chlorite (~25%), albite (~25%), actinolite (~15%), cordierite, epidote, biotite and kaolinite (< 15%). Lesser concentrations of calcite, pyrite, ankerite, sericite, magnetite, and titanite are also observed. This mineral assemblage is

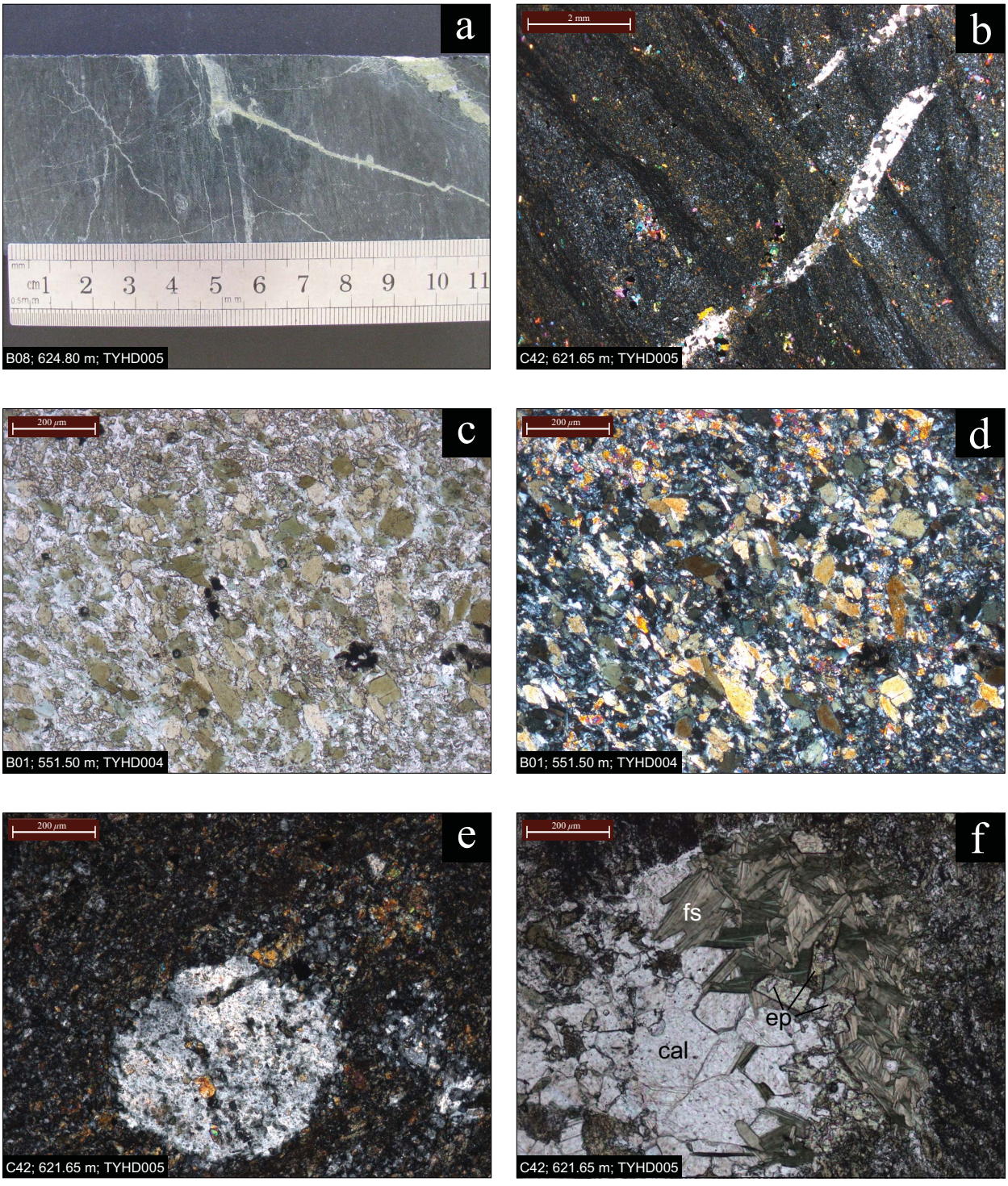

Figure 4.2: (a) Hand specimen of the fine-grained basaltic volcaniclastic unit, showing faint compositional layering of the groundmass, with propylitic related epidote veining and later tension gash carbonate infill veins. (b) Low magnification photomicroscope, showing faint to dark banding, epidote alteration veining (high birefringence) and cross-cutting carbonate tension gashes. XPL. (c) Actinolite and epidote (top) within a felsic groundmass PPL. (d) XPL. (e) An inclusion-rich cordierite porphyryblast displaying faint sector twinning within a chlorite rich groundmass. XPL. (f) Granoblastic calcite (cal), epidote (ep) and fibrous ferrostilpnomelane (fs) infilling a late tension gash. PPL.

interpreted to be the mixed outcome of primary mineralogy, contact metamorphism, hydrothermal alteration and regional deformation.

Texturally, the unit is dominated by blocky to subrounded shaped actinolite grains averaging 10 – 50 μm within a finer grained matrix of chlorite, albite and cordierite; the latter of which also occur as occasional larger crystals to ~200 μm, observed in the least altered of samples. Variations in the proportion of chlorite to plagioclase within the groundmass have produced a banded texture, most obvious at low magnification (Figure 4.2b). This banding is crosscut and offset by variably orientated coarse tension gashes in a manner that suggests it was developed prior to latest deformation.

Actinolite grains are weakly pleochroic between faint yellow to forest green in plane-polarised light, and dominantly yellow-brown to lower second order blue to pink in cross-polarised light (Figure 4.2c,d). Many of the larger grains possess obvious simple twins. Orientations range from random to strongly aligned and from relatively isolated to interlocking, at times occurring in coarser grained aggregates averaging 1 mm in diameter. A reasonable abundance of ragged magnetite/titanomagnetite in all samples suggests it was also likely a primary component. Quartz varies from comprising a minor component of the groundmass to being absent; however the presence of cordierite (Figure 4.2e) suggests that the primary lithology was probably pelitic.

It is clear that the basaltic volcaniclastic unit has been subjected to a number of alteration events. Contact metamorphism to lower hornblende hornfels facies is inferred by the presence of cordierite, biotite and actinolite. This interpretation is consistent with the proximity of intrusive bodies. Contact metamorphic products are best preserved in samples furthest removed from later hydrothermal alteration, where relict platy and fine grained recrystallised biotite are evident. Within intensely altered zones; biotite, cordierite and variable amounts of actinolite are altered to secondary quartz and abundant chlorite.

Pervasive propylitic alteration is also inferred to be the source of groundmass calcite and abundant granular epidote, the latter of which also occurs within neat, fine grained meandering veins, averaging 100 – 500 μm in width and cross-cutting the banded texture.

These veins commonly contain or are associated with pyrite, which occurs as 20 – 200 μm diameter cubes of low to moderate abundance.

A final stage of alteration related to regional deformation has generated sharp-walled coarsely crystalline calcite ± epidote ± quartz tension gashes and ductile kinking of earlier epidote veins. Calcite crystals within tension gashes are granoblastic and often join at 120º triple junctions. In sample C42, ferrous iron bearing ferrostilpnomelane is also a major infill product. This mineral is the metamorphically stable form of stilpnomelane (Yardley et al. 1990), and is present as radiating platy fibres to 200 μm length (Figure 4.2f).

Andesitic volcaniclastics

The andesitic volcaniclastic unit is of a much more variable character than the fine-grained basaltic volcaniclastics. In hand specimen, it consists of a light greenish texturally variable rock, ranging from a fine grained well-sorted matrix to a mixture of sand and finer sized particles (Figure 4.3a). This unit has been intensely affected by later deformation, such that a strong foliation largely overprints original bedding textures.

All samples observed in thin section have undergone intense hydrothermal alteration, reflected by the mineral assemblage of albite, K-feldspar, sericite, epidote, chlorite, quartz, calcite, rutile, pyrite and occasional titanite. Albite is dominant, occurring throughout the groundmass with only minor quartz (< 10%). Albitised porphyryclasts range to 1 mm, however most are fine grained yet inequigranular (Figure 4.3b,c). Other abundant alteration products include granular epidote and flaky sericite, dispersed through the groundmass, along with relatively abundant variably sized (20 – 150 μm) magnetite and less abundant pyrite cubes (Figure 4.3d,e). Chlorite is also a moderately significant, albeit variable alteration component. It occurs predominantly as fine grains dispersed throughout the groundmass. The only preserved primary minerals are trace zircons, which occur as relatively small (~ 20 μm) stumpy crystals.

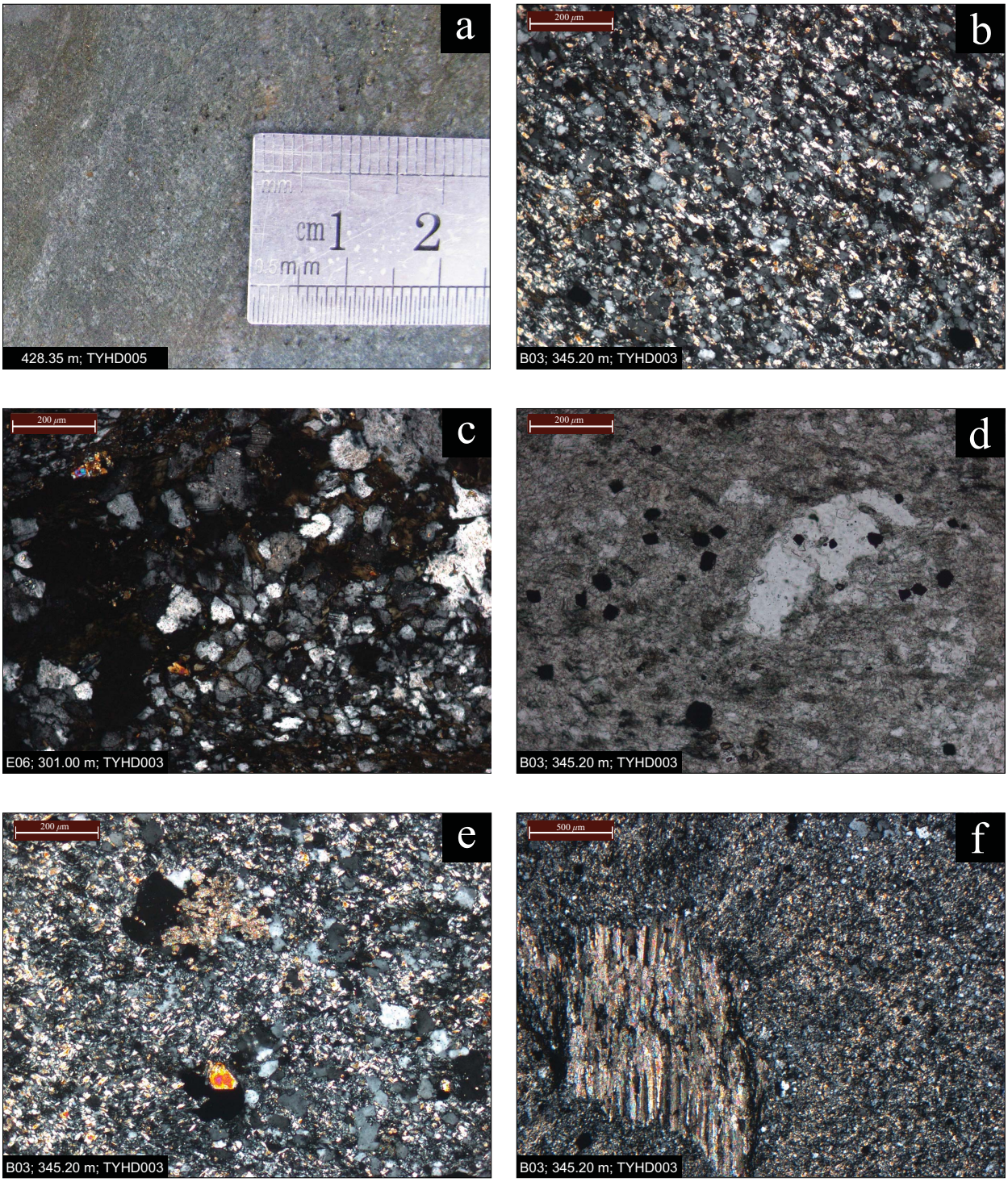

Figure 4.3: Hand specimen and photomicrograph images of the andesitic volcaniclastic unit. (a) Hand specimen photograph of a relatively uniform, chlorite altered andesitic volcaniclastic sample. (b) Fine-grained, relatively equigranular andesitic volcaniclastic sample, dominated by a matrix of optically continuous replacement albite, with interstitial chlorite and sericite. XPL. (c) Coarser-grained example, where some polysynthetic twinning has been preserved. Chlorite is dominant interstitially. XPL. (d) Relatively rare recrystallised quartz clast within a chlorite/ sericite altered matrix, also containing alteration magnetite and lesser epidote (bottom of image). PPL. (e) Variably sized albite grains and alteration magnetite with interstitial sericite and calcite. Bright crystal is epidote. XPL. (f) Syn-tectonic calcite with minor sericite and chlorite, aligned within a late tension gash. XPL.

The abundance of albite, sericite and chlorite along with the variable grain size of this unit suggests the primary rock was likely a feldspathic volcaniclastic of intermediate chemistry.

Some samples display signs of contact metamorphism, including large patches (to 1 mm) of granoblastic interlocking actinolite grains, and recrystallised quartz clasts in aggregates averaging 500 μm. Overall however, contact metamorphism is not as well developed in this unit than the fine-grained basaltic volcaniclastic unit, which may have been a factor in enabling more efficient fluid circulation during later mineralising events. As with the basaltic volcaniclastics, this unit displays significant signs of post hydrothermal alteration deformation. These signs include the foliation of groundmass material, particularly in samples containing high proportions of hydrous alteration products, and the development of calcite filled tension gashes (Figure 4.3f).

4.3.2 Geochemistry

Two samples of the basaltic volcaniclastic unit and two samples of the andesitic volcaniclastic unit were analysed for major, trace and rare earth elements using X-ray fluorescence and ICP-MS. Chemical data is presented in Table 4.1 and Table 4.2.

Considerable loss on ignition values in all samples, particularly those of the andesitic volcaniclastic unit are indicative of high degrees of hydrothermal alteration. As such, most major and many trace elements are likely to vary from initial concentrations. Despite this limitation, a clear distinction between the two units can be observed in a number of elemental abundances. SiO_2 values of 48.06 – 51.21% for the basaltic volcaniclastic unit and 54.28 – 58.17% for the andesitic volcaniclastic unit are consistent with the respective basic and intermediate classifications resolved from the Nb/Y versus Zr/Ti immobile element diagram (Figure 4.1). Consistently higher TiO_2, Fe_2O_3, MgO, Ca, V, Co and Ni concentrations in the basaltic volcaniclastic unit are also strongly indicative of its more mafic chemistry (Rollinson 1993; Winter 2001; Hastie et al. 2007).

The immobile rare earth element series, along with other immobile trace elements including Th, Yb, Ta and Nb are extremely important in providing information regarding the magma source of igneous rocks. This information can be used to infer tectonic setting of formation,

Table 4.1: XRF whole rock geochemical data for volcaniclastic units.

Catalogue no.	HONS557	HONS561	HONS558	HONS562
Sample no.	**B1**	**B8**	**B3**	**B10**
Rock type	BSVC	BSVC	ANVC	ANVC
Major elements (wt%)				
SiO_2	48.06	51.21	58.17	54.28
TiO_2	1.71	1.80	0.97	0.67
Al_2O_3	15.65	15.23	18.35	16.43
***Fe_2O_3**	12.78	11.64	5.87	5.98
MnO	0.26	0.25	0.09	0.00
MgO	6.56	4.65	2.78	1.09
CaO	8.70	7.97	4.23	0.12
Na_2O	3.73	5.18	3.19	5.17
K_2O	1.33	0.71	3.34	1.91
P_2O_5	0.32	0.25	0.38	0.14
S	0.13	0.10	0.55	5.42
O=S	-0.06	-0.05	-0.27	-2.71
LOI	2.23	1.66	5.05	8.99
Total	**101.40**	**100.60**	**102.71**	**97.48**
Trace elements (ppm)				
V	240	216	134	134
Co	56	42	14	36
Cu	148	92	126	3650
Zn	122	119	93	539
Ga	17	15	18	19
As	1	2	1	3
Rb	23	5	47	46
Sr	535	482	464	304
Y	34	37	34	30
Zr	125	145	178	165
Nb	12	10	8	11
Ba	563	471	947	635
La	7	11	35	53
Ce	< 2	42	75	128
Hf	4	6	7	< 1
Pb	4	2	3	8
Th	2.0	1.7	6.5	5.0
U	1.3	0.6	5.7	2.0

*Total iron expressed as Fe_2O_3. Elements predominantly below detection limits were omitted (Ge, Se, Br, Mo, Cd, Sn, Sb, Cs, Ta, W, Hg, Bi).
BSVC = Fine-grained basaltic volcaniclastic. ANVC = Andesitic volcaniclastic.

Table 4.2: ICP-MS whole rock geochemical data for volcaniclastic units.

Catalogue no.	HONS557	HONS561	HONS558	HONS562
Sample no.	**B1**	**B8**	**B3**	**B10**
Rock type	BSVC	BSVC	ANVC	ANVC
Trace and rare earth elements (ppm)				
Ba	557	470	885	624
Ce	32.7	31.3	83.2	113.5
Co	46.1	41.7	13.7	35.4
Cs	0.36	0.06	0.27	0.46
Dy	6.30	6.72	6.03	5.02
Er	3.64	4.08	3.46	2.76
Eu	1.98	1.77	2.49	2.74
Ga	20.3	20.1	20.3	16.0
Gd	5.88	6.17	7.43	7.14
Hf	3.4	3.8	4.4	4.3
Ho	1.29	1.40	1.19	0.96
La	16.1	14.7	42.0	55.5
Lu	0.50	0.57	0.51	0.41
Mo	3	3	3	41
Nb	14.6	12.2	8.6	11.8
Nd	18.0	18.0	40.6	56.8
Pr	3.88	3.91	9.98	14.35
Rb	24.4	6.1	49.7	47.5
Sm	5.11	5.19	8.74	10.45
Sn	2	1	2	4
Sr	576	503	462	293
Ta	0.9	0.8	0.5	0.8
Tb	1.17	1.18	1.17	1.21
Th	1.34	1.66	5.50	5.25
Tm	0.51	0.58	0.49	0.41
U	1.34	1.14	3.32	2.35
V	327	301	171	172
W	1	2	2	3
Y	34.2	37.3	33.4	27.8
Yb	3.28	3.79	3.35	2.64
Zr	146	168	186	179

BSVC = Fine-grained basaltic volcaniclastic. ANVC = Andesitic volcaniclastic.

and can also be useful when correlating units in situations where associations are unclear or there has been significant hydrothermal alteration; such as in the present work.

The rare earth elements comprise the series of 15 metals of atomic numbers 57 (La) to 71 (Lu). They generally possess similar geochemical properties arising from their common stable 3+ ion states. Eu may also form a stable 2+ ion. The small differences in chemical behaviour they do display result from regular decreases in ionic radii with increasing atomic number, which cause the series to become fractionated relative to one another during certain petrological processes (Rollinson 1993).

The series can be divided into two groups, the light rare earth elements (LREE) (La – Eu) possessing atomic numbers of 57 – 63 and the heavy rare earth elements (HREE) (Gd – Yb) with atomic numbers ranging from 64 – 71. These groups differ in their behaviour in alternate arc magma series, consequently producing variations in the slope of a chondrite normalised rare earth element plot. It is these characteristic differences in slope that are indicative of alternate magmatic sources, rather than the total abundances, which are primarily controlled by fractional crystallisation (Winter 2001).

When plotted on a chondrite normalised rare earth element plot, the low-K tholeiitic series possesses a relatively flat slope, which increases slightly with increasing atomic number. The medium-K to high-K series are progressively more enriched in LREE, such that the slope reverses to decreasing with increasing atomic number. This pattern occurs due to the similar behaviour of the LREE's to that of other highly incompatible elements, including K (and other large ion lithophile elements) (Winter 2001). The various proposals for the causes of K-enrichment within melts will be discussed in Chapter Eight.

The rare earth element patterns of the two volcaniclastic units sampled at Yiddah are highly dissimilar (Figure 4.4). The basaltic volcaniclastic pattern, which is tightly constrained between both samples, possesses a relatively flat signature which decreases gently with increasing atomic number. This pattern is consistent with that of a low-K calc-alkaline magma, where the LREE's are only moderately enriched relative to the HREE's (Winter 2001). The andesitic volcaniclastic pattern, which was not as tightly constrained between the two samples, is much steeper (LREE enriched), indicative of a K-enriched magma.

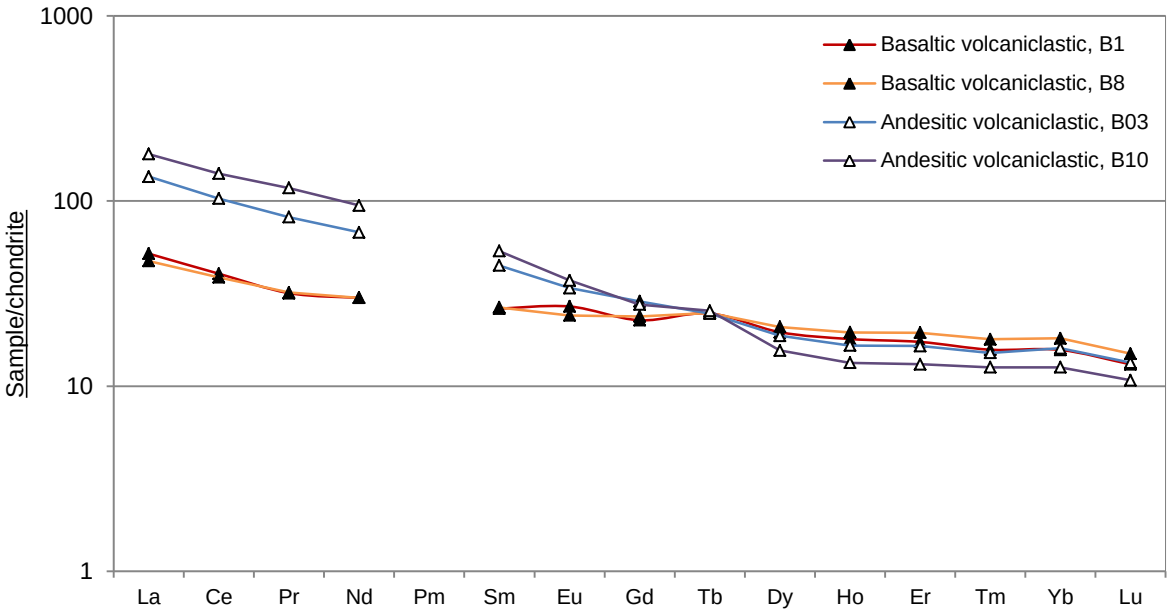

Figure 4.4: Chondrite normalised REE plot for volcaniclastic units. Normalisation values from Boynton (1984). Plotting values from ICP-MS.

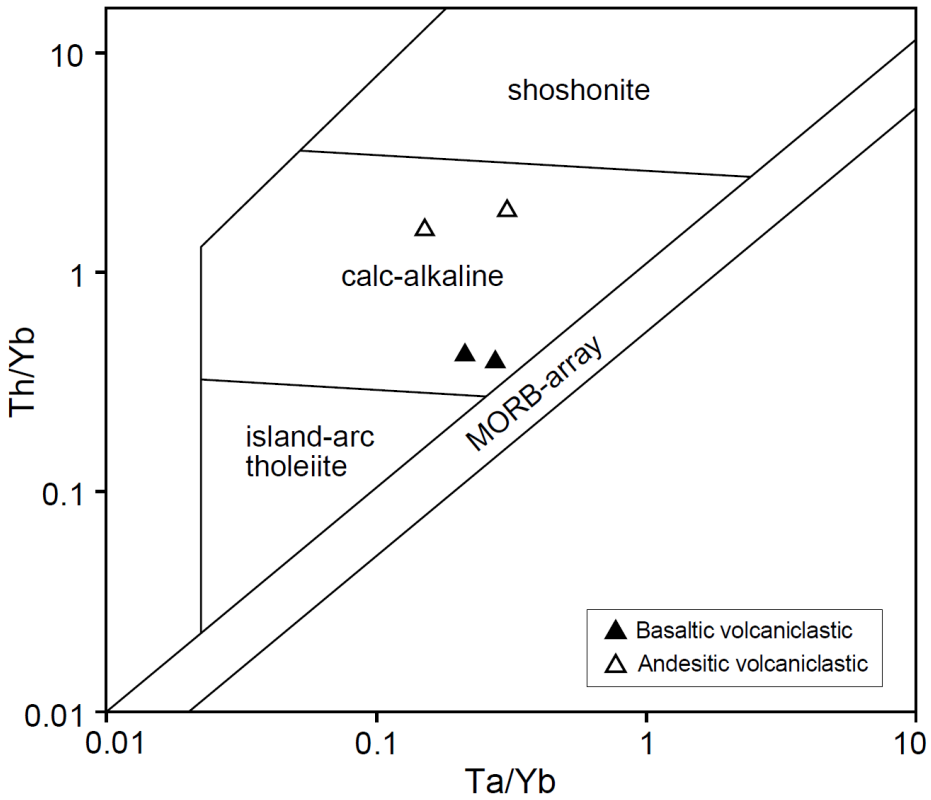

Figure 4.5: Volcaniclastic units plotted on the immobile element magma series discrimination diagram of Pearce (1982).

The Ta/Yb versus Th/Yb magma series discrimination plot of Pearce (1982) has been used to distinguish between the calc-alkaline and shoshonitic magmatic series (Figure 4.5). The key variable, Th, is considered relatively immobile in both weathered conditions and in rocks which have experienced up to sub-amphibolite facies metamorphism (Hastie et al. 2007). Yb is used as the denominator to reduce the effects of partial melting and fractional crystallisation. Th and Ta have similar distribution coefficients for melting and fractional crystallisation, such that mid ocean ridge/within plate igneous rocks form a relatively linear, diagonal array. As Th concentrations are very low in the mantle, any upward deviation from the diagonal trend is thought to be related to Th addition from subducted slab derived fluids (where Ta is not added). Slab derived fluids also introduce other fluid mobile elements, such as Cl, B, Sb, S, Bi, Pb and large ion lithophile elements, including Rb, Cs, Ba, Sr and K. It is this related behaviour that is exploited in differentiating between the tholeiitic, calc-alkaline and shoshonite magma series. Th addition is also considered to occur with the addition of melted crust and/or sediments, where coinciding Ta addition may lead to an accompanying shift to the right (Pearce 1982; Hawkesworth 1997; Richards 2003; Pearce 2008).

Under this classification, the andesitic volcaniclastic unit is classified as high-K calc-alkaline, whilst the basaltic volcaniclastic unit plots as low-K calc-alkaline, consistent with their rare earth element signatures. These findings suggest that the two volcaniclastic units were not derived from the same volcanic source, possibly representing volcanic detritus derived from an arc in transition from low-K calc-alkaline to high-K calc-alkaline. The implications of this outcome will be discussed in Chapter Eight.

4.4 **INTRUSIVE UNITS**

4.4.1. Petrography

Rain Hill Monzodiorite

In hand specimen, the Rain Hill Monzodiorite displays a medium-grained sub-equigranular mesocratic texture consisting of pinkish-cream to white feldspars, as both blocky euhedral and interstitial components, with minor clear quartz patches; and reasonably abundant dark minerals of rectangular to pointed shapes (amphiboles). Accessory diamond shaped dark red to yellowish-cream components (titanite) are also observed (Figure 4.6a).

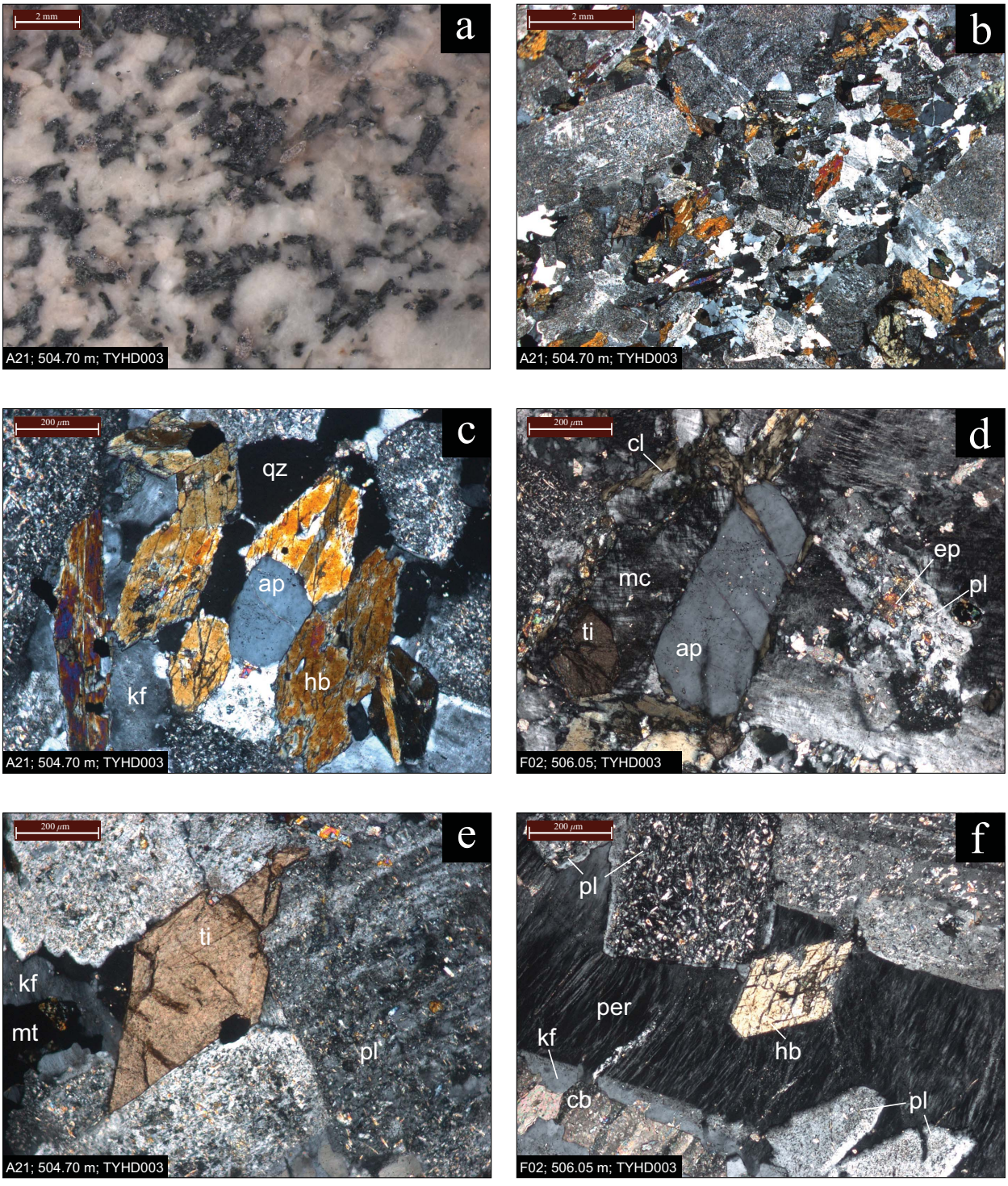

Figure 4.6: (a) The Rain Hill Monzodiorite in hand specimen. (b) Low magnification textural overview, highlighting variably sized plagioclase and amphibole phenocrysts with interstitial anhedral K-feldspar and quartz. XPL. (c) Hornblende (yellow, twinned) and an apatite crystal (centre) within a matrix of K-feldspar and quartz, between variably sized sericitised plagioclase crystals. XPL. (d) Large apatite phenocryst possessing tiny fluid inclusions within microcline, which poikilitically encloses an albitised and epidotised plagioclase phenocryst. XPL. (e) Euhedral igneous titanite crystal predominantly surrounded by plagioclase. XPL. (f) Perthitic recrystallisation of plagioclase and K-feldspar within interstitial areas, also containing a basally cut hornblende phenocryst with 60/120º cleavage. A carbonate vein is evident in the lower left corner. XPL. qz = quartz, kf = K-feldspar, hb = hornblende, ap = apatite, mc = microcline, ti = titanite, ep = epidote, pl = plagioclase, mt = magnetite, per = perthite, cb = carbonate (calcite).

In thin section, the unit displays an interlocking texture (Figure 4.6b) comprised of early euhedral prismatic plagioclase feldspars (to 3 mm, averaging 0.5 – 1.5 mm) and rectangular to diamond shaped amphiboles (to 4 mm, averaging 1 mm); with later interstitial K-feldspar, minor quartz, diamond shaped titanite (200 μm – 1 mm), euhedral apatite (averaging ~ 350 μm length and ~ 100 μm diameter for hexagonal basal cross-sections), along with ragged igneous magnetite (averaging ~ 1 mm diameter) and trace zircons (averaging ~ 40 – 60 μm in length). This mineralogy is distinctive in that no primary pyroxene or biotite is observed, as would possibly be expected in an intermediate arc-related crystallisation mineral assemblage (Winter 2001).

Plagioclase is abundant, comprising ~ 70% of the feldspar component. It frequently possesses complex twinning, although moderate degrees of alteration (sericite ± calcite) variably mask grain surfaces. Late stage plagioclase crystals are often poikilitically enclosed in K-feldspar, characteristically possessing blurred and irregular grain margins (Figure 4.6d). These textures are evident in both heavily altered and relatively fresh samples, and thus are attributed to peritectic reactions during crystallisation, rather than K^+ ion metasomatism. In more altered samples, albitisation or perthitic recrystallisation of plagioclase is common (Figure 4.6f).

Amphiboles are strongly pleochroic, ranging from light forest to yellow green in colour, to occasional light brown. In cross-polarised light, interference colours are predominantly pale yellow to burnt orange, ranging to lower second order blue, with moderately frequent simple twinning (Figure 4.6c). Extinction occurs symmetrical to 60/120º cleavages, which are particularly evident in diamond shaped basal cross sections (Figure 4.6f). These optical properties indicate the phase is hornblende. In more altered samples, amphiboles are completely altered to chlorite pseudomorphs, which retain the prismatic to diamondiferous habit of the former crystal. The presence of primary igneous amphibole is significant as it is only stable in melts of > 3 wt% H_2O and at pressures in excess of 0.1 – 0.2 GPa (> ~3 – 6 km depth; Winter 2001), conditions consistent with those considered appropriate for the formation of porphyry copper systems.

K-feldspar is abundant in interstitial spaces, occurring anhedrally as orthoclase, microcline and intergrown with albite (perthite). Interestingly, K-feldspar is commonly less sericitised than plagioclase, which could possibly be due to the syntectonic recrystallisation of lower

temperature species (K-feldspar) during low-grade regional metamorphism, which post-dates hydrothermal alteration. This event is also predominantly attributed to silicification of the Rain Hill Monzodiorite, which increases with alteration intensity as gauged from the chloritisation of amphiboles.

Despite comprising only a small volumetric constituent, pinkish-brown titanite is a consistent and distinctive component the Rain Hill Monzodiorite. It occurs both as large, euhedral diamond shaped crystals (Figure 4.6e), chiefly within K-feldspar; and as anhedral to granular alteration products. Fluoroapatite ($Ca_5(PO_4)_3F$), confirmed by electron microprobe analysis, is also distinctive; occurring as relatively stubby prisms and hexagonal basal cross-sections. These crystals possess similar optical properties to K-feldspar, however do not extinguish as completely, and commonly contain tiny fluid inclusions on otherwise clear grain surfaces (Figure 4.6d). Euhedral to irregular titanomagnetite occurs throughout interstitial spaces and poikilitically enclosed in amphibole and plagioclase phenocrysts.

An estimated mineralogy by volume for the Rain Hill Monzodiorite at Yiddah guided by petrographic analysis of the least altered samples, F2 and A21 (loss on ignition of 1.96%, and 2.22% respectively) is presented in Table 4.3.

Table 4.3: Estimated primary igneous mineralogy modal abundance (volume %) of the Rain Hill Monzodiorite at Yiddah.

Mineral	**Volume %**
Quartz	4
Plagioclase	56
K-feldspar	20
Amphibole	15
Titanite	2
Titanomagnetite	2
Apatite	1
Zircon	tr
Total	100

This mineralogy is highly similar to descriptions of the Rain Hill Monzodiorite intersected in drilling south of Barmedman, described by Wormald (1993) as 58.2% plagioclase, 15.3% K-feldspar, 12.9% amphibole, 6.0% quartz, 3.2% opaques, 1.9% albite, 0.8% titanite, 0.8% apatite with minor alteration epidote, chlorite and calcite (reverse circulation hole TP327; 535500 mE 6210200 mN AGD 66). The strong petrographic similarity of the two granitoids is particularly significant given the distinctive nature of the mineral assemblage.

All samples display weak, non-texturally destructive alteration; consisting of variable chloritisation of amphiboles, albitisation and sericitation of feldspars, minor carbonate addition and silicification. Granular epidote occurs in the groundmass in minor volumes and in thin, undulating veins with narrow selvedges, along with chlorite ± pyrite. It is likely that the observed alteration assemblage is the product of both the invasion of minor volumes of fluid during weak propylitic alteration, and a later deformation event, which is evidenced by cracked phenocrysts, bent plagioclase twins, transcrystalline fractures and the shadowy, undulose extinction of quartz.

A final noteworthy feature of the Rain Hill Monzodiorite is its pinkish red hue, evident in both thin section and hand specimen. This phenomenon results from the sub-micron sized hematite dusting of secondary feldspars (albite and K-feldsar), indicative of wall rock oxidation by mineralising fluids. The source of iron is likely to be the amphibole and magnetite of the host rock. In alkali porphyries of the Macquarie Arc, hematite dusting is a common wall-rock alteration indicator, and its presence within propylitic assemblages has been used in vectoring exploration drill holes, such as at Ridgeway (Holliday & Cooke 2007). At Yiddah, the intensity of hematite staining ('redness') also increases with proximity to the mineralised zone. Relatively unaltered samples possess creamy pink shades (e.g. A21, Figure 4.6a) while intensely altered samples range to red brick shades (e.g. A19, Figure 4.7). This feature is particularly evident in the late intermediate to acidic dykes evolved off the Rain Hill Monzodiorite, which are both more proximal to the mineralised zone and contain higher proportions of feldspars.

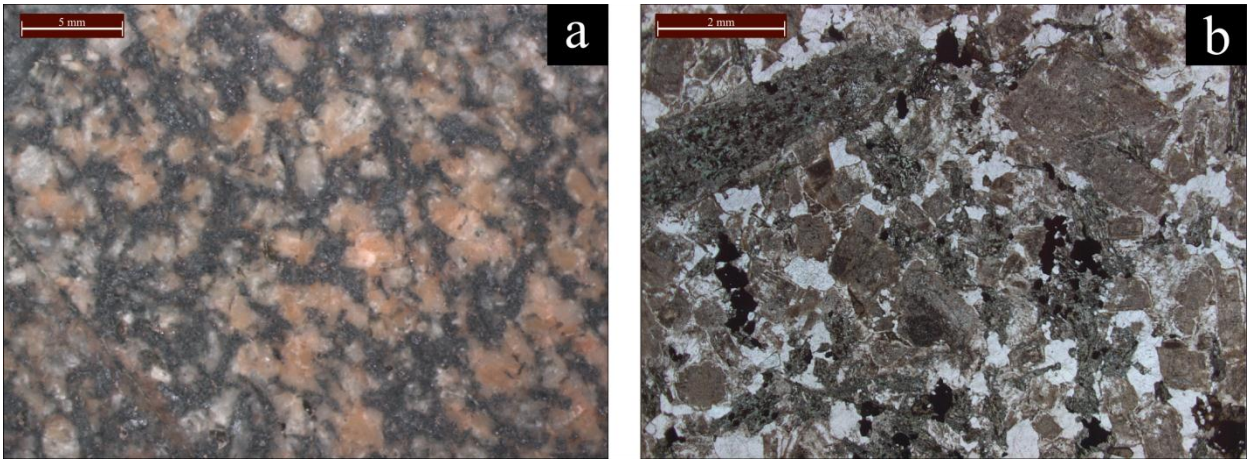

Figure 4.7: Hematite dusting of altered feldspars among chlorite altered amphiboles and secondary quartz in sample A19 (386.90 m; TYDH003), of the Rain Hill Monzodiorite. (a) Hand specimen. (b) PPL.

Porphyry sills/stocks

In the three drill holes studied in detail, the volcaniclastic units are intruded by numerous stock-like porphyry textured bodies that range from tens to hundreds of metres in width. All samples examined display severe hydrothermal alteration, such that the observed mineralogy differs significantly to that of their primary alkali-monzodiorite compositions (Figure 4.1).

In hand specimen, these units predominantly range in colour from pale to very dark greenish grey (Figure 4.8a); with one leucocratic example inferred from cross-cutting relations to be post-mineralisation in emplacement age. Feldspars averaging 1 – 3 mm in length occur as moderate to high density white to cream phenocrysts, with distinctly altered (blurry) margins, occurring within an indistinct green groundmass material. In some samples, feldspars are very faint and the rock appears homogenous in texture. The only other recognisable mineral at hand specimen scale is alteration rutile, which commonly occurs as opaque yellowish-cream patches, generally of < 0.5 mm diameter.

In thin section, textures vary from moderately to densely porphyritic, with mineralised porphyry units tending to possess higher phenocryst to groundmass ratios (phenocrysts > 50% of rock volume; Figure 4.8b). A much lower phenocryst to groundmass ratio is observed in some pre- and post-mineralisation porphyry units (as low as 25% of the rock volume). This suggests that multiple intrusive stages occurred, with possible reinjection of the parental magma chamber. There is no clear textural distinction between mineralised porphyries in the sampled northern and southern holes. A moderate degree of phenocryst foliation is occasionally observed, which is variably attributed to both emplacement (flow) and deformational (rotational) alignment.

Feldspar phenocrysts within porphyry stocks are generally less-variably-sized and slightly smaller (~ 1 mm average) than the feldspars in the Rain Hill Monzodiorite (Figure 4.8c). Their primary compositions are obscured by pervasive albitisation and subsequent sericitation, the latter of which ranges from a sparse speckling of minute (~ 20 μm), highly birefringent flakes to completely matted cover. Relict twinning in the least altered of samples suggests that plagioclase was the dominant feldspar.

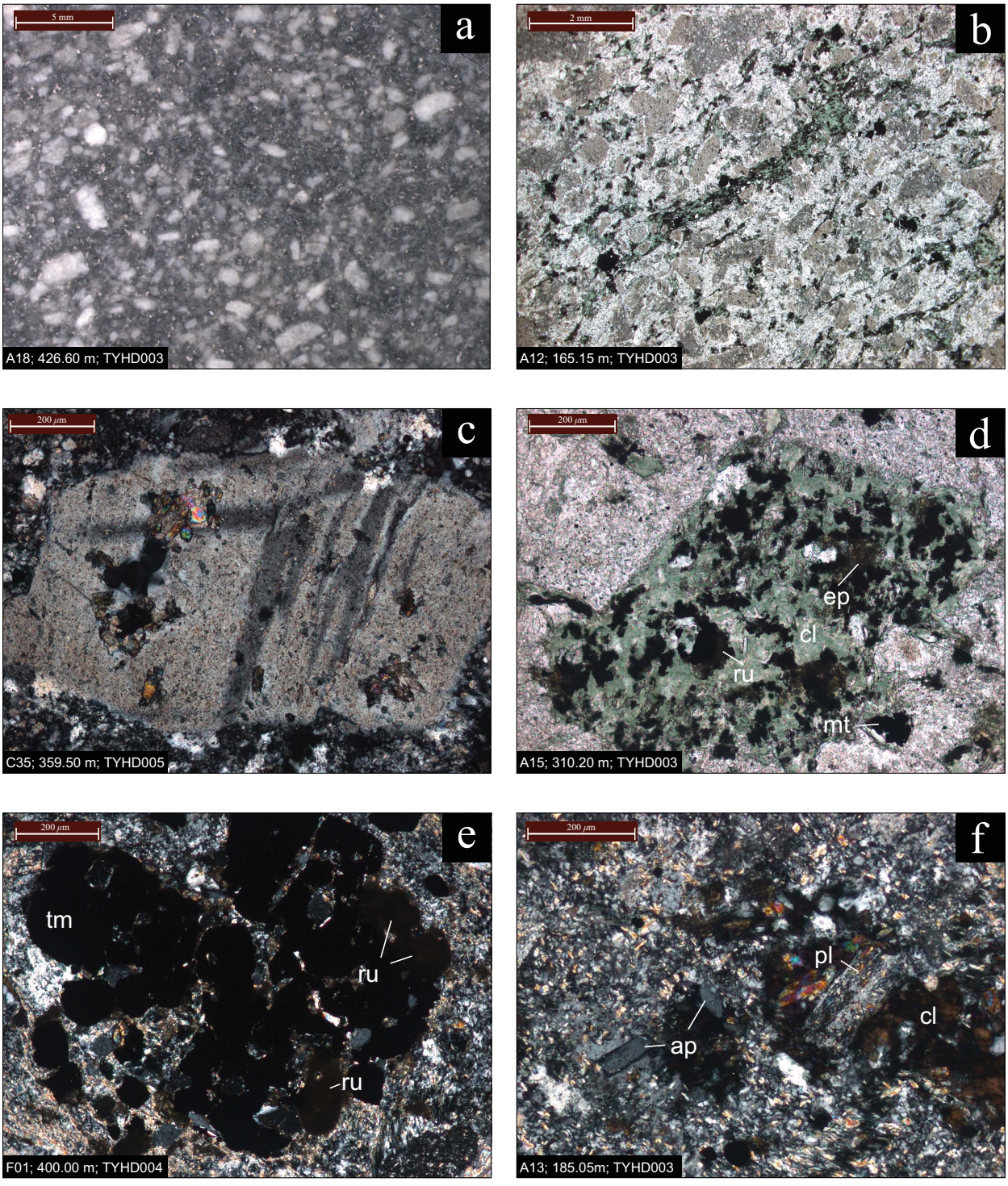

Figure 4.8: (a) Hand specimen of a relatively fresh appearing porphyritic textured intrusive rock. Thin section microscopy reveals feldspars are highly albitised and sericitised. (b) Textural overview showing abundant plagioclase phenocrysts, opaques (predominantly titanomagnetite) and one elongate amphibole pseudomorph (chlorite; centre) within a finer grained feldspar/quartz matrix. PPL. (c) Albitised plagioclase phenocryst. Minor alteration epidote and carbonate are also evident (high birefringence). XPL. (d) Chloritised amphibole phenocryst (cl), with abundant alteration rutile (ru), magnetite (mt) and epidote (ep). PPL. (e) Relict ragged igneous titanomagnetite grain, (tm) altering predominantly to rutile (ru). XPL. (f) Albitised and sericitised groundmass containing alteration chlorite after amphibole (cl), a small plagioclase phenocryst (pl) and two stubby apatite grains (ap). XPL.

The second major phenocryst component consists of pseudomorphic prismatic to diamond shaped fine-grained patches of alteration chlorite (Figure 4.8d). These grains average 1 – 2 mm in length, and are interpreted to be the alteration products of amphibole. The intensity of hydrothermal alteration combined with post-emplacement deformation has remobilised much of this chlorite throughout the groundmass, which has resulted in the green hue in hand specimen. Also associated with the amphibole pseudomorphs is granular-alteration titanite, acicular to granular rutile, magnetite, epidote and infrequent very fine grained relict alteration biotite.

The groundmass is predominantly composed of feldspar (albite) occurring as prismatic to anhedral grains averaging 20 – 100 μm. Quartz is also a major component, however much appears secondary. As a whole, silicification of porphyritic stocks is pronounced.

Opaque minerals observed in the sills and stocks include titanomagnetite, pyrite and chalcopyrite. Common ragged euhedral titanomagnetite grains (Figure 4.8e) suggest that this mineral was a primary igneous component, however alteration magnetite is also commonly observed. Hematite staining affects all feldspar phenocrysts; however the intensity of chlorite alteration throughout the groundmass dominates the appearance of porphyry stocks in hand specimen. Primary apatite is evident as clear stubby to hexagonal grains, generally not more than ~ 50 μm in length but ranging to ~ 200 μm (Figure 4.8f). Small euhedral titanite grains (to 150 μm) occur rarely, with relatively common relict diamondiferous rutile/carbonate clusters suggesting that titanite was a primary igneous component. Prismatic primary igneous zircons are also relatively common, averaging 20 – 70 μm.

4.4.2. Geochemistry

Thirty three samples from intrusive bodies at Yiddah were analysed for whole rock geochemistry using X-ray fluorescence and ICP-MS methods. A further sample from the Rain Hill Monzodiorite south of Barmedman was analysed for trace and rare earth element concentrations. Average values for each unit are presented in Table 4.4 and Table 4.5, with full results listed in Appendix F.

Table 4.4: XRF whole rock geochemical averages for intrusive units.

	Rain Hill Monzodiorite		**RHM late dykes**		**Porphyry stocks (south)**		**Porphyry stocks (north)**		**MHRC537**
Samples	A17, A19, A20, A21, A22, F02		A05, A06, A07, A08, A09, A10, A15, A33		A1, A2, A3, A4, A12, A13, A15, A18, F01		A24, A27, A29, A32, A35		RHM (n = 1)
Major elements (wt%)	*mean*	*SD*	*mean*	*SD*	*mean*	*SD*	*mean*	*SD*	
SiO_2	58.92	1.50	65.29	3.20	62.38	0.83	62.64	0.72	
TiO_2	1.13	0.07	0.69	0.16	0.74	0.05	0.92	0.06	
Al_2O_3	17.11	0.59	15.40	0.92	16.72	1.46	15.99	1.25	
***Fe_2O_3**	6.82	0.63	4.20	1.11	5.38	0.50	6.78	0.94	
MnO	0.11	0.01	0.09	0.03	0.11	0.03	0.13	0.04	
MgO	2.50	0.22	1.47	0.38	1.89	0.15	2.63	0.96	
CaO	4.24	0.60	3.65	1.78	3.20	1.03	1.91	0.44	
Na_2O	4.75	0.99	4.03	1.16	4.49	0.82	4.19	1.15	
K_2O	2.64	0.26	3.45	0.73	1.98	0.51	1.71	0.32	
P_2O_5	0.42	0.02	0.32	0.14	0.31	0.03	0.33	0.04	
S	< 0.01	0.00	0.12	0.13	0.22	0.47	0.50	0.56	
O=S	0.00	0.00	-0.07	0.07	-0.19	0.29	-0.31	0.28	
LOI	3.03	0.80	2.48	0.90	3.52	0.84	3.56	0.76	
Total	**101.66**	**0.92**	**101.14**	**0.82**	**100.83**	**1.85**	**101.03**	**1.02**	
Trace elements (ppm)									
Cl	87	24	108	90	121	97	122	29	315
V	114	36	84	38	99	21	106	18	171
Co	13	7	10	5	8	9	12	9	138
Ni	5	1	5	3	4	4	6	1	14
Cu	49	43	76	71	979	2643	1392	1710	4
Zn	67	16	67	23	96	19	141	29	73
Ga	19	1	16	3	16	2	18	2	39
As	1	1	3	2	1	1	2	0	< 0.5
Rb	37	8	33	5	32	9	35	7	< 0.1
Sr	1027	167	576	292	736	265	312	148	55
Y	26	3	17	4	21	2	17	2	1063
Zr	194	25	145	23	152	14	195	13	21
Nb	22	2	16	4	16	1	22	1	149
Ba	1649	214	1828	1201	1940	1577	764	292	< 1.1
La	55	11	37	6	42	45	41	19	2479
Ce	119	20	63	35	82	71	103	36	35
Hf	6	2	4	1	5	2	2	3	73
Pb	5	2	4	1	5	1	5	1	1
Th	10.4	0.4	14.1	3.3	9.4	2.4	10.2	1.0	0.7
U	6.0	0.3	7.6	1.3	4.7	1.1	3.0	0.8	16.3

*Total iron expressed as F_2O_3. Elements predominantly below detection limits were omitted (Ge, Se, Br, Mo, Cd, Sn, Sb, Cs, Ta, W, Hg, Bi).

Table 4.5: Whole rock ICP-MS trace and rare earth element average for intrusive units.

	Rain Hill Monzodiorite		**RHM late dykes**		**Porphyry stocks (south)**		**Porphyry stocks (north)**		**MHRC537**
Samples	A17, A19, A20, A21, A22, F02		A05, A06, A07, A08, A09, A10, A15, A33		A1, A2, A3, A4, A12, A13, A15, A18, F01		A24, A27, A29, A32, A35		RHM (n = 1)
Trace & rare earth elements (ppm)	*mean*	*SD*	*mean*	*SD*	*mean*	*SD*	*mean*	*SD*	
Ba	1583	205	1723	1111	1827	1383	725	289	2440
Ce	119.0	7.4	81.8	23.8	99.4	46.5	85.2	30.8	113.5
Co	13.6	1.4	8.8	1.6	9.9	2.5	9.9	5.0	11.4
Cr	95	21	123	47	91	47	98	20	140
Cs	0.25	0.13	0.36	0.21	0.27	0.04	0.26	0.06	0.39
Dy	5.06	0.33	3.24	0.86	3.71	0.39	3.35	0.46	3.78
Er	2.46	0.19	1.70	0.44	1.90	0.10	1.71	0.20	1.89
Eu	2.65	0.18	1.68	0.38	1.98	0.54	1.71	0.34	2.14
Ga	21.3	1.2	17.2	2.5	17.8	0.6	21.7	0.6	19.1
Gd	7.28	0.38	4.45	1.17	5.22	1.27	5.03	0.99	5.62
Hf	5.7	0.5	4.5	0.8	4.2	0.4	5.0	0.3	4.6
Ho	0.91	0.06	0.61	0.16	0.69	0.05	0.62	0.08	0.67
La	62.7	3.9	44.8	12.5	53.5	27.4	43.5	16.4	65.4
Lu	0.33	0.03	0.25	0.06	0.28	0.01	0.25	0.02	0.26
Mo	3	0	6	3	4	2	6	4	9
Nb	25.5	1.9	18.6	4.5	18.2	1.3	23.8	1.1	16.4
Nd	54.1	3.5	32.5	10.0	38.8	15.9	37.7	13.2	46.0
Pr	14.01	0.92	8.60	2.78	10.35	4.65	9.69	3.72	12.30
Rb	39.4	8.0	35.4	6.2	34.5	9.6	36.3	7.5	62.1
Sm	9.96	0.58	6.00	1.73	6.97	2.05	7.01	1.97	8.14
Sn	2	0	1	0	1	1	2	1	2
Sr	1023	169	573	287	731	258	304	140	1090
Ta	1.6	0.1	1.3	0.4	1.2	0.1	1.5	0.1	1.0
Tb	1.11	0.09	0.74	0.16	0.85	0.10	0.78	0.10	1.01
Th	10.14	0.93	14.92	4.02	8.80	1.99	10.37	0.91	16.20
Tm	0.33	0.03	0.24	0.06	0.26	0.01	0.23	0.03	0.25
U	3.96	0.45	5.43	1.20	3.08	0.77	2.75	0.58	5.72
V	180	20	107	28	114	17	154	18	167
W	3	1	2	1	2	1	3	2	3
Y	25.2	2.2	16.7	4.3	19.2	1.1	16.7	1.9	20.1
Yb	2.16	0.18	1.59	0.40	1.76	0.07	1.59	0.14	1.70
Zr	247	20	176	29	177	19	220	11	189

Loss on ignition values for all intrusive units range from 1.07 – 5.07%, averaging ~ 3% for the Rain Hill Monzodiorite and ~ 3.5% for porphyritic stocks. Moderately higher values for mineralised stocks are indicative of their greater proportions of sulphides and hydrous minerals, despite sampling targeting the least altered of intersections. Due to the moderate to high levels of alteration, major element abundances have been plotted against TiO_2 in bivariate plots, as TiO_2 is considered to be the least mobile of the major elements during hydrothermal alteration and low grade metamorphism (Rollinson 1993) (Figure 4.9). Titanium is compatible during fractional crystallisation of an intermediate-acid magma, and therefore will decrease with melt evolution for magmas of intermediate to felsic chemistries (Pearce 1996, Winter 2001).

An obvious trend in TiO_2 versus SiO_2 is observed when TiO_2 is plotted against SiO_2 on a bivariate plot, with SiO_2 values increasing from 57.15 – 59.37% for the Rain Hill Monzodiorite to a maximum of 70.20% for the most evolved of the late stage dykes; with a corresponding decrease in TiO_2 from 1.27% to 0.47% (Figure 4.9). A relatively tightly constrained magmatic trend is evident between the Rain Hill Monzodiorite and its late stage dykes, with porphyry stocks plotting as slightly more evolved than the Rain Hill Monzodiorite, on the upper spectra of intermediate in composition. These finding are consistent with those resolved from the Nb/Y versus Zr/Ti immobile element classification diagram of Pearce (1996) (Figure 4.1). This plot revealed a small but consistent distinction in Nb/Y (alkalinity proxy) between porphyry stocks sampled from the northern drill hole (TYDH005; more alkali) and those of the southern two holes (TYHD003 and TYHD004; less alkali). In the TiO_2/SiO_2 bivariate plot, the northern porphyry samples plot on the Rain Hill Monzodiorite magmatic trend, whilst the southern porphyries show a modest depletion in SiO_2. This is probably related to hydrothermal alteration, which Mottl (1983) has noted to cause depletion of SiO_2.

The fractional crystallisation magmatic trend is more tightly constrained when TiO_2 is plotted against P_2O_5, which is also considered relatively immobile (Rollinson 1993). P_2O_5 decreases from ~ 0.5 to 0.2%, consistent with observed magmatic trends of K-enriched melts (Winter 2001). Porphyry units again plot as more evolved than the Rain Hill Monzodiorite, with the southern porphyries appearing to be more fractionated than the northern porphyries

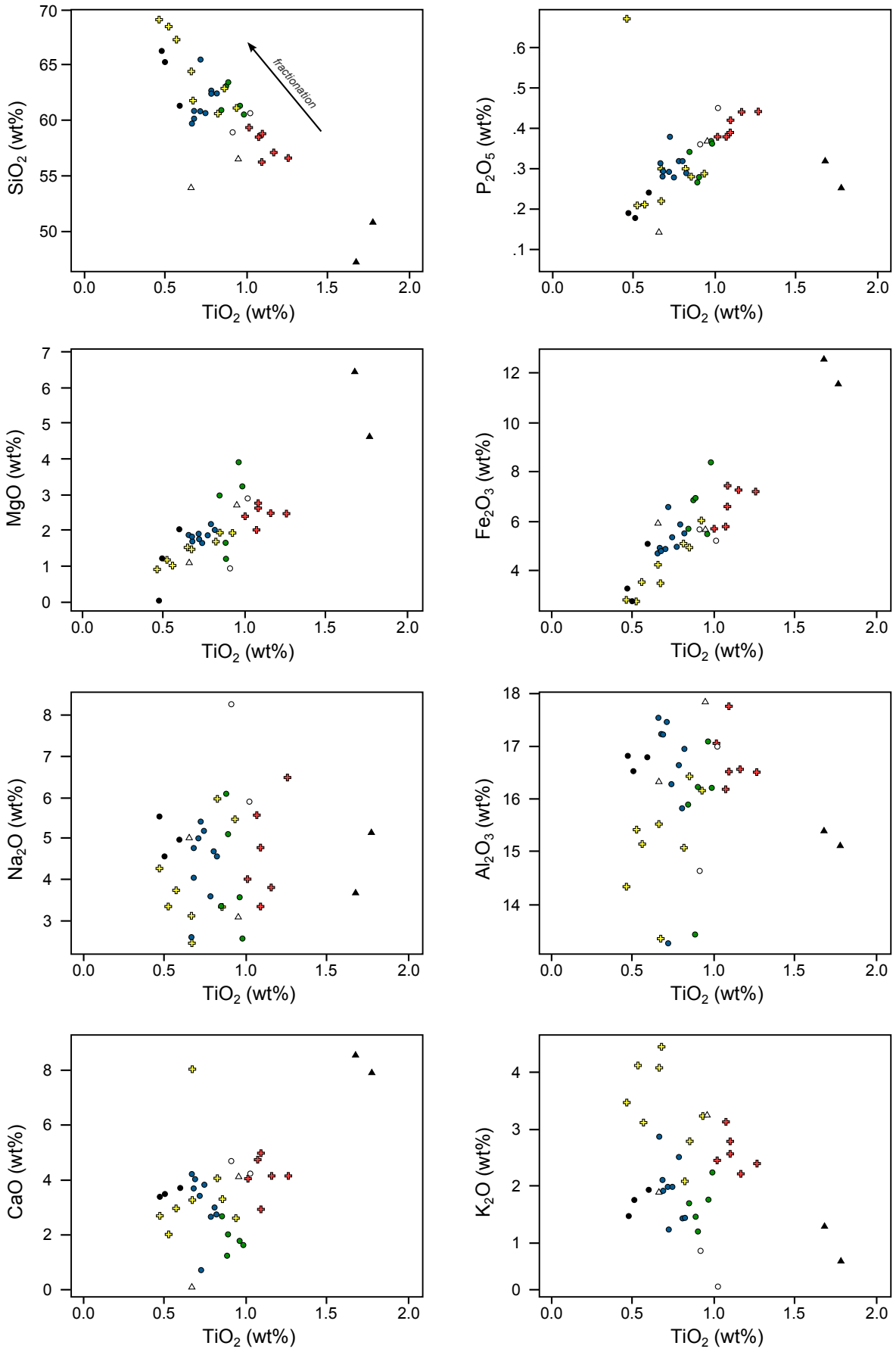

Figure 4.9: Major and selected trace element bivariate plots for volcaniclastic and intrusive units. See adjoining Figure 4.9 (cont.) for symbol labels.

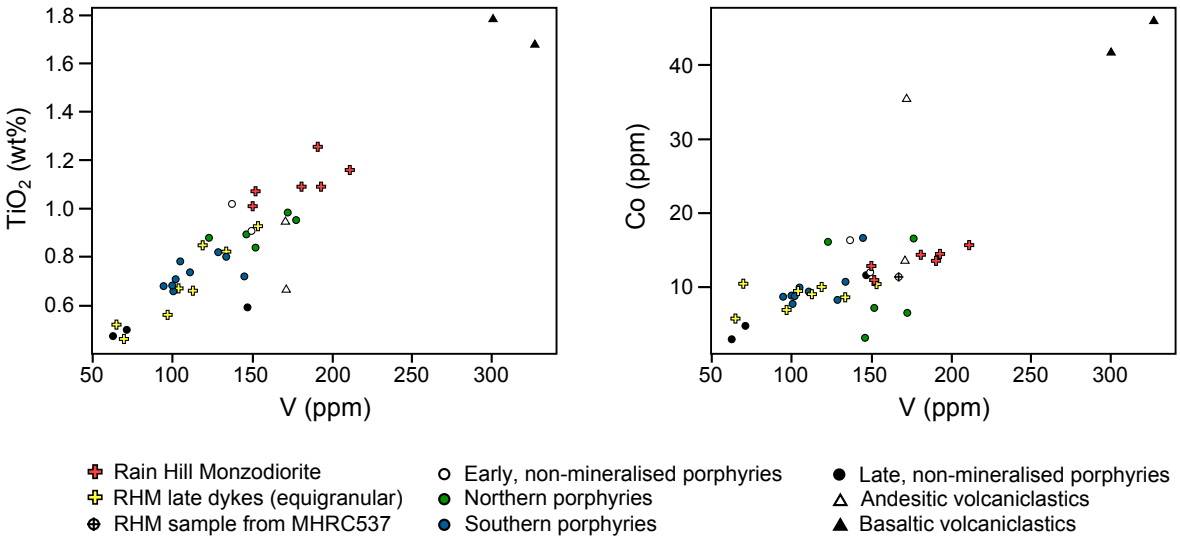

Figure 4.9: continued.

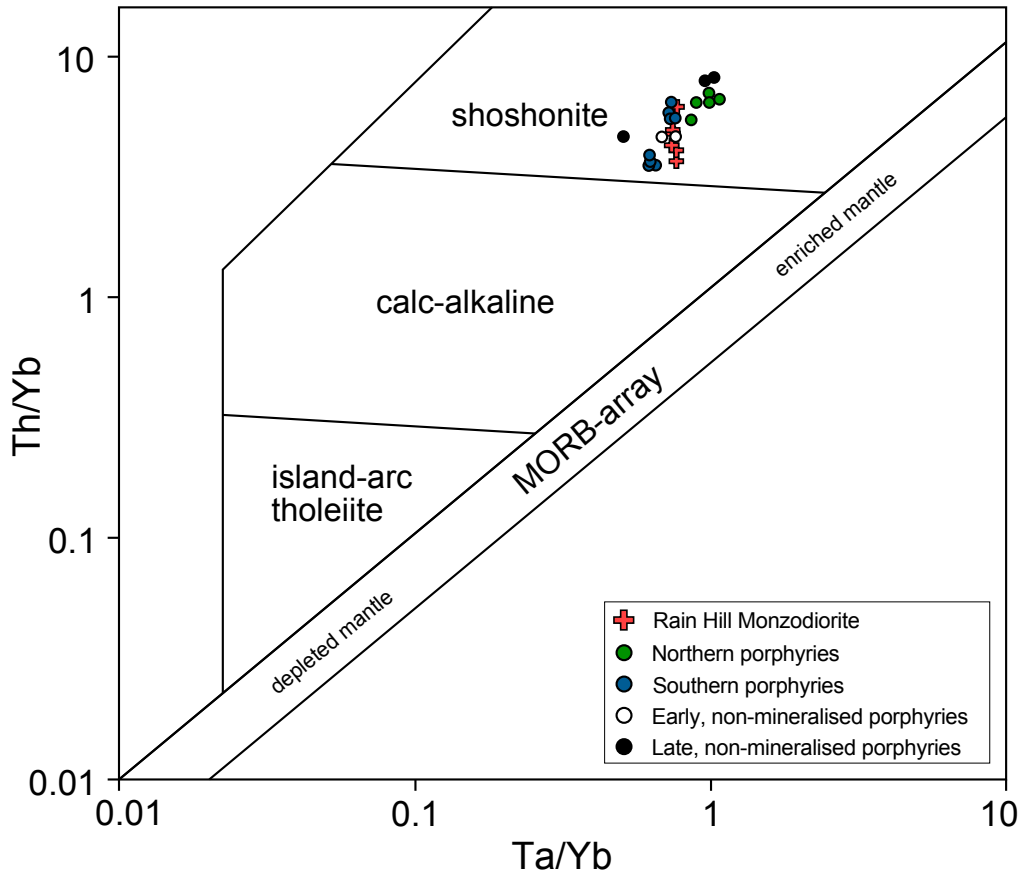

Figure 4.10: Pearce (1982) magma series discrimination diagram, with Yiddah intrusive units plotted. Late acid dykes are not plotted, as they are strongly affected by very late stage fractionation (as are the Rain Hill Monzodiorite samples to a lesser degree) and therefore are not considered representative of the bulk magma. The implication of Ta/Yb versus Th/Yb enrichment of Yiddah intrusives is discussed further in Chapter Eight.

Both MgO (~1 – 3%) and Fe_2O_3 (~ 4 – 8%) correlate positively with TiO_2, consistent with fractional crystallisation trends. Relative to the linear fractionation pattern observed for the Rain Hill Monzodiorite, porphyry units are slightly enriched in MgO and Fe_2O_3.

All units show variable concentrations of Na_2O, Al_2O_3, CaO and K_2O; elements which are considered mobile during both hydrothermal alteration and low grade metamorphism. Na_2O concentrations are scattered, ranging from 2 – 7% and averaging ~ 4.5%. These magnitudes are elevated relative to average K-enriched magmas; with variable internal enrichment (scatter) considered to be primarily due to the albitisation of feldspars. Al_2O_3 concentrations (13 – 18%) are also reasonably highly scattered, particularly for porphyry stocks, which display moderate enrichment relative to the magmatic trend preserved by the Rain Hill Monzodiorite and late dykes.

Relative to average arc melts, CaO concentrations (0.5 – 6%) are depleted. CaO possesses an inverse relationship with alkalinity, such that average CaO values for low-K (tholeiitic), medium-K and high-K andesitic melts decrease from 8.1, 7.1 to 6.0% respectively (Winter 2001). The general depletion of CaO within Yiddah intrusives is therefore attributed to their primary alkali (shoshonitic) chemistries, confirmed by the Ta/Yb versus Th/Yb immobile element magma series discrimination diagram of Pearce (1982) (Figure 4.10). This classification is consistent with the Pearce (1996) diagram (Figure 4.1).

CaO is also depleted in porphyry stocks relative to the magmatic differentiation trend of the Rain Hill Monzodiorite and late dykes; with CaO depletion becoming more pronounced with increasing basicity of primary rock composition. This trend may be partially attributed to the differential alteration susceptibility of certain Ca-bearing minerals. Rocks of more mafic primary compositions initially contain larger proportions of calcium within Ca-plagioclase and hornblende, minerals which at Yiddah are intensely albitised and chloritised, respectively. These processes potentially facilitate the mobilisation and transport of calcium from the rock. In more evolved stocks, a greater proportion of calcium is contained within the later stage minerals of titanite and apatite, which are generally reasonably well preserved within the Yiddah intrusive units.

As the porphyry stocks are not highly fractionated relative to one another, the above explanation is not considered substantial enough to entirely explain the CaO depletion trend.

Another factor may relate to the decreasing fluid volumes experienced by stocks emplaced over time within an evolving hydrothermal system. By this explanation, stocks emplaced at early stages experience greater cumulative fluid volumes than those intruding in the later stages, which results in greater alteration intensity. At Yiddah, such an explanation infers that the slightly more evolved stocks observed in the south of the deposit (TYDH003 and TYDH004) have telescoped the earlier (northern) porphyries, resulting in their enhanced albitisation, chloritisation and subsequent CaO depletion.

K_2O is highly mobile under hydrothermal alteration and metamorphic conditions (Rollinson 1993). In the Yiddah intrusives, concentrations are variable, ranging from ~ 1 – 5% for all units and 2.28 – 3.16% for the (least altered) Rain Hill Monzodiorite. Despite all samples plotting as shoshonitic on both the Pearce (1982) (Figure 4.10) and Pearce (1996) (Figure 4.1) immobile element diagrams, these K_2O concentrations fall below the shoshonite field on traditional SiO_2 versus K_2O plots, where the high-K calc-alkaline/shoshonitic boundary is ~ 3.5% at 59% SiO_2 (Peccerillo & Taylor 1976). It is therefore suggested that intrusive units at Yiddah have suffered depletion of K_2O consistent with increases of Na_2O due to the albitisation of feldspars. Mobilised potassium is likely to have been reprecipitated in intensely altered shear-related sericitic-argillic zones as discussed in Chapter Six. K_2O depletion is considerably more pronounced in the intrusive stocks; which predominantly contain 1 to 3% K_2O. As the porphyry stocks consistently plot as being more fractionated than the Rain Hill Monzodiorite using immobile element indicators, they would be expected to possess higher K_2O concentrations in an undisturbed system. The opposite outcome therefore indicates that alteration of porphyritic stocks was significantly more intense than that of the Rain Hill Monzodiorite.

In addition to SiO_2, P_2O_5, MgO and Fe_2O_3; a number of immobile trace and rare earth elements display relatively tightly constrained magmatic differentiation trends. The strongest correlation is resolved between TiO_2 and vanadium (V). V is compatible during differentiation of intermediate to felsic melts and generally shows a strong decrease with magmatic differentiation in arc related melts (Pearce 1996; Winter 2001). In the Yiddah intrusive units, V decreases from a maximum of 211 ppm for the Rain Hill Monzodiorite, through to ~ 175 – 100 ppm for mineralised porphyry stocks to a minimum of ~ 65 ppm for late stage porphyry intrusives and dykes (ICP-MS values).

The relatively immobile element cobalt (Co) also displays a strong positive correlation with Ti_2O. Co is compatible, and therefore decreases with melt fractionation and increasing SiO_2 (Hastie et al. 2007). For the Yiddah intrusive samples, concentrations decrease from ~ 15 ppm for the Rain Hill Monzodiorite to a minimum of 3.1 ppm for the most fractionated porphyry sample. Co has been plotted against V in Figure 4.9 to enable the examination of sample 'RHM' from drill hole MHRC537, located south of Barmedman. This sample plots within the magmatic fractionation trend of the Yiddah intrusive units, at the more evolved extent of the Rain Hill Monzodiorite sampled at Yiddah; supportive of a common genetic origin, implied by their similar petrography.

The chondrite normalised rare earth element pattern of the Yiddah intrusive units and sample 'RHM' from MHRC537 strongly reflect K-enriched shoshonitic chemistries, with a large degree of LREE enrichment (La – Eu) relative to the HREE's (Gd – Yb) (Figure 4.11). Despite variations in overall magnitude, the slopes of individual units are broadly parallel. This pattern supports the shoshonitic classification resolved from the Pearce (1982) and Pearce (1996) diagrams. The implications of this chemistry in relation to the tectonic setting of formation will be explored in Chapter Eight.

Variations in the overall magnitude of chondrite normalised rare earth element patterns are generally related to fractional crystallisation, which affects the rare earth elements relatively uniformly. In the early stages of fractionation, the rare earth elements are incompatible, due to their poor partitioning into early crystallising minerals such as olivine and pyroxene. This results in the general enrichment of rare earth elements in the melt and their enrichment relative to chondrite values. With increasing fractionation, the rare earth elements become increasingly compatible due to their effective partitioning into later stage minerals including amphibole, titanite, apatite and zircon. This results in the reverse trend, where rare earth element concentrations decrease in magnitude relative to chondrite values (Rollinson 1993).

Within melts of known mineral compositions, the compatibility of an element (its bulk partition coefficient, D_i) can be calculated by summing the individual partition coefficients of each mineral weighted by its proportion within the melt. At $D_i > 1$, the element behaves compatibly, whilst at $D_i < 1$, the element behaves incompatibly. For the Yiddah intrusives, bulk partition coefficients are calculated based on the modal abundance of the Rain Hill Monzodiorite as presented in Table 4.3, as it is considered the least fractionated of units.

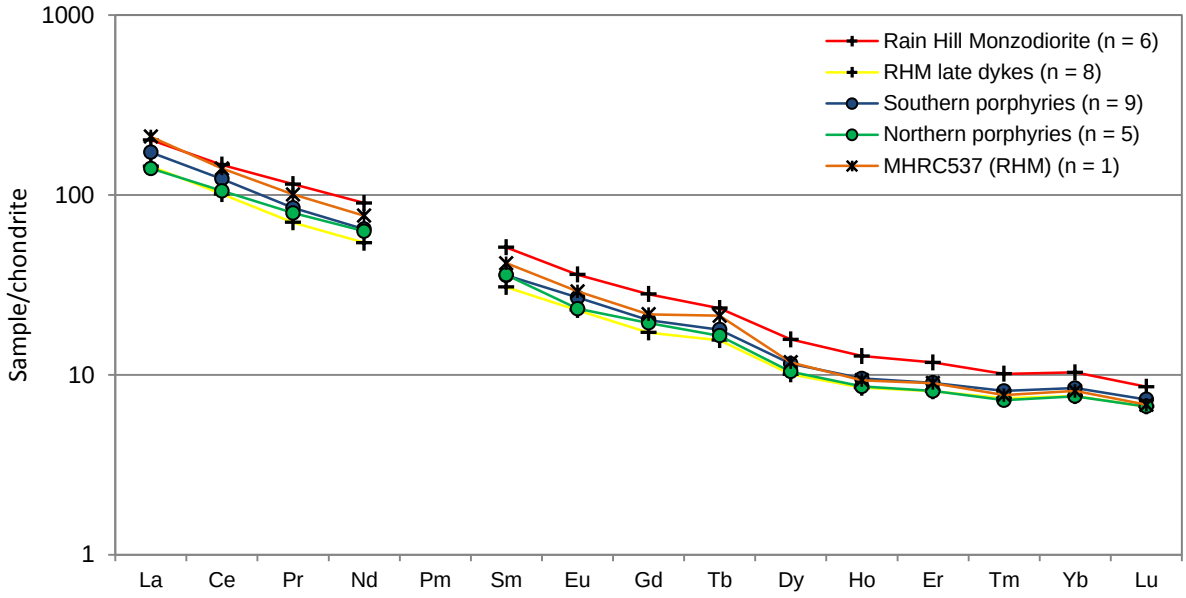

Figure 4.11: Chondrite normalised rare earth element plot for intrusive units. Normalisation values from Boynton (1984). LREE on the left (La – Eu) , HREE on the right (Gd - Lu).

Rare earth element bulk partition coefficients for the Yiddah intrusives are consistently > 1. The calculation of D_i for Sm (Table 4.6) reveals that this value is predominantly driven by the high partition coefficients of amphibole, titanite and apatite (Rollinson 1993). This indicates that further fractionation of the magma from the Rain Hill Monzodiorite composition would generate melts with decreasing rare earth element concentrations, as observed for the porphyry stocks and late dykes in Figure 4.11.

Table 4.6: Calculations for the bulk partition coefficient of Sm.
Partition coefficients from Rollinson (1993), Tables 4.2 and 4.3.

Mineral	Proportion	Partition coefficient	Weighted contribution
Plagioclase	0.56	0.102	0.057
Orthoclase	0.20	0.018	0.004
Amphibole	0.15	3.000	0.450
Quartz	0.04	0.014	0.001
Titanite	0.02	10.00	0.200
Magnetite	0.02	0.300	0.006
Apatite	0.01	46.00	0.460
Zircon	0.002	4.940	0.001
D_i (bulk partition coefficient)			**1.178**

No Europium anomaly is observed for the intrusive units, which is likely indicative of a relatively highly oxidised melt. Eu anomalies generally occur due to the variation in

behaviour of Eu relative to the other rare earth elements when it exists in the 2+ vacancy state. In oxidised melts however, Eu^{3+} is dominant, and hence Eu behaves concordantly with the other rare earth elements, all of which exist at 3+ valencies (Rollinson 1993). The significance of an oxidised melt, which is also suggested by the dominance of magnetite as the Ti-Fe oxide phase; is that dissolved sulphur is contained as sulphate, which inhibits the chalcophile elements Cu and Au from forming sulphide complexes as the melt fractionates. The metals are then available to be scavenged by volatiles such as Cl^-, H_2S and SO_2 which partition into the fluid phase upon exsolution (Richards 2003; Sillitoe 2010).

4.4.3. Summary of key points

The various petrographic and geochemical evidence presented suggests that all intrusive units sampled at Yiddah were initially of relatively similar chemistry and mineralogy, comprising amphibole monzodiorites of shoshonitic affinity. The consistent, slightly more fractionated chemistry of porphyritic stocks to the Rain Hill Monzodiorite suggests that stocks were likely to have been evolved from the more slowly cooling granitoid.

Alteration has affected the major element chemistry of all units; however its effects are most profound within the mineralised stocks. The most significantly affected elements are Na, K and Ca. The alteration of these elements appears to have been driven by the intense albitisation of feldspars, which has resulted in the depletion of K and Ca and the enrichment of Na within intrusive units. These effects are represented diagrammatically on the IUGS Quartz, Alkali feldspar Plagioclase, Feldspathoid (QAPF) diagram (Figure 4.12).

In the broader regional context, the geochemical and petrological evidence presented here suggest that the Rain Hill Monzodiorite at Yiddah is genetically related to the Rain Hill Monzodiorite identified in drilling south of Barmedman, described by Wormald (1993). This implies that a relatively large magmatic event was responsible for emplacement of a significant, *mineralisation related* melt, the implications for which will be discussed in Chapter Eight.

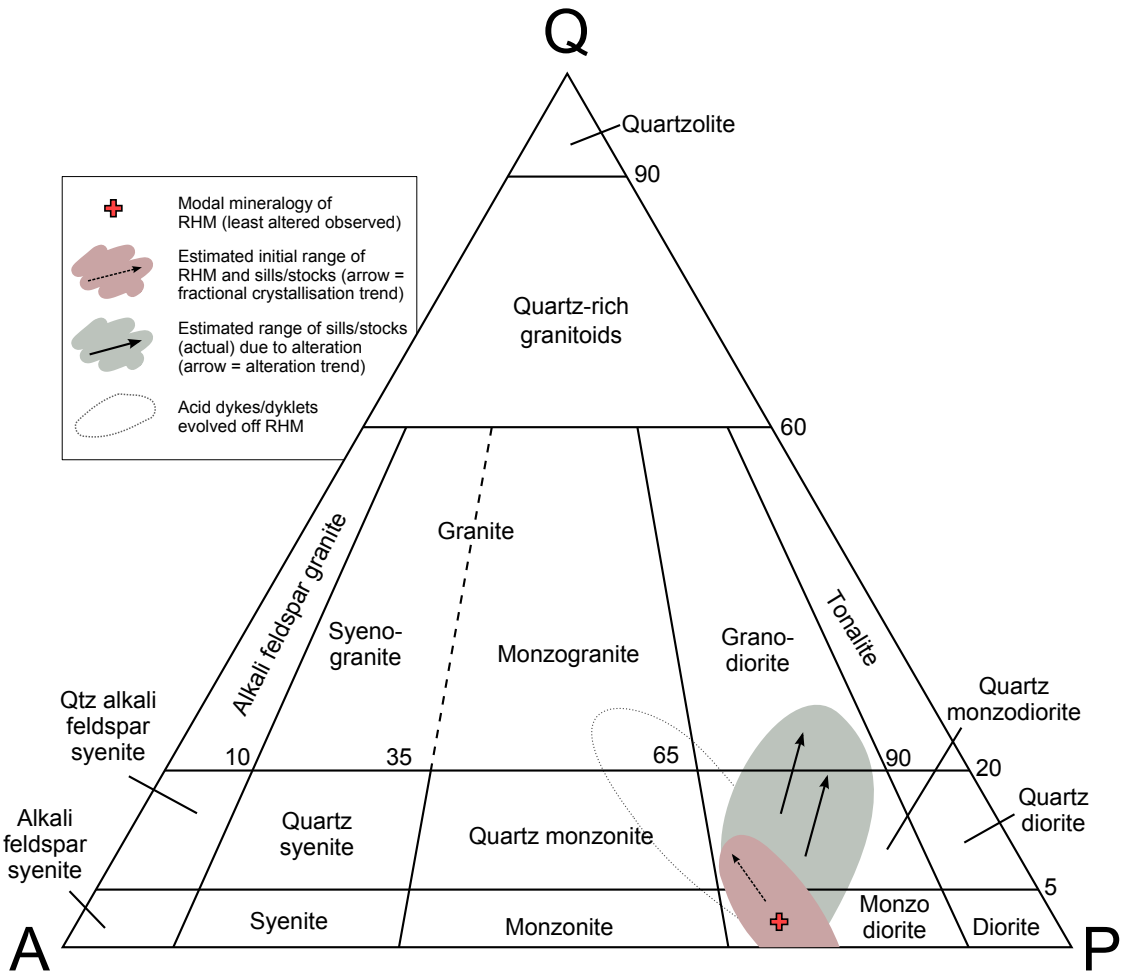

Figure 4.12: IUGS QAPF classification diagram displaying primary rock compositions and alteration trends for Yiddah intrusive units.

CHAPTER FIVE

U-Pb ZIRCON GEOCHRONOLOGY

5.1. INTRODUCTION

This chapter utilises the U-Pb zircon dating method to compare the age of mineralisation-related intrusive stocks at Yiddah to the Rain Hill Monzodiorite and other magmatic events within the Gidginbung Volcanics. Previous dating of these events has largely focused on intrusions and flows associated with the Gidginbung Au-(Ag) deposit; where a date of 435 ± 2.5 Ma (SHRIMP-1) has been obtained by Perkins et al. (1990) for zircons of an andesite flow and a date of 436.4 ± 3.1 Ma has been obtained for zircons initially interpreted as hydrothermal in origin (Lawrie et al. 2007) but later concluded to be magmatic (Fu et al. 2009). The Rain Hill Monzodiorite south of Barmedman has been dated by C. Perkins (Ar-Ar hornblende; cited in Wormald 1993) at 434.9 ± 2.3 Ma from a drill hole north of the Gidginbung pit. In addition, a number of workers have recently used U-Pb zircon and Re-Os molybdenite techniques to date a selection of the porphyry style deposits which flank the Rain Hill Monzodiorite; however at the time of writing, none of these results were available to the author.

5.2. FIELD RELATIONS

Two samples of intrusive material contained within drill core at Yiddah were collected for dating. Sample F2 (504.25 – 506.05 m; TYHD003) was sourced from the Rain Hill Monzodiorite, which is intersected at the base of drill holes TYHD003 and TYHD004. Above and to the east are the hornfelsed fine-grained basaltic volcaniclastic and andesitic volcaniclastic units, which are intruded by mineralisation-related porphyritic sills and stocks. Sample F1, a chlorite-sericite altered intrusive phase (400.00 – 402.00 m; TYHD004) was collected from a ~ 150 m section of drill core intersecting a porphyry sill/stock. Cross-sectional representations of these relationships and sample locations are presented in Chapter Six (Figure 6.4 and Figure 6.5).

No definitive cross-cutting relationships were observed between the Rain Hill Monzodiorite and intrusive stocks in the three drill holes observed; attributed to (1) their largely spatially separated nature, (2) the lack of well-developed selvedges where the units are contacted

against one another and (3) the limitation of interpreting spatial relationships in (complexly deformed) drill core. However, the presence of mineralised quartz-seam veins within the Rain Hill Monzodiorite suggests that this unit was emplaced either before or contemporaneously to the porphyritic sills/stocks.

5.3. **U-Pb ZIRCON DATING**

5.3.1 Introduction

The determination of absolute ages via U-Pb zircon geochronology exploits the natural process of radioactive decay; where the nucleus of an unstable isotope undergoes spontaneous breakdown (or a series of breakdowns) in order for it to form a stable isotope. This process occurs at characteristic rates for each element and isotope, independent of other known chemical and physical parameters (summarised by Williams 1998). The absolute age (t) is determined through measuring the ratio of daughter atoms produced (D) to parent atoms remaining (P) where the decay constant (λ) is known, through:

$$D/P = e^{\lambda t} - 1$$

The decay constant is generally expressed in terms of its half-life ($T_{½}$), which represents the time taken for half of a given amount of the radioisotope to decay. The decay constant and half-life are related by:

$$T_{½} = \ln 2/\lambda$$

The half-life is a major determinant when selecting an isotopic system. Suitable radioisotopes require half-lives small enough for significant proportions of the daughter isotope to accumulate but large enough for measurable proportions of the parental isotope to remain. In the U-Pb system, two independent isotopic systems exist:

^{238}U decays to ^{206}Pb at $T_{½}$ = 4.47 Ga and
^{235}U decays to ^{207}Pb at $T_{½}$ = 704 Ma

The main advantage of the U-Pb system is that it is paired, enabling a further age determination to be produced by combining the daughter isotopes ($^{207}Pb/^{206}Pb$). This provides an independent measure which can be compared to the $^{238}U/^{206}Pb$ and $^{235}U/^{207}Pb$ parent/daughter ratios to assess if the system is undisturbed (closed), or has been affected by

secondary processes (open). This comparison is most commonly performed visually, through plotting on a 'Wetherill' or 'Tera-Wasserburg' concordia diagram. The Tera-Wasserburg diagram ($^{238}U/^{206}Pb$ versus $^{207}Pb/^{206}Pb$ bivariate plot, Tera & Wasserburg 1972) is advantageous over the Wetherill diagram ($^{207}Pb/^{235}U$ versus $^{206}Pb/^{238}U$ bivariate plot) in that all variables plotted are as directly measured, in contrast to the Wetherill plot in which the ^{235}U value is calculated from ^{238}U based on the accepted modern $^{238}U/^{235}U$ ratio of 137.88 (Williams 1998).

Zircon ($ZrSiO_4$) is the most effective and commonly used mineral to perform U-Pb isotope age determinations. Foremost, zircon can incorporate trace amounts of U and Th in its crystal lattice upon formation, whilst it strongly discriminates against Pb (Hoskin & Schaltegger 2003). Therefore, any Pb detected in the zircon, in principle, has formed by radioactive decay. Zircon is also a relatively common accessory mineral in igneous (particularly felsic) rocks, and is sufficiently robust to survive episodes of weathering, erosion, transport and metamorphism (Davis et al. 2003). Evidence of these events may be preserved through a number of textural and zoning features which can be identified through cathodoluminescence imaging and precisely targeted using a high resolution microprobe such as the Sensitive High Resolution Ion Microprobe (SHRIMP).

5.3.2 Description of zircons

Thin sections of each sample were initially examined in transmitted light to identify the textural relationships of contained zircons. Moderately abundant zircon populations were identified in both samples, interspersed evenly throughout other mineral constituents. Zircons from samples F2 and F1 were subsequently extracted via the methods outlined in Section 1.4.6 by Shane Paxton of the Research School of Earth Sciences at The Australian National University. The zircon yield from both samples was high; with > 300 grains obtained from each 1 kg sample. Full petrographic descriptions and geochemical properties of each sample are provided in Appendix C and Appendix F, respectively.

Zircons from the Rain Hill Monzodiorite (sample F2) average 50 – 200 μm, with aspect ratios typically ~ 2:1 (Figure 5.1). They are predominantly prismatic in habit and well preserved, occurring mostly as euhedral to subhedral whole grains. Grain terminations are often faceted, while the lengthwise margins are generally straight. Zircons of the porphyritic

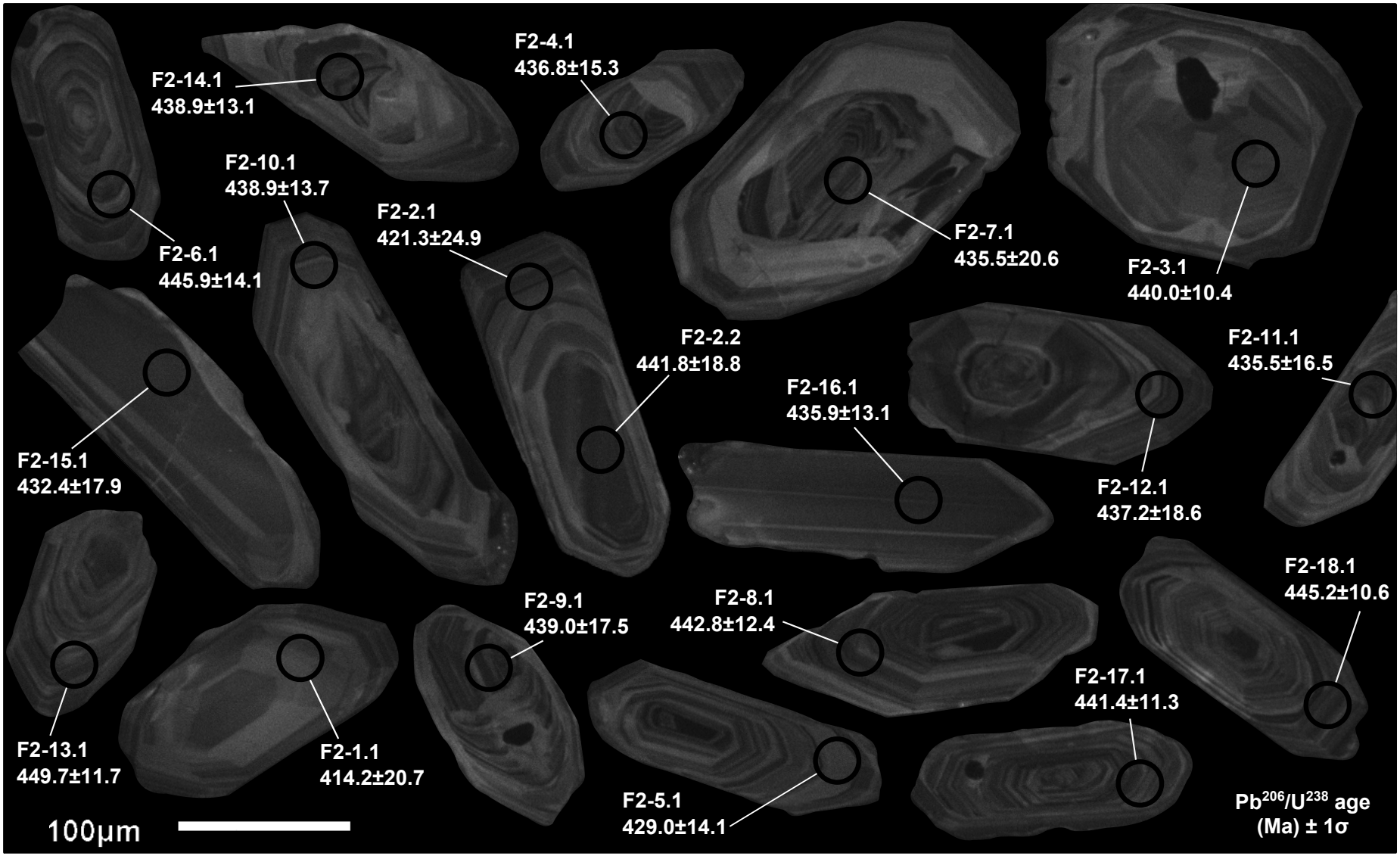

Figure 5.1: Cathodoluminescence images and analysis positions of zircons extracted from the Rain Hill Monzodiorite (sample F2), at 504.25 - 506.05 m TYHD003.

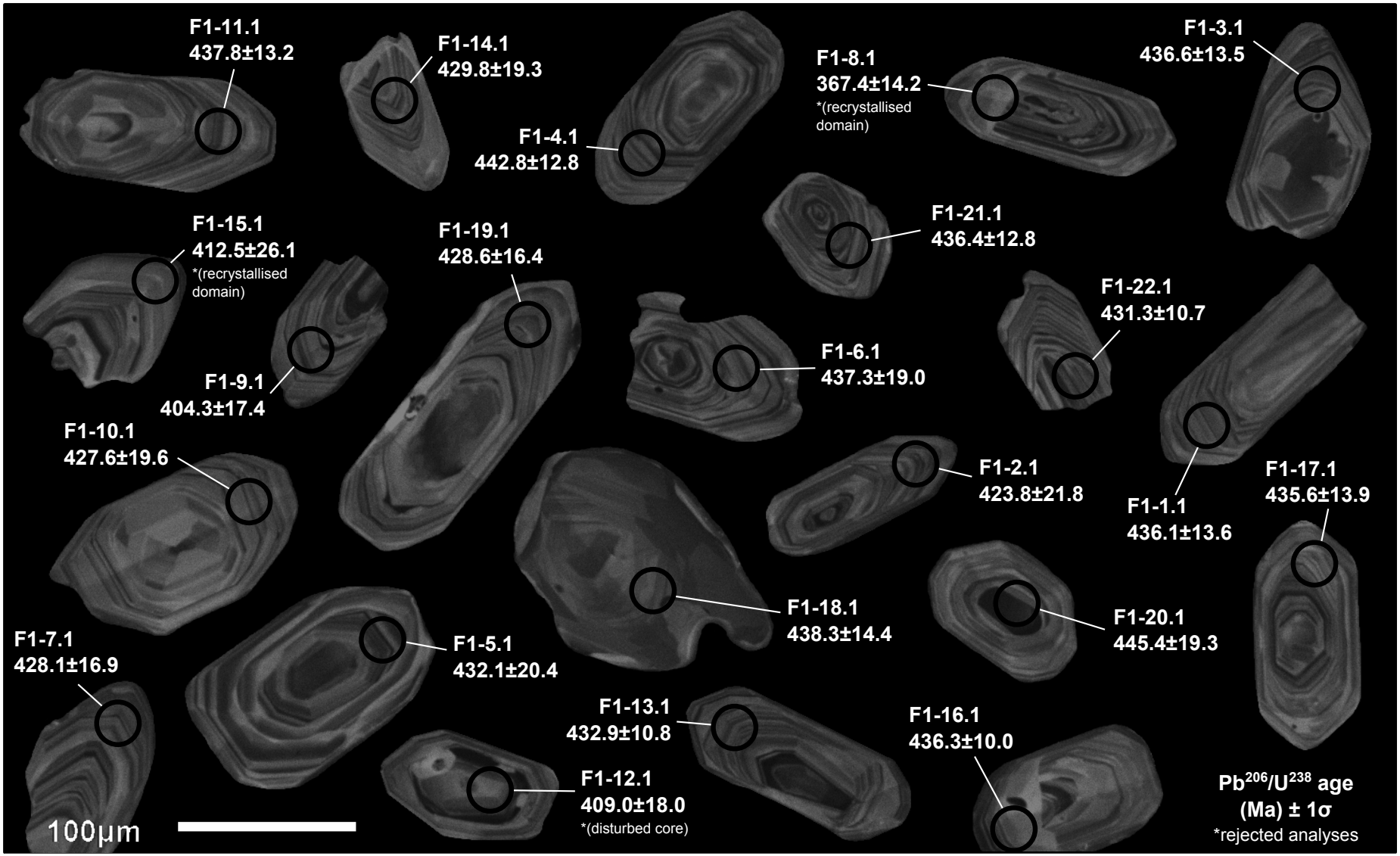

Figure 5.2: Cathodoluminescence images and analysis positions of zircons extracted from sample F1, a monzodiorite sill/stock within the mineralised zone at 400.0 - 402.0 m, TYHD004.

stock (sample F1) are somewhat smaller than those of the Rain Hill Monzodiorite, averaging 20 – 150 μm (Figure 5.2). This is consistent with a more rapid late stage cooling related to porphyry emplacement. A greater proportion of these zircons are fragmented and grain boundaries are somewhat more pitted than those observed for F2. Otherwise, the habit and aspect ratios of zircons from sample F1 are broadly similar to those of sample F2.

Virtually all zircon grains observed from both samples possess weak to well-developed growth zoning, apparent in cathodoluminescence images. These patterns are typical of primary magmatic zircons (Corfu et al. 2003). In sample F2, zoning ranges from broad to oscillatory, with relatively faint changes in luminescence between zoning bands. In sample F1, fine oscillatory zoning is dominant; and a larger discrepancy between end-members has produced greater contrasts in luminosity. These features may be related to the slightly more felsic primary chemistry of porphyry stocks (sample F1), as magma differentiation has been related to the narrowing of growth zoning (Hoskin 2000).

Instances of growth zoning truncation are relatively common in zircons of both samples. These textural discontinuities are generally rimmed with recrystallised or newly grown domains, which are more homogenous and lighter in appearance than the internal region. Where these zones are targeted in dating (F1-8.1; F1-15.1), resultant ages plot discordantly, indicating the U-Pb isotope system has been disturbed.

A final characteristic feature observed in zircon extracts from sample F1 and sample F2 are moderately frequent bleb-like opaque inclusions, averaging ~ 5 – 10 μm and ranging to 40 μm in diameter. These inclusions are generally but not always contained nearer to the rim of zircon grains, often within recrystallised domains; suggesting they could possibly represent immiscible sulphide droplets emplaced contemporaneously to mineralisation.

5.3.3 Analysis

Samples F2 and F1 were cast in an epoxy resin 1 inch disc (mount W5) with fragments of the standard TEMORA-2 (417 Ma; Black et al. 2004), ground down and polished to reveal cross sections of grains. Eighteen grains of sample F2 and 22 grains of sample F1 were analysed on the SHRIMP IIe at Geoscience Australia, Canberra. The SHRIMP is a double-focusing secondary ion mass spectrometer (SIMS) instrument which

operates by focusing a primary beam of oxygen ions onto a ~ 20 μm spot, sputtering material from the target to produce secondary ions which are focused and filtered according to their energy and mass by a large turning radius electromagnet (see summary by Williams 1998).

Cathodoluminescence images were used to target analysis sites, with the aim of capturing a range of primary igneous, potential core and potentially recrystallised sites. Analysis sites are presented in Figure 5.1 and Figure 5.2. All grains were analysed only once, except F2.2, in which a potential core and rim were analysed. Analysis of samples F2, F1 and TEMORA-2 were undertaken during a single session, interleaved, such that three to four unknown grains were analysed between each TEMORA-2 standard (Figure 5.3). Reported ages are derived from $^{206}Pb/^{238}U$ ratios, as is consistent for Phanerozoic grains. The $^{206}Pb/^{238}U$ calibration error based on the 13 TEMORA-2 analyses was 0.9%. This was added in quadrature to the largely counting statistics errors in the measurement of ^{206}Pb and ^{238}U, so that external comparisons could be made with other age determinations. Tera-Wasserburg and cumulative Gaussian distribution plots were generated using ISOPLOT (Ludwig 1999).

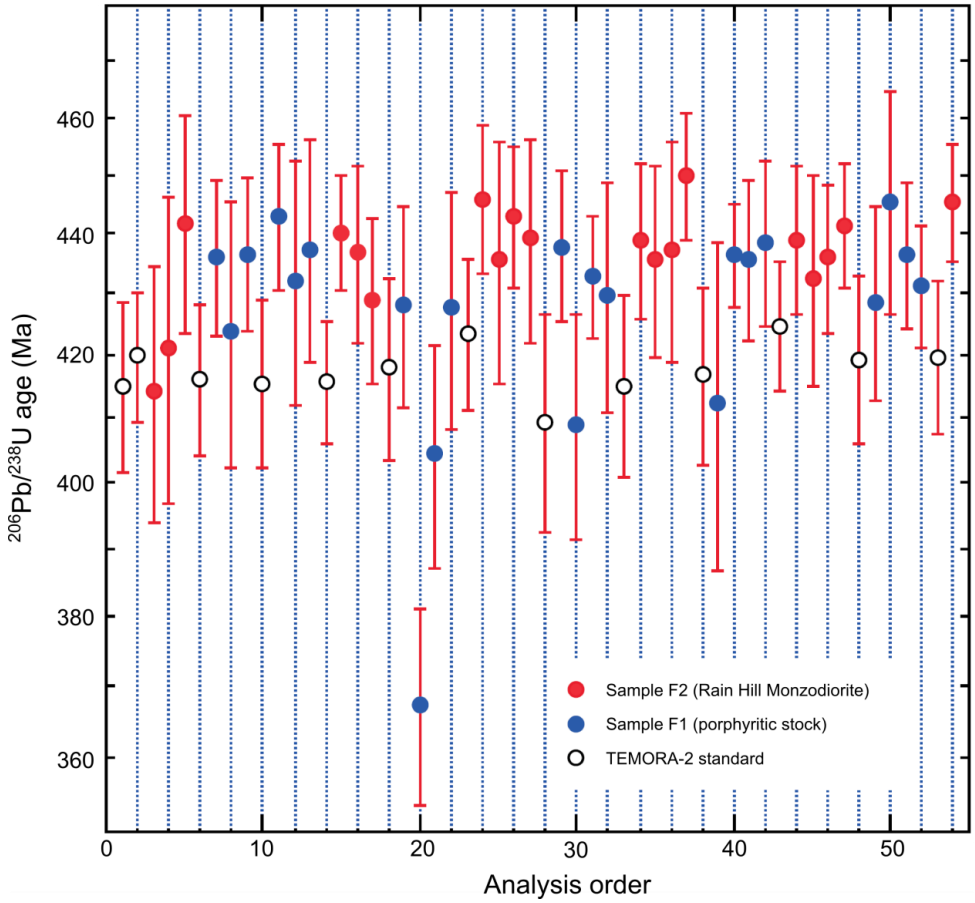

Figure 5.3: Time sequence plot of all analyses performed on sample F2, sample F1 and TEMORA-2 in mount E5. Diagram produced by A. Nutman.

5.3.4 Results

Rain Hill Monzodiorite

All analyses of zircons from sample F2 plot close to concordia, indicating little disturbance to the isotopic system. They also show negligible common Pb, based on measured ^{204}Pb. All analyses are within statistical error of one another, with no difference resolved between apparent rims and cores (Table 5.1, Figure 5.4a). All grains are interpreted to represent a single normal population (Figure 5.5a). As such, a final weighted mean ^{206}Pb/^{238}U age of 439.2 ± 6.4 Ma (n = 19, MSWD=0.24) is obtained. All analyses plot close to concordia; indicating the U/Pb isotopic system is relatively undisturbed.

Mineralisation related porphyry stock

Sample F1 also produced a single normal population, of similar ^{206}Pb/^{238}U age to sample F2 (Table 5.2). Analysed sample F1 zircon domains are however apparently slightly less concordant, with greater variation observed in ^{206}Pb/^{238}U ages (Figure 5.4b). Two recrystallised domains and one disturbed core produced apparently younger ages than the majority of analyses (Figure 5.5b). Excluding these datum points from the final age determination produces a weighted mean ^{206}Pb/^{238}U age of 433.8 ± 6.4 Ma (n = 22; MSWD=0.27).

5.4. **INTERPRETATION**

High Th/U ratios (> 0.4) in all zircons analysed and well-developed oscillatory zoning in the majority of zircons analysed are consistent with zircon grown from magma rather than in high temperature hydrothermal and/or metamorphic environments. Thus, the U/Pb ages reported here are interpreted to reflect magmatic events.

The ^{206}Pb/^{238}U dates obtained for zircon populations of both samples F2 and F1 represent single magmatic events statistically indistinguishable in age. This suggests that the two units were emplaced either contemporaneously or within a reasonably short time period of one another. This result is consistent with petrographic and geochemical findings that suggest the Rain Hill Monzodiorite and porphyry sills/stocks are genetically related.

Table 5.1: Sample F2 U/Pb SHRIMP analyses.

Labels	Site	U (ppm)	Th (ppm)	Th/U	$^{238}U/^{206}Pb$ ratio	$^{206}Pb/^{238}U$ date (Ma)
F2-1.1	m,p	105	47	0.44	15.069 ± 0.776	414.2 ± 20.7
F2-2.1	e,osc,p	303	186	0.61	14.807 ± 0.903	421.3 ± 24.9
F2-2.2	c,p	292	206	0.71	14.096 ± 0.620	441.8 ± 18.8
F2-3.1	c,osc,anh	211	90	0.43	14.157 ± 0.346	440.0 ± 10.4
F2-4.1	c,osc,p	249	111	0.45	14.263 ± 0.516	436.8 ± 15.3
F2-5.1	e,osc,p	185	93	0.50	14.533 ± 0.494	429.0 ± 14.1
F2-6.1	e,osc,p	316	154	0.49	13.962 ± 0.425	445.9 ± 13.1
F2-7.1	c,osc,anh	264	132	0.50	14.307 ± 0.699	435.5 ± 20.6
F2-8.1	e,osc,p	301	143	0.47	14.064 ± 0.407	442.8 ± 12.4
F2-9.1	c,osc,anh	341	197	0.58	14.188 ± 0.583	439.1 ± 17.5
F2-10.1	e,osc,p	247	121	0.49	14.195 ± 0.458	438.9 ± 13.7
F2-11.1	m,osc,p	247	111	0.45	14.309 ± 0.560	435.5 ± 16.5
F2-12.1	e,osc,p	256	177	0.69	14.252 ± 0.628	437.2 ± 18.6
F2-13.1	e,osc,p,f	266	145	0.54	13.840 ± 0.373	449.7 ± 11.7
F2-14.1	c,osc,p	240	111	0.46	14.193 ± 0.438	438.9 ± 13.1
F2-15.1	m,p	201	140	0.69	14.414 ± 0.617	432.4 ± 17.9
F2-16.1	m,p	293	230	0.79	14.296 ± 0.443	435.4 ± 13.1
F2-17.1	e,osc,p	344	175	0.51	14.110 ± 0.372	441.4 ± 11.3
F2-18.1	e,osc,p	327	201	0.62	13.987 ± 0.343	445.2 ± 10.6
						439.2 ± 6.4
						95% conf. MSWD=0.24

m = middle, e = edge, p = prismatic, anh = anhedral, osc = oscillatory zoned, f = fragment. Errors are expressed at the 1 sigma level.

Table 5.2: Sample F1 U/Pb SHRIMP analyses.

Labels	Site	U (ppm)	Th (ppm)	Th/U	$^{238}U/^{206}Pb$ ratio	$^{206}Pb/^{238}U$ date (Ma)
F1-1.1	e,osc,p,f	179	108	0.61	14.288 ± 0.459	436.1 ± 13.6
F1-2.1	e,osc,p	217	127	0.59	14.717 ± 0.782	423.8 ± 21.8
F1-3.1	e,osc,p	185	97	0.52	14.271 ± 0.456	436.6 ± 13.5
F1-4.1	e,osc,p	245	161	0.66	14.064 ± 0.420	442.8 ± 12.8
F1-5.1	e,osc,p	274	202	0.74	14.424 ± 0.702	432.1 ± 20.4
F1-6.1	e,osc,p,f	180	99	0.55	14.247 ± 0.639	437.3 ± 19.0
F1-7.1	e,osc,p,f	249	164	0.66	14.564 ± 0.592	428.1 ± 16.9
F1-8.1	**e,rex,p**	**99**	**59**	**0.59**	**17.053 ± 0.678**	**367.4 ± 14.2**
F1-9.1	e,osc,p,f	224	212	0.95	15.499 ± 0.686	404.3 ± 17.4
F1-10.1	e,osc,p	219	174	0.79	14.581 ± 0.690	427.6 ± 19.6
F1-11.1	e,osc,p	259	136	0.53	14.229 ± 0.443	437.8 ± 13.2
F1-12.1	**c,p**	**178**	**112**	**0.63**	**15.268 ± 0.692**	**409.0 ± 18.0**
F1-13.1	e,osc,p	236	152	0.65	14.397 ± 0.372	432.9 ± 10.8
F1-14.1	m,osc,p,f	188	122	0.65	14.504 ± 0.672	429.8 ± 19.3
F1-15.1	**e,rex,p,f**	**156**	**82**	**0.53**	**15.133 ± 0.985**	**412.5 ± 26.1**
F1-16.1	e,osc,p	82	32	0.39	14.280 ± 0.323	436.3 ± 9.6
F1-17.1	e,osc,p	148	79	0.54	14.306 ± 0.470	435.6 ± 13.9
F1-18.1	m,anh	134	58	0.43	14.213 ± 0.481	438.3 ± 14.4
F1-19.1	m,osc,p	225	147	0.65	14.547 ± 0.575	428.6 ± 16.4
F1-20.1	m,osc,p	498	413	0.83	13.980 ± 0.627	445.4 ± 19.3
F1-21.1	e,osc,p,f	300	240	0.80	14.277 ± 0.431	436.4 ± 12.8
F1-22.1	m,osc,p,f	222	162	0.73	14.453 ± 0.370	431.3 ± 10.7
						433.8 ± 6.4
						95% conf. MSWD=0.27

m = middle, e = edge, p = prismatic, anh = anhedral, rex = recrystallised, osc = oscillatory zoned, f = fragment. Errors are expressed at the 1 sigma level. Samples in bold represent disturbed sites which were excluded from the final age calculation.

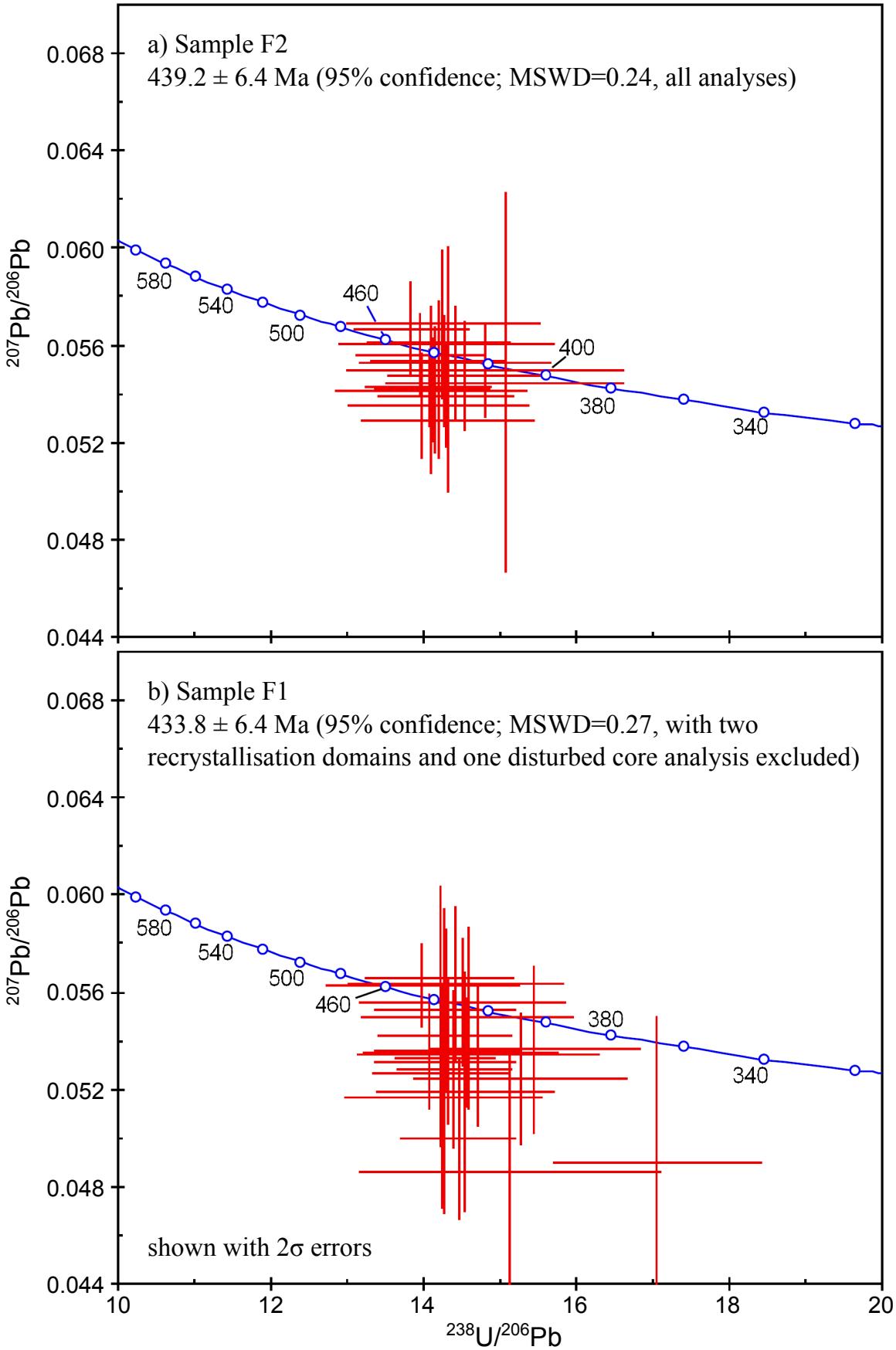

Figure 5.4: Terra-Wasserburg plots. (a) Sample F2, the Rain Hill Monzodiorite. (b) Sample F1, a porphyritic stock from within the mineralised zone. Diagrams produced by A. Nutman.

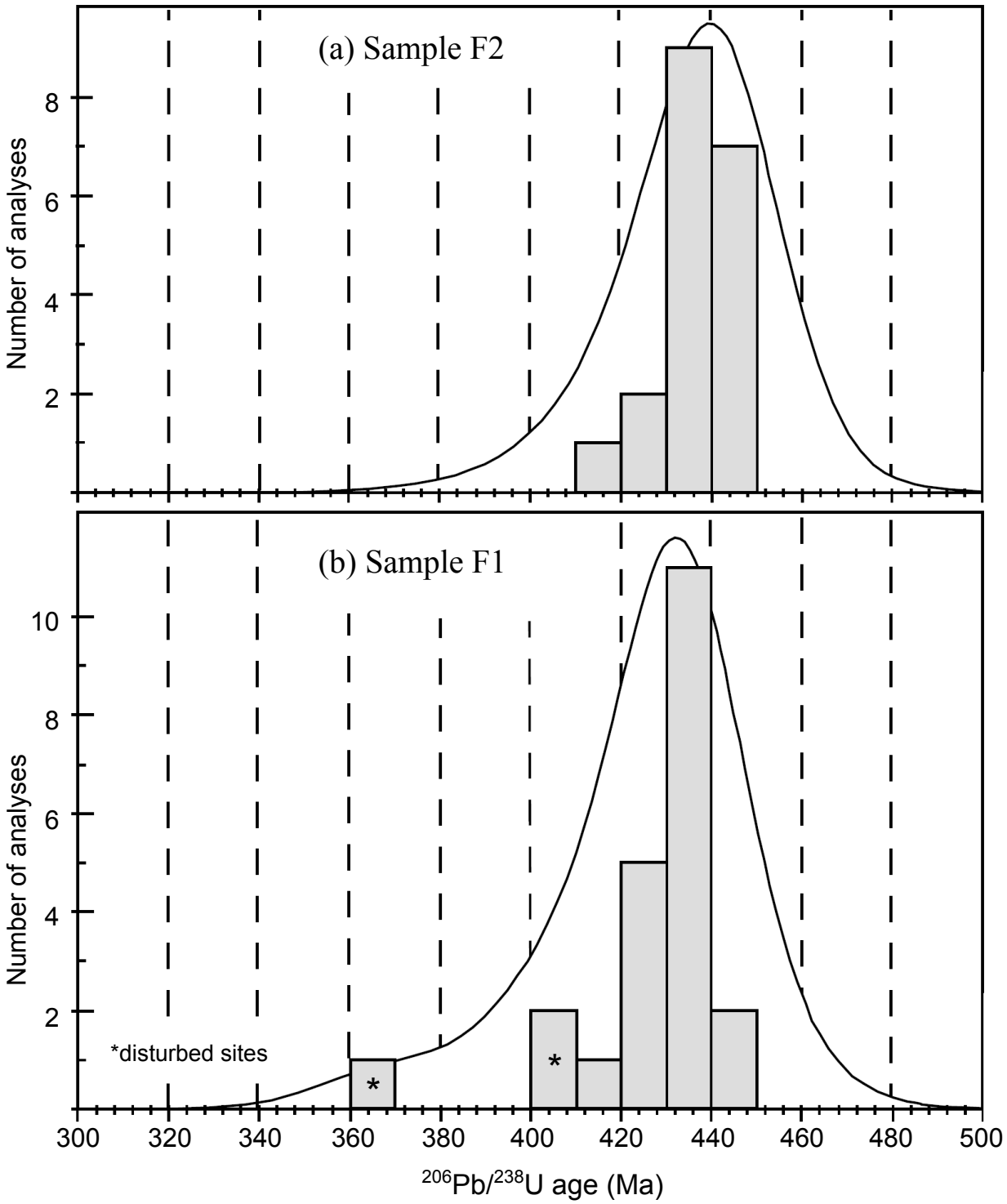

Figure 5.5. Cumulative Gaussian distribution plots. (a) Sample F2, the Rain Hill Monzodiorite. (b) Sample F1, a porphyritic stock from the mineralised zone. Diagrams produced by A. Nutman.

Despite the recognition of growth zoning truncation, no older (inherited) cores were identified from U-Pb analysis. The lack of inherited cores is consistent with (although not exclusive to) a hot, initially zircon undersaturated melt, most likely of subcrustal origin (Nutman and Hiess 2009 and references therein). The truncation of growth zoning and development of recrystallised domains are attributed to either resorption during complex evolution of the magma system, hydrothermal alteration associated with mineralisation or a combination of these factors. The common occurrence of opaque inclusions (possibly sulphides) in recrystallised rims suggests that hydrothermal alteration was likely a factor; however Fu et al. (2009) also note the possibility of a primary magmatic origin for quartz, rutile and pyrite inclusions contained within zircons sourced from the Gidginbung open pit. The more intense nature of hydrothermal alteration in porphyritic sills/stocks to that of the Rain Hill Monzodiorite may also be linked to the slightly less concordant nature of sample F1 zircon U-Pb analyses to that of sample F2.

The ages acquired for intrusive units at Yiddah are within error of those obtained by Perkins et al. (1990) (435 ± 2.5 Ma), C. Perkins (cited in Wormald 1993) (434.9 ± 2.3 Ma) and Lawrie et al. (2007) (436.4 ± 3.1 Ma) for magmatic bodies sampled from the southern portion of the Gidginbung Volcanics. Zircons of sample F2 and F1 are also very similar in size, shape, aspect ratio, zoning and contain similar inclusions to those described by Lawrie et al. (2007) for zircons extracted from the Gidginbung pit. This suggests that it is likely the intrusive bodies identified in the southern and northern Gidginbung Volcanics were emplaced in the same magmatic event, from a common mantle source.

This potentially links the origins of dispersed mineralisation in the Rain Hill district to a single, relatively large-scale magmatic event of early Silurian age, which has emplaced the metaluminous, oxidised Rain Hill Monzodiorite and associated mineralised stocks. This further increases the prospectivity of the Rain Hill Monzodiorite unit, which is yet to be explored intensively on its western margin.

Constraining the timing of mineralisation related intrusive activity is also important in the broader regional context, as it allows the contained deposits to be tied into the development, endowment and cessation of Macquarie Arc volcanism. These themes will be discussed in Chapter Eight.

CHAPTER SIX

ALTERATION AND MINERALISATION

6.1. INTRODUCTION

Hydrothermal alteration is the outcome of fluid-rock interaction, where chemical reactants are delivered and aqueous reaction products are removed through the circulation of heated fluids (Reed 1997). As discussed in Section 3.3, spatial and/or temporal zonation of broad-scale hydrothermal alteration and mineralisation styles are common characteristics of porphyry Cu systems (Lowell & Guilbert 1970; Sillitoe 2010). Zonation is produced through the gradation of factors such as temperature, salinity, pH and oxidation state within lithologies and across lithological boundaries (Reed 1997).

In addition to porphyry related alteration, the Yiddah prospect has been subjected to considerable post-mineralisation low-grade regional metamorphism, discussed further in Chapter Seven. Greenschist facies metamorphism typically produces alteration products similar to propylitic facies hydrothermal alteration in porphyry systems (chlorite, epidote ± albite and calcite) (Beane 1982; Beane & Bodnar 1995). During prograde metamorphism macroscale dissolution and mechanical mobilisation of base metal sulphides also occurs above temperatures from ~ 300 – 400 ºC at 2-3 kbar (Marshall & Gilligan 1987; Wagner et al. 2005). In addition to temperature, factors controlling mineralisation mobilisation include pressure gradients, chemical conditions, fluid/rock ratios, rock structure and rock porosity (Hobbs 1987; Cox et al. 1987).

In this chapter, petrographic observations (Appendix C), X-ray diffraction results (Appendix D) and electron microprobe analysis results (Appendix E) are integrated to describe the alteration, veining and mineralisation styles observed in the Yiddah prospect.

6.2. ALTERATION SUITES AND ZONING

In the three holes studied, four dominant alteration styles are recognised to be related to initial porphyry-style alteration. These are chlorite-magnetite, chlorite-sericite, sericitic and propylitic. Also, a late, pervasive ‘regional propylitic’ (deformation related) alteration style

overprints the above assemblages, along with a more localised, intense sericitic-argillic assemblage.

The chlorite-magnetite zone (Figure 6.1a,b) is best developed in the porphyry stocks and andesitic volcaniclastic material immediately overlying the basal fine-grained basaltic volcaniclastic unit. This assemblage consists of magnetite, chlorite, albite, quartz, sericite, epidote, rutile, titanite, pyrite and hematite. Alteration magnetite occurs as both pervasive fine-grained (10 – 100 μm) disseminations (Figure 6.1c) and within veins, ranging from vein 'trails', to neat, mineralised quartz-seam veins with associated quartz/magnetite flooding. In the latter case, magnetite grains may be significantly larger (to 500 μm). Alteration magnetite differs from primary (titano)magnetite commonly observed in the intrusive units in that it is generally more variable in size, anhedral in shape and less ragged in condition.

Magnetite alteration products and mineralised quartz-seam veins are typically observed within deep/core positions in porphyry systems. Along with K-feldspar and biotite, these products are characteristic of potassic-style alteration (Seedorff et al. 2005; Sillitoe 2010). If the chlorite-magnetite alteration zone at Yiddah is indeed indicative of porphyry copper style potassic alteration, then the altered porphyritic stocks would be the site of central, early and deep alteration in the Yiddah porphyry system. However, the main problem with this interpretation is the lack of K-feldspar and biotite within this alteration style at Yiddah. The lack of alteration K-feldspar at Yiddah may be due to an initial absence of K^+ ion metasomatism (possibly with an alternate deep sodic zone) or the later albitisation of K-feldspar products due to regional deformation.

In contrast to a lack of K-feldspar in the chlorite-magnetite alteration suite at Yiddah, there is some evidence of the former presence of biotite. One line of evidence is the occurrence of alteration chlorite grains displaying platy habits highly resemblant of non-chlorite micas (Figure 6.1d). Some of these crystals also display dislocation glide typical of deformed micas, with subsequent precipitation of rutile along glide planes. This process was described for chlorite altered biotite in the Miéville shear-zone, Switzerland by Kerrich et al. (1998). A second feature is very fine-grained reddish brown granules which are common spatially associated with amphibole pseudomorph chlorite aggregates, which may consist of fine-grained biotite, however may alternatively comprise fine-grained iron oxides (Figure 6.1e).

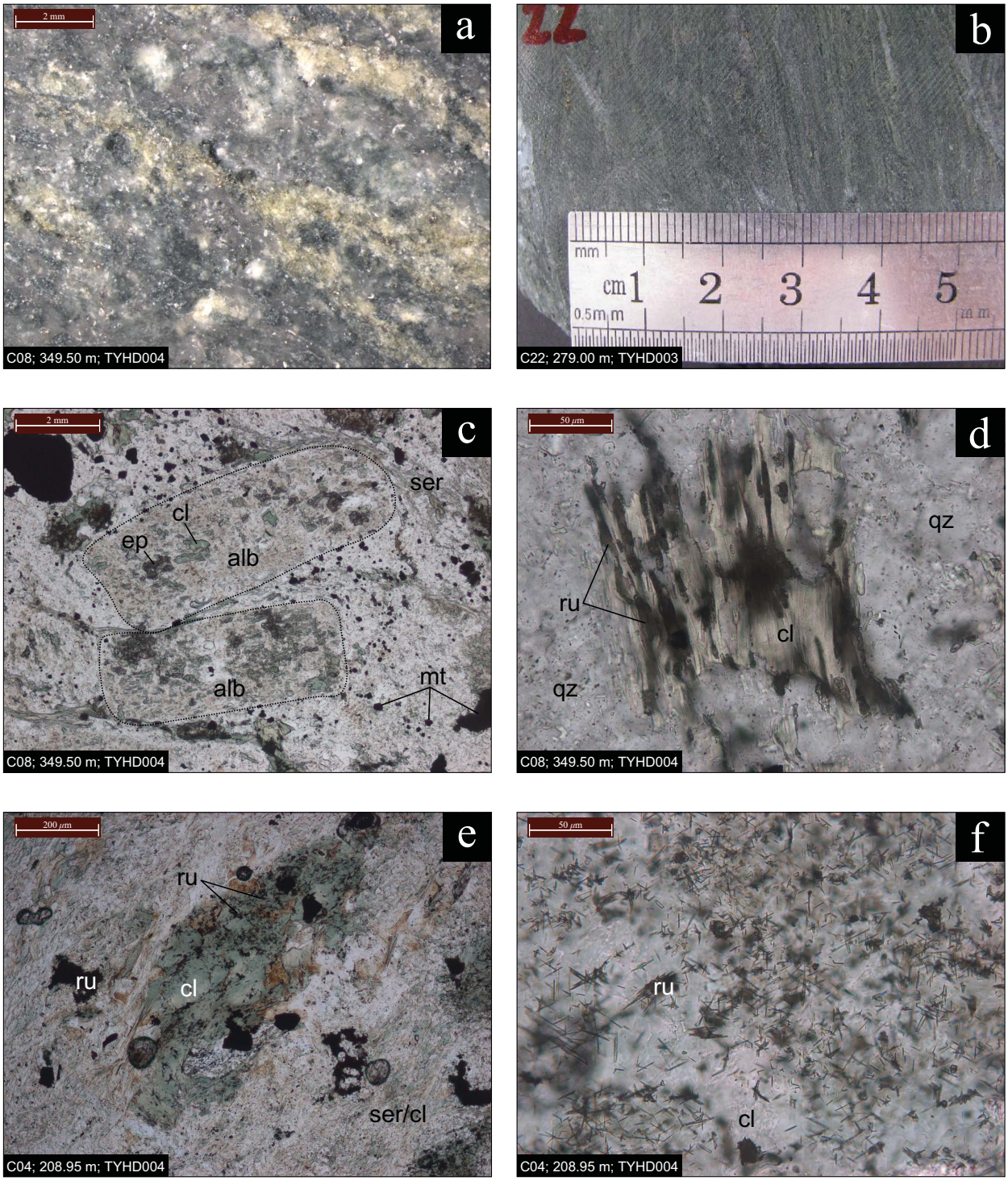

Fig 6.1: Chlorite-magnetite related alteration observed at Yiddah. (a) Hand specimen displaying representative chlorite-magnetite alteration in a porphyritic intrusive sample. (b) Hand specimen of chlorite-magnetite alteration in an andesitic volcaniclastic sample. (c) Disseminated magnetite in a porphyry intrusive sample; also possessing albitised feldspars, chlorite, sericite and epidote alteration products. Dashed lines surround albitised plagioclase phenocrysts. PPL. (d) Possible alteration biotite which has been further altered to chlorite, possessing a platy habit; with alteration rutile precipitating along cleavages. PPL. (e) Amphibole pseudomorph altered to biotite and subsequently chlorite, indicated by orientated rutile inclusions. Associated fine-grained brown material is probably either biotite or fine-grained iron oxides. PPL. (f) Higher magnification photomicrograph of orientated rutile in (e) PPL. alb = albite, cl = chlorite, ep = epidote, ser = sericite, mt = magnetite, qz = quartz, ru = rutile.

A third and stronger line of evidence for the former presence of biotite is the occurrence of asterisk-shaped inclusions of rutile oriented at ~ 60º to one another within pseudomorphous chlorite aggregates (Figure 6.1e.f), a phenomenon attributed by Shau et al (1991) to the formation of rutile during the breakdown of biotite controlled by the mutually parallel crystallographic planes possessed by biotite and rutile.

The pseudomorphous chlorite aggregates in which the asterisk-shaped rutile inclusions occur (e.g. Fig 6.1e) appear from their size and shape to be after primary igneous amphibole (see Section 4.4.1). Both amphibole and biotite expel rutile during alteration caused by the introduction of sulphur by the following respective equations (Mongkolip & Ashworth 1983; Force 1991):

$$\underset{\text{(hornblende)}}{Ca_2(Fe,Mg,Ti,Al)_5Si_7AlO_{22}(OH,F)_2} + \underset{\text{(sulphur)}}{S_2} \rightarrow \underset{\text{(actinolitic hornblende)}}{Ca_2(Mg,Fe)_5Si_8O_{22}(OH,F)_2} + \underset{\text{(pyrite)}}{FeS_2} + \underset{\text{(rutile)}}{TiO_2} + \underset{\text{(alumina)}}{Al_2O_3}$$

$$\underset{\text{(biotite)}}{K(Fe,Mg)_2(Fe,Al,Ti)Si_3AlO_{10}(OH,F)_2} + \underset{\text{(sulphur)}}{S_2} \rightarrow \underset{\text{(phlogopitic biotite)}}{K(Mg,Fe)_3Si_3AlO_{10}(OH,F)_2} + \underset{\text{(pyrite)}}{FeS_2} + \underset{\text{(rutile)}}{TiO_2}$$

As discussed above, rutile formed by the breakdown of biotite has the characteristic asterisk pattern, whereas that formed by amphibole alteration does not. Since the Yiddah pseudomorphous chlorite aggregates contain both 60º oriented rutile as well as randomly dispersed rutile inclusions, it is proposed here that biotite was in some cases an intermediate alteration product of amphibole alteration, and was itself subsequently altered to chlorite during regional greenschist-facies alteration and deformation.

The magnetite-chlorite zone grades upward into the pervasive chlorite-sericite zone (Figure 6.2a), which possesses similar alteration products to the former, but with lesser volumes of magnetite and greater volumes of sericite, carbonate and pyrite (Figure 6.2b,c,d). Feldspars are similarly albitised, yet are more intensely sericitised. White-micas are predominantly muscovite; however phengite, glauconite and lepidolite are also identified. Chlorite occurs in dense patches after amphibole and also variably throughout the groundmass, along with calcite and granular epidote, rutile and titanite. Various combinations of chlorite, carbonate, quartz and pyrite also comprise late but generally significantly deformed veins. With

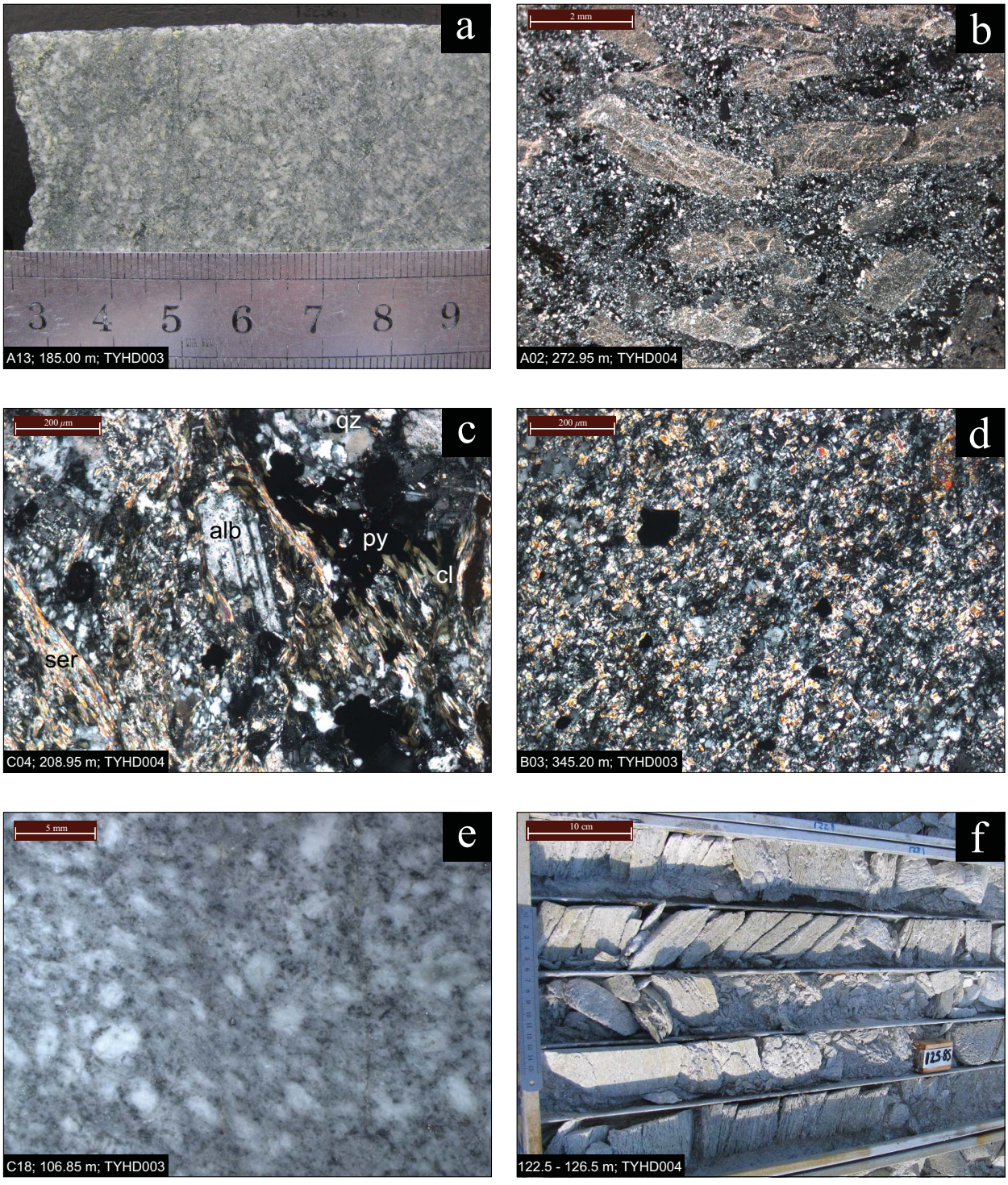

Figure 6.2: Chlorite-sericite to sericitic-argillic related alteration observed at Yiddah. (a) Hand specimen of representative chlorite-sericite alteration in a porphyritic intrusive sample. (b) Strongly sericitised feldspar phenocrysts in a matrix of alteration albite, chlorite, sericite, rutile and carbonate. XPL. (c) Chlorite-sericite altered porphyry intrusive sample displaying characteristic alteration products of this assemblage (ser = sericite, alb = albite, qz = quartz, py = pyrite, cl = chlorite). (d) Chlorite-sericite altered andesitic volcaniclastic sample, composed of similar (finer grained) products to those observed in the intrusive stock. (e) Sample gradational from chlorite – sericite to sericitic alteration zones. Significant sericite volumes give this rock a bleached appearance. (f) Tray overview of sericitic-argillic altered (quartz, sericite, kaolinite, pyrite) rocks of unknown primary lithology.

increasing abundances of sericite in this assemblage, these rocks develop a bleached appearance.

Further above the chlorite-sericite zone, sericitisation becomes much more intense, occurring as flood-like fine grains throughout the groundmass and covering feldspar phenocryst surfaces (Figure 6.2e). The volume of clay minerals, pyrite and quartz increases while the volume of chlorite decreases; indicative of more intense alteration conditions probably caused by higher fluid/rock ratios (Beane 1982). These products give rocks of the sericitic zone a white 'sheen-like' appearance and a relatively friable texture. These mineralogical trends intensify up-hole into the sericitic-argillic zone, where clay minerals (kaolinite and halloysite) become more abundant. X-ray diffraction results show the most intensely altered rocks sampled are composed almost entirely (> 95%) of quartz, sericite and kaolinite in roughly equal proportions, with minor volumes of chlorite and pyrite. These rocks are preserved very poorly and are generally very strongly foliated (Figure 6.2f). This assemblage cross-cuts and destroys mineralisation at Yiddah and is therefore considered to have formed during later regional deformation preferentially in the weaker (chlorite-sericite/sericitic) porphyry alteration assemblage (rather than constituting an argillic lithocap). Ar-Ar dating of micas from this zone would clarify this interpretation.

Propylitic alteration is typically developed at lower fluid/rock ratios, lower temperatures (~ 200 – 300 ºC) and distally to potassic and sericitic alteration zones (Sillitoe 2010). At Yiddah, the propylitic mineral assemblage consists of albite, epidote, chlorite, calcite, pyrite, hematite, quartz, rutile and sericite. This style is best developed within the basal fine-grained basaltic volcaniclastic unit and (more variably) within the Rain Hill Monzodiorite (Figure 6.3a,b). Lower fluid/rock ratios may have been experienced within the basaltic volcaniclastic unit due to its hornfelsed character, which is characterised by a reduced porosity due to the interlocking nature of secondary minerals. Fluid conduits in this unit range from narrow to very wide and voluminous veins; composed predominantly of epidote with lesser calcite and pyrite (Figure 6.3a,c). Similar veins also are observed within the Rain Hill Monzodiorite however these veins are generally more sinuous and do not develop to the equivalent widths of those observed within the basaltic volcaniclastic unit (Figure 6.3b,d).

Late, cross-cutting carbonate/quartz/chlorite filled tension gashes within propylitic zones suggest that propylitic-style alteration products were probably generated during both initial

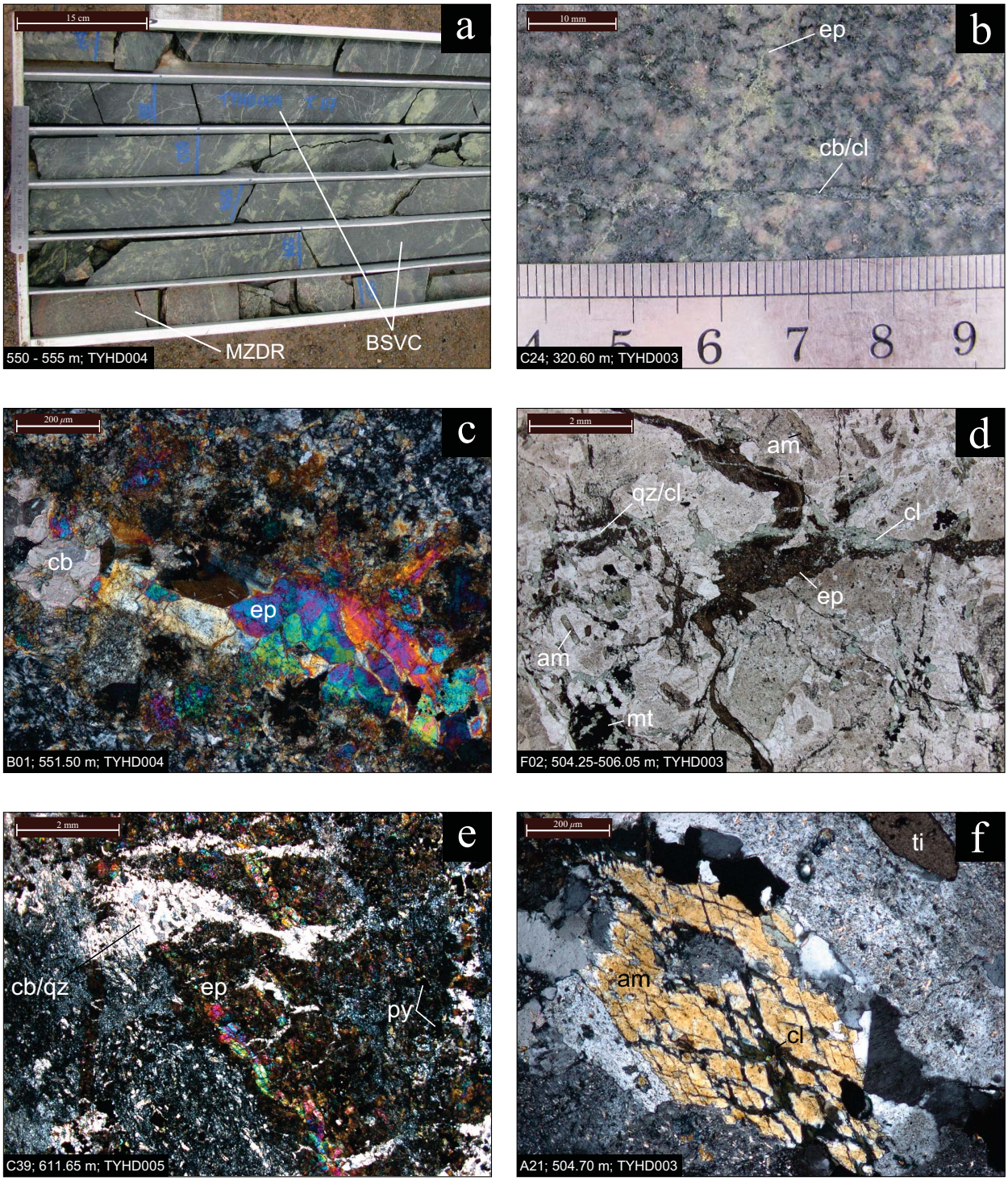

Figure 6.3: Propylitic style alteration observed at Yiddah. (a) Tray overview of propylitic alteration within the basaltic volcaniclastic (BSVC) and Rain Hill Monzodiorite (MZDR) units, displaying abundant epidote. (b) Hand specimen of the Rain Hill Monzodiorite containing epidote veining, hematite staining of feldspars, chlorite alteration of amphiboles and later crosscutting carbonate/chlorite veining. (c) Epidote/carbonate/pyrite vein within the basaltic volcaniclastic unit. XPL. (d) Sinuous fine-grained epidote vein within the Rain Hill Monzodiorite with minor crosscutting quartz, carbonate and chlorite. PPL. (e) Fine epidote veining with associated pyrite crosscut and offset by carbonate/quartz filled tension gashes. (f) Amphibole phenocryst altering to chlorite preferentially along basal cleavage planes. XPL. ep = epidote, cb = carbonate, cl = chlorite, qz = quartz, am = amphibole, mt = magnetite, py = pyrite, ti = titanite.

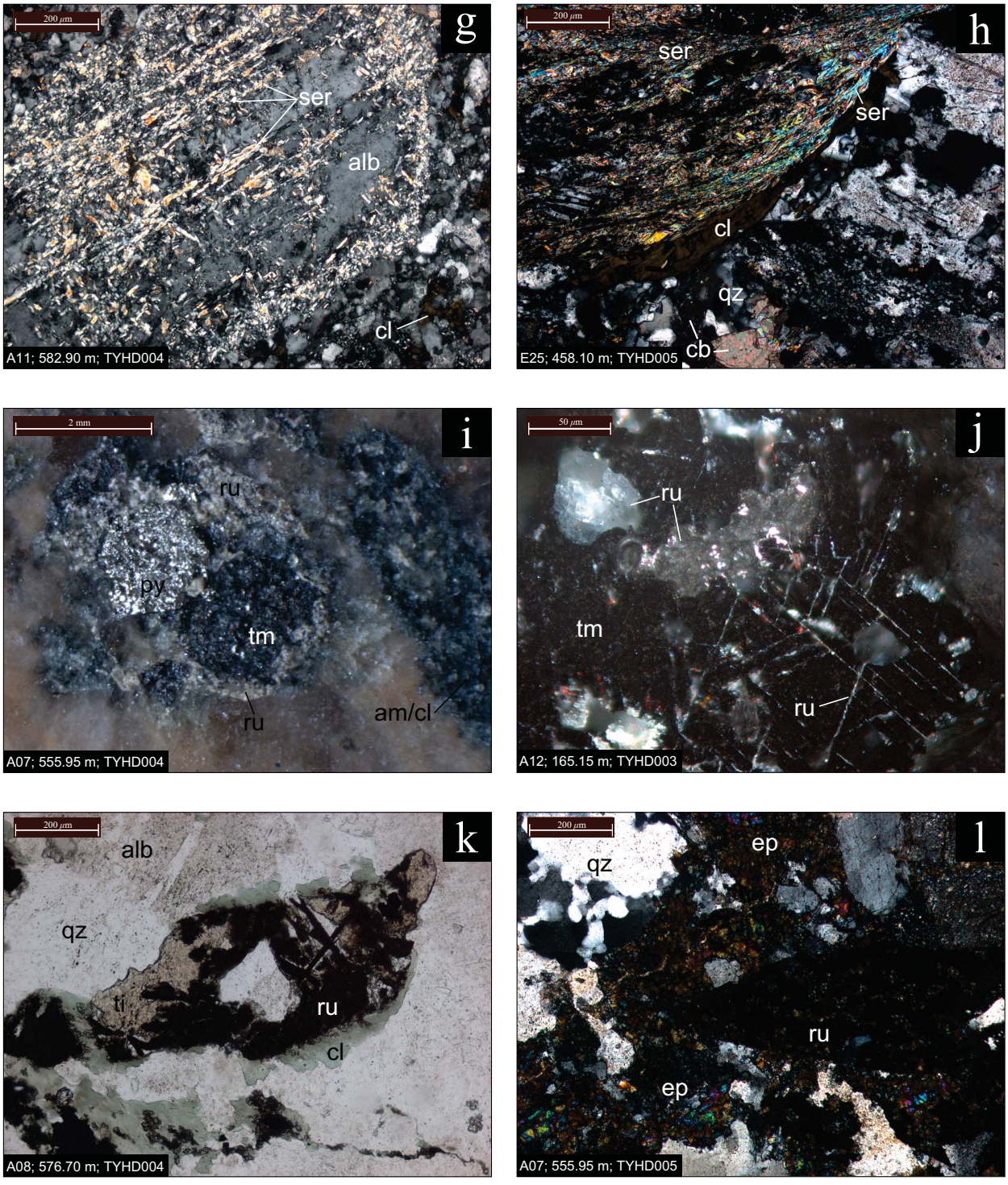

Figure 6.3 continued: Regional propylitic style alteration products. (g) Albitised feldspar phenocryst within a late porphyry intrusive displaying minor to moderate sericite alteration developed during regional deformation. (h) Syn-kinematic sericite and chlorite intergrown within the matrix of a porphyritic intrusive sample. XPL. (i) Hand specimen photograph of a magnetite crystal altering to rutile and pyrite, contained within a late dyke of the Rain Hill Monzodiorite. (j) Magnetite crystal altering to rutile along cleavages. Cross polarised reflected light (non-polished section). (k) Titanite phenocryst altering to rutile within a late dyke of the Rain Hill Monzodiorite. (l) Alteration epidote, quartz and rutile (after titanite) within a late dyke of the Rain Hill Monzodiorite. ser = sericite, alb = albite cl = chlorite, qz = quartz, cb = carbonate, py = pyrite, ru = rutile, tm = titanomagnetite, am = amphibole, ti = titanite, ep = epidote.

porphyry-related hydrothermal alteration and later regional deformation (Figure 6.3e). These alteration products are common in varying abundances in all alteration suites, indicating that a 'regional-propylitic' (deformational) assemblage overprints the prospect. The most ubiquitous forms of alteration are the chloritisation of ferromagnesian minerals (Figure 6.3f) and the albitisation and sericitation of feldspars (Figure 6.3g). Intergrown syn-kinematic (aligned) chlorite and sericite fibres are also very common throughout the groundmass of samples from across the prospect (Figure 6.3h), along with granular fine-grained to coarser replacement epidote. Turbid brown granular rutile is commonly observed within and flanking amphibole pseudomorphs (chlorite), titanomagnetite and titanite. Titanomagnetite expels rutile on its margins and within cleavages via reaction (1) (Figure 6.3i,j) while titanite alters to rutile and calcite in the presence of a carbonate-rich fluid via reaction (2) (Figure 6.3k,l) (Force 1991). In each case, rutile appears to possess a close spatial association with the parental mineral.

$$\underset{\text{(titanomagnetite)}}{2(Fe,Ti)_3O_4} + \underset{\text{(sulphur)}}{S_2} \rightarrow \underset{\text{(magnetite)}}{Fe_3O_4} + \underset{\text{(pyrite)}}{FeS_2} + \underset{\text{(rutile)}}{TiO_2} \qquad (1)$$

$$\underset{\text{(titanite)}}{CaTiSiO_5} + \underset{\text{(carbon dioxide)}}{CO_2} \rightarrow \underset{\text{(rutile)}}{TiO_2} + \underset{\text{(calcite)}}{CaCO_3} + \underset{\text{(quartz)}}{SiO_2} \qquad (2)$$

The spatial configuration of the alteration suites described above as evident in the three holes studied is summarised in Figure 6.4, Figure 6.5 and Figure 6.6. It is evident that rather than the concentric zonation patterns described in traditional porphyry models such as that of Lowell & Guilbert (1970), patterns of alteration zoning in the recognised mineralised zone at Yiddah are asymmetrical. This may be due to the contrasting permeability of the basaltic volcaniclastic and andesitic volcaniclastic units as considered above. The likely lesser porosity of the hornfelsed basaltic volcaniclastic unit may have resulted in lower fluid/rock ratios both within this unit and the within the underlying Rain Hill Monzodiorite, generating the dominant propylitic style of alteration observed. Conversely, in the andesitic volcaniclastic unit, greater porosity may have enabled higher fluid/rock ratios, resulting in greater degrees of porphyry-related alteration.

An alternative explanation may be that post-emplacement deformation has resulted in the realignment of porphyry stocks to more energetically favourable positions (parallel to the dominant foliation and regional north-northwest trends), such that the spatial relationship between any such primary alteration zonation and sills/stocks has been largely modified.

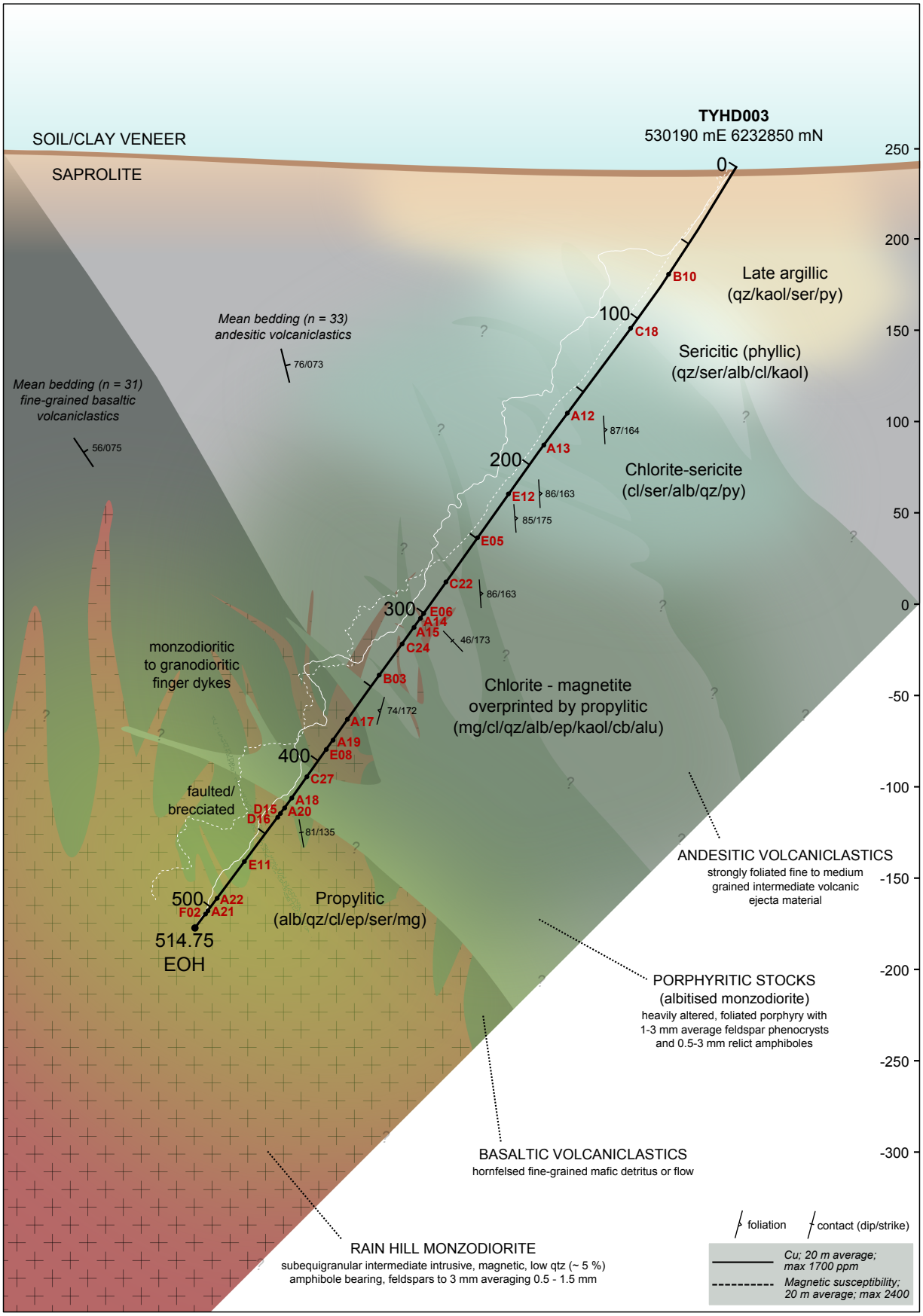

Figure 6.4: Cross-sectional representation of diamond-hole TYHD003 (530190 mE 6232850 mN) displaying the spatial arrangement of lithologies and alteration suites.

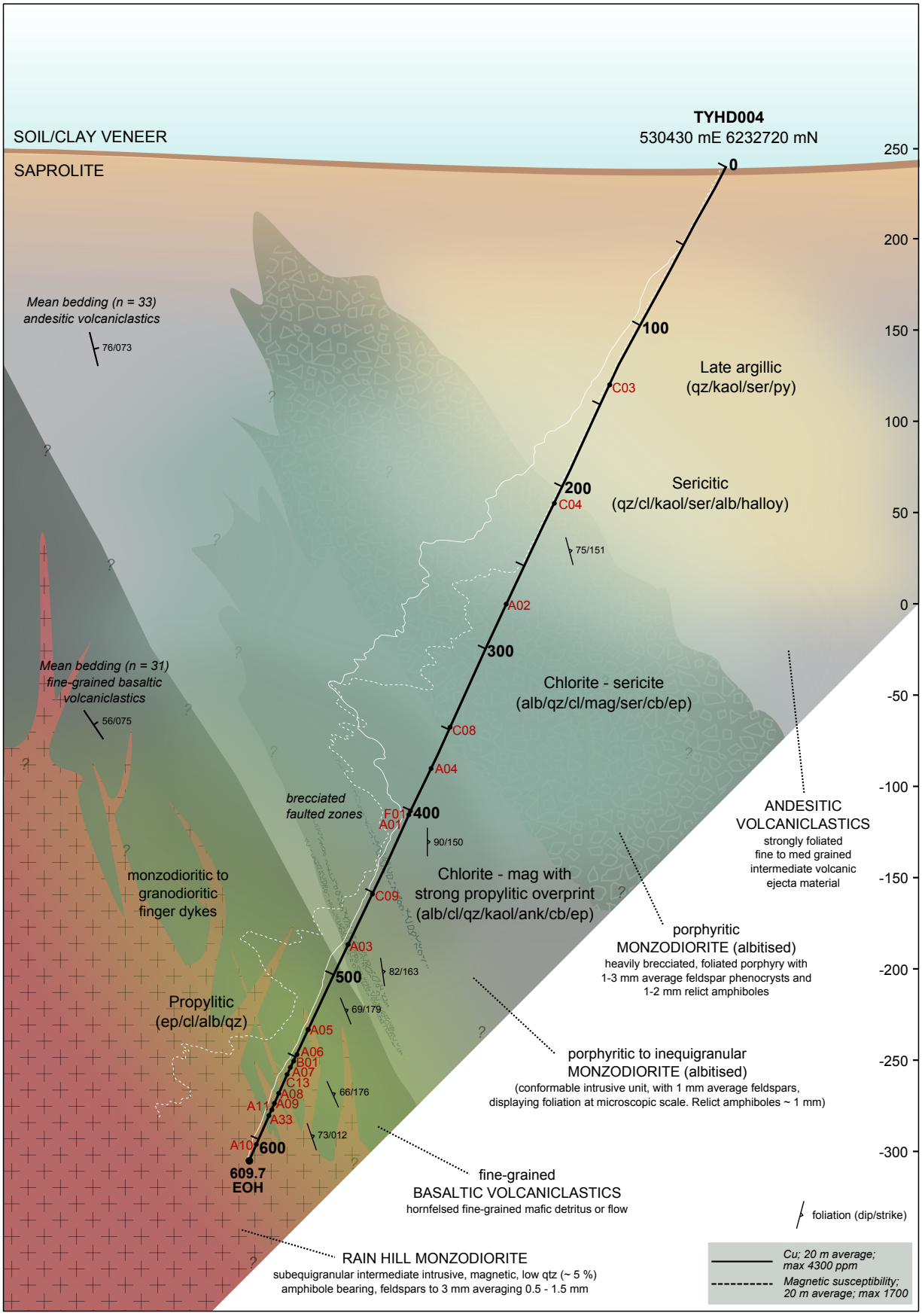

Figure 6.5: Cross-sectional representation of diamond-hole TYHD004 (530430 mE 6232720 mN) displaying the spatial arrangement of lithologies and alteration suites.

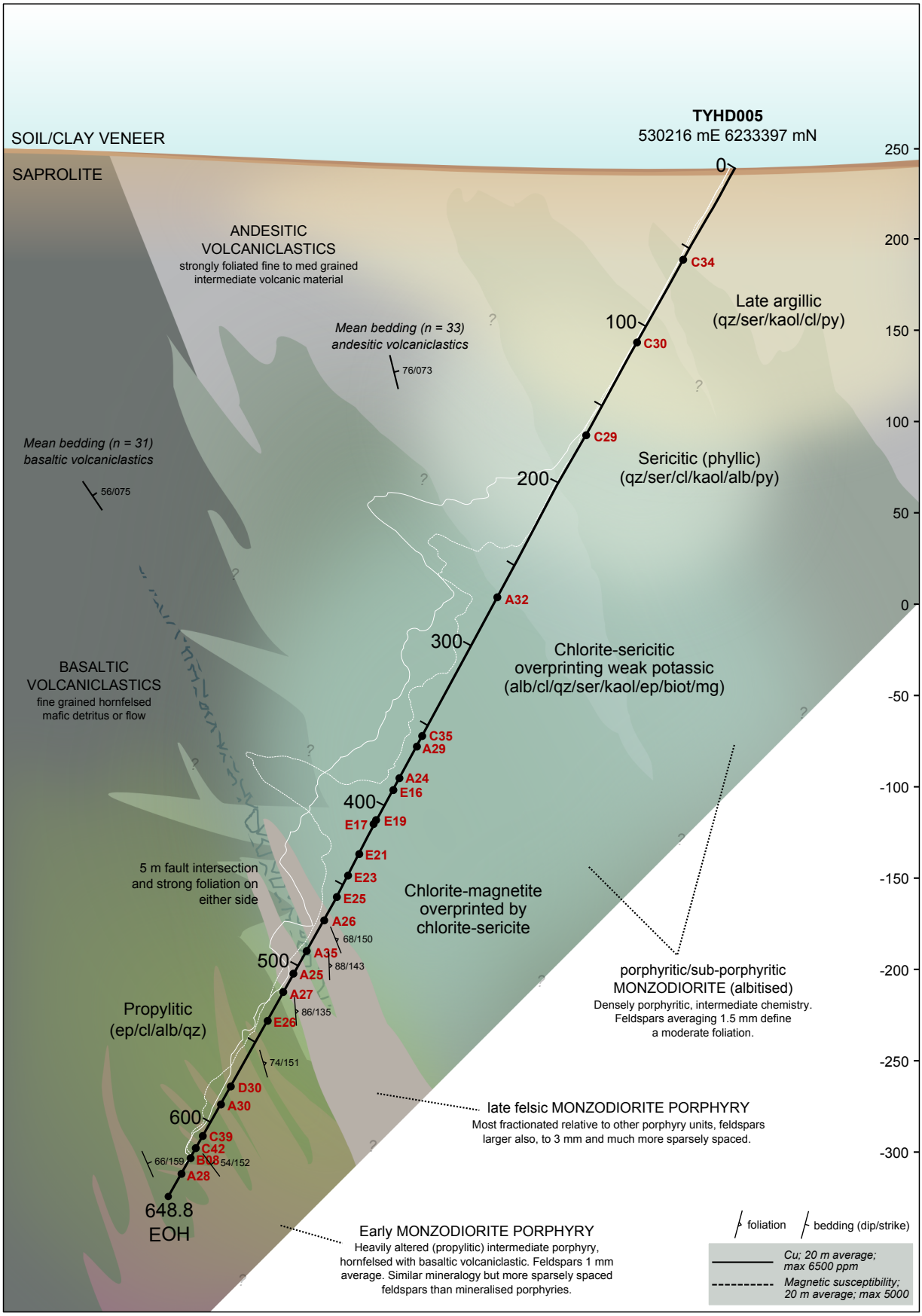

Figure 6.6: Cross-sectional representation of diamond-hole TYHD005 (530216 mE 6233397 mN) displaying the spatial arrangement of lithologies and alteration suites.

6.3. **MINERALISATION TEXTURES**

Cu and Mo mineralisation at Yiddah occurs as both disseminated and vein hosted sulphides, in both porphyry-related and remobilised mineralisation styles. The only Cu-sulphide species apparent in the three holes observed is chalcopyrite. No Au was observed in hand specimen or thin section, reflecting its low-grade and finely disseminated nature.

As aforementioned, quartz-seam veins are associated with the early chlorite-magnetite alteration zone. These features occur within all lithologies and are typically 0.5 – 2 cm in width, consisting of crystalline, interlocking quartz (to ~ 2 mm) healed centrally by magnetite, pyrite, chalcopyrite and minor molybdenite (Figure 6.7a-f). Molybdenite mineralisation additionally occurs on fracture surfaces, which may represent early veins which have faulted preferentially due to the layered structure of molybdenite (Figure 6.7g). A number of seam-veins also contain central calcite, epidote and chlorite; however cross-cutting textures suggest these minerals were probably emplaced during later deformation (Figure 6.7c). Molybdenite and magnetite may also occur on the outer margin of these veins (Figure 6.7b), emplaced early in the vein paragenesis with subsequent inward growth of quartz and latest crystallisation of chalcopyrite. The volume of chalcopyrite in the seam varies considerably as a proportion of the overall vein (*cf.* Figure 6.7a and Figure 6.7b).

Within these seam-veins, pyrite is generally well-preserved and cubic in habit, while chalcopyrite is more pitted and blebby. Both pyrite and chalcopyrite often contain inclusions of one another, suggesting their emplacement occurred contemporaneously. A shard-like habit is observed for molybdenite aggregates (Figure 6.7f), which occur texturally either before or contemporaneously to chalcopyrite. Chalcopyrite also occurs to varying abundances in vein selvedges, which are generally insignificant in the Rain Hill Monzodiorite but larger in the more intensely altered andesitic volcaniclastics and porphyritic stocks. In these units, the ‘quartz-seam’ style of mineralisation generally is replaced by a more pervasive quartz/magnetite ‘flooding’, containing disseminated chalcopyrite (Figure 6.7h,i).

In addition to early quartz veining, later porphyry-related quartz/pyrite/carbonate veins are relatively common, predominantly within the chlorite-sericite alteration zone. These veins do not contain visible mineralisation; however in one sample examined, minor chalcopyrite was contained as blebs within pyrite (Figure 6.7j).

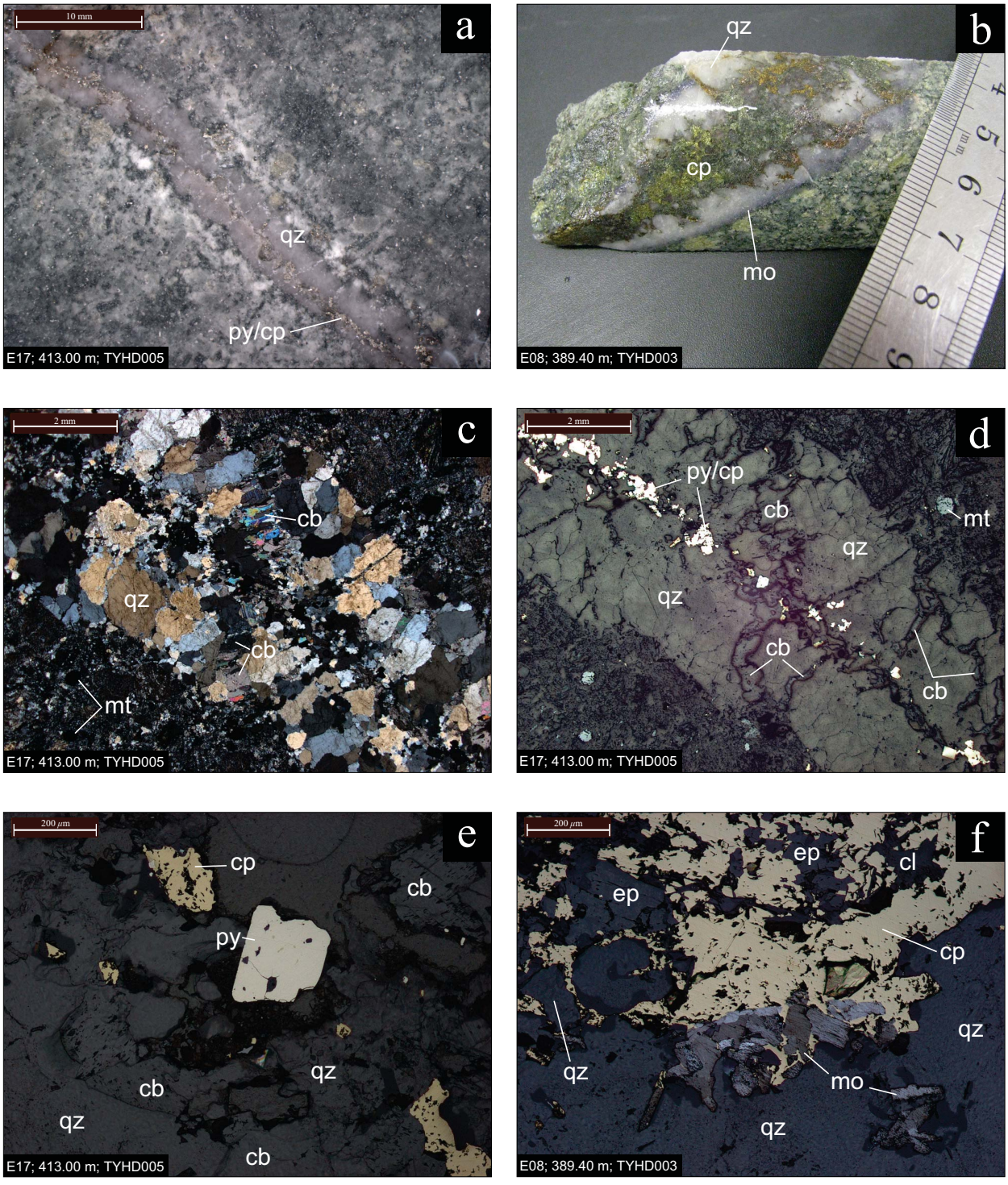

Figure 6.7: Mineralisation and veining related features at Yiddah. (a) Quartz-seam vein contained within a porphyritic stock, possessing a moderate sericite alteration selvedge and post-emplacement carbonate filled deformation fractures. (b) Large, neat quartz-seam vein contained within the Rain Hill Monzodiorite with molybdenite evident on the margins and voluminous chalcopyrite in the seam. Note the abrupt vein margin. (c) Photomicrograph of (a), displaying the crystalline nature of quartz and a cross-cutting carbonate tension gash. XPL. (d) Plane polarised reflected light photomicrograph of (c). (e) Higher magnification photomicrograph of (d) displaying the blebby and pitted texture of chalcopyrite contained within the seam, and the cubic habit of pyrite. The central pyrite crystal contains minute chalcopyrite inclusions while the chalcopyrite grain in the upper left possesses a small pyrite inclusion on its left margin. Plane polarised reflected light. (f) Chalcopyrite and molybdenite mineralisation contained proximally to the margin of the seam vein in (b). Shard-like molybdenite occurs texturally before blebby chalcopyrite, intergrown with quartz, epidote and chlorite gangue. Plane polarised reflected light. ser = sericite, qz = quartz, py = pyrite, cp = chalcopyrite, mo = molybdenite, cb = carbonate, mt = magnetite, ep = epidote.

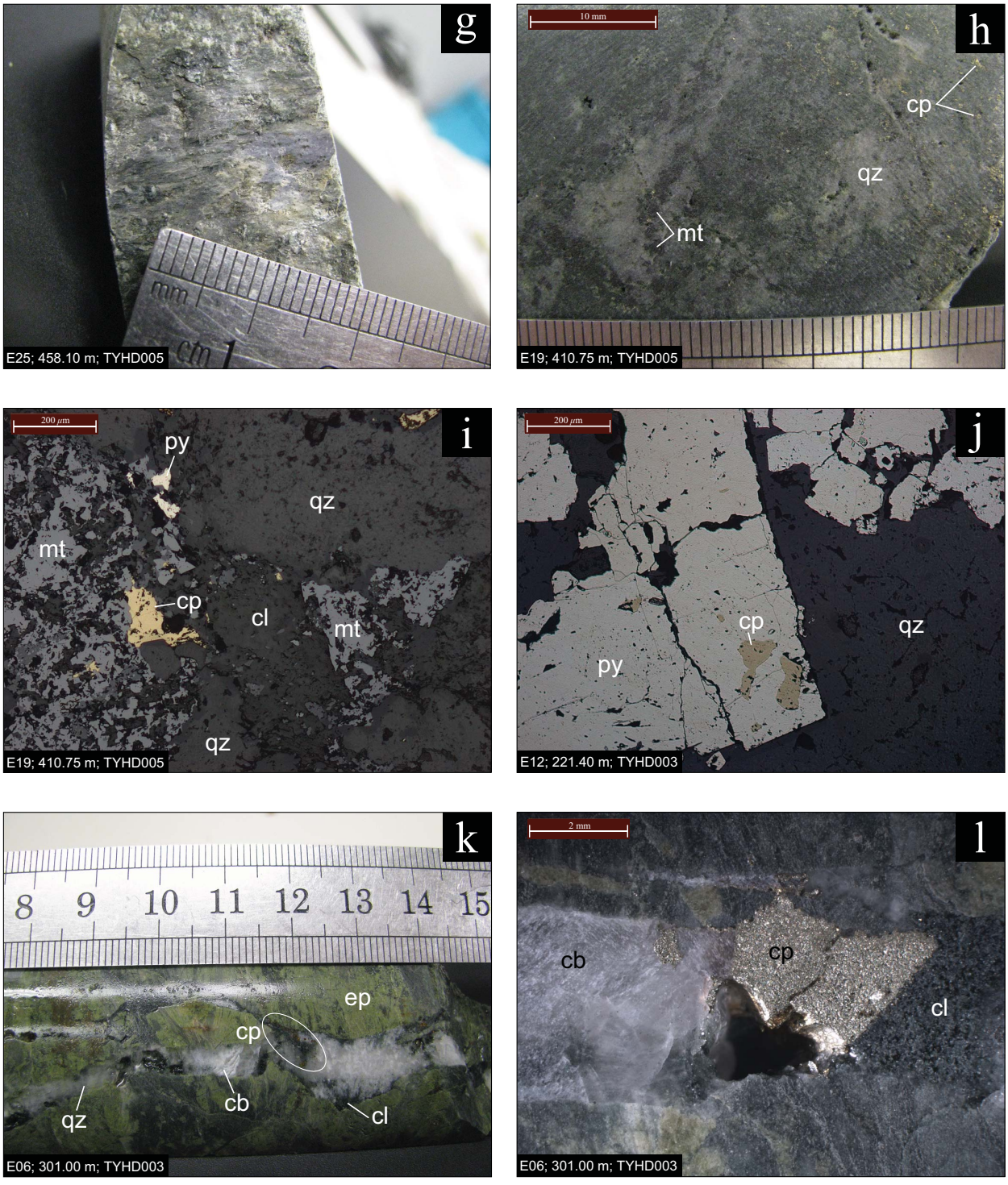

Figure 6.7 continued: (g) Molybdenite coating a fracture surface of a porphyritic intrusive sample. (h) Quartz-magnetite 'flooding' and disseminated chalcopyrite associated with a quartz vein (bottom right) in a porphyritic stock. (i) Photomicrograph of (h) displaying contemporaneous chalcopyrite, pyrite and magnetite within quartz gangue. Plane polarised reflected light. (j) Chalcopyrite contained as an inclusion within fractured cubic pyrite emplaced in a quartz-pyrite-carbonate vein of the chlorite-sericite alteration assemblage. Plane polarised reflected light. (k) Deformation related carbonate/quartz/chlorite/chalcopyrite tension gash cross-cutting intensely epidote altered volcaniclastic material. (l) Massive chalcopyrite contained within a carbonate/quartz/chlorite tension gash. The vug likely contained chlorite which is often weathered out due to surface exposure, revealing euhedral quartz and calcite habits (not observed in this sample). mt = magnetite, qz = quartz, cp = chalcopyrite, py = pyrite, cl = chlorite, ep = epidote, cb = carbonate.

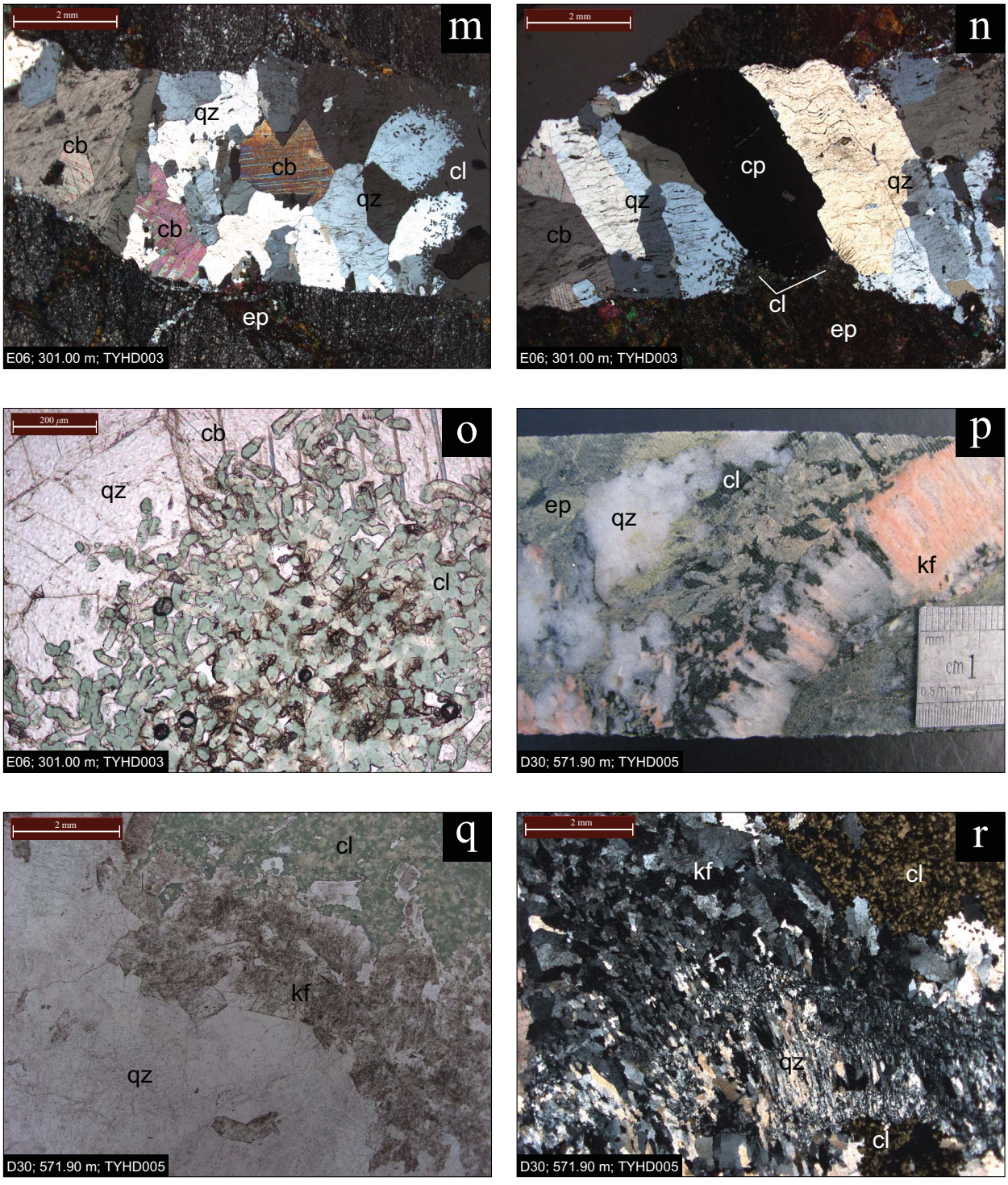

Figure 6.7 continued: (m) Crystalline carbonate and quartz contained within a late tension gash along with granular chlorite (right of field). Note the sharp vein contacts cross-cutting the chlorite-epidote altered host rock. XPL. (n) Massive chalcopyrite and stressed, deformed quartz within with same vein as (m). XPL. (o) 'Worm-like' or 'booklet' habit typical of granular chlorite crystallised into space within the tension gashes at Yiddah. PPL. (p) 'Cocks-comb' texture displayed by intergrown quartz, K-feldspar, chlorite and minor carbonate. Note the less distinct (more 'mushy') margins of this vein. (q) Plane polarised photomicrograph of quartz, K-feldspar and chlorite contained in (p). K-feldspar displays a reddish/brown speckled appearance due to hematite staining. (r) Cross polarised photomicrograph of elongate, intergrown syn-kinematic quartz and feldspar within (p). cb = carbonate, qz = quartz, cl = chlorite, ep = epidote, kf = K-feldspar.

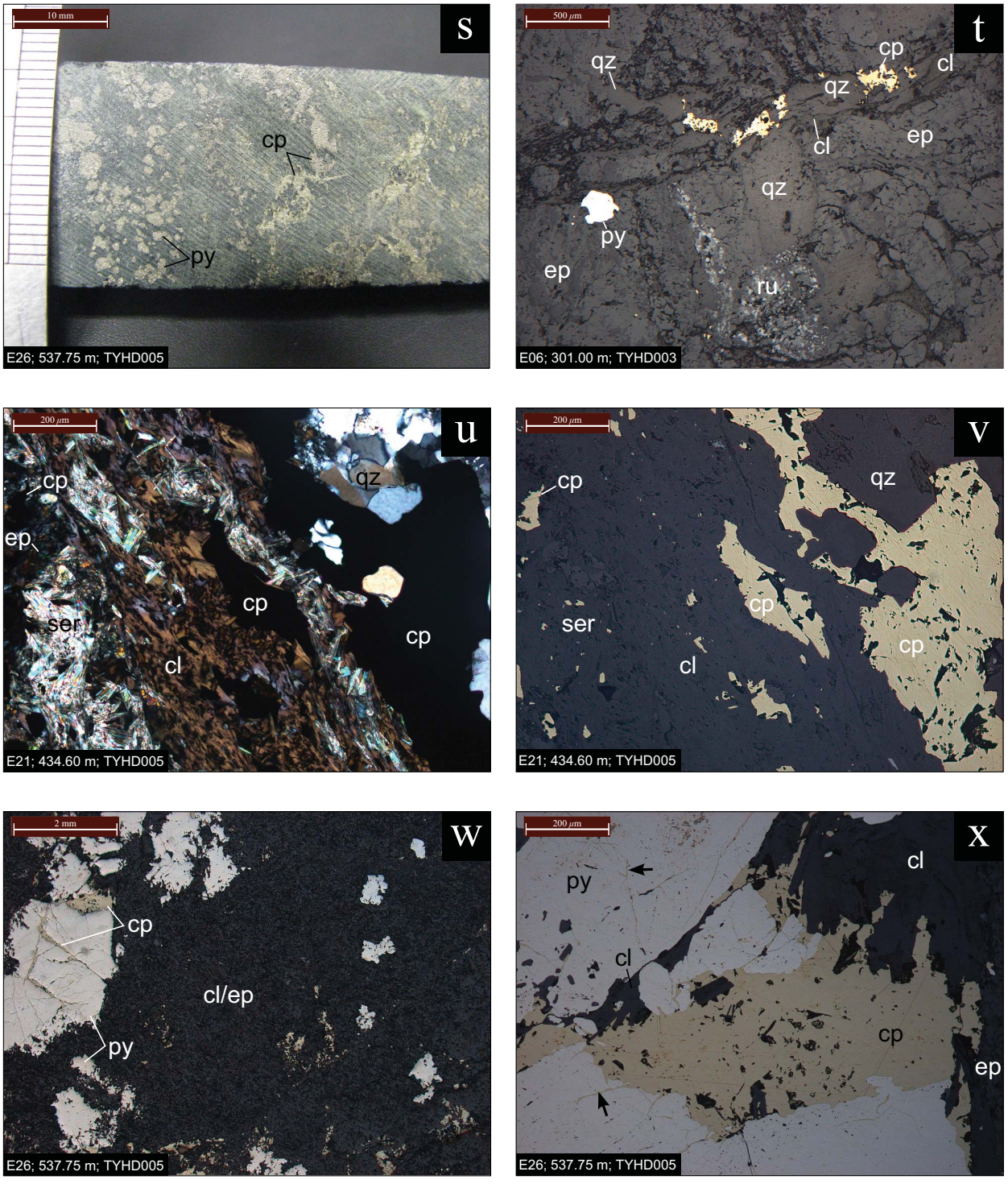

Figure 6.7 continued: Textural features associated with remobilisation of mineralisation. (s) 'Stringy' remobilised chalcopyrite and more globular to subrounded pyrite contained within a highly chlorite-epidote altered sample of the fine-grained basaltic volcaniclastic unit. (t) Quartz/chlorite conduit containing remobilised chalcopyrite. The host rock is strongly chlorite-epidote altered. Plane polarised reflected light. (u) Intergrown recrystallised chalcopyrite, sericite, quartz and iron-rich chlorite contained within a highly chloritised porphyry stock sample. XPL. (v) Reflected light photomicrograph of (u), highlighting the intergrown texture of chalcopyrite and chlorite/sericite/ quartz gangue minerals. Plane polarised reflected light. (w) Disseminated pyrite and minor remobilised chalcopyrite, contained within (s). Note the presence of chalcopyrite infilling pyrite fractures. Plane polarised reflected light. (x) Higher magnification photomicrograph of a fractured pyrite crystal possessing infilling recrystallised chalcopyrite (arrows). Plane polarised reflected light. cp = chalcopyrite, py = pyrite, qz = quartz, ep = epidote, ru = rutile.

As is the case with alteration assemblages, primary porphyry-related mineralisation at Yiddah has been strongly affected by overprinting shear-related deformation.

The most obvious evidence of this process is the occurrence of large clots of chalcopyrite in late, cross-cutting tension gashes which are relatively common to decimetre widths (Figure 6.7k-n). In addition to crystalline chalcopyrite, these veins contain coarse-grained quartz, calcite and dense aggregates of finer-grained chlorite. Quartz and calcite crystals range to 5 mm in diameter, while chlorite grains typically average ~ 30 μm in width, range up to 300 μm in length and occur in clumps of similar dimensions to other vein components. The platy 'booklet' habit of chlorite (Figure 6.7o) suggests it has crystallised into open space, either contemporaneously to deformation or following the dissolution of an alternate vein-fill mineral component.

Late infill veins are generally slightly sinuous, possessing sharp contacts, without selvedges. Some syn-kinematic veins however possess less distinct margins, with one example containing intergrown quartz, chlorite and K-feldspar (adularia) in a 'cocks-comb' texture (Figure 6.7p-r). K-feldspar contained within these veins is pink, due to the incorporation of very fine-grained hematite. Carbonate within these late veins also often possesses a light pink hue, which may be due to the incorporation of minor amounts of Mn.

Chalcopyrite occurring throughout the groundmass of all units at Yiddah commonly possesses textures indicative of remobilisation. These textures include a 'stringy' appearance in hand specimen and thin section; and intergrowth with chlorite and sericite in fluent, aligned aggregates. (Figure 6.7s-v). These microveinlets are the probable source conduits for macroscale tension-gash infill veins. Other associated minerals are commonly pyrite, epidote, quartz and rutile; characteristic of the overprinting deformation-related alteration assemblage. Remobilised pyrite and chalcopyrite analysed by electron microprobe in sample E05 (250.50 m; TYHD003) contained no Au, suggesting that Au mineralisation occurs as free Au or possibly was liberated from sulphides during remobilisation.

Pyrite does not display the equivalent remobilisation textures as described for chalcopyrite. Rather, much of the (porphyry related) pyrite situated proximally to remobilised chalcopyrite possesses fine-scale fractures, often filled with chalcopyrite (Figure 6.7w,x). These textures

suggest that pyrite has not undergone chemical remobilisation subsequent to porphyry system formation. This contrast in sulphide behaviour can be explained by the difference in temperature necessary to generate syn-kinematic recrystallisation of the two sulphide species. This process occurs in chalcopyrite from ~ 300ºC, whilst not until ~ 550ºC is reached for pyrite. Below 450ºC, cataclasis of pyrite is considered to dominate (Marshall & Gilligan 1987). This suggests that temperatures obtained during regional deformation of the Yiddah porphyry prospect were broadly within the range of 300 – 450ºC, where pyrite undergoes fracturing and chalcopyrite may recrystallise simultaneously.

As primary porphyry-related and remobilised mineralisation styles are observed in close spatial association at Yiddah, it is not considered that shear-related remobilisation of mineralisation was effective in transporting chalcopyrite on a large spatial scale.

6.4. MINERALISATION ZONATION

Associations between alteration assemblages, host lithologies and mineralisation grades have been explored by linking pre-existing assay data (Cu, Mo and Au grades) collected at 1 m intervals across the Yiddah prospect with corresponding alteration and lithology information extracted and interpreted from diamond hole logging provided by Goldminco Corporation.

Analysis of Variance (ANOVA) tests performed on the substantial resulting dataset (n = 4981) using JMP statistical software (v. 7.0.2) show that Cu grade varies significantly with alteration style at Yiddah ($F_{3,4980} = 458.7$, $P < .0001$). Cu mineralisation is greatest within the chlorite-magnetite and chlorite-sericite alteration zones; while average Cu values within the propylitic and overprinting sericitic-argillic alteration zones are much lower (Figure 6.8). Cu grade also varies significantly with host lithology ($F_{3,4980} = 50.0$, $P < .0001$), with the andesitic volcaniclastics and porphyry stocks containing significantly higher Cu concentrations than the Rain Hill Monzodiorite and basaltic volcaniclastic units.

Au grades display broadly similar trends to Cu, with significant variations identified between both Au and alteration assemblage ($F_{3,4980} = 44.3$, $P < .0001$) and Au and host lithology ($F_{3,4980} = 253.9$, $P < .0001$). As with Cu, the chlorite-magnetite and chlorite-sericite alteration

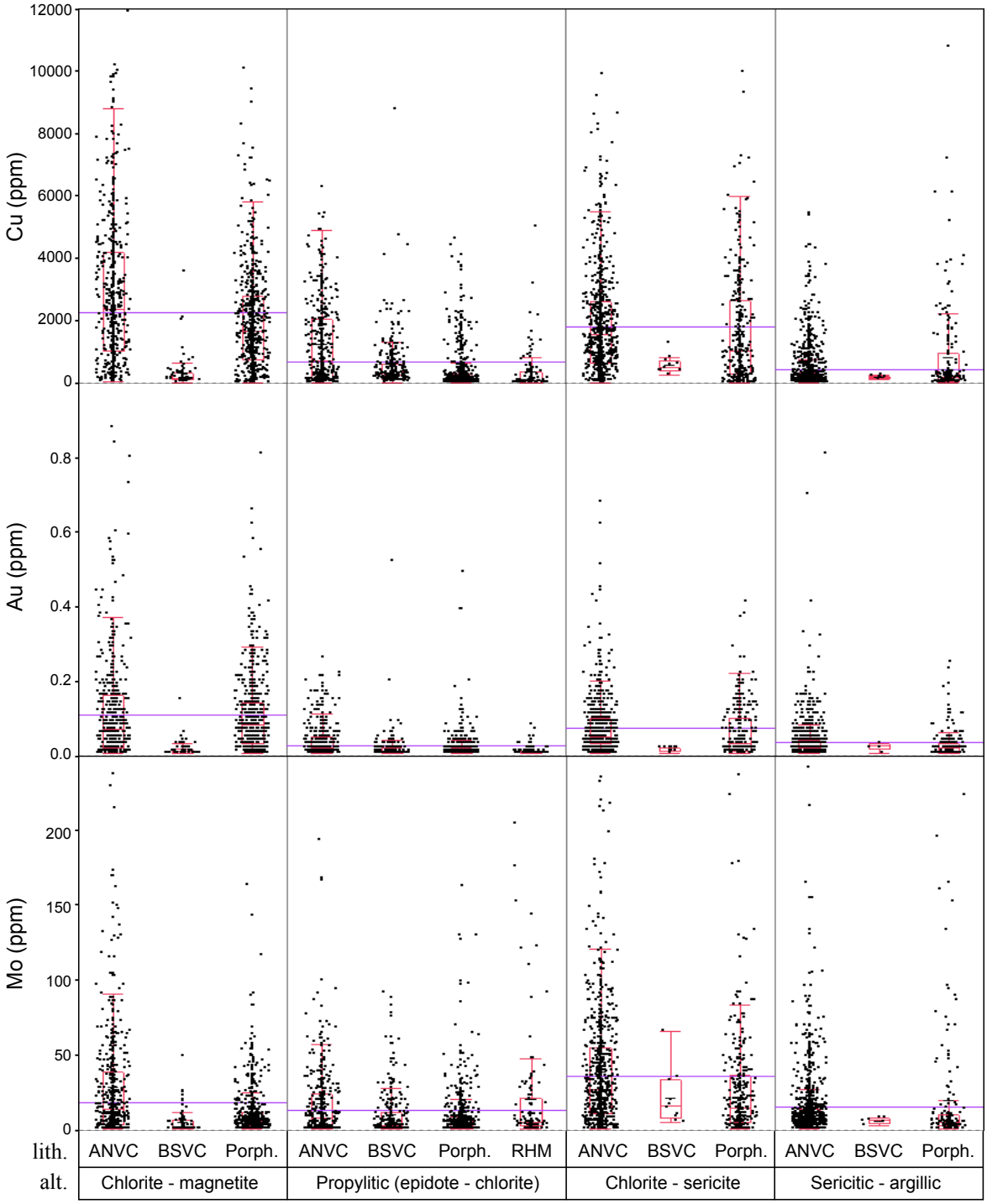

Figure 6.8: Box and whisker 'jitter' plots of Cu, Au and Mo assay grades at Yiddah; divided and grouped by lithology and alteration types. Each dot represents a 1 m drill core intersection (Goldminco Corporation assay data; *n* = 4981). Data from all holes were included where rock and alteration type could be confidently assigned from company logging. Large outlier values were excluded to enable effective scaling of the y-axis to capture the majority of datum points. Purple lines indicate group means. ANVC = Andesitic volcaniclastics; BSVC = Basaltic volcaniclastics; Porph. = porphyritic stocks; RHM = Rain Hill Monzodiorite.

zones contain the highest average Au grades, along with the andesitic volcaniclastic and porphyry stock lithologies.

Mo grades at Yiddah also vary significantly with alteration assemblage ($F_{3,4980} = 124.6$, $P < .0001$) and host lithology ($F_{3,4980} = 124.6$, $P < .0001$); however they differ to Cu and Au in that the chlorite-sericite alteration zone contains the highest average Mo mineralisation, while concentrations of Mo within the chlorite-magnetite, propylitic and sericitic-argillic zones are roughly equivalent. This variation in alteration association is further reflected by the relatively weak correlation observed between Cu and Mo compared to that of Cu and Au (Figure 6.9).

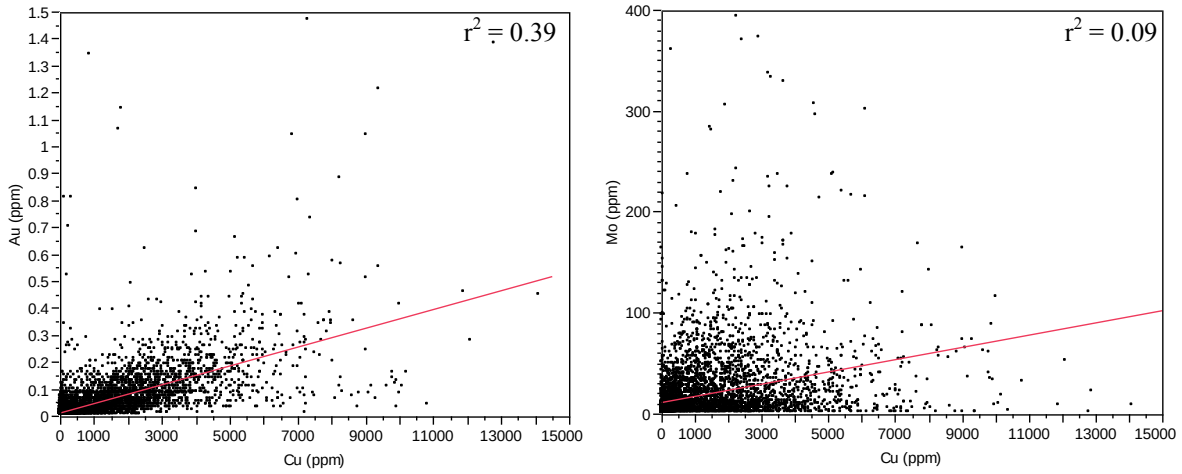

Figure 6.9: Bivariate plots of mineralisation grades at Yiddah, highlighting the moderately well-correlated nature of Cu and Au grades and relatively weak correlation of Cu and Mo. *n* = 4981.

On the basis of these trends and spatial associations, mineralisation zonation at Yiddah can be summarised as consisting of a central Cu-Au dominated zone associated with chlorite-magnetite alteration, which grades upward to a chlorite-sericite alteration zone containing substantial (yet lower) Cu and Au, and increased Mo. Decreasing Cu:Mo and Au:Mo ratios occurring with upward movement from the early chlorite-magnetite zone are similar to trends described at E26 (Goonumbla) by Radclyffe (1995), who found that Mo concentrations increased outward erratically from the high Cu grade zone over ~ 400 m. Above the chlorite-sericite zone, shearing related to later deformation is likely to have developed preferentially within the marginal (porphyry-related) sericitic alteration zone, which has produced argillic assemblage alteration products and cross-cut mineralisation.

CHAPTER SEVEN

STRUCTURE

7.1. INTRODUCTION

Regional structures associated with porphyry deposits are recognised to play significant roles in the localisation of intrusions and the creation of dilational environments that may host mineralisation (Hildreth & Moorbath 1988). On a deposit scale, structural features of preferred orientation are generally related to the release of mechanical energy with fluid exsolution in the form of quartz stockworks or sub-parallel sheeted arrays (Burnham 1979; Sillitoe 2010).

By virtue of their collisional margin settings and the apparent association between regional structures and mineralisation, many porphyry systems display evidence of post-mineralisation deformation. In the Macquarie Arc, this is particularly pertinent due to the relatively ancient age of lithologies and their exposure to numerous orogenic events. The ability of deformational activity to mobilise and redistribute mineralisation is a further consideration; as observed both at Yiddah on a small spatial scale (Chapter Six) and at Gidginbung, where the development of a rheologically distinct shear-related advanced argillic alteration zone is thought to have focused mineralised hydrothermal fluids (Allibone et al. 1995).

7.2. REGIONAL STRUCTURE

Due to very poor outcrop in the Rain Hill district, interpretation of regional geology and structural patterns has been undertaken using regional and local gravity imagery in conjunction with information gained from exploration drilling.

7.2.1. Aeromagnetics

The Gidginbung Volcanics appear in aeromagnetic imagery as a discrete, elongate, curvilinear north-northwest striking package of relatively high magnetic intensity, bounded by regions of lower magnetic intensity to the west and east (Figure 7.1a). This appearance is broadly consistent with other volcanic piles in the Macquarie Arc (Mowat & Smith 2006). The western margin of the Gidginbung Volcanics consists of a sharp contact which

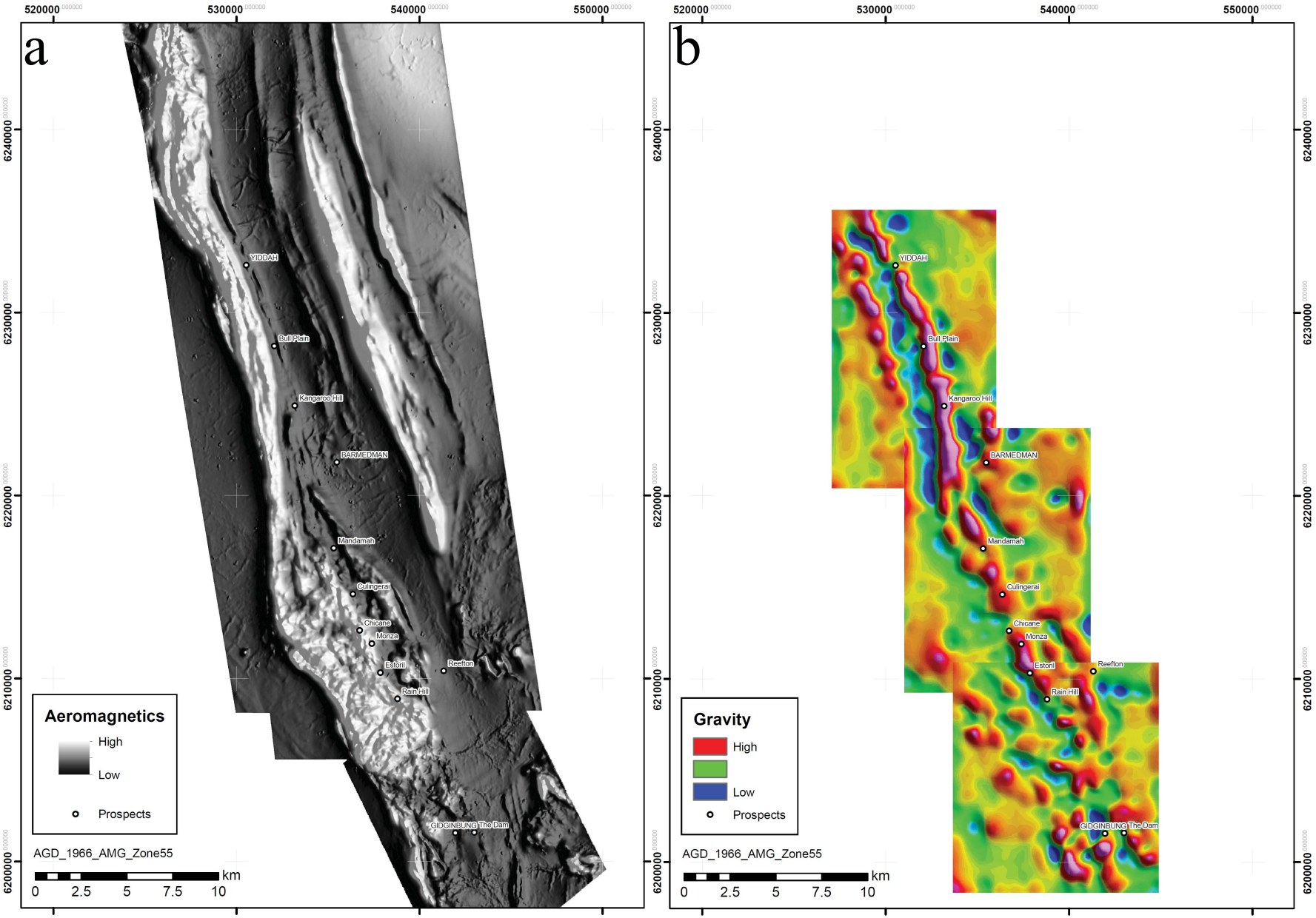

Figure 7.1: (a) Grey-scale continuous reduced-to-pole aeromagnetic image of the Rain Hill district. Illumination from the east. (b) RGB composite stitched image of regional gravity, at station spacing of 500 m. Goldminco Corporation company data.

corresponds with the Gilmore Fault, the boundary between the central and eastern subprovinces of the Lachlan Orogen. Internally, the Gidginbung Volcanics contain a number of cross-structures of varying orientation, principally north-northwest, north and northeast.

The package is at its greatest width in the southern third of its extent, where a highly magnetic, noisy region measures roughly 10 x 4 km^2 and strikes northwest to north-northwest. Within this region, a number of cross-structures define a high textural complexity, most prominently of northeast and northwest orientations.

With northward progression, the magnetic high narrows substantially into an elongate belt 1.25 – 2 km in width, that persists north/north-northwest for *ca* 15 km. Texturally, the region exhibits smooth, slightly sinuous, sub-parallel trends that may represent alternating stratigraphy, folded strata, deformational structures or a combination of such features. These trends continue to a lesser degree into the northern third of the Gidginbung Volcanics, where the texture returns to the noisy, structurally complex response observed in the southern extent; and the package again widens, to *ca* 3 km.

Regions of low magnetism occur on either side of the magnetic high, subparallel to its curvilinear elongate north-northwest strike. The Yiddah, Bull Plain, Kangaroo Hill, Mandamah, Culingerai, Chicane, Monza, Estoril and Rain Hill prospects are all located in relatively quiet regions of low magnetic response, each within 1 km of the high/low magnetic margin. The nature of the margin is sharp; however at Yiddah it is slightly more diffuse, with the prospect situated in a slight magnetic high in an overall low. The Gidginbung deposit is also located in an area of low magnetism, at the base of the highly magnetic region. The particularly low magnetic response at Gidginbung is attributed to magnetite destructive Devonian shearing, which is thought to have remobilised and concentrated earlier mineralisation (Allibone et al. 1995).

To the east of the Gidginbung Volcanics, the Ordovician Belimebung Volcanics are characterised by linear magnetic highs striking subparallel to the Gidginbung package. The volcanic features are contained within magnetic lows of Silurian sedimentary rocks of the Yiddah and Combaning Formations. The similarity of these features in magnetic response and orientation to that of the Gidginbung Volcanics, combined with the steep dip of volcanic units observed in the region suggests they could possibly represent fault repetitions.

On the western margin of the Gidginbung package, the metasedimentary Wagga Group, and contained intrusions are characterised as regions of low magnetic intensity, with little internal variance.

7.2.2. Gravity

The gravity signature of the Gidginbung Volcanics consists of an elongate, north-northwest striking low density region, which extends northward over roughly the same extent as the highly magnetic region to the northern truncation of the survey (Figure 7.1b). Bounding the gravity low on either side are high gravity regions, also striking north-northwest. This pattern is most pronounced in the northern portion of the gravity image, where it is relatively unbroken. The Yiddah prospect is unique in that it sits within a low gravity area contained within this gravity high. A similar break in the gravity high exists on the opposing (western) margin of the gravity low, which may or may not be related.

7.2.3. Interpretation

The most dominant feature resolved within the geophysical imagery is the coincident magnetic high/gravity low that extends from just north of the Gidginbung pit to the northern extent of the Gidginbung Volcanics. Drilling within the wide, southern region (MHRC537, Goldminco Corporation exploration drill hole; TP-327, Wormald 1993) has intersected the Rain Hill Monzodiorite, which contains significant accessory magnetite and is inferred by its mineral assemblage to be of lower than average crustal density. It is therefore suggested that the Rain Hill Monzodiorite is the primary unit responsible for the high magnetic/low gravity signature, and thus extends as one unit throughout the Gidginbung Volcanics (Figure 7.2). The high textural complexity observed and elongate nature of the intrusive unit suggests it has undergone significant post-emplacement shearing; however variations in volcanic units that possibly overlie it (e.g. due to bedding, imbrication, magnetite destructive alteration) also likely affect this pattern.

Areas of low magnetic intensity and high density situated on the margins of the Rain Hill Monzodiorite are interpreted to represent volcanic rocks of the Gidginbung Volcanics; including the andesitic volcaniclastic unit and fine-grained basaltic volcaniclastic unit described within the Yiddah prospect.

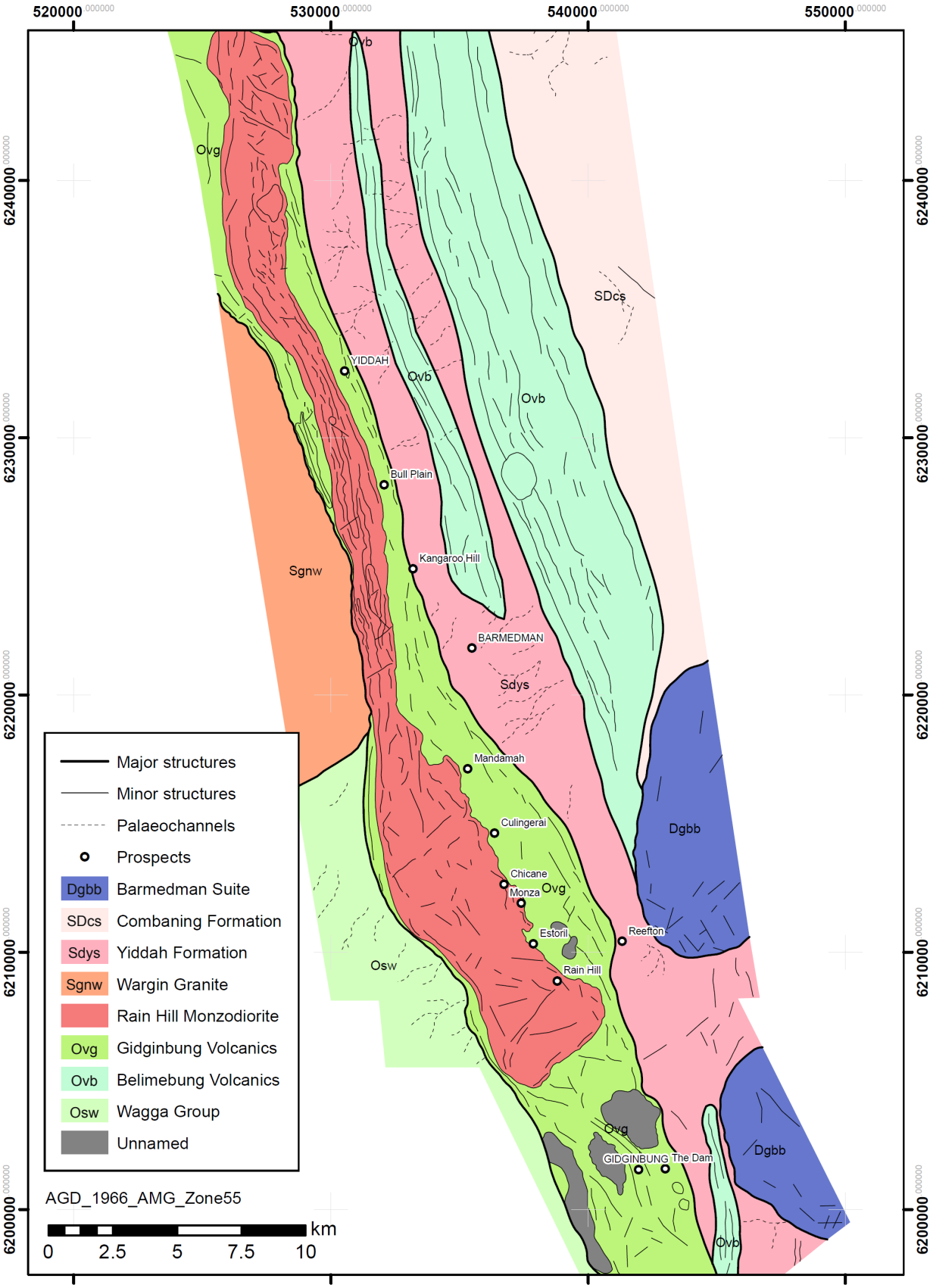

Figure 7.2: Structural and geological interpretation of the Rain Hill district derived from aeromagnetic and gravity imagery, showing the inferred northern extent of the Rain Hill Monzodiorite. Note the likelihood that the volcanic rocks into which the Rain Hill Monzodiorite intrudes overlie the intrusion at shallow depths.

It is unclear from aeromagnetic imagery alone as to whether the intrusive unit was (1) emplaced prior to major east-west compressional activity (unrelated to a major structure), with subsequent deformation elongating the unit; (2) emplaced during or prior to major deformation, along a major regional structure (the Gilmore Fault Zone) or (3) emplaced following major deformation, with magma ascent preferentially focusing along the Gilmore Fault Zone (with later orogenic activity shearing the unit). Following the porphyry model paradigm, the presence of a regional structure is considered a potential transport conduit for magmatic ascent and fluid focusing, which would favour options 2 and 3.

The earliest measured movement along the Gilmore Fault Zone (observed in the Tumut region) corresponds with the Bindian-Bowning Orogeny; however Stuart-Smith (1991) has suggested that the structure was probably active from the earlier Benambran Orogeny. Movement is considered to be dominantly sinistral transpressional throughout this period (Stuart-Smith 1991). In the study area, the contact of the Gilmore Fault Zone is sinuous; suggesting that strike-slip movement would be considerably constrained. In contrast, the Belimebung Volcanics to the east are relatively straight. This suggests that much of the deformation may have developed preferentially in this zone, at least for the latest movement. This transfer may be related to the presence of the S-type Wargin Granite (Sgnw), abutting the Gidginbung Volcanics on its western margin. Such a resistant body may have focused oblique compression on the central region of the Gidginbung Volcanics during later deformation, elongating the intrusive body and deforming the Gilmore Fault contact.

7.3. DEFORMATION

7.3.1. Foliation and deformational features

A consistent north-northwest trending foliation of varying intensity overprints all lithologies at Yiddah (76/071º; n = 438; Figure 7.3a). This foliation is considered to have developed during the same shearing event/s that remobilised and concentrated mineralisation within the Gidginbung deposit (Warren et al. 1995), dated by Perkins et al. (1995; K-Ar illite) at 413 ± 4 Ma and 423 ± 5 Ma. It is thought that the sericitic-argillic alteration assemblage (quartz/sericite/kaolinite/pyrite; Figure 7.4a; See Section 6.2) observed at Yiddah was also developed at this time, as it appears to cross-cut mineralisation. Ar-Ar dating would clarify this interpretation; however this is beyond the time-frame of the current work.

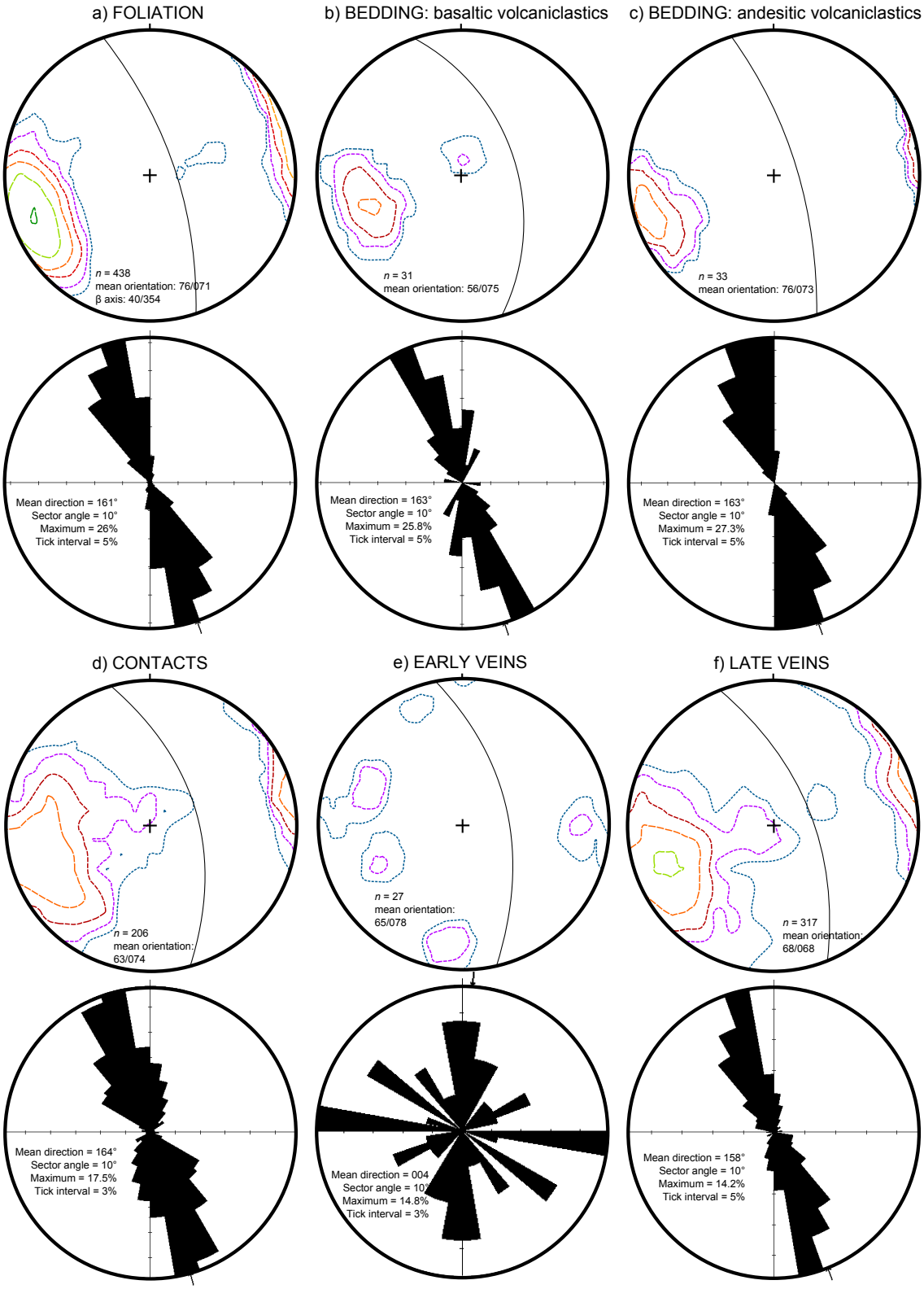

Figure 7.3: Dominant structural trends of the Yiddah porphyry system, as presented by contoured stereoplots and strike frequency rose diagrams. Mean orientations are dip/dip direction. (a) Foliation (contours are 1, 2, 4, 8, 16 and 32% per 1% area). (b) Bedding; basaltic volcaniclastics (contours are 4, 8, 16 and 32% per 1% area). (c) Bedding; andesitic volcaniclastics (contours are 4, 8, 16, and 32% per 1% area). (d) Contacts (contours are 1, 2, 4 and 8% per 1% area. (e) Early porphyry qz ± mg/mo/cp veins (contours are 4 and 8% per 1% area) (f) Late veins (cl/cb/py) (contours are 1, 2, 4, 8 and 16% per 1% area). All measurements relate to true north. Note the overwhelmingly dominant north-northwestern trend and easterly to vertical dip in all plots except early porphyry related veins.

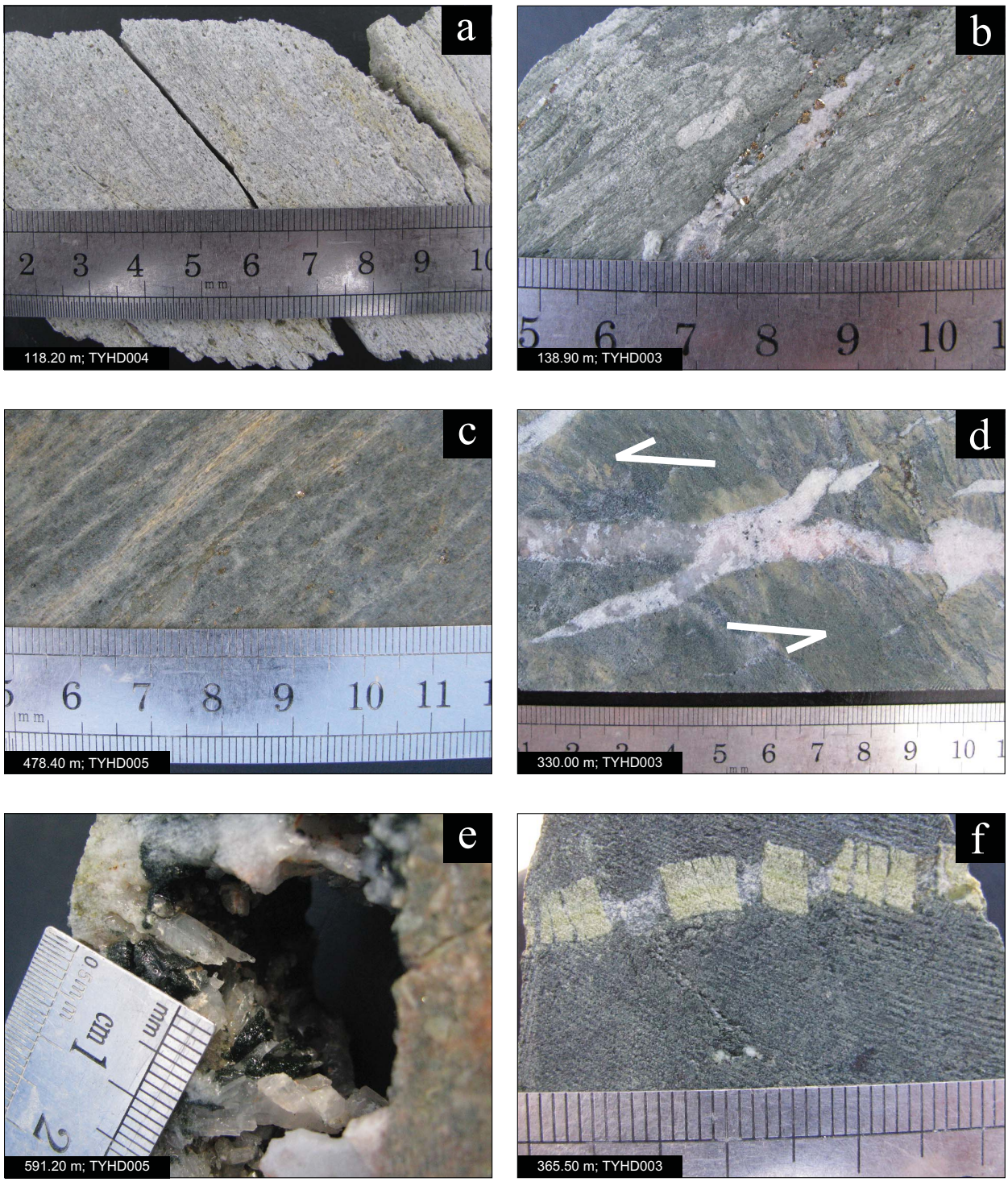

Figure 7.4: Macrostructural deformation features. (a) Foliation developed within sericite/kaolinite/quartz/pyrite (argillic) alteration andesitic volcanics. (b) Foliation developed within chlorite/sericite altered andesitic volcaniclastics; dismembering a late porphyry carbonate/pyrite vein. (c) Strain developed in monzodiorite porphyry located proximal to a significat late fault. (d) Hornfelsed andesitic volcaniclastics with quartz/ carbonate tension gashes. (e) Quartz crystals which have grown into a cavity, within a coarse grained quartz/ carbonate/chlorite vein as in d (chlorite has weathered out with exposure to elements to reveal euhedral quartz crystals). (f) Brittle boudinaged coarse-grained porphyry related epidote vein which has suffered partial carbonate alteration.

Outside the sericitic-argillic assemblage; the intensity of foliation is largely correlated with the abundance of hydrated alteration products. Rocks containing significant volumes of sericite, kaolinite and/or chlorite display the strongest foliation, evident both in hand specimen (Figure 7.4a,b) and at a microscopic scale. In the latter, mineral alignment is pronounced, producing microfabrics (Figure 7.5a) and 'wrapped' textures, where foliated micas have moulded around resistant minerals such as pyrite, apatite and quartz (Figure 7.5b). Chlorite pressure shadows and aligned chlorite/sericite growths within cracked grains or other low pressure zones are also commonly observed (Figure 7.5c,d). Where porphyritic units are contained in intensely altered zones, significant alteration of groundmass minerals to hydrated minerals has enabled rotation and weak alignment of feldspar phenocrysts. Another common ductile deformation feature observed is mechanical twinning of calcite, which occurs in all units along with undulose extinction of quartz (Figure 7.5e).

In the least hydrothermally altered units (the Rain Hill Monzodiorite, hornfelsed volcaniclastic rocks and some porphyry stocks), deformational features are characteristically more brittle. Tension gashes to decimetre widths are infilled with coarse-grained quartz, calcite, chlorite ± chalcopyrite (Figure 7.4d,e). Veins associated with post-mineralisation deformation are also observed on a microscopic scale, where parallel elongate calcite crystals are aligned perpendicular to vein margins, cross-cutting all other fabrics. Epidote veins emplaced hydrothermally during porphyry system formation are commonly boudinaged in a brittle manner, healed by calcite or quartz (Figure 7.4f); whilst numerous cracked feldspar and amphibole crystals within the Rain Hill Monzodiorite are observed, in addition to transcrystalline fractures (Figure 7.5d,f).

Zones of fault breccia are common within the moderately altered lithologies outside of the more intensely sericitic-argillic altered zone. The three-dimensional nature of these features is difficult to ascertain in drill core; however they do not appear associated with major offsets. A substantial zone of high strain (~ 35 m) and a faulted section from 487.0 – 492.4 m is intersected at the base of TYHD005, within a weakly altered late porphyry monzodiorite stock (Figure 7.4c).

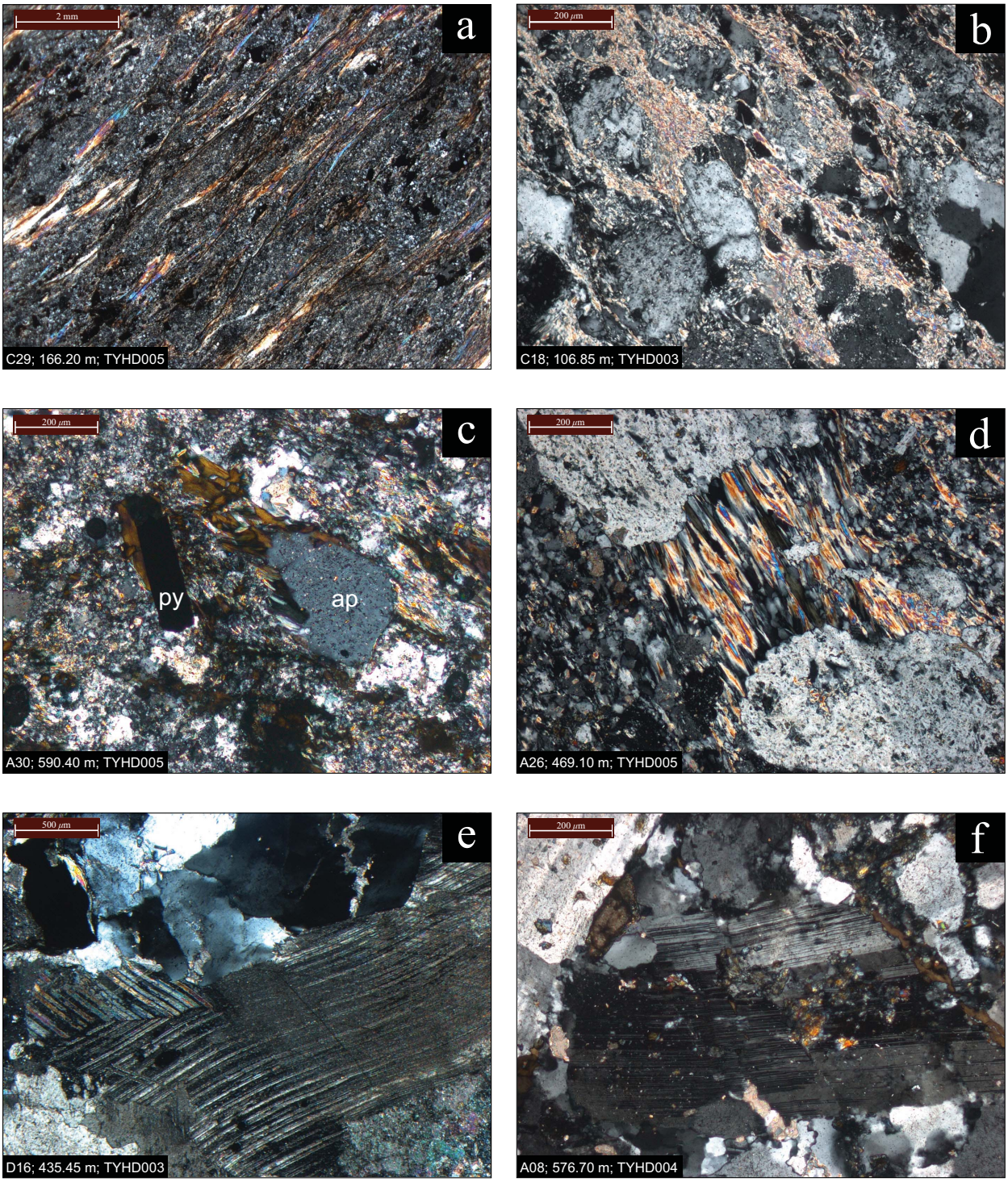

Figure 7.5: Cross-polarised light photomicrographs of microstructural deformation features. (a) Aligned sericite defining foliation in highly altered andesitic volcaniclastics. (b) Wrapped sericite textures surrounding somewhat aligned feldspar and secondary quartz phenocrysts in a porphyritic intrusion. (c) Chlorite pressure shadows fringing pyrite (py) and apatite (ap). (d) Boudinaged feldspar phenocryst with aligned syn-kinematic sericite-chlorite. (e) Mechanically twinned, bent calcite crystal and quartz crystals displaying undulose extinction. (f) Dislocated feldspar phenocryst.

7.3.2. Bedding and contacts

Bedding orientations are broadly similar in volcaniclastic units of the Yiddah prospect. The fine-grained basaltic volcaniclastic dips moderately to steeply east, striking north-northwest (56/075º; *n* = 31; Figure 7.3b), while the andesitic volcaniclastic unit possesses a moderate easterly to vertical dip, also striking north-northwest (76/073º; *n* = 33; Figure 7.3c). These results are consistent with the regional north-northwest strike, while the steepness of dip suggests the units are either intensely folded or are imbricated fault slices.

Measurable lithological contacts within the Yiddah prospect dip moderately to steeply east, through to steeply west; with a greater range but broadly similar average orientation to that of bedding (63/073º; *n* = 206; Figure 7.3d). The greater variability likely relates to the more unpredictable nature of intrusive activity, particularly observed for dykes at the margin of the Rain Hill Monzodiorite. The broad conformability of contacts and bedding planes may be due to (1) intrusive units being emplaced as sills; possibly along weakened planes due to a differential stress regime or (2) post-emplacement deformation compressing porphyry stocks and their host units into the dominant north-northwestern orientation.

7.3.3. Porphyry-related veins

Only a broad discrimination of ‘early’ and ‘late’ veins could be achieved due to the nature of interpreting pre-collected orientated core measurements. ‘Early veins’ include only quartz veins containing magnetite, chalcopyrite and/or molybdenite, to eliminate quartz tension veins which may have been generated during later deformation. The resulting strike frequency rose diagram displays a range of orientations; with major sectors striking north, east, north-northeast and northwest (Figure 7.3e; 65/168º; *n* = 27). Veins containing minerals generally associated with propylitic or retrograde alteration including carbonate, chlorite and pyrite (Sillitoe 2010) were plotted as ‘late veins’. These features possess a gentle eastern through to vertical dip and a tightly constrained north-northwest strike (68/068; *n* = 317). The similarity of propylitic alteration products to those produced by lower greenschist facies metamorphism in conjunction with the broad similarity in orientation to that of foliation however suggests that many of these veins were likely formed from recrystallised alteration products, or have been realigned into the foliation plane along with their host rocks during later deformation (e.g. Figure 7.4b).

7.3.4. Temperature of deformation

Chlorite, a common product of hydrothermal alteration and greenschist facies metamorphism; is recognised to comprise an effective proxy for estimating the physiochemical conditions which prevailed during its formation (de Caritat et al. 1993).

Chlorite compositions of crystals contained within six Yiddah samples associated with a variety of mineral phases have been determined via electron microprobe spectrometry (Table 7.1). All chlorite grains analysed plot within the chamosite (Fe-end member) – clinochlore (Mg-end member) solid solution continuum (Figure 7.6). Chlorites from TYHD003 contained slightly higher Mg than Fe while those from TYHD005 were closer to parity.

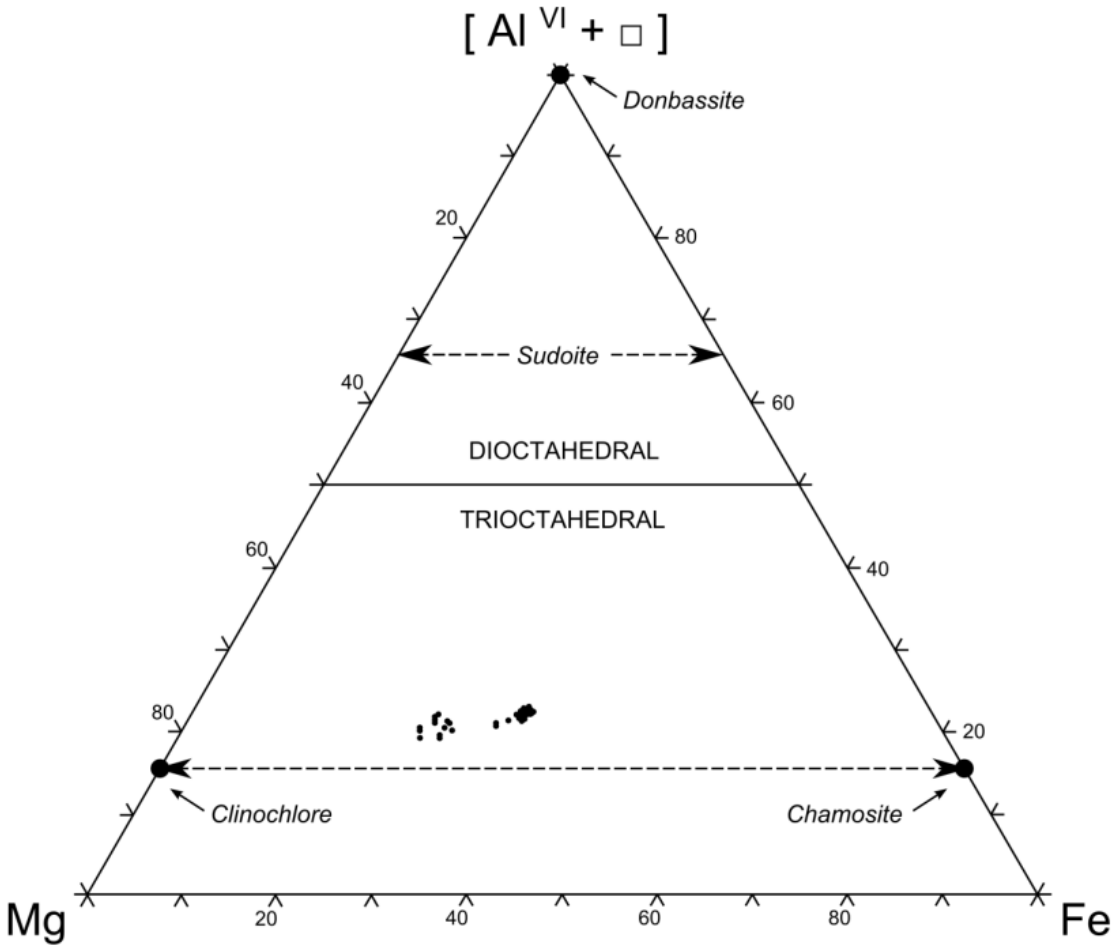

Figure 7.6: Chlorite classification diagram after Zane & Weiss (1998). The left cluster (higher cationic Mg), are samples from TYHD003; while the right cluster are samples from TYHD005.

Table 7.1: Chlorite microprobe results and geothermometry calculations; as for a half cell, based on the ideal formula $(Mg_2Fe)_2Al(AlSi_3O_{10})(OH)_8$. Methodologies used are T1: Cathelineau & Nieva 1985 (Al^{IV}); T2: Cathelineau & Nieva 1985 (vacancies); T3: Cathelineau 1988; T4: Jowett 1991.

Sample	E05						E06						E17					
Analysis	cl-2	cl-3	cl-4	cl-5	cl-6	cl-7	cl-1	cl-2	cl-3	cl-5	cl-6	cl-7	cl-1	cl-2	cl-3	cl-4	cl-5	cl-6
Chlorite association	Pyrite/ Chalcopyrite veining	Pyrite/ Chalcopyrite veining	Pyrite/ Chalcopyrite veining	groundmass	groundmass	groundmass	coarse qz/cl/cb/ep vein	altered amphibole	groundmass	coarse qz/cl/cb/ep vein	groundmass	coarse qz/cl/cb/ep vein	altered amphibole	altered amphibole	altered amphibole	quartz seam vein	altered amphibole	quartz seam vein
K_2O	0.03	0.05	0.01	0.06	0.01	0.01	0.01	0.02	0.01	0.00	0.04	0.01	0.02	0.06	0.00	0.01	0.02	0.02
CaO	0.03	0.01	0.02	0.09	0.02	0.04	0.02	0.06	0.06	0.01	0.03	0.05	0.03	0.04	0.04	0.03	0.04	0.02
Na_2O	0.02	0.06	0.01	0.06	0.00	0.03	0.02	0.02	0.02	0.03	0.12	0.01	0.04	0.08	0.01	0.00	0.00	0.01
FeO*	18.12	18.39	18.44	18.04	17.55	18.75	19.66	17.71	18.93	19.11	19.00	19.13	23.74	23.28	22.71	23.21	22.16	23.44
MgO	20.10	20.07	20.24	20.09	21.08	20.02	19.64	21.05	19.85	19.93	19.50	20.40	15.45	15.29	16.67	15.64	17.35	15.91
SiO_2	28.10	27.88	27.79	27.89	28.89	27.73	28.28	29.53	28.09	28.40	28.09	28.78	26.16	26.18	27.20	24.39	27.56	26.66
MnO	0.41	0.39	0.45	0.45	0.43	0.44	0.73	0.57	0.64	0.71	0.67	0.67	0.99	1.02	0.99	0.87	0.90	0.85
TiO_2	0.01	0.02	0.01	0.07	0.02	0.01	0.00	0.04	0.05	0.00	0.04	0.00	0.04	0.04	0.04	0.05	0.06	0.03
Cr_2O_3	1.04	0.59	0.70	0.03	0.38	0.59	0.02	0.25	0.06	0.01	0.05	0.00	0.01	0.02	0.00	0.02	0.01	0.02
F	0.16	0.08	0.04	0.10	0.15	0.08	0.05	0.20	0.10	0.17	0.13	0.15	0.00	0.08	0.18	0.01	0.15	0.00
Al_2O3	19.09	20.07	20.26	19.72	19.01	20.23	19.36	17.94	19.56	19.82	19.93	18.72	20.87	20.80	19.87	20.86	19.50	21.22
Total	**87.10**	**87.61**	**87.96**	**86.60**	**87.55**	**87.93**	**87.79**	**87.79**	**87.79**	**87.79**	**87.79**	**87.79**	**87.35**	**86.90**	**87.73**	**85.08**	**87.75**	**88.19**
Fe/(Fe+Mg)	0.47	0.48	0.48	0.47	0.45	0.48	0.50	0.46	0.49	0.49	0.49	0.48	0.61	0.60	0.58	0.60	0.56	0.60
Si (full cell)	5.75	5.67	5.63	5.73	5.85	5.63	5.77	6.00	5.74	5.75	5.73	5.85	5.50	5.53	5.67	5.28	5.72	5.53
Si IV	2.88	2.83	2.81	2.86	2.92	2.81	2.89	3.00	2.87	2.88	2.87	2.93	2.75	2.77	2.83	2.64	2.86	2.76
Al IV	1.12	1.17	1.19	1.14	1.08	1.19	1.11	1.00	1.13	1.12	1.13	1.07	1.25	1.23	1.17	1.36	1.14	1.24
Al VI	1.18	1.24	1.23	1.25	1.19	1.24	1.21	1.14	1.23	1.24	1.26	1.17	1.34	1.36	1.27	1.31	1.25	1.36
Fe 2+	1.55	1.56	1.56	1.55	1.48	1.59	1.68	1.50	1.62	1.62	1.62	1.63	2.09	2.06	1.98	2.10	1.92	2.03
Mg 2+	3.07	3.04	3.06	3.07	3.18	3.03	2.99	3.19	3.02	3.01	2.97	3.09	2.42	2.41	2.59	2.53	2.68	2.46
Mn 2+	0.04	0.03	0.04	0.04	0.04	0.04	0.06	0.05	0.06	0.06	0.06	0.06	0.09	0.09	0.09	0.08	0.08	0.07
6-ΣVI (□)	0.16	0.12	0.11	0.09	0.11	0.10	0.06	0.12	0.07	0.07	0.09	0.06	0.06	0.09	0.07	-0.01	0.07	0.07
$Fe^{2+}/\Sigma R^{2+}$	0.33	0.34	0.34	0.33	0.32	0.34	0.35	0.32	0.34	0.35	0.35	0.34	0.45	0.45	0.43	0.45	0.41	0.45
TºC 1	255.9	265.0	269.3	258.9	246.1	269.2	254.1	230.3	257.2	255.9	258.4	245.5	282.6	279.6	265.0	305.9	259.6	279.8
TºC 2	262.2	267.1	268.1	270.8	268.6	269.0	274.5	267.7	272.7	273.5	270.2	274.8	274.0	271.1	273.3	282.6	273.2	272.5
TºC 3	299.6	313.3	319.9	304.1	284.7	319.7	296.8	260.7	301.5	299.6	303.4	283.8	340.0	335.5	313.4	375.3	305.1	335.7
TºC 4	304.3	318.0	324.5	308.8	288.9	324.5	302.4	265.3	306.6	304.8	308.7	289.0	348.6	344.0	321.3	383.3	312.6	344.0
TºC average	**280.5**	**290.8**	**295.4**	**285.7**	**272.1**	**295.6**	**281.9**	**256.0**	**284.5**	**283.4**	**285.2**	**273.3**	**311.3**	**307.6**	**293.3**	**336.8**	**287.6**	**308.0**

***Total Fe expressed as FeO. Microprobe results in wt%. Calculations as for a half cell, except where stated.

Table 7.1: (continued)

Sample	E19				E21					E26				
Analysis	cl-1	cl-2	cl-3	ep-2	cl-1	cl-2	cl-3	cl-4	mu-1	cl-1	cl-2	cl-3	cl-4	cl-5
Chlorite association	within pyrite/ magnetite/ chalcopyrite	quartz/ magnetite seam vein	groundmass	qz/mg seam vein	chalcopyrite veining	chalcopyrite veining	quartz/ chalcopyrite veining	with sericite; fibrous habit	with sericite; fibrous habit	chlorite	chlorite with chalcopyrite	pressure shadow of pyrite	groundmass	pyrite/ chalcopyrite mineralisation
K_2O	0.01	0.02	0.02	0.01	0.01	0.00	0.01	0.00	0.01	0.00	0.00	0.01	0.01	0.02
CaO	0.05	0.03	0.05	0.01	0.02	0.00	0.01	0.04	0.01	0.04	0.04	0.00	0.03	0.02
Na_2O	0.02	0.01	0.03	0.02	0.02	0.00	0.03	0.00	0.00	0.00	0.03	0.02	0.00	0.00
FeO*	23.60	23.21	23.67	24.15	23.17	23.55	23.76	23.37	23.29	23.87	23.46	23.74	23.88	23.48
MgO	15.45	16.01	15.76	15.69	16.16	16.06	16.00	15.57	16.26	15.57	15.81	16.20	15.62	16.08
SiO_2	26.11	26.81	26.47	26.06	26.96	26.69	26.08	25.59	26.58	25.76	26.31	26.43	25.90	26.29
MnO	0.98	0.96	0.97	0.99	0.76	0.82	0.80	0.72	0.72	0.95	0.92	0.91	0.98	0.92
TiO_2	0.04	0.13	0.06	0.01	0.04	0.03	0.05	0.02	0.05	0.05	0.02	0.01	0.03	0.03
Cr_2O_3	0.01	0.03	0.05	0.02	0.01	0.00	0.01	0.01	0.02	0.01	0.02	0.05	0.00	0.00
F	0.04	0.05	0.07	0.04	0.00	0.09	0.01	0.07	0.14	0.02	0.01	0.04	0.00	0.00
Al_2O3	20.71	20.75	21.01	21.01	20.56	20.75	20.86	20.68	20.38	20.97	20.26	20.26	20.74	20.44
Total	**87.79**	**87.79**	**87.79**	**87.79**	**87.79**	**87.79**	**87.79**	**87.79**	**87.79**	**87.79**	**87.79**	**87.79**	**87.79**	**87.79**
Fe/(Fe+Mg)	0.60	0.59	0.60	0.61	0.59	0.59	0.60	0.60	0.59	0.61	0.60	0.59	0.60	0.59
Si (full cell)	5.51	5.57	5.51	5.46	5.61	5.56	5.47	5.46	5.57	5.44	5.56	5.54	5.47	5.53
Si IV	2.76	2.79	2.76	2.73	2.81	2.78	2.73	2.73	2.78	2.72	2.78	2.77	2.73	2.76
Al IV	1.24	1.21	1.24	1.27	1.19	1.22	1.27	1.27	1.22	1.28	1.22	1.23	1.27	1.24
Al VI	1.33	1.33	1.34	1.32	1.33	1.33	1.31	1.33	1.30	1.33	1.30	1.27	1.31	1.30
Fe 2+	2.08	2.02	2.06	2.11	2.02	2.05	2.08	2.09	2.04	2.11	2.07	2.08	2.11	2.06
Mg 2+	2.43	2.48	2.45	2.45	2.51	2.49	2.50	2.48	2.54	2.45	2.49	2.53	2.46	2.52
Mn 2+	0.09	0.08	0.09	0.09	0.07	0.07	0.07	0.07	0.06	0.09	0.08	0.08	0.09	0.08
6-ΣVI (□)	0.06	0.09	0.07	0.03	0.08	0.06	0.04	0.04	0.05	0.03	0.05	0.03	0.03	0.04
$Fe^{2+}/\Sigma R^{2+}$	0.45	0.44	0.45	0.45	0.44	0.44	0.45	0.45	0.44	0.45	0.45	0.44	0.45	0.44
TºC 1	281.3	275.1	281.5	287.6	271.0	276.7	286.4	286.9	275.6	289.7	276.7	278.5	286.4	279.9
TºC 2	273.9	271.1	272.9	277.6	271.9	274.4	276.9	276.5	274.8	277.1	275.0	277.4	277.4	276.8
TºC 3	338.2	328.6	338.4	347.7	322.5	331.2	345.9	346.6	329.4	350.9	331.1	333.9	345.8	336.0
TºC 4	346.7	336.8	346.7	356.1	330.6	339.4	354.1	354.9	337.5	359.3	339.4	342.1	354.2	344.2
TºC average	**310.0**	**302.9**	**309.9**	**317.3**	**299.0**	**305.4**	**315.8**	**316.2**	**304.3**	**319.3**	**305.6**	**307.9**	**315.9**	**309.2**

***Total Fe expressed as FeO. Microprobe results in wt%. Calculations as for a half cell, except where stated.

The ability of chlorite to constitute an effective geothermometer is related to its non-stoichiometric chemical behaviour, whereby both decreases in Si^{IV} (and converse increases in Al^{IV}); and decreases in VI vacancies are correlated with increasing formation temperatures (Cathelineau & Nieva 1985). Si^{IV}, Al^{IV} and VI vacancies (□) are calculated through substituting the cationic values of Mg, Fe, Mn, Al and Si into the following general formula:

$$[Mg_a,Fe_b,Mn_c,Al_{d-[4-e]},\square_{(6-a-b-c-(d-[4-e]))}]^{VI}[Si_eAl_{4-e}]^{IV}O_{10}(OH)_8$$

These values are then substituted into a variety of formulas, applicable for formation temperatures under 325ºC, (Jowett 1991) (Table 7.2).

Table 7.2: Formulae of various methods used to calculate chlorite formation temperatures.

Method	**Formula**
1. Cathelineau & Nieva (1985) Al^{IV}	TºC = (Al^{IV} + 0.0826)/0.00471
2. Cathelineau & Nieva (1985) □	TºC = (□-2.41)/(-0.00857)
3. Cathelineau (1988)	TºC = -61.92 + (321.98*Al^{IV})
4. Jowett (1991)	TºC = {319*(Al^{IV}+[0.1*Fe/(Fe+Mg)])}-69

The average of these four methods produced resultant temperatures in the range of 256.0 – 336.8ºC, with the majority falling within the 270 – 320ºC range (Figure **7**.7). Results were most consistent among various methods at the lower temperature spectra, with deviations of around 60ºC observed between methods at high formation temperatures. Samples E05 and E06 produced the lowest temperatures (~280 – 290ºC); while samples E17, E19. E21 and E26 characteristically were between 290 – 320ºC. These two groupings correspond with their sample origins, with the former sourced from the central TYHD003 and the latter from the northern TYHD005. They are also distinguished by their Fe/Mg ratios, as demonstrated in Figure **7**.6. Fe - Mg contents are not considered to be highly correlated with formation temperatures, however some methodologies such as that of Jowett (1991) account for this variable. If the results of Jowett (1991) are examined in isolation, the same increase in formation temperature is observed from samples from TYHD005.

No clear correlation was resolved between chlorite mineral association and formation temperature. Alternate mineral settings included chlorite within quartz-seam veins, within the groundmass, after amphibole, with chalcopyrite, with magnetite, within late deformation related coarse quartz/carbonate veins and as ‘flowing’ fibrous grains associated with sericite

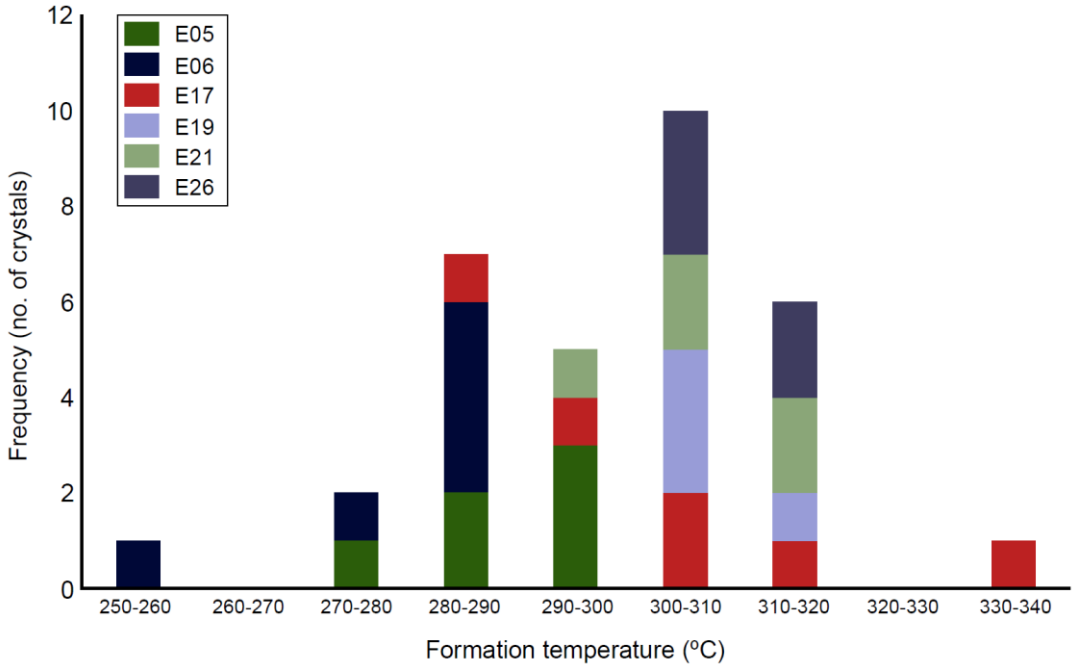

Figure 7.7: Frequency histogram diagram for average chlorite formation temperatures. E05 = 250.50 m, TYHD003; E06 = 301.00 m, TYHD003; E17 = 391.00 m, TYHD005; E19 = 413.00 m, TYHD005; E21 = 434.60 m TYHD005; E26 = 537.75, TYHD005.

(see Table 7.1). Samples analysed also represented those from a relatively broad range of alteration facies; from which a broader range of temperatures would likely be expected if chlorite was representative of conditions during porphyry emplacement.

These temperatures are therefore interpreted to be representative of later deformational conditions, which have resulted in widespread recrystallisation of hydrothermal chlorite and likely the initial formation of much metamorphic chlorite within the Rain Hill Monzodiorite. Regional metamorphism is thus inferred to be sub to lower greenschist facies, dominated by chlorite, epidote, and carbonate products.

The slightly higher formation temperature of chlorites sourced from the northern drill hole TYHD005 than the central drill hole TYHD003 may be related to the mapped boundary of 'schist' at the northern and southern extents of the prospect, which here refers to a unit of indistinguishable primary lithology (see Figure 2.7). It is possible that during shearing, intrusive stocks helped prevent deformation of the lower andesitic pile; with stress therefore being transferred predominantly through the overlying (and weakest) sericitic alteration zone, resulting in the intense overlying sericitic-argillic alteration assemblage as outlined in Chapter Six.

7.3.5. Three-dimensional configuration

East-west gravity cross-sections of 100 m spacing spanning the strike of the Yiddah prospect (6231700 mN – 6234000 mN; Goldminco Corporation company data) enable a three-dimensional assessment of the spatial relationship between units of contrasting densities (Figure 7.8). In conjunction with knowledge gained from spatially referenced diamond core, gravity patterns can be loosely assigned as: low density (dark blue) = Rain Hill Monzodiorite and larger intrusive stocks; high density (yellow – pink) = basaltic volcaniclastics and intermediate density (light blue – light green) = andesitic volcaniclastics and transitional zones.

Following this classification, the prospect scale geology can be described as a package of elongate, discrete units which strike north-northwesterly and are possibly fault repeated. It is clear that at around 6232500 – 800 mN this pattern is significantly disrupted by what appears to be a cross-structure with left-lateral offset. The emplacement of mineralised stocks in this zone (as observed in TYHD003 and TYHD004) could possibly be related to this structure, which may represent the source point of magmas and hydrothermal fluids from the Rain Hill Monzodiorite, as portrayed in Figure 7.8.

The presence of rare mineralised quartz-seam veins in the Rain Hill Monzodiorite (TYHD003, 389.4; 434.0 m), along with its weakly mineralised character suggests that while post-mineralisation deformation was significant, it did not result in a large-scale offset of mineralised sills/stocks from the underlying 'parental' Rain Hill Monzodiorite. Instead, it is suggested that *in situ* compression of all units uniformly resulted in the strong north-northwest trending alignment of bedding, contacts and foliation.

Under this interpretation, it is possible that mineralisation continues both to the east of the area currently explored, under the Silurian Yiddah Formation contact and down-dip to the south, where it is envisioned the source of mineralised stocks/sills is located (Figure 7.8).

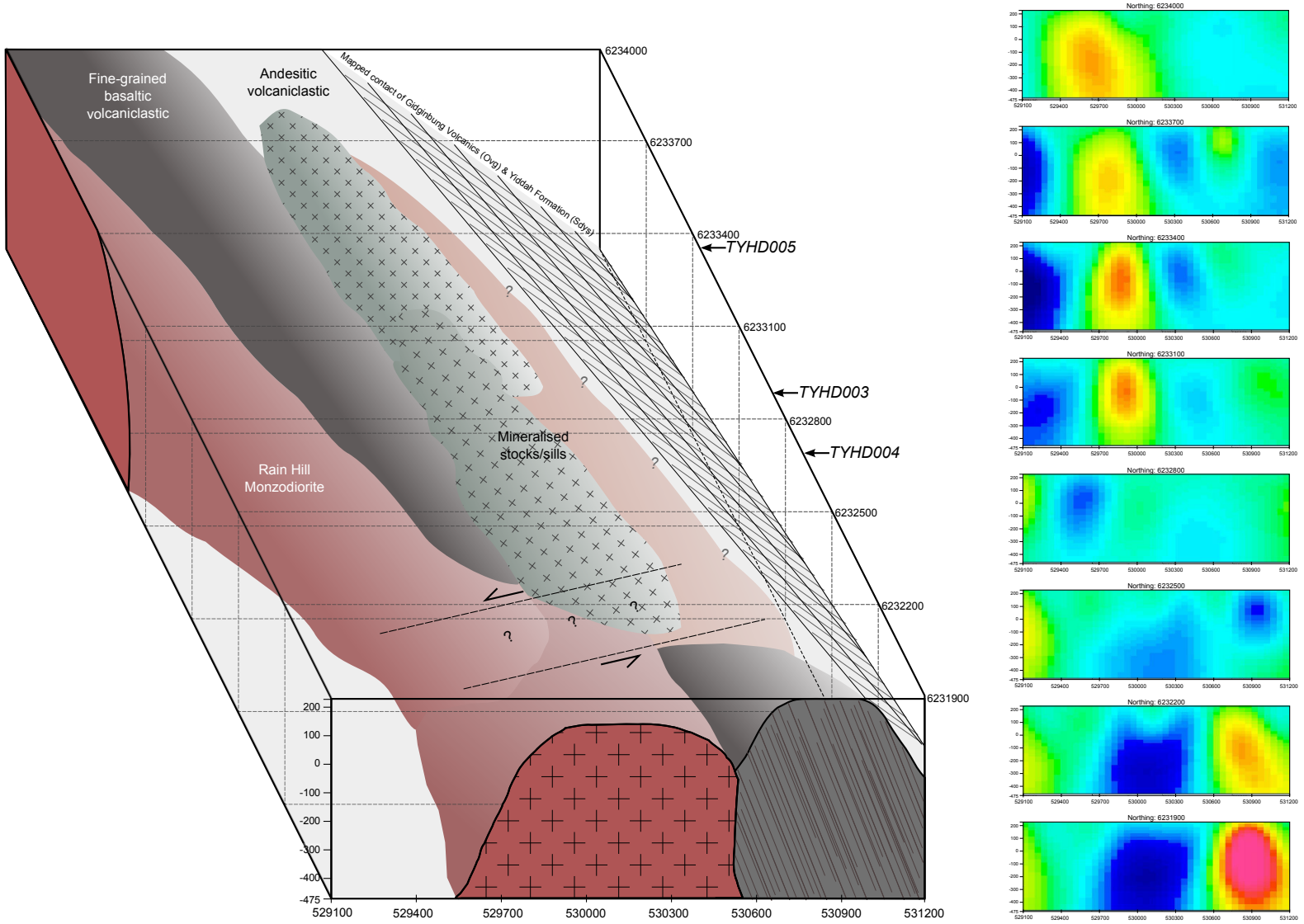

Figure 7.8: Selected gravity cross-sections spanning the Yiddah prospect at 300 m spacings (right) and interpreted three-dimensional block diagram (left), where each vertical slice corresponds to a gravity image. Gravity response: low = dark blue, high = pink.

CHAPTER EIGHT

TECTONIC SETTING AND REGIONAL CONTEXT

8.1. INTRODUCTION

Spatial and/or genetic associations between particular mineralisation styles and tectonic formational settings have long been documented. These associations are particularly strong for hydrothermal mineralisation styles, where the presence of a magmatic heat source is intimately linked to the tectonic setting or regime experienced by the region at the time of mineralisation. As discussed in Chapter Three, the vast majority of modern porphyry systems are observed in convergent margin settings, chiefly within the active Pacific Rim. In the Lachlan Orogen, the numerous porphyry and porphyry-related systems contained within elongate volcanic belts of the Macquarie Arc have thus been interpreted to infer analogous subduction-related settings. Subduction-related settings are also suggested by the calc-alkaline to shoshonitic geochemical affinities of volcanic rocks, which have been interpreted by Crawford et al. (2007a), Glen et al. (2007a) and Percival & Glen (2007) in their four phase Macquarie Arc evolutionary model (see Section 2.2 and Figure 2.5).

In this chapter, the tectonic signature of the Yiddah intrusive units is examined through geochemical discrimination methods and discussed in the context of petrological, geochronological and structural findings presented throughout previous chapters. The tectonic formational setting is further appraised in relation to the aforementioned four phase Macquarie Arc model and other mineralised units of the Macquarie Arc; namely Copper Hill (medium-K calc-alkaline), Goonumbla (high-K calc-alkaline/shoshonitic) and Cadia (shoshonitic). Blevin (2002) has published geochemical profiles for all three of these porphyry copper sites, for samples within the 55 – 60 wt% SiO_2 range. To enable a rigorous comparison between the geochemistry of the intrusive rocks at Yiddah and those at Copper Hill, Goonumbla, and Cadia the following discussion excludes Yiddah samples deviating significantly from the 55 – 60 wt% SiO_2 range.

8.2. GEOCHEMICAL TECTONIC DISCRIMINATION

8.2.1. Background

In the past forty years, a large number of methods have been developed that use predominantly immobile trace element abundances to discriminate between rocks formed in alternate tectonic settings (e.g. Pearce & Cann 1973; Winchester & Floyd 1977; Pearce et al. 1984; Müller et al. 1992; Pearce 1996). Initially, the majority of these studies focused simply on identifying elementary patterns between the abundances (or ratios) of elements within (young) rocks of particular, known tectonic settings; with these patterns then being used to infer the tectonic formational setting of (generally) older, unknown samples. In the years to follow however, greater attention has been paid to understanding the geological processes responsible for these associations.

The result has been a large body of literature pertaining to the many variables (i.e. enrichment and depletion processes) responsible for generating the distinct signatures possessed by rocks formed in differing tectonic environments. A sophisticated understanding of these processes enables not only the discrimination of broader tectonic formational settings, but the identification of more subtle variations in geochemical character which may occur with changes in the tectonic regime, or evolution of magmatism within a region. One such commonly observed pattern in collisional margin settings is that of a spatial and/or temporal progression from tholeiitic through calc-alkaline to shoshonitic magmatic affinity (Morrison 1980). This variation has particular significance in the Macquarie Arc due to the apparent association of K-enrichment with mineralisation (Blevin 2002; Cooke et al. 2007).

8.2.2. MORB normalised abundances

The mid ocean ridge basalt (MORB) normalised multiple-element (spider) diagram provides the most fundamental information regarding the source and enrichment/depletion history of rocks of intermediate composition (Rollinson 1993). In Figure 8.1, samples are normalised and ordered using the scheme of Pearce (1983), with the large ion lithophile (LIL) elements located on the left and the high field strength (HFS) elements located on the right. The compatibility of each element relative to the mantle increases outward from Ba and Th.

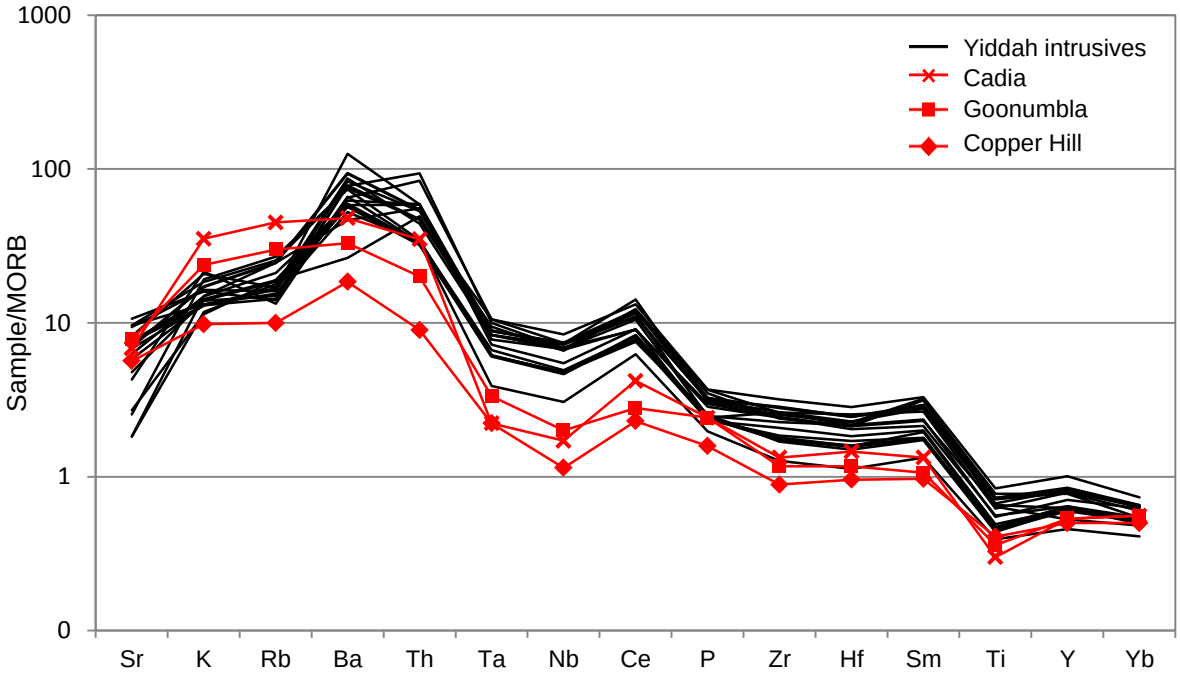

Figure 8.1: Mid ocean ridge basalt normalised plot for intrusive units at Yiddah and other mineralised intrusive bodies of the Macquarie Arc (representative values from Blevin 2002). Average MORB normalisation values and ordering scheme of Pearce (1983). LIL on the left and HFS on the right, with increasing compatibility outwards from Ba-Th.

The MORB normalised abundances of Yiddah intrusives are relatively consistent, with the greatest internal scatter observed for the mobile LIL elements; Sr, K, Rb and Ba. The mobility of K was demonstrated in the TiO_2 versus K_2O bivariate plot presented in Figure 4.9, where intrusive samples displayed inconsistent values of around 1 – 4 wt% K_2O despite the Nb/Y and Th immobile element proxies indicating alkaline (shoshonitic) affinities. It is thus considered that K and Rb are depleted relative to their initial concentrations; due to the observed breakdown of feldspars and micas at Yiddah related to hydrothermal alteration and processes related to the Gilmore Fault Zone. To the right of Ba (the HFS elements), very little internal scatter is observed, suggesting these abundances are largely unaffected by hydrothermal alteration and/or metamorphic processes.

With the exception of K and Rb, the Yiddah MORB normalised enrichment/depletion patterns are broadly similar to those of the Copper Hill, Goonumbla and Cadia suites. All samples display characteristic arc-related enrichment of the LIL elements, negative Ta-Nb anomalies, depletion of Ti, Y and Yb relative to the MORB and enrichment of Ce and Sm (Pearce et al. 1984; Pearce & Peate 1995). The most notable difference is the overall more enriched character of the Yiddah intrusive units than the Copper Hill, Goonumbla and Cadia

suites. Yiddah samples also possess a less pronounced Ta-Nb trough, and the distinction between the LIL and HFS elements is not as great.

These observations can be explained through examining the processes responsible for subduction-related melt enrichment. The first major process is related to the addition of an aqueous fluid phase during dehydration of the down-going crust and/or associated sediments. LIL elements partition into this fluid phase readily due to their large ionic radii and low valencies, whilst the immobile HFS elements do not partition into the fluid phase and thus the two groups are fractionated relative to one another, with the HFS elements remaining at abundances similar to the MORB (Pearce et al. 1984; Saunders et al. 1991; Pearce & Peate 1995). Th is unique in that it is the most immobile element that is also non-conservative (i.e. partitions into the fluid phase), only doing so at comparatively greater depth and heat. These properties make it the most appropriate element for substitution of K in immobile element discrimination diagrams such as those of Pearce (1982) and Hastie et al. (2007).

The second major enrichment process occurs due to partial melting of the subducting crust and/or sediments derived from the subducting crust. This process introduces HFS elements along with additional Th and LREE's, which are mobilised more readily in siliceous than aqueous fluids. These elements could also be introduced through the incorporation of a siliceous crustal component during magma ascent and/or emplacement (McDermott et al. 1993; Pearce & Peate 1995; Sun et al. 2008).

Variations in overall enrichment also occur due to the level of initial mantle enrichment. Possible processes responsible include (1) depletion by melt extraction from the column, (2) depletion by deep advection into the wedge (possibly due to back-arc spreading), (3) enrichment by incorporation of enriched lithosphere, and (4) enrichment by the advection of plume-enriched mantle into the wedge (Pearce & Peate 1995).

Due to the HFS element abundances plotting similarly to the MORB for the Copper Hill, Goonumbla and Cadia suites; and the similar age of the Yiddah, Goonumbla and Cadia systems, it can be assumed that the initial mantle was relatively 'normal' (i.e. not greatly depleted or enriched). Enrichment patterns observed for the Copper Hill, Goonumbla and Cadia suites are thus interpreted to be predominantly the result of an aqueous fluid

subduction component, possibly with a very minor sediment/crustal component contributing to the Goonumbla and Cadia suites.

The enrichment of LIL *and* HFS elements within the Yiddah intrusives however indicates it is likely that both a fluid and sediment (or crustal) component has contributed to the melt. It is not considered that enrichment could have been the product of very late host rock assimilation, as the LIL and HFS element concentrations of the host volcaniclastic units are considerably lower than those of the intrusives.

8.2.3. Tectonic discrimination plots

To investigate the involvement of a crustal component in the Yiddah intrusive source melt, the tectonic discrimination diagrams of Pearce et al. (1984) (Figure 8.2) and Müller et al. (1992) (Figure 8.3) are implemented. The granite (*s.l.*) discrimination plots of Pearce et al. (1984) are the most commonly applied tectonic discrimination methods for igneous rocks containing normative quartz. These plots use combinations of the trace elements Nb, Ta, Y, Yb and Rb to distinguish between volcanic-arc, within-plate, ocean-ridge and syn-collisional settings. Post-collisional melts generally span the volcanic-arc/syn-collisional spectra.

As highlighted in the MORB spider diagram, the HFS elements Nb and Ta are conservative in respect to an aqueous fluid phase (not added to the mantle wedge) and incompatible during mantle melting. Therefore, Nb and Ta values will remain low in the absence of an initially enriched mantle, sediment addition or crustal contamination (i.e. ocean-ridge melts and under 'normal' subduction conditions) (Pearce 1996). Y and Yb are highly incompatible during (deep) spinel lherzolite mantle melting yet only moderately incompatible during (shallower) garnet lherzolite melting. This is due to the high partition coefficients of Y and Yb into garnet, which may be retained as a residual phase. The depletion of Y and Yb thus occurs at depths where garnet lherzolite mantle is melted (plate boundaries), while more abundant Y and Yb results from deeper level melts, where spinel lherzolite is the substrate (ocean ridge and within-plate melts) (Pearce et al. 1984; Pearce 1996; Pearce 2008).

These properties are exploited in Figure 8.2a and Figure 8.2b, where the Yiddah intrusive samples plot similarly to Copper Hill, Goonumbla and Cadia on the x-axis (Yb and Y), which divides the fields of volcanic-arc and ocean-ridge granites. This suggests that all melts were

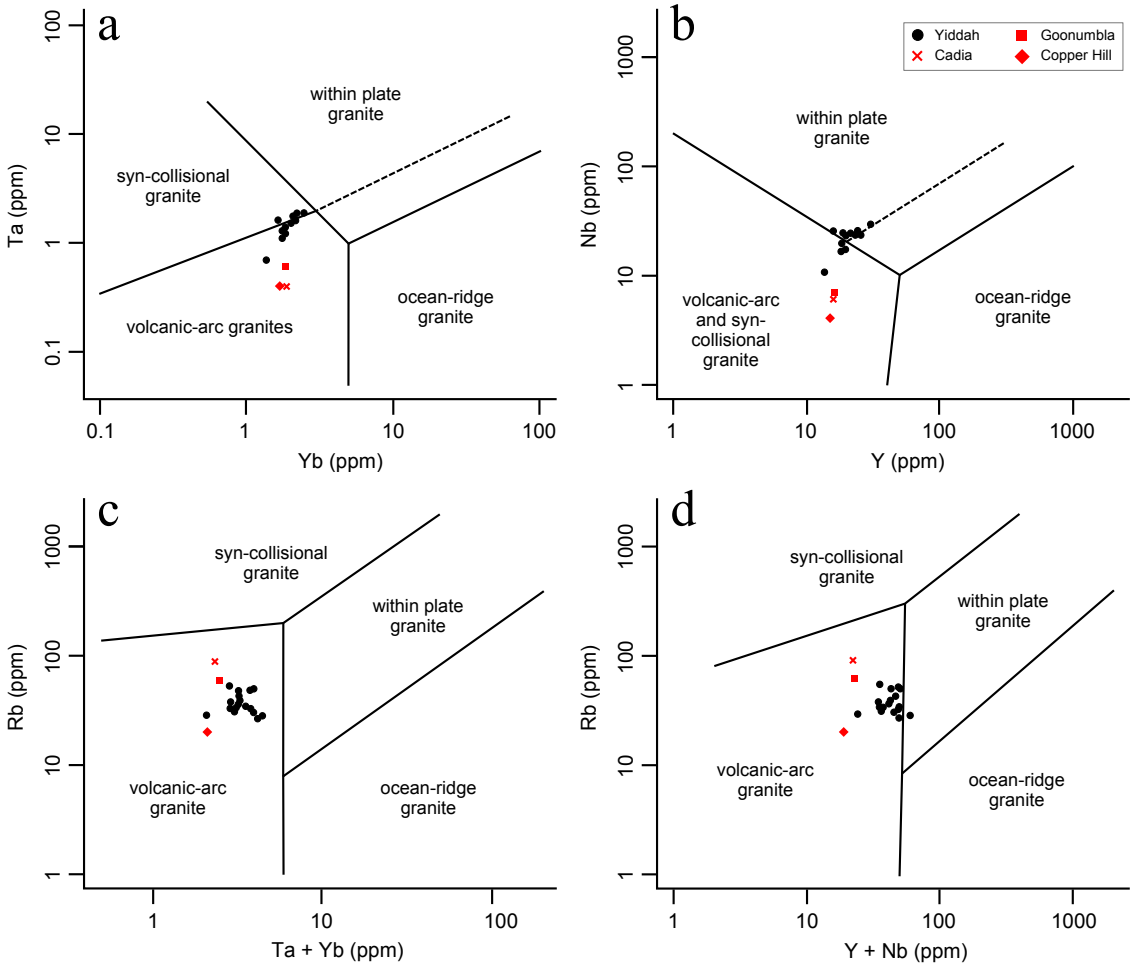

Figure 8.2: Granite (*s.l.*) trace element tectonic discrimination diagrams of Pearce et al. (1984). Cadia, Goonumbla, Copper Hill average values from Blevin (2002).

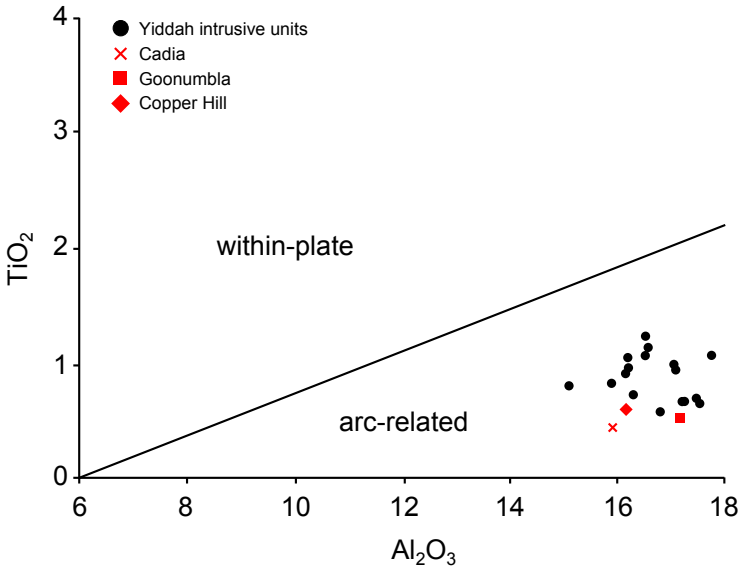

Figure 8.3: Al_2O_3 versus TiO_2 tectonic discrimination diagram of Muller et al. (1992). Cadia, Goonumbla, Copper Hill average values from Blevin (2002).

derived from mantle of similar (garnet bearing) composition. On the y-axis (Ta-Nb), the Yiddah intrusives plot significantly higher than those of other Macquarie Arc units, falling on the boundary of volcanic-arc, syn-collisional and within-plate melts, indicating again that a greater sediment and/or crustal component contributed to the Yiddah melt.

Rb, the only incompatible LIL element used in the plots of Pearce et al. (1984), is enriched by both fluid additions to the wedge and sediment/crustal incorporation. In Figure 8.2c and Figure 8.2d, Rb is used on the y-axis to discriminate between volcanic-arc granites and syn-collisional granites. In these diagrams, the Yiddah samples plot as volcanic-arc in origin, however they do not plot as closely to the syn-collisional field as in Figure 8.2a and Figure 8.2b. This is considered to be due to the depletion of Rb by hydrothermal/metamorphic alteration processes, as discussed for the MORB normalised plot. On the x-axis, combinations of the Y-Yb and Ta-Nb pairs again result in the Yiddah samples plotting slightly closer to the within-plate fields than the Copper Hill, Goonumbla and Cadia suites.

The Yiddah samples fall more definitively within the volcanic-arc field when plotted on the Al_2O_3 versus TiO_2 plot of Müller et al. (1992) (Figure 8.3). This plot was developed from a database of > 2200 shoshonitic volcanic rock analyses, where it was recognised that alkaline samples from within-plate settings possess very high abundances of Ti (a HFS element) relative to those formed in arc-related settings. The relatively immobile nature of both TiO_2 and Al_2O_3 make this plot applicable to rocks affected by secondary alteration processes.

8.2.4. Magmatic affinity

In Chapter Four, chondrite normalised rare earth element plots and the immobile element Ta/Yb versus Th/Yb diagram of Pearce (1982) were used to discriminate between the magmatic affinities of the units identified at Yiddah. It was demonstrated that the basaltic volcaniclastic unit is of low-K, calc-alkaline affinity, plotting only marginally above the (normal) MORB array in the Pearce (1982) plot (Figure 4.5), while the andesitic volcaniclastic unit plotted further from the MORB array as high-K calc-alkaline in affinity. The intrusive units exhibited high LREE and Th abundances, plotting as shoshonitic on the Pearce (1982) plot (Figure 4.10) and alkaline on the Pearce (1996) plot.

In Figure 8.4, the Yiddah intrusive samples are plotted on the Pearce (1982) immobile element magmatic series discrimination plots alongside other mineralised Macquarie Arc suites (Copper Hill, Goonumbla and Cadia). A variant of the Ta/Yb versus Th/Yb plot is also included which incorporates Ce, which behaves similarly to Th during both subduction and mantle melting (Pearce 1996). In both diagrams, the Yiddah samples plot furthest into the shoshonite field. The Copper Hill, Goonumbla and Cadia units are characterised by increasing Th with no definitive increase in Ta, interpreted as an increasing fluid subduction component with little crustal involvement. Assuming a common 'normal' MORB substrate, the Yiddah samples show an increase both upward and rightward to the shoshonite field, indicating the probable interaction of both fluid and sediment (or crustal) components.

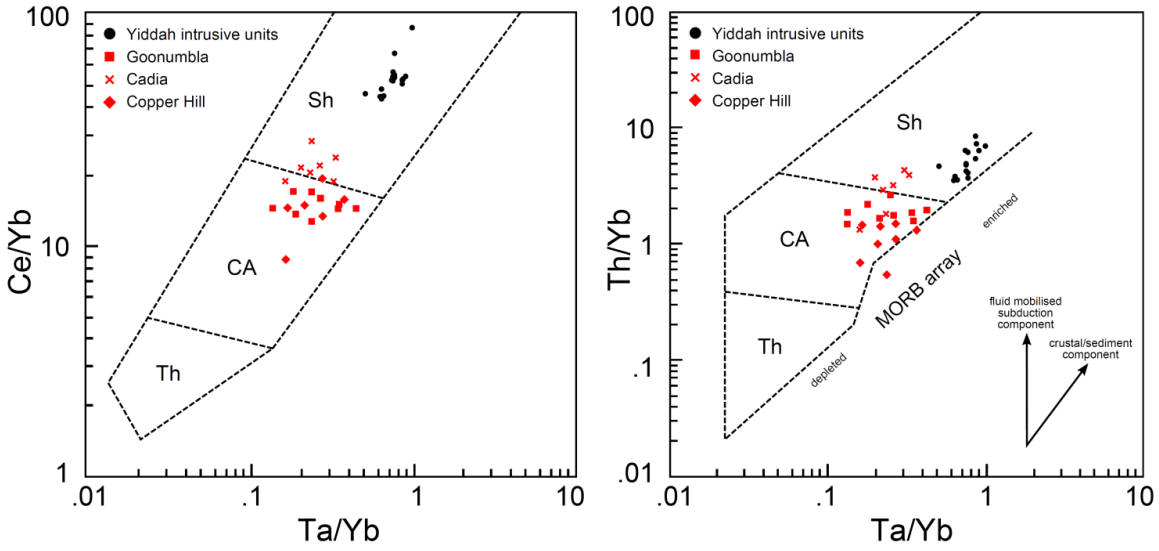

Figure 8.4: Discrimination diagrams of Pearce (1982) for intrusive units at Yiddah and other mineralised intrusive bodies of the Macquarie Arc. Copper Hill, Goonumbla and Cadia data from Blevin (2002). Plot adapted from Blevin (2002). Th = tholeiitic, CA = calc-alkaline, Sh = shoshonitic.

8.3. SHOSHONITES

Shoshonites are rocks of the potassic volcanic rock group, that s*ensu stricto* possess high K_2O/Na_2O ratios (> 0.5), LIL element enrichment, high $Na_2O + K_2O$ (> 5 wt%), high Al_2O_3 (> 9 wt%) and (generally) low TiO_2 (Morrison 1980; Müller & Groves 1993). Unlike calc-alkaline rocks, which are largely restricted to convergent margin settings, shoshonites are documented in a number of tectonic environments; including within-plate, continental arc, initial oceanic arc, late oceanic arc and post-collisional arc (Müller et al. 1992). Genetic associations have been recognised between Au-Cu mineralisation and K-enriched igneous

suites in late oceanic arcs (e.g. Cadia & Goonumbla), continental arcs (e.g. Bingham, U.S.A.) and post-collisional arcs (e.g. Porgera, Papua New Guinea) (Müller & Groves 1993).

The wide range of tectonic settings that shoshonites form within relates to the number of mechanisms which may generate K-enriched melts. Such mechanisms include (1) a small degree partial melt of the mantle, (2) addition of fluid mobile LIL elements from an aqueous subduction component, (3) incorporation of a sediment and/or crustal component, and (4) melting of an already enriched mantle. It is possible (and likely) that many K-enriched melts form due to a combination of these factors (Müller et al. 1992; Pearce 1996).

In ocean arc settings, spatio/temporal zonation patterns are commonly observed where shoshonites are younger, stratigraphically higher and located at greater height above the Benioff zone (i.e. further from the trench) than tholeiitic and calc-alkaline affinity rocks (Morrison 1980; Müller et al. 1992).

One explanation for trench-normal spatial zonation is that with increasing depth, the ability of the dehydrating slab to generate an aqueous fluid phase diminishes, which results in a smaller degree of partial melting and hence a more incompatible enriched mantle melt (Richards 2003; Kearey et al. 2009). In the Lachlan Orogen, dismemberment of volcanic belts and the likelihood of multiple subduction zones/multiple periods of arc-related volcanism make the recognition of any such spatial zonation extremely difficult.

The temporal zonation of increasing K-enrichment in late-oceanic arcs is considered to be related to increasing sediment addition with greater proximity to the continent (and associated collision) (Morrison 1980; Pearce & Peate 1995). This theory is supported by along-arc compositional variations recognised in the North Luzon Arc (Philippines), where the approach of the continent-collision has been demonstrated isotopically to be accompanied by increasing incompatible element enrichment, derived from wholesale melting of terrigenous sediment (McDermott et al. 1993). Morrison (1980) suggests that late-arc shoshonism may also be related to steepening of the subduction zone and eventual flipping during the termination of a subduction phase or transition of tectonic regimes.

The generation of shoshonitic affinity rocks in post-collisional settings is governed by less predictable processes. Post-collisional melts are produced through lithospheric thinning and

asthenospheric upwelling associated with relaxation following collision (Pearce et al. 1984; Wang et al. 1999). The melt source therefore will vary according to tectonic setting. The generation of small degree partial melts, crustal assimilation and the melting of pre-enriched mantle are all considered potential causes of shoshonitic affinity post-collisional melts.

In the Northern Taiwan Volcanic Zone, tholeiitic to shoshonitic affinity volcanism is attributed to post-collisional extensional collapse since Plio-Pleistocene time, despite ongoing collision in central and southern Taiwan (Wang et al. 1999). Of significant note, the whole orogenic spectrum of mountain building to extensional collapse is considered by Teng (1996) to have occurred within only a few million years; with the collision of the Luzon arc to the Asian continental margin occurring at ~ 10 Ma and the intrusion of post-collisional magmas from ~ 2.8 Ma. Due to the subduction-enriched source of the Northern Taiwan Volcanic Zone magmas, these rocks possess 'arc-like' signatures, characterised by high LIL/HFS element ratios. A southwestward spatial zonation of increasing shoshonism (LIL enrichment) is explained by a corresponding southwestward weakening extensional regime, which results in decreasing degrees of partial melting and thus enrichment of incompatible elements (Wang et al. 1999).

8.4. **DISCUSSION**

The significant variation in geochemical affinity (K-enrichment) of the volcaniclastic and intrusive units observed at Yiddah indicates that their emplacement was not coeval, but rather was offset spatially and/or temporally. Although limited geochronology has been performed on volcaniclastic material from the Gidginbung Volcanics, an $^{40}Ar/^{39}Ar$ illite age of 461.5 ± 1.1 Ma obtained from the Gidginbung pit (Perkins et al. 1995) indicates that volcaniclastic material may be considerably older than the intrusive bodies. The calc-alkaline affinity of volcaniclastic units suggests that this material was most likely extruded during 'normal' subduction conditions in an island-arc setting, possibly during Phase 2 volcanism recognised to have occurred in the Goonumbla-Trangie belt during the Middle to Late Ordovician (Glen et al. 2007a).

Numerous lines of evidence presented in the current study have indicated that the Rain Hill Monzodiorite at Yiddah, intrusive stocks at Yiddah and the Rain Hill Monzodiorite in the southern Gidginbung Volcanics are genetically related. Such factors include similar mineral

assemblages, similar geochemical abundances and evolutionary trends, similar and spatially connected geophysical signatures and tightly constrained geochronological age determinations. These findings have a number of implications in linking intrusive activity at Yiddah into the broader context of Macquarie Arc volcanism. Firstly, previously published absolute ages for intrusive bodies in the Gidginbung Volcanics (see Figure 2.8) can be collated with age determinations from this study (439.2 ± 6.4 Ma and 433.8 ± 6.4 Ma) to infer that magmatic emplacement most likely occurred at around 437 – 435 Ma, coinciding within error with mineralisation-related intrusive activity at Cadia (Wilson et al. 2007) and Goonumbla (Lickfold et al. 2003). Secondly, rather than viewing mineralisation at Yiddah as an isolated event (e.g. such as at Copper Hill and Marsden), mineralisation within the Gidginbung Volcanics is considered as a large-scale event, occurring with emplacement of a relatively large-volume of hydrous, oxidised melt (e.g. such as at Cadia and Goonumbla). Under the four phase Macquarie Arc model of Crawford et al. (2007a), Glen et al. (2007a) and Percival & Glen (2007), the Rain Hill district intrusives are geochemically, petrologically and chronologically consistent with Phase 4, which is characterised by more evolved, shoshonitic affinity melts than previous phases. This phase represents the final stage of magmatism before cessation of Macquarie Arc volcanism, which is considered to have commenced from around 438 Ma with arc-continent collision (Glen et al. 2007a). Phase 4 appears to be the most economically significant period of Macquarie Arc volcanism, as it includes the Cadia Intrusive Complex and Goonumbla Volcanic Complex intrusives.

Despite their geochemical and chronological similarities, a number of disparities are recognised between the Yiddah and Cadia/Goonumbla porphyry systems. At Cadia and Goonumbla, shoshonitic intrusive units have been emplaced into broadly coeval volcanic host rocks of largely shoshonitic-andesitic geochemical character (Blevin 2002). At Yiddah however, volcaniclastic units are of calc-alkaline affinity, with no coeval volcanic material identified in the current study. Volcaniclastic units also differ in that at Yiddah, they dip steeply to vertically and are possibly fault imbricated. Intrusion of mineralisation related stocks appears to have occurred predominantly along bedding, sub-parallel to the elongate parental Rain Hill Monzodiorite. It is unclear however if this geometric relationship was the product of initial intrusion or if it has been generated in response to later deformation occurring with movement along the Gilmore Fault Zone.

Enrichment of HFS elements in the Yiddah intrusives relative to the Cadia and Goonumbla suites is indicative of a greater sediment and/or crustal component within the Rain Hill Monzodiorite source melt (Pearce & Peate 1995). The origins of such an input may be (1) sediment subducted with the down-going plate and/or (2) incorporation of continental crust during emplacement. While it is considered that subducted sediment was a likely contributor, the possibility of continental crust involvement will now be considered.

The late nature of intrusion of the Rain Hill Monzodiorite (~ 437 – 435 Ma) relative to the evolutionary history of the Macquarie Arc makes it quite possible that its emplacement post-dated onset of arc-continent collision, considered to have commenced at ~ 438 Ma (i.e. emplacement was syn-collisional) (Glen et al. 2007a, 2007b). As discussed earlier, the approach and eventual collision of an oceanic arc to a continental margin is considered to be accompanied by an increasing supply of terrigenous sediment to the trench, leading to greater volumes of subducted sediment and a temporal gradation of increasing LIL and HFS element abundances (Morrison 1980; McDermott et al. 1993; Pearce & Peate 1995). It is therefore not unexpected that the latest stages of Macquarie Arc volcanism will display overall enrichment relative to the MORB. Indeed, Pb isotope studies (Carr et al. 1995; Forster et al. 2011) and the MORB normalised enrichment plot (Figure 8.1) indicate that the Cadia and Goonumbla systems are characterised by very minor crustal components.

For this mechanism to explain the significantly more LILE-HFSE enriched nature of the Rain Hill Monzodiorite melt however, it is considered that emplacement would have to have occurred somewhat later, following much larger volumes of sediment subduction. Although the time-frame required to produce such further enriched melts is probably not great, the coincidence in timing of mineralisation events in the Lachlan Orogen (the 440 Ma 'mineralisation epoch') cannot be ignored. The emplacement of a number of world-class Au deposits of differing styles (orogenic Au at Bendigo and Stawell and porphyry Cu-Au at Cadia and Goonumbla), along with a number of smaller deposits suggests it is likely that a major tectonic event occurred at this time. Squire & Miller (2003) have suggested that this event consisted of the subduction of a seamount or microcontinental block. Regardless of the mechanism, if mineralisation was coeval within the Rain Hill, Cadia and Goonumbla districts, an alternate explanation is necessary to explain the overall greater LIL and HFS element enrichment of the Rain Hill district.

One such explanation is that subduction occurred obliquely, producing an along-arc gradation of increasing sediment flux toward the Gondwanan margin. Strike-slip offset of the Goonumbla Trangie and Molong Volcanic Belts with anti-clockwise rotation as outlined in the model of Fergusson (2009) could also result in a greater terrigenous sediment yield within the southern trench region of the Goonumbla Trangie Volcanic Belt at this time.

An alternative explanation centres on the possibility that the emplacement mechanism of the Rain Hill district magmas was post-collisional. In this scenario, it is envisioned that the Yiddah melt would have an 'arc-like' signature due to an arc-enriched mantle source in common with other Phase 4 intrusive units, however would be additionally enriched in LIL and HFS elements due to the incorporation of crustal material with magma ascent through a Benambran-thickened continental crust. A possible modern analogue of this proposal may be the middle to late Miocene Porgera deposit (Papua New Guinea), in which shoshonitic mineralisation-related plugs, stocks and dykes are considered on structural and geochemical grounds to have been emplaced post-collisionally in essentially an arc-setting (Müller & Groves 1993).

Observations in the active Northern Taiwan Volcanic Zone have demonstrated the ability of oblique convergence to generate complex stress regimes, whereby a gradation from collisional to extensional conditions occurs over only a few hundred kilometres (Wang et al. 1999). Furthermore, this configuration has been shown by Teng (1996) to have developed entirely within a period of ~ 5 Ma, suggesting that in very active systems, the progression from onset of collision to post-collisional collapse may occur in a relatively short time period.

Under the post-collisional scenario, it is hence envisioned that the onset of the Benambran Orogeny at ~ 438 Ma resulted in accretion of the Goonumbla-Trangie Volcanic Belt, generating the thrust imbricated volcaniclastic configuration observed for the Gidginbung and adjacent Belimebung Volcanics. With the northward migration of the collisional regime (due to oblique convergence), post-collisional collapse may have occurred in this region coinciding with relatively 'normal' subduction (albeit syn-collisional) arc-volcanism elsewhere. Post-collisional collapse in the Rain Hill district is envisioned to have enabled the endowed melt that had previously been stalled at the base of the crust to advect upward, focusing along the major regional structure of the Wagga Metamorphic Belt/accreted volcanics contact (the Gilmore Fault Zone). This explanation accounts for the reasonably

intact yet highly elongate nature of the Rain Hill Monzodiorite. It also presents a potential link between major Phase 4 mineralised zones and major crustal structures; with the intrusion along the Gilmore Fault Zone possibly akin to the intrusion of the Cadia – Goonumbla systems along the proposed Lachlan Transverse Zone (Glen & Walshe 1999).

The post-collisional theory is partly supported by the work of Forster et al. (2011), who use $^{208}Pb/^{204}Pb$ and $^{207}Pb/^{204}Pb$ isotopic ratios interpreted using the plumbotectonic model of Carr et al. (1995) to differentiate between the relative contribution of crustal and mantle sources to mineralised systems of the Macquarie Arc, including Cadia, Goonumbla and Gidginbung. It is demonstrated that the Cadia and Goonumbla deposits possess Pb isotope ratios consistent with partial melting of a LIL element enriched mantle-like source that has undergone little exchange with more evolved crustal rocks. The Gidginbung deposit contrastingly displays a minor to moderate level of crustal enrichment relative to the mantle. As significant amounts of Pb are unlikely to be incorporated into marine sediments due to the short residence time of Pb (Wombacher & Münker 2000), this enrichment is considered by Forster et al. (2011) to be more likely the result of crustal contamination. There is also however the possibility that Pb isotopes may have homogenised with those of the adjacent sedimentary and metasedimentary rocks during the proposed remobilisation of mineralisation in Devonian shearing events of Allibone et al. (1995). For this reason, it is considered that more conclusive isotopic evidence would be attained from targeting one of the better preserved porphyry-style deposits within the Rain Hill district, such as Culingerai or Mandamah.

8.5. **ECONOMIC IMPLICATIONS**

The evidence presented in this study suggests that the Rain Hill magmas were likely to have been sourced from the same mantle reservoir as the world-class Cadia and Goonumbla systems and emplaced roughly contemporaneously, during Phase 4 of Macquarie Arc volcanism. Key similarities include the more evolved, shoshonitic chemistry of magmas, the late nature of intrusion (probably coinciding with the onset of the Benambran Orogeny) and the provincial, clustered nature of mineralised systems. If a post-collisional emplacement mechanism is responsible for the observed LILE-HFSE enrichment, the effect of crustal incorporation could possibly be a degree of mineralisation dilution, or other unknown effect on the chemical and physical characteristics of the melt (e.g. oxygen fugacity).

It can be commented however, that the broad similarities between world-class mineralised systems at Cadia and Goonumbla and those emerging in the Rain Hill district is encouraging for the potential discovery of further large tonnage, low-grade, porphyry Cu or epithermal Au style mineralisation in the Rain Hill district. Exploration of this region is difficult due to a number of factors; including the significant volumes of transported sediment cover, lack of distinct geophysical signatures where mineralised systems are recognised and the strong deformational overprint which has generated 'regional propylitic alteration' (sub to lower greenschist metamorphism). Alkaline porphyry systems in general are also considered to be more difficult exploration targets than calc-alkaline systems, due to smaller overall volumes of altered rocks and narrower intrusion dimensions (Cooke et al. 2007).

The recognition of shoshonitic related mineralisation in the Rain Hill district further affirms the Macquarie Arc's position as the second major alkaline porphyry province in the world behind British Columbia, Canada (Cooke et al. 2007). This in turn increases the overall prospectivity of the Macquarie Arc volcanic rocks and also potentially other units of a similar tectonic setting to the Gidginbung Volcanics at the time of emplacement under the post-collisional collapse scenario.

CHAPTER NINE

PARAGENESIS AND CONCLUSIONS

The current work has identified a complex depositional, intrusive and deformational history for the Yiddah porphyry Cu-(Au-Mo) system. The oldest rocks consist of a relatively primitive low-K, calc-alkaline affinity basaltic volcaniclastic unit and a high-K calc-alkaline affinity andesitic volcaniclastic unit; deposited separately in time and/or space during Ordovician Macquarie Arc volcanism. These units dip steeply east and strike north-northwesterly, parallel to the proximal Gilmore Fault and typifying the trends observed throughout the entire Gidginbung Volcanics.

Intrusion of mineralisation-related shoshonitic affinity magmas occurred during the early Silurian, either; (1) during the late stages of Macquarie Arc island-arc formation, as more Gondwanan derived sediment was subducted prior to arc collision, or (2) within a post-collisional collapse setting whereby magmas were intruded into already deformed Macquarie Arc volcanic rocks (the Gidginbung Volcanics). Geochemical, petrographic, geochronological and geophysical consistencies link the intrusive units at Yiddah to those described in the southern extent of the Gidginbung Volcanics (the Rain Hill Monzodiorite); suggesting this magmatic event was voluminous and constituted the causative agent for the emplacement of the number of porphyry-related systems currently recognised on the eastern margin of the Rain Hill Monzodiorite.

Intrusion of the Rain Hill Monzodiorite at Yiddah resulted in contact metamorphism of the volcaniclastic units, particularly the basally located fine-grained basaltic volcaniclastics. This generated an interlocking matrix of secondary minerals which decreased the ensuing permeability of this unit. Mineralised porphyritic textured sills/stocks intruded mostly within the andesitic volcaniclastics either contemporaneously or subsequent to the more slowly cooling sub-equigranular Rain Hill Monzodiorite, from the same broad magmatic source. SHRIMP analysis of zircons extracted from the Rain Hill Monzodiorite granitoid and a mineralised porphyry stock indicate that both are of the same early Silurian age (439.2 ± 6.4 Ma and 433.8 ± 6.4 Ma, respectively) within error. The relatedness of these two units has been shown through; (1) their similar primary mineralogy (plagioclase, K-feldspar, amphibole, quartz, titanite, titanomagnetite, apatite, zircon), (2) their similarity in immobile

element classification and tectonic discrimination plots and (3) their comparable fractionation trends as revealed on immobile element bivariate diagrams (e.g. SiO_2/TiO_2, TiO_2/P_2O_5, TiO_2/V, V/Co). All of the mineralisation related porphyritic textured stocks sampled in the current work plot as slightly more evolved than the Rain Hill Monzodiorite, but not as evolved as the very late, narrow, equigranular dykes that probably also evolved from the Rain Hill Monzodiorite.

Mineralised fluids interpreted to have exsolved from the porphyritic stocks generated a central, early chlorite-magnetite alteration assemblage with associated quartz/magnetite/ chalcopyrite disseminated mineralisation and quartz-seam veins containing molybdenite and chalcopyrite. This assemblage grades upwards into a chlorite-sericite zone with greater concentrations of Mo and, in turn, into an overlying lesser-mineralised sericitic zone. These alteration styles and the bulk of mineralisation were developed predominantly within porphyry stocks and the andesitic volcaniclastic country rocks, where Cu correlates reasonably well with Au but not with Mo.

Beneath the chlorite-magnetite alteration zone, propylitic-style alteration was developed within the basaltic volcaniclastic and Rain Hill Monzodiorite units. This alteration style produced pervasive chloritisation and voluminous epidote veining in the basaltic unit and more selective vein-related epidote and albite alteration within the Rain Hill Monzodiorite. Significant carbonate addition also occurred related to propylitic hydrothermal alteration. Infrequent neat (well-preserved) mineralised quartz-seam veins contained within the Rain Hill Monzodiorite were probably emplaced erratically during early porphyry system evolution, but never to the extent of generating significant mineralisation in this this unit.

Following porphyry-related mineralisation, the Yiddah system underwent a deformation event, or series of events that produced abundant macro- and micro-structural features (e.g. tension gashes, cracked phenocrysts) and a strong overprinting north-northwest foliation consistent with regional trends. It is thought that this deformation was related to successive periods of movement along the nearby Gilmore Fault, which probably represents a major crustal-scale discontinuity or possibly even a suture between the Macquarie Arc and the Gondwanan continent. Silurian – Devonian ages (413 ± 4 Ma and 423 ± 5 Ma) obtained from K-Ar illite dating within the southern Gidginbung Volcanics by Perkins et al. (1995) are considered to constrain the timing of such deformation. It is likely however that shearing

occurred episodically over a reasonably protracted time period related to the number of orogenic events that affected the Lachlan Orogen subsequent to the emplacement of the Rain Hill district magmas.

Deformation also resulted in a pervasive chlorite/albite/sericite/epidote/calcite/rutile ('regional-propylitic') alteration assemblage at Yiddah possibly along with a more localised, intense sericitic-argillic shear assemblage (sericite/kaolinite/quartz/pyrite). Chlorite geothermometry and textural observations related to sulphide mobilisation suggest that the temperature of deformation related to 'regional-propylitic' alteration was ~ 300ºC. These conditions led to the recrystallisation and mobilisation of disseminated chalcopyrite throughout the groundmass and to within coarsely crystalline late tension-gash (infill) veins (± carbonate, quartz, chlorite and K-feldspar). The coexistence of early resistant quartz-seam veins and recrystallised chalcopyrite indicates that mobilisation of mineralisation did not occur on a large spatial scale at Yiddah. The prospect is therefore most accurately described as a porphyry copper system possessing a strong deformational (or shear) overprint.

This overprint constitutes the key difference between the Yiddah prospect and other known porphyry copper systems of the Macquarie Arc. Of these, Yiddah is most similar to the shoshonitic Cadia and Goonumbla porphyry systems. Despite whole-rock K concentrations plotting in the field of high-K calc-alkaline; immobile trace element proxies (Th and Ce) have demonstrated the primary shoshonitic chemistry of the Yiddah intrusive units. Coupled with the late Macquarie Arc age obtained from U-Pb zircon dating, these findings suggest that magmatism within the Rain Hill district occurred during Phase 4 volcanism within the Macquarie Arc model of Percival & Glen (2007), Crawford et al. (2007b) and Glen et al. (2007a); sharing a common petrogenetic history with the Cadia and Goonumbla systems. Further similarities include common alteration styles (early magnetite, later sericite and albite assemblages; Smith et al. 2004), the slightly more evolved chemistry of intrusives at Yiddah than average Macquarie Arc volcanism and the regional clustering of mineralised systems.

The Yiddah (Rain Hill) system differs however in that the causative magmas appear to have incorporated a crustal component, inferred primarily from elevated HFS element abundances relative to the MORB. This is attributed either to an increased volume of subducted terrestrial sediment with increasing proximity to the Gondwanan continent during late stage arc-magmatism, or to greater crustal interaction due to emplacement through a Benambran

thickened crust during post-collisional collapse. In the latter scenario, it is hypothesised that the Gilmore Fault Zone may have acted as an efficient conduit for melts of an arc-enriched mantle origin essentially akin to the Cadia and Goonumbla melt sources to be transported to mid/shallow crustal levels where porphyry system evolution could ensue. Whichever the emplacement mechanism, the primary shoshonitic chemistry of the Rain Hill Monzodiorite as identified at Yiddah and relatively late stage of its intrusion relative to Macquarie Arc volcanism is a positive indicator for the ongoing exploration prospectivity of the Rain Hill district, a highly obscured region of the Macquarie Arc.

REFERENCES

Allibone, A., Cordery, G., Gregg, W., Jaireth, S. & Lindhorst, J. (1995) Synchronous advanced argillic alteration and deformation in a shear zone-hosted magmatic hydrothermal Au-Ag deposit at the Temora (Gidginbung) Mine, New South Wales, Australia. *Economic Geology* **90**: 1570-1603.

Beane, R. (1982) Hydrothermal alteration in silicate rocks. *In* Titley, S. ed. *Advances in the Geology of the Porphyry Copper Deposits, Southwestern North America*, pp.117-137. University of Arizona Press, Tuscon, Arizona.

Beane, R. & Bodnar, R. (1995) Hydrothermal fluids and hydrothermal alteration in porphyry copper deposits. *In* Pierce, F., & Bohm, J. eds. *Porphyry Copper Deposits of the American Cordillera*, pp.83-93. Arizona Geological Society Digest, Tuscon, Arizona.

Bierlein, F., Gray, D. & Foster, D. (2002) Metallogenic relationships to tectonic evolution-the LachlanOrogen, Australia. *Earth and Planetary Science Letters* **202**: 1-13.

Black, L., Kamo, S., Allen, C., Davis, D., Aleinikoff, J., Valley, J., Mundil, R., Campbell, I., Korsch, R.,Williams, I. & Foudoulis, C. (2004) Improved $^{206}Pb/^{238}U$ microprobe geochronology by the monitoring of a trace-element-related matrix effect; SHRIMP, ID–TIMS, ELA–ICP–MS and oxygen isotope documentation for a series of zircon standards. *Chemical Geology* **205** (1-2): 115-140.

Black, L., Kamo, S., Williams, I,. Mundil, R., Davis, D., Korsch, R. & Foudoulis, C. (2003) The application of SHRIMP to Phanerozoic geochronology; a critical appraisal of four zircon standards. *Chemical Geology* **200** (1-2): 171-188.

Blevin, P. (1998) A re-evaluation of mineralized Ordovician intrusives in the Lachlan Fold Belt: implications for tectonic and metallogenic models. *Geological Society of Australia, Abstracts* **49**: p. 43.

Blevin, P. (2002) The petrographic and compositional character of variably K-enriched magmatic suites associated with Ordovician porphyry Cu – Au mineralisation in the Lachlan Fold Belt, Australia. *Mineralium Deposita* **37**: 87-99.

Blevin, P. & Chappell, B. (1995) Chemistry, origin and evolution of mineralized granites in the Lachlan Fold Belt, Australia: The metallogeny of I- and S-Type granites. *Economic Geology* **90**: 1604-1619.

Boynton, W. (1984) Geochemistry of the rare earth elements: meteorite studies. *In* Henderson, P. ed. *Rare earth element geochemistry*, pp. 63-114. Elsevier

Braun, J. & Pauselli, C. (2004) Tectonic evolution of the Lachlan Fold Belt, southeastern Australia constraints from coupled numerical models of crustal deformation and surface erosion driven by subduction of the underlying mantle. *Physics of The Earth and Planetary Interiors* **141** (4): 281-301.

Burnham, C. (1979) Magmas and hydrothermal fluids. *In* Barnes, H. ed. *Geochemistry of hydrothermal ore deposits*, pp.71-136. John Wiley & Sons

Butera, K., Williams, I., Blevin, P. & Simpson, C. (2001) Zircon U–Pb dating of Early Palaeozoic monzonitic intrusives from the Goonumbla area, New South Wales. *Australian Journal of Earth Sciences* **48** (3): 457-464.

Campbell, T., Ballard, J., Palin, J., Allen, C. & Faunes, A. (2006) U- Pb zircon geochronology of granitic rocks from the Chuquicamata-El Abra porphyry copper belt of northern Chile: Excimer laser ablation ICP-MS analysis. *Economic Geology* **101**: 1327-1344.

Candela, P. & Holland, H. (1984) The partitioning of copper and molybdenum between silicate melts and aqueous fluids. *Geochemica et Cosmochimica Acta* **48**: 373-380.

Candela, P. & Holland, H. (1986) A mass transfer model for copper and molybdenum in magmatic hydrothermal systems: the origin of porphyry-type copper deposits. *Economic Geology* **81**: 1-18.

Candela, P. & Piccoli, P. (2005) Magmatic processes in the development of porphyry-type ore systems. *Economic Geology* (100th Anniversary Volume): 25-37.

Carr, G., Dean, J., Suppel, D. & Heithersay, P. (1995) Precise lead isotope fingerprinting of hydrothermal activity associated with Ordovician to Carboniferous metallogenic events the Lachlan Fold Belt of New South Wales. *Economic Geology* **90**: 1467-1505.

Casselman, M., McMillan, W. & Newman, K. (1995) Highland Valley porphyry copper deposits near Kamloops, British Columbia: A review and update with emphasis on the Valley deposit. *Canadian Institute of Mining, Metallurgy and Petroleum* Special Volume **46**: 161-191.

Cathelineau, M. (1988) Cation site occupancy in chlorites and illites as a function of temperature. *Clay Minerals* **23**: 471-485.

Cathelineau, M. & Nieva, D. (1985) A chlorite solid solution geothermometer, The Loz Azufres (Mexico) geothermal system. *Contributions to Mineralogy and Petrology* **91**: 235-244.

Chivas, A. & Nutter, A. (1975) Copper Hill porphyry-copper Prospect. *In* Knight, C. ed. *Economic Geology of Australia and Papua New Guinea*, pp.716-720. Australian Institute of Mining and Metallurgy, Melbourne.

Clemens, J. & Mawer, C. (1992) Granitic magma transport by fracture propagation. *Tectonophysics* **204**: 339-360.

Collins, W. (2002) Hot orogens, tectonic switching, and creation of continental crust. *Geology* **30** (6): 535-538.

Colquhoun, G., Fergusson, C. & Tye, S. (1999) Provenance of early Palaeozoic sandstones, southeastern Australia, Part 2: cratonic to arc switching. *Sedimentary Geology* **125** (3-4): 153-163.

Coney, P. (1992) The Lachlan Belt of eastern Australia and Circum-Pacific tectonic evolution. *Tectonophysics* **214** (1-4): 1-25.

Cooke, D., Hollings, P. & Walshe, J. (2005) Giant Porphyry Deposits: characteristics, distribution, and tectonic controls. *Economic Geology* **100** (5): 801-818.

Cooke, D., Wilson, A., House, M., Wolfe, R., Walshe, J., Lickfold, V. & Crawford, A. (2007) Alkalic porphyry Au - Cu and associated mineral deposits of the Ordovician to Early Silurian Macquarie Arc, New South Wales. *Australian Journal of Earth Sciences* **54** (2): 445-463.

Corfu, F., Hanchar, J., Hoskin, P. & Kinny, P. (2003) Atlas of zircon textures. *In* Hanchar, J. & Hoskin, P. eds. *Reviews in Mineralogy & Geochemistry*, *Volume 53. Zircon*. pp. 468-500.

Cox, S., Etheridge, M. & Wall, V. (1987) The role of fluids in syntectonic mass transport, and the localization of metamorphic vein-type ore deposists. *Ore Geology Reviews* **2** (1-3): 65-86.

Crawford, A., Cooke, D. & Fanning, C. (2007b) Geochemistry and age of magmatic rocks in the unexposed Narromine, Cowal and Fairholme Igneous Complexes in the Ordovician Macquarie Arc, New South Wales. *Australian Journal of Earth Sciences* **54** (2): 243-271.

Crawford, A., Meffre, S., Squire, R., Barron, L. & Falloon, T. (2007a) Middle and Late Ordovician magmatic evolution of the Macquarie Arc, Lachlan Orogen, New South Wales. *Australian Journal of Earth Sciences* **54** (2): 181-214.

Davis, D., Williams, I. & Krogh, T. (2003) Historical development of zircon geochronology. *In* Hanchar, J. & Hoskin, P. eds. *Reviews in Mineralogy & Geochemistry*, *Volume 53. Zircon.* pp.145-181.

De Caritat, P., Hutcheon, I. & Walshe, J. (1993) Chlorite Geothermometry: A Review. *Clays and Clay Minerals* **41** (2): 219-239.

Deckart, K., Clark, A., Aguilar, C., Vargas, R., Bertens, A., Mortensen, J. & Fanning, M. (2005) Magmatic and hydrothermal chronology of the giant Rio Blanco porphyry copper deposit, central Chile: Implications of an integrated U-Pb and $^{40}Ar/^{39}Ar$ database. *Economic Geology* **100**: 905-934.

Downes, P., McEvilly, R. & Raphael, N. (2004) Mineral deposits and models, Cootamundra 1:250,000 map sheet area. *Geological Survey of New South Wales Quarterly Notes* **116**: p. 38.

Emmons, W. (1924) Primary Downward Changes in Ore Deposits. *American Institution of Mining and Metallurgy Engineers Transcripts* **70:** 964.

Fergusson, C. (2003) Ordovician-Silurian accretion tectonics of the Lachlan Fold Belt, southeastern Australia. *Australian Journal of Earth Sciences* **50** (4): 475-490.

Fergusson, C. (2009) Tectonic evolution of the Ordovician Macquarie Arc, central New South Wales: arguments for subduction polarity and anticlockwise rotation. *Australian Journal of Earth Sciences* **56** (2): 179-193.

Fergusson, C. & Coney, P. (1992) Convergence and intraplate deformation in the Lachlan Fold Belt of Southeastern Australia. *Tectonophysics* **214** (1-4): 417-439.

Fergusson, C. & Fanning, C. (2002) Late Ordovician stratigraphy, zircon provenance and tectonics, Lachlan Fold Belt, southeastern Australia. *Australian Journal of Earth Sciences* **49**: 423-436.

Fergusson, C. & Tye, S. (1999) Provenance of early Palaeozoic sandstones, southeastern Australia, Part 1: vertical changes through the Bengal fan-type deposit. *Sedimentary Geology* **125** (3-4): 135-151.

Force, E. (1991) Titanium oxide minerals in other igneous suites. *In Geology of Titanium-Mineral Deposits, The Geological Society of America, Special Paper 259*. The Geological Society of America, Boulder, pp. 47-50.

Forster, D. (2004) Controls on skarn mineralization and alteration at the Cadia Deposits, New South Wales, Australia. *Economic Geology* **99** (4): 761-788.

Forster, D., Carr, G. & Downes, P. (2011) Lead isotope systematics of ore systems of the Macquarie Arc - Implications for arc substrate. *Gondwana Research* **19** (3): 686-705.

Foster, D. & Gray, D. (2000) Evolution and Structure of the Lachlan Fold Belt (Orogen) of Eastern Australia. *Annual Review of Earth and Planetary Sciences* **28**: 47-80.

Fu, B., Mernagh, T., Kita, N., Kemp, A. & Valley, J. (2009) Distinguishing magmatic zircon from hydrothermal zircon: A case study from the Gidginbung high-sulphidation Au–Ag–(Cu) deposit, SE Australia. *Chemical Geology* **259** (3-4): 131-142.

Glazner, A. (1991) Plutonism, oblique subduction, and continental growth: An example from the Mesozoic of California. *Geology* **19** (8): 784-786.

Glen, R. (1992) Thrust, extensional and strike-slip tectonics in an evolving Palaeozoic orogen—a structural synthesis of the Lachlan Orogen of southeastern Australia. *Tectonophysics* **214**: 341–380.

Glen, R. (1995) Thrusts and thrust-associated mineralization in the Lachlan Orogen. *Geology* **90**: 1402-1429.

Glen, R., Crawford, A. & Cooke, D. (2007a) Tectonic setting of porphyry Cu - Au mineralisation in the Ordovician - Early Silurian Macquarie Arc, Eastern Lachlan Orogen, New South Wales. *Australian Journal of Earth Sciences* **54** (2): 465-479.

Glen, R., Korsch, R., Direen, N., Jones, L., Johnstone, D., Lawrie, K., Finlayson, D. & Shaw, R. (2002) Crustal structure of the Ordovician Macquarie Arc, Eastern Lachlan Orogen, based on seismic-reflection profiling. *Australian Journal of Earth Sciences* **49**: 323-348.

Glen, R., Meffre, S. & Scott, R. (2007b) Benambran Orogeny in the Eastern Lachlan Orogen, Australia. *Australian Journal of Earth Sciences* **54** (2): 385-415.

Glen, R., Saeed, A., Quinn, C. & Griffin, W. (2011) U–Pb and Hf isotope data from zircons in the Macquarie Arc, Lachlan Orogen: Implications for arc evolution and Ordovician palaeogeography along part of the east Gondwana margin. *Gondwana Research* **19** (3): 670-685.

Glen, R., Spencer, R., Willmore, A., David, V. & Scott, R. (2007c) Junee – Narromine Volcanic Belt, Macquarie Arc, Lachlan Orogen, New South Wales: components and structure. *Australian Journal of Earth Sciences* **54** (2): 215-241.

Glen, R. & Walshe, J. (1999) Cross-structures in the Lachlan Orogen: the Lachlan Transverse Zone example. *Australian Journal of Earth Sciences* **46** (4): 641-658.

Glen, R., Walshe, J., Barron, L. & Watkins, J. (1998) Ordovician convergent-margin volcanism and tectonism in the Lachlan sector of east Gondwana. *Geology* **26**: 751-754.

Glen, R. & Wyborn, D. (1997) Inferred thrust imbrication, deformation gradients and the Lachlan Transverse Zone in the Eastern Belt of the Lachlan Orogen, New South Wales. *Australian Journal of Earth Sciences* **44** (1): 49-68.

Goldminco Corporation (2010) Exploration Update; Vancouver, BC, July 22, 2010; Goldminco Corporation (TSXV: GCP) News Release. p.10.

Gradstein, F., Ogg, J. & Smith, A. (2004) *A Geological Time Scale 2004*, Cambridge University Press, Cambridge.

Gray, D. & Foster, D. (1998) Character and kinematics of faults within the turbidite-dominated Lachlan Orogen: implications for tectonic evolution of eastern Australia. *Journal of Structural Geology* **20** (12): 1691-1720.

Gray, D. & Foster, D. (2004) Tectonic evolution of the Lachlan Orogen, southeast Australia: historical review, data synthesis and modern perspectives. *Australian Journal of Earth Sciences* **51**: 773-817.

Gray, D., Foster, D. & Bucher, M. (1997) Recognition and definition of orogenic events in the Lachlan Fold Belt. *Australian Journal of Earth Sciences* **44**: 489-501.

Gustafson, L. (1978) Some major factors of porphyry copper genesis. *Economic Geology* **73**: 600-607.

Gustafson, L. & Hunt, J. (1971) Evolution of mineralisation at El Salvador, Chile. *Economic Geology Abstracts* **66**: 1266-67.

Gustafson, L. & Hunt, J. (1975) The porphyry copper deposit at El Salvador, Chile. *Economic Geology* **70**: 857-912.

Harris, A. & Golding, S. (2002) New evidence of magmatic-fluid – related phyllic alteration: Implications for the genesis of porphyry Cu deposits. *Geology* **30** (4): 335-338.

Hastie, A., Kerr, A., Pearce, J. & Mitchell, S. (2007) Classification of altered volcanic island arc rocks using immobile trace elements: development of the Th-Co discrimination diagram. *Journal of Petrology* **48** (12): 2341-2357.

Hawkesworth, C. (1997) U-Th isotopes in arc magmas: implications for element transfer from the subducted crust. *Science* **276** (551): 551-555.

Heinrich, C., Gunther, D., Audetat, A., Ulrich, T. & Frischknecht, R. (1999) Metal fractionation between magmatic brine and vapor, determined by microanalysis of fluid inclusions. *Geology* **27** (8): 755-758.

Heithersay, P. & Walshe, J. (1995) Endeavour 26 North; a porphyry copper-gold deposit in the Late Ordovician, shoshonitic Goonumbla volcanic complex, New South Wales, Australia. *Economic Geology* **90** (6): 1506-1532.

Hildreth, W. & Moorbath, S. (1988) Crustal contributions to arc magmatism in the Andes of central Chile. *Contributions to Mineralogy and Petrology* **98**: 455-489.

Hobbs, B. (1987) Principles involved in mobilization and remobilization. *Ore Geology Reviews* **2** (1-3):37-45.

Holland, H. (1972) Granites, solutions, and base metal deposits. *Economic Geology* **67** (3): 281-301.

Holliday, J. & Cooke, D. (2007) Advances in geological models and exploration methods for copper ± gold porphyry deposits. *In* Milkereit, B. ed. *Proceedings of Exploration 07: Fifth Decennial International Conference on Mineral Exploration,* pp.791-809. Toronto.

Holliday, J., Wilson, A., Blevin, P., Tedder, I., Dunham, P. & Pfitzner, M. (2002) Porphyry gold – copper mineralisation in the Cadia district, eastern Lachlan Fold Belt, New South Wales, and its relationship to shoshonitic magmatism. *Mineralium Deposita* **37** (1): 100-116.

Hoskin, P. (2000) Patterns of chaos: fractal statistics and the oscillatory chemistry of zircon. *Geochimica et Cosmochimica Acta* **64** (11): 1905-1923.

Hoskin, P. & Schaltegger, U. (2003) The composition of zircon and igneous and metamorphic petrogenesis. *In* Hanchar, J. & Hoskin, P. eds. *Reviews in Mineralogy & Geochemistry, Volume 53. Zircon*. pp.27-62.

Hough, M., Bierlein, F. & Wilde, A. (2007) A review of the metallogeny and tectonics of the Lachlan Orogen. *Mineralium Deposita* **42**: 435-448.

Hunt, J. (1991) Porphyry Copper Deposits. *Economic Geology* (Monograph **8)**: 192-206.

Ickert, R. & Williams, I. (2011) U–Pb zircon geochronology of Silurian–Devonian granites in southeastern Australia: implications for the timing of the Benambran Orogeny and the I–S dichotomy. *Australian Journal of Earth Sciences* **58** (5): 501-516.

Ishihara, S. (1981) The granitoid series and mineralization. *Economic Geology* (75th Anniversary Volume): 458-484.

Jaques, A., Jaireth, S. & Walshe, J. (2002) Mineral systems of Australia: an overview of resources, settings and processes. *Australian Journal of Earth Sciences* **49** (4): 623-660.

Jowett, E. (1991) Fitting iron and magnesium into the hydrothermal chlorite geothermometer. In *GAC/MAC/SEG Joint Annual Meeting, May 27-29, 1991, Program with Abstracts 16*, p.A62. Toronto.

Kearey, P., Klepeis, K. & Vine, F. (2009) *Global Tectonics,* 3rd ed., Wiley-Blackwell, West Sussex.

Kerrich, R., Allison, I. & Barnett, R., 1998. Interaction of chemical and mechanical factors in biotite deformation. *In* Snoke, A., Tullis, J. & Todd, T. eds. *Fault-related Rocks: A Photographic Atlas*, Princeton University Press, pp. 470-471, Princeton.

Kesler, S. (1973) Copper, molybdenum and gold abundances in porphyry copper deposits. *Economic Geology* **68**: 106-112.

Kesler, S., Jones, L. & Walker, R. (1975) Intrusive rocks associated with porphyry copper mineralization in island arc areas. *Economic Geology* **70** (3): 515-526.

Kilinc, I. & Burnham, C. (1972) Partitioning of chloride between a silicate melt and coexisting aqueous phase from 2 to 8 kilobars. *Economic Geology* **67**: 231-235.

Lang, J. & Baker, T. (2001) Intrusion-related gold systems: the present level of understanding. *Mineralium Deposita* **36** (6): 477-489.

Lawrie, K., Mernagh, T. & Ellis, P. (1997) Host rock control on localisation of the Gidginbung epithermal high sulfidation Au deposit. *Geological Society of Australia, Abstracts* **44**: p.45.

Lawrie, K., Mernagh, T., Ryan, C., Achterbergh, E. & Black, L. (2007) Chemical fingerprinting of hydrothermal zircons: an example from the Gidginbung high sulphidation Au-Ag-(Cu) deposit, New South Wales, Australia. *Proceedings of the Geologists' Association* **118**: 37-46.

Li, Z. & Powell, C. (2001) An outline of the palaeogeographic evolution of the Australasian region since the beginning of the Neoproterozoic. *Earth-Science Reviews* **53** (3-4): 237-277.

Lickfold, V., Cooke, D., Crawford, A. & Fanning, C. (2007) Shoshonitic magmatism and the formation of the Northparkes porphyry Cu - Au deposits, New South Wales. *Australian Journal of Earth Sciences* **54** (2): 417-444.

Lickfold, V., Cooke, D., Smith, S. & Ulrich, T. (2003) Endeavour copper-gold porphyry deposits, Northparkes, New South Wales: Intrusive history and fluid evolution. *Economic Geology* **98** (8): 1607-1636.

Lindgren, W. (1933) *Mineral Deposits,* 4th ed., McGraw-Hill, New York.

Lowell, J. & Guilbert, J. (1970) Lateral and vertical alteration-mineralization zoning in porphyry ore deposits. *Economic Geology* **65** (4): 373-408.

Ludwig, K. (1999) *Using ISOPLOT/EX Version 1.00b: A Geochronological Toolkit for Microsoft Excel*. Berkeley Geochronology Center, p.1. (Special Publication).

MacCorquodale, F. (1997) *EL1563, Barmedman North, Barmedman, NSW, annual exploration progress report 19th Feb 1996 - Feb 1997*, Gold Mines of Australia (NSW) Pty Ltd, pp. 8

Marshall, B. & Gilligan, L. (1987) An introduction to remobilization: Information from ore-body geometry and experimental considerations. *Ore Geology Reviews* **2**(1-3): 87-131.

Mason, D. (1996) *Petrographic Descriptions and Interpretations for Ten Rock Samples, Drill Hole PY12 (Yiddah Prospect)*, Mason Geoscience Australia Pty Ltd, pp. 1-42

McDermott, F., Defant, M., Hawkesworth, C., Maury, R. & Joron, J. (1993) Isotope and trace element evidence for three component mixing in the genesis of the North Luzon lavas (Philippines). *Contributions to Mineralogy and Petrology* **113**: 9-23.

Meffre, S., Scott, R., Glen, R. & Squire, R. (2007) Re-evaluation of contact relationships between Ordovician volcanic belts and the quartz-rich turbidites of the Lachlan Orogen. *Australian Journal of Earth Sciences* **54** (2): 363-383.

Meyer, C. & Hemley, J. (1967) Wall rock alteration. *In* Barnes, H. ed. *Geochemistry of hydrothermal ore deposits.* pp.166-235. Holt, Rinehart and Winston, New York.

Miles, I. & Brooker, M. (1998) Endeavour 42 deposit, Lake Cowal, New South Wales: A structurally controlled gold deposit. *Australian Journal of Earth Sciences* **45** (6): 837-847.

Mongkoltip, P. & Ashworth, J. (1983) Exsolution of ilmenite and rutile in hornblende. *American Mineralogist* **68:**.143-155.

Morrison, G. (1980) Characteristics and tectonic setting of the shoshonite rock association. *Lithos* **13:** 97-108.

Mottl, M. (1983) Metabasalts, axial hot springs, and the structure of hydrothermal systems at mid-ocean ridges. *Geological Society Of America Bulletin* **94**: 161-180.

Mowat, B. & Smith, S. (2006) Characteristics of porphyry Au-Cu systems in the Ordovician Macquarie Arc of NSW. *In* Lewis, P. ed. *Mineral Exploration Geoscience in New South Wales: SMEDG Mines and Wines Conference*, pp.11-17.Mudgee, New South Wales.

Müller, D. & Groves, D. (1993) Direct and indirect associations between potassic igneous rocks, shoshonites and gold-copper deposits. *Ore Geology Reviews* **8** (5): 383-406.

Müller, D., Rock, N. & Groves, D. (1992) Geochemical discrimination between shoshonitic and potassic volcanic rocks in different tectonic settings: A pilot study. *Mineralogy and Petrology* **46** (4): 259-289.

Munro, S. (2010) Developments at Goldminco's Temora Exploration Project. In *Mineral Exploration Geoscience in New South Wales: SMEDG Mines and Wines Conference*. pp.1-6. Cessnock, New South Wales.

Nutman, A. & Hiess, J. (2009) A granitic inclusion suite within igneous zircons from a 3.81 Ga tonalite (W. Greenland): Restrictions for Hadean crustal evolution studies using detrital zircons. *Chemical Geology* **261**: 76-81.

Pearce, J. (1982) Trace element characteristics of lavas from destructive plate boundaries. *In* Thorpe, R. ed. *Andesites: Orogenic Andesites and Related Rocks,* pp.525-548. John Wiley & Sons.

Pearce, J. (1983) Role of the subcontinental lithosphere in magma genesis at active continental margins. *In* Hawkesworth, C. & Norry, M. eds. *Continental basalts and mantle xenoliths,* pp.230-249. Shiva, Natwich.

Pearce, J. (1996) A users guide to basalt discrimination diagrams. *In* Wyman, D. ed. *Trace Element Geochemistry of Igneous Rocks: Applications for Massive Sulphide Exploration: Geological Association of Canada, Short Course Notes* (12): pp.79-113.

Pearce, J. (2008) Geochemical fingerprinting of oceanic basalts with applications to ophiolite classification and the search for Archean oceanic crust. *Lithos* **100** (1-4): 14-48.

Pearce, J. & Cann, J. (1973) Tectonic setting of basic volcanic rocks determined using trace element analyses. *Earth and Planetary Science Letters* **19**: 290-300.

Pearce, J., Harris, N. & Tindle, A. (1984) Trace element discrimination diagrams for the tectonic interpretation of granitic rocks. *Journal of Petrology* **25** (4): 956-983.

Pearce, J. & Peate, D. (1995) Tectonic implications of the composition of volcanic arc magmas. *Annual Review of Earth and Planetary Sciences*, **23**: 251-285.

Peccerillo, A. & Taylor, S. (1976) Geochemistry of Eocene calc-alkaline volcanic rocks from the Kastamonou area, northern Turkey. *Contributions to Mineralogy and Petrology* **58**: 63-81.

Percival, I. & Glen, R. (2007) Ordovician to earliest Silurian history of the Macquarie Arc, Lachlan Orogen, New South Wales. *Australian Journal of Earth Science* **54** (2): 143-165.

Perkins, C., McDougall, I. & Claoue-Long, J. (1990) Dating of ore deposits with high precision: Examples from the Lachlan Fold Belt, NSW, Australia. In *Pacific Rim Conference 90,* pp.105-112. Australasian Institute of Mining and Metallurgy Melbourne.

Perkins, C., Walshe, J. & Morrison, G. (1995) Metallogenic episodes of the Tasman Fold Belt System, Eastern Australia. *Economic Geology* **90**: 1443-1466.

Porter, T. (1998) An overview of the world's porphyry and other hydrothermal copper and gold deposits and their distribution. *In* Porter, T. ed. *Porphyry and Hydrothermal Copper and Gold Deposits, a Global Perspective*, pp.3-17. Australian Mineral Foundation, Perth.

Radclyffe, D. (1995) *Regional scale propylitic alteration in the Northparkes mineral field, Parkes, New South Wales*. Bsc hons thesis, University of Tasmania (unpublished).

Reed, M. (1997) Hydrothermal alteration and its relationship to ore fluid composition. *In* Barnes, H. ed. *Geochemistry of Hydrothermal Ore Deposits,* pp.303-365. John Wiley & Sons.

Richards, J. (2003) Tectono-magmatic precursors for porphyry Cu-(Mo-Au) deposit formation. *Economic Geology* **98**: 1515-1533.

Robb, L. (2007) *Introduction to Ore-Forming Processes,* 4th ed., Blackwell Publishing, Malden.

Rollinson, H. (1993) *Using Geochemical Data: Evaluation, Presentation, Interpretation*, Pearson Prentice Hall, Essex.

Royden, L. (1993) The tectonic expression slab pull at continental convergent margent boundaries. *Tectonics* **12**: 303-325.

Sales, R. & Meyer, C. (1948) Wallrock alteration, Butte, Montana. *American Institution of Mining and Metallurgy Engineers Transcripts* **178**: 9-35.

Saunders, A., Norry, M. & Tarney, J. (1991) Fluid influence on the trace element composition of subduction zone magmas. *Philosophical Transactions of the Royal Society* **335**: 377-392.

Scheibner, E. (1973) A plate tectonic model of the Palaeozoic tectonic history of New South Wales. *Journal of the Geological Society of Australia* **20** (4): 405-426.

Scheibner, E. (1989) The tectonics of New South Wales in the second decade of application of plate tectonics paradigm. *Royal Society of New South Wales Journal and Proceedings* **122:** 35-74.

Seedorff, E., Dilles, J., Proffett, J., Einaudi, M., Zurcher, L., Stavast, W., Johnson, D. & Barton, M. (2005) Porphyry deposits: Characteristics and origin of hypogene features. *Economic Geology* (100th Anniversary Special Edition): 251-298.

Shau, Y., Yang, H. & Peacor, D. (1991) On oriented titanite and rutile inclusions in sagenitic biotite. *American Mineralogist* **76**: 1205-1217.

Sillitoe, R. (1973) The tops and bottoms of porphyry copper deposits. *Economic Geology* **68**: 799-815.

Sillitoe, R. (1993) Gold-rich porphyry copper deposits: geological model and exploration implications. *In* Kirkham, R., Sinclair, W., Thorpe, R., & Duke, J. eds. *Mineral Deposit Modeling: Geological Association of Canada Special Edition 4*. pp.465-478.

Sillitoe, R. (1997) Characteristics and controls of the largest porphyry copper-gold and epithermal gold deposits in the circum-Pacific region. *Australian Journal of Earth Sciences* **44** (3): 373-388.

Sillitoe, R. (2010) Porphyry Copper Systems. *Economic Geology* **105**: 3-41.

Sillitoe, R. & Gappe, I. (1984) *Philippine porphyry copper deposits: geologic setting and characteristics*, Committee for Coordination of Joint Prospecting for Mineral Resources in Asian Offshore Areas (CCOP), Technical Publication, 14: 89p

Smith, S., Mowat, B. & Sharry, M. (2004) Macquarie Arc porphyry Au–Cu systems: a review of the critical exploration features. *In* Bierlein, F. & Hough, M. eds. *Tectonics to Mineral Discovery—Deconstructing the Lachlan Orogen. Geological Society of Australia Abstracts* **74**: pp.51 – 62.

Squire, R. & Crawford, A. (2007) Magmatic characteristics and geochronology of Ordovician igneous rocks from the Cadia - Neville region, New South Wales: implications for tectonic evolution. *Australian Journal of Earth Sciences* **54** (2): 293-314.

Squire, R. & Miller, J. (2003) Synchronous compression and extension in East Gondwana: Tectonic controls on world-class gold deposits at 440 Ma. *Geology* **31** (12): 1073-1076.

Stuart-Smith, P. (1991) The Gilmore Fault Zone - the deformational history of a possible terrane boundary within the Lachlan Fold Belt, New South Wales. *BMR Journal of Australian Geology & Geophysics* **12** (1): 35-50.

Sun, L., Wang, Y., Fan, W. & Zi, J. (2008) Post-collisional potassic magmatism in the Southern Awulale Mountain, western Tianshan Orogen: Petrogenetic and tectonic implications. *Gondwana Research* **14** (3): 383-394.

Suppel, D., Warren, A., Watkins, J., Chapman, J., Woods, K. & Barron, L. (1986) A reconnaissance study of the geology and gold deposits of the West Wyalong - Temora - Adelong district. *Geological Survey of New South Wales Quarterly Notes* **64**: 1-23.

Taylor, H. (1974) The application of oxygen and hydrogen isotope studies to problems of hydrothermal alteration and ore deposition. *Economic Geology* **69**: 843-883.

Taylor, H. (1997) Oxygen and hydrogen isotope relationships in hydrothermal mineral deposits. *In* Barnes, H. ed. *Geochemistry of Hydrothermal Ore Deposits*, pp.229-302. John Wiley & Sons.

Teng, L. (1996) Extensional collapse of the northern Taiwan mountain belt. *Geology* **24**: 949-952.

Tera, F. & Wasserburg, G. (1972) U-Th-Pb systematics in three Apollo 14 basalts and the problem of initial Pb in lunar rocks. *Earth and Planetary Science Letters* **14**: 281-304.

Titley, S. (1975) Geological characteristics and environment of some porphyry copper occurrences in the southwestern Pacific. *Economic Geology* **70** (3): 499-514.

Tosdal, R. & Richards, J. (2001) Magmatic and structural controls on the development of porphyry Cu ± Mo ± Au deposits. *Economic Geology Reviews* **14**: 157-181.

VandenBerg, H. (1999) Timing of orogenic events in the Lachlan Orogen. *Australian Journal of Earth Sciences* **46**: 691-701.

Wagner, T., Jonsson, E. & Boyce, A. (2005) Metamorphic ore remobilization in the Hällefors district, Bergslagen, Sweden: constraints from mineralogical and small-scale sulphur isotope studies. *Mineralium Deposita* **40** (1): 100-114.

Walshe, J., Heithersay, P. & Morrison, G. (1995) Toward an understanding of the metallogeny of the Tasman Fold Belt System. *Economic Geology* **90**: 1382-1401.

Wang, K., Chung, S., Chen, C.Hw., Shinjo, R., Yang, T. & Chen, C.Ho. (1999) Post-collisional magmatism around northern Taiwan and its relation with opening of the Okinawa Trough. *Tectonophysics* **308** (3): 363-376.

Warren, A., Gilligan, L. & Raphael, N. (1995) *Geology of the Cootamundra 1:250,000 map sheet*, Geological Survey of New South Wales, Sydney.

Whitney, J. (1975) Vapor generation in a quartz monzonite magma: a synthetic model with application to porphyry copper deposits. *Economic Geology* **70** (2): 346-358.

Williams, I. (1998) U-Th-Pb Geochronology by ion microprobe. *In* McKibben, M., Shanks III, W. & Ridley, W. eds. *Reviews in Economic Geology, 7. Applications of Microanalytical Techniques to Understanding Mineralizing Processes*. pp.1-34.

Wilson, A., Cooke, D. & Harper, B. (2003) The Ridgeway gold-copper deposit: A high-grade alkalic porphyry deposit in the Lachlan Fold Belt, New South Wales, Australia. *Economic Geology* **98**: 1637-1666.

Wilson, A., Cooke, D., Stein, H., Fanning, C., Holliday, J. & Tedder, I. (2007) U-Pb and Re-Os geochronologic evidence for two alkalic porphyry ore-forming events in the Cadia District, New South Wales, Australia. *Economic Geology* **102** (1): 3-26.

Winchester, J. & Floyd, P. (1977) Geochemical discrimination of different magma series and their differentiation products using immobile elements. *Chemical Geology* **20**: 325-343.

Winter, J. (2001) *An Introduction to Igneous and Metamorphic Petrology,* Prentice Hall, New Jersey.

Wombacher, F. & Münker, C. (2000) Pb, Nd and Sr isotopes and REE systematics of Cambrian sediments from New Zealand: implications for the reconstruction of the Early Palaeozoic Gondwana margin along Australia and Antarctica. *The Journal of Geology* **108** (6): 663–686.

Wormald, R. (1993) *The petrology and geochemistry of Mid to Late Palaeozoic magmatism in the Temora Region, New South Wales*. Ph.D thesis, La Trobe University (unpublished).

Wyborn, D. (1992) The tectonic significance of Ordovician magmatism in the eastern Lachlan Fold Belt. *Tectonophysics* **214** (1-4): 177-192.

Yardley, B., MacKenzie, W. & Guilford, C. (1990) *Atlas of Metamorphic Rocks and their Textures*, Longman Scientific & Technical, Essex.

Zane, A. & Weiss, Z. (1998) A procedure for classifying rock-forming chlorites based on microprobe data. *Rendiconti Lincei Scienze Fisiche e Naturali Serie* **9**: 51-56.

APPENDIX A

SAMPLE LIST

Sample	Hole ID	Depth (m)	Thin section?		XRD	XRF	ICP-MS	Micro-probe	U-Pb SHRIMP	Brief description
			stnd	pol						
A1	TYHD004	403.55	✓			HONS527	✓			Mineralisation related porphyry
A2	TYHD004	272.95	✓			HONS528	✓			Mineralisation related porphyry
A3	TYHD004	474.40				HONS529	✓			Mineralisation related porphyry
A4	TYHD004	367.30				HONS530	✓			Mineralisation related porphyry
A5	TYHD004	530.48				HONS531	✓			Finger dyke evolved off the Rain Hill Monzodiorite
A6	TYHD004	549.50				HONS532	✓			Finger dyke evolved off the Rain Hill Monzodiorite
A7	TYHD004	555.95	✓			HONS533	✓			Finger dyke evolved off the Rain Hill Monzodiorite
A8	TYHD004	576.70	✓			HONS534	✓			Rain Hill Monzodiorite/late stage RHM
A9	TYHD004	582.30				HONS535	✓			Finger dyke evolved off the Rain Hill Monzodiorite
A10	TYHD004	602.95				HONS536	✓			Finger dyke evolved off the Rain Hill Monzodiorite
A11	TYHD004	582.90	✓			HONS537	✓			Late post-mineralisation porphyry
A12	TYHD003	165.15	✓			HONS538	✓			Mineralisation related porphyry
A13	TYHD003	185.05	✓			HONS539	✓			Mineralisation related porphyry
A14	TYHD003	304.00				HONS540	✓			Finger dyke evolved off the Rain Hill Monzodiorite
A15	TYHD003	310.20	✓			HONS541	✓			Mineralisation related porphyry
A17	TYHD003	371.95				HONS542	✓			Rain Hill Monzodiorite
A18	TYHD003	426.60	✓			HONS543	✓			Mineralisation related porphyry
A19	TYHD003	386.90	✓			HONS544	✓			Rain Hill Monzodiorite
A20	TYHD003	430.10				HONS545	✓			Rain Hill Monzodiorite
A21	TYHD003	504.70	✓			HONS546	✓			Rain Hill Monzodiorite
A22	TYHD003	496.90				HONS547	✓			Rain Hill Monzodiorite
A24	TYHD005	385.40				HONS548	✓			Mineralisation related porphyry
A25	TYHD005	506.30				HONS549	✓			Late stage, poorly mineralised porphyry intrusive
A26	TYHD005	469.10	✓			HONS550	✓			Late stage, poorly mineralised porphyry intrusive
A27	TYHD005	518.40				HONS551	✓			Mineralisation related porphyry
A28	TYHD005	632.50				HONS552	✓			Pre-mineralisation porphyry
A29	TYHD005	365.00	✓			HONS553	✓			Mineralisation related porphyry
A30	TYHD005	590.40	✓			HONS554	✓			Pre-mineralisation porphyry
A32	TYHD005	271.05				HONS555	✓			Mineralisation related porphyry
A33	TYHD004	585.30				HONS556	✓			Finger dyke evolved off the Rain Hill Monzodiorite
A35	TYHD005	488.60	✓			HONS560	✓			Mineralisation related porphyry
B1	TYHD004	551.50	✓			HONS557	✓			Fine-grained basaltic volcaniclastic/metabasalt
B3	TYHD003	345.20	✓			HONS558	✓			Andesitic volcaniclastic

Sample	Hole ID	Depth (m)	Thin section?		XRD	XRF	ICP-MS	Micro-probe	U-Pb SHRIMP	Brief description
			stnd	pol						
B8	TYHD005	624.80	✓			HONS561	✓			Fine-grained basaltic volcaniclastic/metabasalt
B10	TYHD003	71.70	✓			HONS562	✓			Andesitic volcaniclastic
F1	TYHD004	400.00-402.00	✓			HONS563	✓		✓	Mineralisation related porphyry
F2	TYHD003	504.25-506.05	✓			HONS564	✓		✓	Rain Hill Monzodiorite
RHM	MHR537	-				HONS631	✓			Rain Hill Monzodiorite from south of Barmedman
C03	TYHD004	142.10			X6252					Late, shear related argillic alteration in unknown host
C04	TYHD004	208.95	✓		X6253					Chlorite-sericite alteration in porphyry intrusive
C08	TYHD004	349.50	✓		X6254					Chlorite-magnetite alteration in porphyry intrusive
C09	TYHD004	450.60	✓		X6255					Propylitic (chlorite-epidote) alteration in Rain Hill Monzodiorite
C13	TYHD004	559.25	✓		X6256					Propylitic + hematite alteration in Rain Hill Monzodiorite
C18	TYHD003	106.85	✓		X6257					Sericite-chlorite alteration in porphyry intrusive
C22	TYHD003	279.00	✓		X6258					Chlorite-magnetite alteration in volcaniclastics
C24	TYHD003	320.60	✓		X6259					Propylitic alteration in Rain Hill Monzodiorite
C27	TYHD003	413.85	✓		X6260					Albite/sodic alteration in porphyry stock in porphyry intrusive
C29	TYHD005	166.20		✓	X6261					Late, shear related argillic alteration
C30	TYHD005	111.60	✓		X6262					Sericitic-argillic alteration in porphyry intrusive
C34	TYHD005	60.00	✓		X6263					Sericitic-argillic alteration in porphyry intrusive
C35	TYHD005	359.50	✓		X6264					Chlorite-sericite alteration in porphyry intrusive
C39	TYHD005	611.65	✓		X6265					Propylitic alteration in fine-grained volcaniclastic
C42	TYHD005	621.65	✓		X6266					Propylitic alteration in fine-grained volcaniclastic
E05	TYHD003	250.50		✓				✓		Blebby (remobilised) chalcopyrite in fine-grained volcaniclastic
E06	TYHD003	301.00		✓				✓		Late (syn-tectonic) qtz/chlorite/carbonate/chalcopyrite infill vein
E08	TYHD003	389.40		✓						Mineralised quartz seam vein
E11	TYHD003	469.05		✓				✓		Carbonate vein containing hematite
E12	TYHD003	221.40		✓						Quartz-pyrite flooding/vein
E16	TYHD005	391.00		✓						Disseminated sulphides in quartz-chlorite-magnetite altered host
E17	TYHD005	413.00		✓				✓		Mineralised quartz seam vein with peripheral magnetite
E19	TYHD005	410.75		✓				✓		Disseminated sulphides in quartz-chlorite-magnetite altered host
E21	TYHD005	434.60		✓				✓		Stringy (remobilised) chalcopyrite in altered intrusive unit
E23	TYHD005	444.00		✓						Coarse infill quartz-carbonate-chalcopyrite vein
E25	TYHD005	458.10		✓						Molybdenite on fracture, disseminated sulphides in foliated host
E26	TYHD005	537.75		✓				✓		Stringy (remobilised) chalcopyrite in altered volcaniclastic
D15	TYHD003	434.00		✓						Mineralised quartz seam vein
D16	TYHD003	435.45	✓		X6267					Late (syn-tectonic) quartz/carbonate infill vein
D30	TYHD005	571.90	✓		X6268					Late (syn-tectonic) quartz/K-feldspar/chlorite/carbonate infill vein

APPENDIX B

SUMMARY LOGS

Hole TYHD003

mFrom	mTo	Rock	Texture	Alt-group	Alt-subgroup	Alteration minerals	Alt/10	Veins	Sample	@ m	t/s?	Structures	@ m	dip	dip dir		Cu ppm	S %	Magsus	Additional Comments
0.00	2.00	SOIL															40	0.14	500	
2.00	18.00	SAPR															56	0.36	97	
18.00	70.20	ANVC	foliated	Argillic		qz/kaol/ser/cl/goeth	9										106	0.33	91	More 'intact' than cl-ser alt (kaol = malleable), but very soft
70.20	100.95	ANVC	foliated	Chl-ser		ser/qz/cl/kaol/py	7	cl/cb	B10	71.70	✓						1347	3.51	65	Broken into soft rock chips, most not >5cm length
100.95	138.45	PP	~equigranular	Chl-ser		alb/ser/cl/qz/py/kaol	7	qz/py/cp	C18	106.85	✓						949	2.52	99	Plag ~1-3mm diam heavily albitised
138.45	142.00	ANVC	foliated	Chl-ser		alb/ser/cl/qz/py/kaol	7	cb/cl/py									796	2.40	73	Cb veins show late shearing nicely
142.00	155.50	PP	~equigranular	Chl-ser		cl/alb/ser/py	7	cb/cl/py/cp				qz/cb/cl vn	159.20	89	20	E	897	2.51	92	
												cb/qz/cl vn	159.70	65	140	E				
155.50	167.40	PP	~porphyritic	Chl-ser		alb/cl/ser/py/qz/leu	3	crse qz/cb/cl/cp/ksp	A12	165.15	✓	cb/qz/cl/cp vn	160.80	66	354	W	252	0.28	428	Intrusive = much more intact here. Late cb/cl tension gashes have opened up but the rock itself has remained conformable. Somewhat flow aligned plag in some samples.
												foliation	162.05	87	74	E				
												qz/cb/cl/mo vn	163.30	74	4	E				
												qz/cb/cl vn	164.20	64	3	E				
												cb/cl/py vn	165.05	82	29	E				
167.40	179.15	ANVC	foliated	Chl-ser		cl/ser/py/ep	6	qz/py,cb/cl/py									1739	2.11	162	Very broken up again
179.15	186.50	PP	~equigranular	Chl-ser		cl/ser/alb/py/ep	6	crse qz/cb/cl/ksp/cl	A13	185.05	✓	qz/cb/cl/py/mo vn	184.40	67	3	E	1017	0.74	151	Fairly conformable
												qz/cb/cl/cp/mo vn	185.40	64	338	W				
												qz/cl/cb/mo vn	185.70	64	6	E				
												qz/cb/cl/mo vn	186.00	74	12	E				
186.50	205.40	ANVC	foliated	Chl-ser		cl/alb/ser/ep/py	5	cb/cl/ep/py/mo									724	2.02	109	
205.40	207.35	PP	foliated	Chl-ser		cl/alb/ser/ep/py/cb	5	cb/cl/py; ep									830	2.30	94	
207.35	225.00	ANVC	foliated	Chl-ser	chl	cl/ser/ep/py/qz/mg	4	cb/cl/py; ep; cp; mg	E12	221.40	✓	foliation	213.85	86	73	E	612	2.80	236	
225.00	249.75	ANVC	foliated	Chl-ser		ep/cl/py/ser/qz	5	cb/ep/cl/py/cp/mg; crse qz/cb				foliation	228.20	80	267	W	743	2.60	135	
												foliation	229.75	85	85	E				
249.75	251.60	ANVC	foliated	Chl-mag		cl/mg/py/ep	4	cb/cl/py ;cp	E05	250.50	✓						3775	3.27	248	
251.60	260.50	PP	foliated	Chl-ser	ser	cl/ser/alb/ep/py/cb	7	cl/cb/ep/py									589	2.79	232	
260.50	266.70	PP	foliated	Chl-ser	chl	alb/cl/ser/ep/py/cb	7	qz; qz/mg/cp; cb/qz/cl									519	0.60	271	Mafic minerals altered expelling Ti (anatase/rutile specks). Early mushy qz vns + later cb/cl/qz
266.70	267.15	ANVC	foliated	Chl-ser	ser	ep/cl/alb/py	7	cb/cl/ep; early qz									259	0.13	505	Late cb more pure than in PP; early qz vn
267.15	271.40	PP	foliated	Chl-ser	ser	alb/cl/ser/ep/py/cb	7	qz; qz/mg/cp; cb/qz/cl									419	0.76	405	
271.40	273.35	ANVC	foliated	Chl-ser	chl	cl/alb/ep/ser/py/mg	6	cb/py/cl									1625	1.14	490	
273.35	278.10	ANVC	banded/ laminated	Chl-ser	chl	cl/alb/ep/ser/py	5	cb/cl/py				foliation	276.15	83	65	E	381	1.06	317	
												qz/cb/cl/mg/py vn	277.24	70	89	E				
278.10	278.80	PP	porphyritic	Chl-mag		cl/ep/mg	4	cb/cl				contact	278.80	84	257	W	209	1.57	114	
278.80	303.55	ANVC	foliated	Chl-mag	ep	ep/cl/mg/py/qz	6	ep/cb/cl/py; late qz/cb/ksp±cp	C22	279.00	✓	foliation	279.15	76	83	E	295	0.80	915	Faint mushy kspar veins + later tension qz/cb/kspar. Lots of epidote
									E06	301.00	✓	qz/py/cl/cp/mg vn	297.35	34	34	E				
												banding	299.37	71	78	E				
												contact	303.55	46	83	E				
303.55	304.50	MZDR	equigranular		hem	kf/ep/cl/alb/py/mg	4	cb/ep/cl	A14	304.00		contact	304.50	62	110	E	303	0.43	491	Very felsic (few dark phenocrysts, lots of pink kspar) and silicic.
304.50	306.50	ANVC	hornsfelsed	Chl-mag		cl/mg/ep/cb/qz/py/ kspar	7	cb/cl/ep/py									277	0.36	2138	Fine to medium sized (1-50 mm) monzodioritic finger dykes in interval (same as either side). Contacts mostly ~perpendicular to core length
306.50	306.80	MZDR	equigranular	Chl-mag	hem	kf/ep/cl/alb/py/mg	6	ep/cl/cb				contact	306.80	24	96	E	175	0.35	2940	
306.80	310.00	ANVC	foliated	Chl-mag		cl/mg/ser/py/ep	6	cb/cl/mg/10cm qz/ser/py vn				banding	307.65	66	81	E	171	1.08	559	
												qz/cb/py/cp/mo vn	308.10	74	263	W				
												contact	310.00	86	212	W				
310.00	315.45	PP	~porphyritic	Chl-mag		alb/mg/ser/py/ep	4	cb/cl/py/qz	A15	310.20	✓	cb/qz vn	311.90	65	339	W	47	0.05	2080	Feint plag, fine titanite/rutile specks, conformable section
												qz/cb/cl/py vn	312.60	85	110	E				
												contact	315.45	58	50	E				
315.45	315.60	ANVC	hornsfelsed	Chl-mag		ep/cl/mg/kspar/cb	7	cb/cl				contact	315.60	26	72	E	52	0.06	1790	Clasts in intrusive? Or psuedoclasts?
315.60	316.00	MZDR	equigranular	Chl-mag		ep/mg/cl/qz/py	3	cb/cl/qz/py; cp				contact	316.00	66	79	E	52	0.06	1790	

Hole TYHD003 cont.

mFrom	mTo	Rock	Texture	Alt-group	Alt-subgroup	Alteration minerals	Alt/10	Veins	Sample	@ m	t/s?	Structures	@ m	dip	dip dir		Cu ppm	S %	Magsus	Additional Comments
316.00	316.20	ANVC	banded	Chl-mag		cl/mg/cb	7	cb/cl; cp									783	0.26	2110	
316.20	316.45	MZDR	~equigranular	Chl-mag	hem	kf/cl/mg/py/he	6	cb/cl				cb/cl/cp vn	316.25	87	53	E	783	0.26	2110	Small finger dykes from the RHM
316.45	319.75	ANVC	hornsfelsed	Chl-mag	ep	ep/cl/mg/he	7	cb/cl/ep/mg/py/cp				banding	318.18	56	76	E	524	0.35	1010	Looks like early qz/kspar alt underlying ep
												qz/cl/mg/he/py vn	318.22	89	59	E				
												foliation	319.20	66	78	E				
												contact	319.60	22	86	E				
319.75	320.60	MZDR	~equigranular	Chl-mag	hem	kf/ep/cl/mg/py/he	6	cb/qz/cl/py	C24	320.60	✓						95	0.25	110	
320.60	326.45	ANVC	banded	Chl-mag	ep	cl/ep/qz/py	6	cl/cb/ep				contact	326.70	84	62	E	305	0.25	2418	
326.45	328.05	MZDR	~equigranular	Chl-mag	hem	kf/ep/cl/mg/he	6	cb/cl; qz/cp				contact	328.05	86	215	W	1210	0.79	261	
328.05	338.10	ANVC	hornsfelsed, banded	Chl-mag	ep	cl/mg/ep/kspar/qz/py		crse cb/cl/py; kspar;qz				foliation	329.10	63	11	E	610	0.63	1466	Qz seam vn, plus early looking acid veins & late tension gashes
												qz/cb/cl/py/cp vn	332.30	28	317	W				
338.10	339.60	PP	V.porphyritic	Chl-mag	ep	cl/ep/alb		ep stringers; kspar stringer cut by cl				banding	338.30	71	72	E	199	0.45	1925	
												banding	338.40	82	101	E				
339.60	347.40	ANVC	banded	Chl-mag	ep	cl/kspar/mg/cb/ep	3	cb/cl/kspar/ep/py/ cp	B03	345.20	✓	banding	339.65	71	80	E	384	1.27	625	ANVC are very fine grained in this section
												qz/cl/py/mg/he vn	346.00	82	280	W				
												contact	347.40	84	257	W				
347.40	348.00	MZDR	equigranular	Chl-mag	hem	ep/cl/alb/mg/he	3	cb/ep/cl/qz/py				contact	348.00	48	90	E	302	0.39	106	
348.00	353.30	ANVC	hornfelsed	Chl-mag	ep	ep/cl/mg/py	3	cb/cl/py; kspar dyklets									1303	1.04	719	Has 5-10 cm MZDR bands, highly altered
353.30	353.60	MZDR	equigranular	Chl-mag	hem	kf/ep/cl/mg/py/he	3	cb/cl/ep									5040	0.49	5	
353.60	358.45	ANVC	hornsfelsed	Chl-mag		cl/mg/ep/kspar		cb/cl/ep/				qz/ep/cb/cl/cp vn	353.80	74	262	W	2408	0.58	2775	
												foliation	353.90	74	262	W				
358.45	358.75	MZDR	equigranular	Chl-mag	hem	kspar/cl/mg/ep		cl/ep									1550	0.42	1510	
358.75	359.70	PP	porphyritic	Chl-mag	ep	cl/mg/ep	8	cl/ep									119	0.18	3060	Porphyritic texture evident from alteration of plag (ep).
359.70	363.25	ANVC	hornsfelsed	Chl-mag		ep/cl/mg/he		cb/cl cut earlier ep				contact	363.25	53	63	E	1263	0.64	2503	Contains ?mg vein with kspar selvedge
363.25	363.90	PP	feint ~ eq	Chl-mag		alb/cl/ser/mg	8	cb/cl; early									581	0.71	1920	
363.90	366.25	ANVC	hornsfelsed	Chl-mag		ep/cl/mg/kspar/py	5	cb/cl; ksp dyklets									2175	0.65	2875	Thin altered intrusive dykes
366.25	368.20	MZDR	equigranular	Chl-mag		ep/cl/mg/he/ser	5	cb/cl/ep									486	0.08	241	
368.20	368.87	BSVC	hornsfelsed	Chl-mag		cl/mg/ep	5	cb/cl									2010	0.35	1350	
368.87	408.80	MZDR	equigranular	Chl-mag		ep/alb/cl/mg/he/ksp/ gyp?	5	cb/cl; ep; minor qz	A17	371.95		qz/cb/cl/cp/mo vn	405.70	74	156	E	437	0.17	1053	Some late cb/cl vns
									A19	386.90	✓	qz/cl/cp/mo vn	406.40	66	280	W				
									E08	389.40		contact	408.80	88	284	W				
408.80	428.65	PP	v.porphyritic	Chl-mag	alb	alb/ser/cl/mg/ep	3	cb/cl	C27	413.85	✓	qz/cb/cl vn	421.30	81	209	W	7	0.05	2033	Smaller phenocrysts (~1mm average vs 2.5 for RHM), very porphyritic. A few very coarse qz/cb/cl vns. A18 = very similar to A12
									A18	426.60	✓	contact	428.65	81	45	E				
428.65	433.25	MZDR	equigranular	Propylitic		cl/mg/he/kspar/ep	5		A20	430.10							123	0.10	2051	Seam vein present. Also contains a few kspar vns offset by late chlorite
433.25	452.80	MZDR	equigranular	Propylitic	hem	cl/ep/mg/he/kspar	5	cb/cl	D15	434.00	✓						267	0.16	996	Late ep wash here. Ksp/hem dusted vns still present (although rare). Significant mineralised quartz seam vein here.
									D16	435.45	✓									
452.80	454.20	FAULT				he/?gyps/cl/mg/ep		hem on fracs									10	0.04	31	Slickensides on fracture surfaces. Later than cl/mg/ep alt
454.20	461.15	MZDR	equigranular	Propylitic	ep/cl	alb/cl/ep/ser/mg	3	cb/cl				contact	461.15	81	66	E	13	0.03	1753	
461.15	462.05	BSVC	hornsfelsed	Propylitic	ep/cl	ep/cl/mg	3	cb/cl				contact	462.05	15	151	E	13	0.04	1040	Very dark, fine grained uniform texture
462.05	467.60	MZDR	equigranular	Propylitic	ep/cl	alb/cl/ep/mg/he	4	cb/cl/he				contact	467.6	58	111	E	30	0.03	540	
467.60	481.90	BSVC	hornsfelsed	Propylitic	ep/cl	ep/cl/mg/qz/he	3	cb/cl/qz/ksp/he/ser/ mo	E11	469.05	✓	cb/cl/he/cp vn	468.95	13	91	E	212	0.06	2896	Mg veins throughout + mushy sinuous early qz & kspar (?late fractionates)
												cb/cl/he/py vn	469.7	13	129	E				
												banding	471.4	52	75	E				
481.90	491.60	MZDR	equigranular	Propylitic	ep/cl	alb/cl/mg/ep/he	3	cb/cl/cp									262	0.05	982	Early qz with kspar selvedges; ep over/p
491.60	495.75	BSVC	hornsfelsed	Propylitic	ep/cl	ep/cl/mg/he	3	cb/cl/ep/he									21	0.03	1343	
495.75	514.75	MZDR	equigranular	Propylitic	ep/cl	cl/mg/alb/ksp/ep/he	3	cb/cl/qz/ep	A22	496.90							2	0.03	2057	Very dark (mt & dark cl), lots of qz vns with pink kspar selvage & ?ksp replaced ep vns. Fairly coarse grained (plag to 5 mm)
									A21	504.70	✓									
									F2	504.25-506.05	✓									

Hole TYHD004

mFrom	mTo	Rock	Texture	Alt-group	Alt-subgroup	Alteration minerals	Alt/10	Veins	Sample	@ m	t/s?	Structures	@ m	dip	dip dir		Cu ppm	S %	Magsus	Additional Comments
0.00	1.50	SOIL																		
1.50	70.00	SAPR	strongly foliated	Argillic		qz/ka/ser/py/goethite	9	qz									60	0.68	17	Extremely altered and weathered. Hard to distinguish any original rock fabric.
70.00	204.25	ANVC	strongly foliated	Arg/ sericitic		ser/ka/qz/py	8	qz/py	C03	142.10							655	5.26	10	Very altered and strongly fol. Dissem py, qz veining & ?malachite staining. Primary lithologies/textures cannot be easily identified.
204.25	252.40	PP	strongly altered	Sericitic	ser/cl	cl/ser/alb/py/ka/qz	5	qz/py/cb/mo/cp	C04	208.95	✓	foliation	231.40	75	061	E	1896	2.86	17	
252.40	259.40	PP	~equigranular	Sericitic	ser/cl	cl/ser/py/alb	5	qz/cb/py/cl									2869	0.89	16	
259.40	339.50	PP	~equigranular	Chl-ser	cl/mg	cl/ser/alb/qz/mag	5	qz/cl/cb/py/cp	A02	272.95	✓						3027	0.85	506	Elongated plag, albitised; strong cl alt
339.50	358.90	PP	~equigranular	Chl-ser	cl/mg	cl/py/mag/ep/ser/cb	3	qz/py/cp	C08	349.50	✓	qz/cb/cl/py vn	351.90	82	060	E	4200	0.67	1523	VERY hard to see any texture- could be intrusive. Broken up/brecciated- get thin sections
												cb/cl/py/cp vn	352.10	47	299	W				
358.90	368.30	PP	~ porphyritic	Chl-ser	cl/mg	cl/alb/ser/mag/py	3	qz/cb/cl,py	A04	367.30							2265	0.36	1540	More conformable section (~ 5 m), intrusive unit very consistent
368.30	373.70	PP	~ porphyritic	Propylitic	ep/cl	cl/ep/alb/ser/mag/py	2	qz/ep/cl									2192	0.93	729	Ep alt selvedges and semi pervasive 'patches'
373.70	380.10	PP	~ porphyritic	Propylitic	cl/mg	cl/alb/ser/mag/ep	3	qz/cb/cl/ep									900	0.39	1742	
380.10	388.45	PP	~ porphyritic	Propylitic	ep/cl	ep/cl/alb/mag	3	cb/cl/py									2184	0.57	1348	
388.45	410.20	PP	~ porphyritic	Propylitic	cl/mg	alb/cl/mg/ser/ep/cb	3	cb/qz/cl/py/ep/cp/ mo	A01	403.55	✓	foliation	408.80	90	060	E	127	0.66	499	Original texture fairly obscured but certainly porphyritic intrusive
									F01	400-402	✓									
410.20	436.70	PP	~ porphyritic	Propylitic	ep/cl	ep/cl/alb/mag/ser	3	qz/cb/cl/py/mo									135	0.18	117	Starting to get coarse qz/cb/cl vns (to 1m) ±cp and Mo around fracts.
436.70	437.53	FAULT	foliated	Sericitic	ser/cl	ser/cl/alb	4	qz/cb/cl/mo									355	0.69	13	Fault zone; likely source of late qz/cb/cl vns and Mo minz
437.53	472.20	PP	~ porphyritic	Propylitic	ep/cl	ep/ser/cl/alb	3	qz/cb/ep/py/mo	C09	450.60	✓						129	0.38	263	More coarse qz/cb/cl present
472.20	478.80	PP	~ porphyritic	Propylitic	cl/mg	cl/alb/mag/ser	3	cb/cl/qz	A03	474.40							19	0.14	996	Fairly unbroken interval. Plag phenocrysts albitised, titanite specks
478.80	479.70	FAULT	faulted pp	Propylitic	ep/cl	ep/cl/ser/alb	4	cb/cl												
479.70	485.80	PP	~porphyritic	Propylitic	ep/cl	ep/cl/ser/alb	4	cb/cl									64	0.58	29	Broken/foliated intrusive
485.80	488.50	FAULT	faulted pp	Sericitic	ser/cl	cl/ser/alb	4	cb/cl									870	1.39	33	
488.50	490.00	PP	~porphyritic	Sericitic	ser/cl	cl/ser/ep/alb	4	cb/cl									308	1.22	14	Porphyritic to more equigranular
490.00	492.45	ANVC	foliated, veined	Propylitic	cl/mg	ep/cl/mg/py	3	cb/ep/cl/mg/py/cp				foliation	490.20	82	073	E	702	0.55	2945	Possibly very altered intrusive. More foliated/can't see phenocrysts (otherwise very similar)
492.45	494.00	PP	~equigranular	Propylitic	cl/mg	ep/cl/alb/ser	3	cb/cl				foliation	493.60	86	268	W	364	0.29	921	Hard to see texture, looks a bit like RHM
494.00	530.48	BSVC	banded/foliated	Propylitic	ep/cl	ep/cl/mag/py/ser/he	3	cb/ep/cl/py				foliation	494.90	81	271	W	136	0.52	733	Dark green (cl pervasive) with many fine cb and ep veinlets roughly parallel to banding. Rock appears hornsfelsed
												banding	502.85	81	094	E				
												foliation	507.90	69	089	E				
												foliation	510.65	53	121	E				
												cb/ep/cl/py vn	517.90	89	278	W				
												foliation	520.90	76	134	E				
												contact	530.48	53	064	E				
530.48	530.55	QZ-SYEN/ MZDR	equigranular	Propylitic	ep/cl	kspar/ep/hem/cl	5	cb;ep/cl/py	A05	530.48							104	0.37	92	Finger dyke presumed from RHM; very pink. Feldspars look altered but amphiboles still relatively intact. Also shows post- emplacement deformation (cb tension veins)
530.55	539.00	BSVC	banded/foliated	Propylitic	ep/cl	ep/cl/mag/py/ser/he	4	cb/ep/cl/py				contact	536.60	25	238	W	98	0.39	113	
												banding	537.33	52	024	E				
												contact	537.40	61	046	E				
539.00	539.60	MDPP	~porphyritic	Propylitic	ep/cl	cl/ep/alb/kspar	3	cb/ep/cl/py									83	0.20	114	
539.60	549.40	BSVC	banded/foliated	Propylitic	ep/cl	ep/cl/mag/py/ser/he	4	cb/ep/cl/py/qz				banding	545.70	28	231	W	139	0.51	665	
												contact	548.30	53	128	E				
549.40	549.50	MZDR	equigranular	Propylitic	kf	alb/kspar/ep	5		A06	549.50										Mushy sinuous margined finger dyke

Hole TYHD004 cont.

mFrom	mTo	Rock	Texture	Alt-group	Alt-subgroup	Alteration minerals	Alt/10	Veins	Sample	@ m	t/s?	Structures	@ m	dip	dip dir		Cu ppm	S %	Magsus	Additional Comments
549.50	554.55	BSVC	banded/foliated	Propylitic	ep/cl	ep/cl/mag/py/qz/ser/he	4	cb/ep/cl/py	B01	551.50	✓	banding	550.45	46	130	E	204	0.20	401	Very dark (looks like no qz), hornsfelsed
												contact	554.55	86	078	E				
554.55	556.40	MZDR	equigranular	Propylitic	ep/cl	alb/kspar/ep/cl	5	qz/cb/cl coarse(late)	A07	555.95	✓	contact	556.40	62	035	E	33	0.08	89	Very pink- hem kspar, also late qz/cb/cl vein
556.40	559.20	BSVC	banded/foliated	Propylitic	ep/cl	ep/cl/qz/mag/py	4	cb/ep/cl/py				cb/cl/he vn	559.15	61	071	E	271	0.24	2041	
559.20	559.75	MZDR	equigranular	Propylitic	ep/cl	qz/alb/kspar/ep/mag/cl/he	5	qz/cb/cl/he	C13	559.25	✓	contact	559.75	12	211	W	24	0.16	1600	Red/purple staining. Looks late, sourced from fractures
559.75	572.35	BSVC	banded/foliated	Propylitic	ep/cl	ep/cl/qz/mag/ser	4	cb/ep/cl/py/mg/mo				banding	569.38	66	086	E	282	0.66	891	
												qz/cb/cl/py/cp/mo	572.30	87	005	E				
572.35	572.90	MZDR	equigranular	Propylitic	ep/cl	qz/alb/kspar/ep/mag/cl/he	5	qz/cb/cl/he												
572.90	573.15	BSVC	banded/foliated	Propylitic	ep/cl	ep/cl/qz/mag/ser	4	cb/ep/cl/py/mg/mo									282	0.66	891	
573.15	573.30	MZDR	equigranular	Propylitic	ep/cl	qz/alb/kspar/ep/mag/cl/he	5	qz/cb/cl/he/?gyps				qz/cb/cl/cp/mo vn	573.50	77	161	E				
573.30	574.05	BSVC	banded/foliated	Propylitic	ep/cl	ep/cl/qz/mag/ser	4	cb/ep/cl/py/mg/mo									282	0.66	891	
574.05	577.05	MZDR	equigranular	Propylitic	ep/cl	alb/kspar/he/ep/cl/mg	5	qz/cb/cl/ep	A08	576.70	✓	contact	574.05	60	068	E	95	0.06	3428	Late tension filling qz/cb/kspar vns are cutting through here, roughly parallel to drill trace.
577.05	578.60	BSVC	banded/foliated	Propylitic	ep/cl	ep/cl/mag	4	ep/qz/cb/cl/py/mg									161	0.15	1373	Ep replaced ?kspar veins?
578.60	579.10	MZDR	equigranular	Propylitic	ep/cl	cl/alb/ep/he/mg	5	cb/cl/ep									103	0.22	616	
579.10	579.35	BSVC	banded/foliated	Propylitic	ep/cl	ep/cl/mag/py	4	cb/cl/ep									182	0.05	2600	
579.35	582.40	MZDR	equigranular	Propylitic	ep/cl	cl/mg/ep/he/alb/kspar	5	cb/cl	A09	582.30							91	0.04	1128	
582.40	584.05	PP	porphyritic	Propylitic	ep/cl	ep/cl/mg/alb/hem/kspar	3	cb/cl	A11	582.90	✓						108	0.33	1231	Texture = porphyry proper. Distinct from RHM
584.05	584.70	BSVC	banded/foliated	Propylitic	ep/cl	ep/cl/mag	4	cb/ep/cl									5	0.09	2280	
584.70	587.80	MZDR	Equi/porph margin	Propylitic	ep/cl	cl/mg/ep/kspar/he	5	cb/cl/he				foliation	587.10	73	102	E	307	0.42	341	
												contact	587.80	74	099	E				
587.80	589.40	BSVC	banded/foliated	Propylitic	ep/cl	ep/cl/mag	3	cb/cl/mg; ser/he									494	0.12	395	
589.40	609.70	MZDR	equigranular	Propylitic	ep/cl	ep/cl/mg/he	5	cb/cl/he	A33	585.30							39	0.17	1251	Strongly altered but resembles RHM texture from TYHD003
									A10	602.95										

Hole TYHD005

mFrom	mTo	Rock	Texture	Alt-group	Alt-subgroup	Alteration minerals	Alt/10	Veins	Sample	@ m	t/s?	Structures	@ m	dip	dip dir		Cu ppm	S %	Magsus	Additional Comments
0.00	3.60	SOIL															14	0.02	157	
3.60	20.30	ANVC		SAPR		kaol/qz/hem/goethite	10										30	0.05	54	Intensely weathered to kaolinite, quartz and goethite
20.30	56.70	ANVC	foliated	SAPR		kaol/qz/goeth/hem	10	cb									48	0.39	67	
56.70	61.70	PP	foliated	Argillic	qz/ser/py	kaol/ser/qz/py/hem/alb	8	qz	C34	60.00	✓						30	1.61	38	Quartz and sericite dominant (~35% each) +cl/kaol/py. Silvery sheen suggests ser rather than kaol
61.70	74.30	PP	foliated	Argillic	qz/ser/py	ser/cl/qz/kaol/alb	8	qz									32	1.89	83	Nodular quartz- highly silicified
74.30	92.40	ANVC	foliated	Argillic	qz/ser/py	ser/cl/qz/kaol	8	cb/qz									30	1.40	36	
92.40	110.40	PP	foliated	Argillic	qz/ser/py	ser/cl/qz/kaol/alb	8	qz									45	5.57	51	Quartz-sericite dominant, low Cu
110.40	119.10	PP	porphyritic	Argillic	qz/ser/py	qz/cl/ser/kaol/py/alb	8	qz	C30	111.60	✓						68	4.90	85	Quartz, chlorite, sericite, kaol
119.10	124.30	PP	porphyritic	Argillic	qz/ser/py	qz/cl/ser/kaol/alb	6	qz									33	0.92	92	Largish quartz veins
124.30	143.10	PP	intensely fol	Argillic	qz/ser/py	qz/ser/kaol/cl/py/alb	8	qz									67	5.97	50	
143.10	167.00	PP	intensely fol	Sericitic	ser/py	qz/ser/kaol/cl/py/alb	8		C29	166.20	✓						85	5.05	98	Quartz, ser, kaol, cl, py(~2%), gypsum
167.00	180.10	PP	intensely fol	Sericitic	qz/ser/py	qz/ser/kaol/py/alb	10										293	3.89	42	
180.10	202.00	PP	intensely fol	Sericitic	ser/cl	qz/cl/ser/kaol/py/alb	8										424	3.49	105	Transitioning from intense qz-ser-kaol alt. into cl-ser ('phyllic') zone with some magnetite. Less clay rich but very broken up (chips).
202.00	232.30	ANVC	foliated	Sericitic	ser/cl	qz/cl/ser/kaol/py/	8	qz									2251	5.77	93	Occasional cp. Dissem. zone. Some wide qz/py veins/flooded areas.
232.30	257.60	ANVC	foliated	Chl-ser		cl/mg/ser/py	6	qz									5468	2.84	1004	

Hole TYHD005 cont.

mFrom	mTo	Rock	Texture	Alt-group	Alt-subgroup	Alteration minerals	Alt/10	Veins	Sample	@ m	t/s?	Structures	@ m	dip	dip dir		Cu ppm	S %	Magsus	Additional Comments
257.60	261.10	ANVC	foliated	Chl-ser		cl/ser/kaol/py	8	qz									3680	5.13	41	Abrupt significant ser/cl alt., has destroyed mag and weakened rock
261.10	268.00	ANVC	foliated	Chl-ser		cl/mg/ser/py	8	qz									6871	3.50	5347	Strong mag alt, strong pervasive Cl alt
268.00	273.80	PP	porphyritic	Chl-ser		cl/mg/qz/kf	6	qz	A32	271.05							1280	1.75	556	Very strong chlorite alteration
273.80	274.90	VN	veined	Chl-ser	qz	cl	2	qz									77	0.55	58	
274.90	275.60	PP	foliated	Chl-ser		kaol/cl/py/ser/qz/alb	8										1520	3.03	125	
275.60	289.10	PP	porphyritic	Chl-ser		cl/mg/alb/qz	6	qz									1714	1.31	791	
289.10	290.00	PP	foliated	Chl-ser		kaol/cl/py/ser/alb/qz	6										1380	1.85	68	
290.00	316.00	PP	porphyritic	Chl-ser		cl/mg/ser/py/qz/alb	8	qz				ser vn	298.7	35	105	E	2325	1.29	575	
316.00	317.90	PP	foliated	Chl-ser		kaol/cl/py/ser/alb/qz	10										1950	2.43	81	
317.90	325.40	PP	porphyritic	Chl-ser		cl/mg/ser/alb/cl	8										1649	1.76	78	
325.40	326.10	PP	foliated	Chl-ser	kaol	kaol/ser/qz/py/hem	10										2130	2.72	188	Intensely altered zone - gouge
326.10	350.70	PP	porphyritic	Chl-ser		cl/mg/alb/qz	8	qz				chl vn	348.6	56	105	E	1459	0.87	958	
350.70	395.50	PP (dense)	porphyritic, but densely packed	Chl-ser		cl/mg/kaol/ser/py/qz	8	qz	A24	385.40							1926	1.73	437	Albite (25%), chlorite (25%), quartz (20%), ser (10%)
									C35	359.50	✓									
									A29	365.00	✓									
									E16	391.00	✓									
395.50	425.20	PP	porphyritic	Chl-mag		cl/mg/py/kf/cp/alb	8	qz/kf	E19	410.75	✓						2664	1.16	3879	
									E17	413.00	✓									
425.20	443.90	PP	foliated	Chl-mag		cl/mg/py/cp/mo	8	qz/kf	E21	434.60	✓						2423	1.63	896	
443.90	444.20	VEIN	coarse	Chl-mag	qz	cl/qz/cp/py/kf	2	qz/kfeld/cl/cp	E23	444.00	✓						2980	4.92	166	
444.20	466.40	PP	foliated	Chl-mag	cl/mg	cl/qz/py/ser/kf/cb/cp	6	cb/qz	E25	458.10	✓						2485	1.66	484	
466.40	487.00	MDPP (late)	porphyritic & highly porphyritic	Late sericitic	qz/ser/py	ser/py/cb	2	cb/qz	A26	469.10	✓	folitation	471.5	68	60	E	117	0.52	107	Felsic and highly porphyritic (low phenocryst/ matrix ratio). MDPP, with larger plag phenocrysts than other sills/stocks. Appears later than the containing PP unit. More resistant to flting, displays foliation but not fractured as the PP. No minz apparent; some py.
												qz vn	481.4	86	44	E				
												folitation	486.6	78	55	E				
487.00	492.40	FAULTED PP	foliated	Chl-mag	ser/cl	cl/ser/hem/cb/py	8	he/qz/cb	A35	488.60	✓	fault zone (brecciated/high strain)	487.3	88	53	E	4716	2.73	171	ANVC confirmed by XRF (plots differently to adjoining late MDPP). Weakness plane faulted between the two more resistant, silicic porphyries. Doesn't appear to have been major offset along fault (similar units on either side-A27 + A29 in immobile element plots)
492.40	515.00	MDPP (late)	foliated & highly porphyryitic	Late sericitic	qz/ser/py	hem/cl/qz/py/ser	5	he/qz veining is strong close to fault, then qz/kf;qz/cb in fol'	A25	506.30		folitation	494	82	91	E	191	0.50	344	Similar to above MDPP, however slightly less altered. Light pink feldspars, to quite large (8 mm).
												folitation	495.2	79	103	E				
												qz/chl vn	496.2	72	92	E				
												qz vn	499.5	86	44	E				
												qz/chl vn	500.05	72	52	E				
												gyp vn	502.6	73	56	E				
												cb vn	506.5	90	194	W				
												gyp vn	510.7	82	144	E				
												qz vn	514.2	77	246	W				
515.00	526.00	PP (dense)	dense PP, looks equigranualr	Propylitic	ep/cl	cl/ser/py/ep	8	qz/kf	A27	518.40		folitation	515	86	45	E	71	0.17	140	Relatively coarse grained, densely packed porphyritic intrusive, similar to above A29. Chlorite rich.
												folitation	517	88	233	W				
												qz/chl/gyp Vn	530.3	87	5	E				
526.00	542.90	BSVC	banded	Propylitic	ep/cl	ep/qz/kf/py/cl	6	qz/kf; coarse qz/cb/cl	E26	537.75	✓	py/cpy vn	537.7	75	40	E	519	1.66	354	Stringy late cp mineralisation is present; propylitic style. Rare and variable- therefore assay data probably reflects occasional good grade, but fairly low overall. Host rock is intensely cl alt'd.
												py/cb/cpy vn	538.5	90	71	E				
												ep vn	542.9	10	15	E				

Hole TYHD005 cont.

mFrom	mTo	Rock	Texture	Alt-group	Alt-subgroup	Alteration minerals	Alt/10	Veins	Sample	@ m	t/s?	Structures	@ m	dip	dip dir		Cu ppm	S %	Magsus	Additional Comments
542.90	550.00	MDPP (late)	porphyritic	Propylitic	ep/cl	kf/ep/cl/py	8	ep				qz/chl gpy contact	542.91	15	351	W	5	0.73	67	Dark rock with mostly small (< 2mm), but up to 10 mm white to light green epidote altered phenocryts (phenocrysts are highlighted by ep alt). Also more pervasive epidote. Similar texture to late MDPP further downhole, just appears to have had more intense cl alt.
												d/ss vn	544.5	73	340	W				
550.00	559.10	BSVC	laminated	Propylitic	ep/cl	kf/qz/ep/cl/py	8	ep				py/mag contact	550.2	72	50	E	777	0.38	527	
												ep fln	554.1	88	270	W				
												ss vn/fln	555.4	74	61	E				
												qz/py/ep contact	559.2	87	265	W				
559.10	580.60	MDPP (late)	porphyritic	Propylitic	ep/cl	cl/ep/py	6	ep/py	D30	571.90	✓	pz/plag vn	568.7	87	32	E	205	0.70	426	Texture similar to other MDPP in this hole, but intense chlorite alteration. Feldspar phenocrysts mostly small (< 3mm), highlighted by epidote alteration/albitisation possibly. Earlier alteration phase involving silica addition and possibly k-spar. Large coarse qz-kspar-cb-cl vein. Later strong ep-cl=py veining and semi-pervasive.
												d/ss vn	572.8	85	224	W				
580.60	589.30	BSVC	laminated	Propylitic	ep/cl	cl/ab/qz/ep/py/cb	8	ep/py				ss/md cb bedding	585.05	45	72	E	171	1.65	744	
												qz/chl cntct	589.4	28	42	E				
589.30	593.90	MDPP (late)	porphyritic	Propylitic	ep/cl	cl/ab/ep/kf	5	qz/ep	A30	590.40	✓	ep cntct	593	75	66	E	109	2.25	152	
593.90	603.70	BSVC	laminated	HNFLSD	ep/cl	cl/ep/py/qz/kf	6	qz, coarse qz/cb/cl				ep/py bedding	598.9	55	65	E	142	2.53	259	
												ss/md vn	602.6	65	73	E				
												ep contact	603.6	90	72	E				
603.70	611.50	MDPP (late)	porphyritic	Propylitic	ep/cl	cl/ep/kf/qz/ep/py	5	ep;qz/kf				contact	605.5	55	79	E	98	1.64	94	Small randomly orientated feldspars, rounded-elongate, fairly sparse. Hint of pink + overall porphyritic texture suggests late MDPP dyke.
												ep contact	607.2	64	86	E				
611.50	615.80	BSVC	laminated	HNFLSD	ep/cl	ep/cl/py	6	ep/py	C39	611.65	✓	ep vn	613.85	65	73	E	910	1.23	1052	
615.80	618.40	MDPP	porphyritic	Propylitic	ep/cl	kf/ep/py	6	kf				ep contact	618.4	57	51	E	644	1.22	564	
618.40	629.60	BSVC	laminated	HNFLSD	ep/cl	ep/cl/py	6	ep/py	C42	621.65	✓	md/ss vn	629.2	65	62	E				
									B08	624.80	✓	py/cb bedding	628.5	54	62	E				
629.60	630.80	MDPP	porphyritic	Propylitic	ep/cl	kf/ep/py	6	kf												
630.80	632.20	BSVC	laminated	HNFLSD	ep/cl	kf/qz/ep/cb/ga	6	qz/kf				ep contact	632.2	63	56	E				
632.20	634.70	MDPP	porphyritic	Propylitic	ep/cl	kf/qz/ep/cpy	6	qz/kf	A28	632.50		ep contact	634.7	90	66	E				
634.70	648.80	BSVC	laminated	HNFLSD	ep/cl	kf/qz/ga/ep/py	6	ep/py				ep vn	642.25	57	52	E				
												bedding	644.4	66	69	E				

SAPR = saprolite; ANVC = andesitic volcaniclastics; PP = porphyritic textured intrusive; MZDR = monzodiorite; BSVC = basaltic volcaniclastic; MDPP = monzodiorite porphyry; HNFLSD = hornfelsed unit.

APPENDIX C

PETROGRAPHIC DESCRIPTIONS

Sample: A01 (403.55 m – TYHD004)

Hand specimen: Medium grey to green coloured rock with a moderate to high number of indistinct margined pale cream coloured plagioclase phenocrysts (0.5 – 3 mm). Small (< 0.5 mm) opaque cream coloured specks are present uniformly but in lower abundance, inferred to be altered titanate. Image #: 261-267.

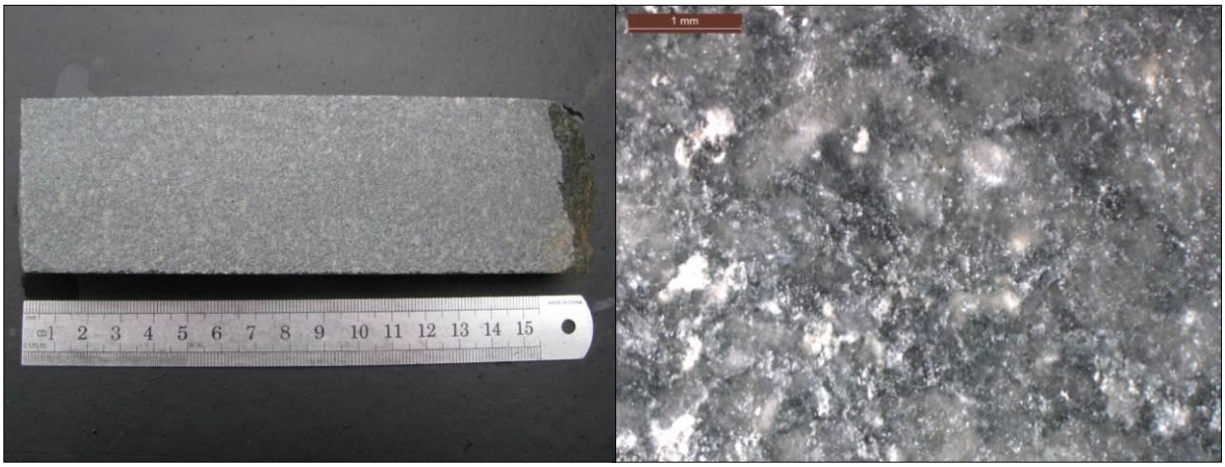

Figure 1: Sample A01 (TYHD004; 403.55 m) section offcut.

Texture& grainsize	Porphyritic to inequigranular (larger phenocrysts in a medium groundmass). Strongly foliated. Feldspars to 2mm (average 1 mm); aligned/elongated along foliation. 'Groundmass' from 200 μm to very fine sericite flakes
Primary mineralogy	Based on apparent twinning, plagioclase is the most abundant feldspar with orthoclase also evident (~ 70/30). Very few primary quartz phenocrysts are evident; those observed (~20% of rock volume) are probably alteration products/recrystallised quartz rather than primary igneous. Ragged magnetite is evident; some sub-euhedral grains appear to be primary relicts. Rare apatite crystals are small and blocky. Zircons observed occasionally occur with chlorite or altered magnetite so some could be hydrothermal. Evidence of former ferromagnesian minerals (chlorite patches), but no substantial primary texture has been preserved to enable identification. Some potential relict grain outlines suggest a blocky habit (possibly amphibole).
Alteration minerals	Sericite is very abundant, foliated in the groundmass and altering all feldspars. Chlorite occurs replacing former ferromagnesian minerals, with a spatial relationship to magnetite and ?rutile/ilmenite aggregates. Numerous discrete calcite crystals, to 1 mm length are present throughout the section (~20 % of phenocrysts). They appear associated with chlorite, magnetite and turbid ?rutile/ilmenite crystals, often in a shape that suggests replacement of a former prismatic or diamond shape primary mineral (possibly titanate or a ferromagnesian). Some are also present as coarse adjacent crystals, suggestive of vein fill. Traces of pyrite.
Alt intensity	7/10
Veining	None obvious in this section. Possibly deformed calcite.
Deformation	Foliated texture, with feldspars appearing to have been rotated into the foliation plane. Much of the sericite has obviously grown synchronously with deformation (e.g. elongated fibres in pressure shadows).
Other	This rock displays intense pervasive alteration with key minerals being sericite and chlorite. The conditions of initial alteration are difficult to estimate due to a lack of indicator mineralogy such as biotite, which may have been present but subsequently has altered to chlorite. Deformation post-emplacement has generated further sericitic alteration, aligned mineralogy from phenocryst to groundmass scale and likely introduced a carbonate fluid which can be attributed to the coarse calcite minerals observed.
Classification	Mineralisation related porphyry.

Sample: A02 (272.95 m – TYHD004)

Hand specimen: Light to medium grey-green plutonic looking rock with visible pale grey somewhat aligned rectangular phenocrysts to 4 mm length. Groundmass of darker grey/green undifferentiated minerals. Possible magnetite/pyrite opaques. Image #: 272-274.

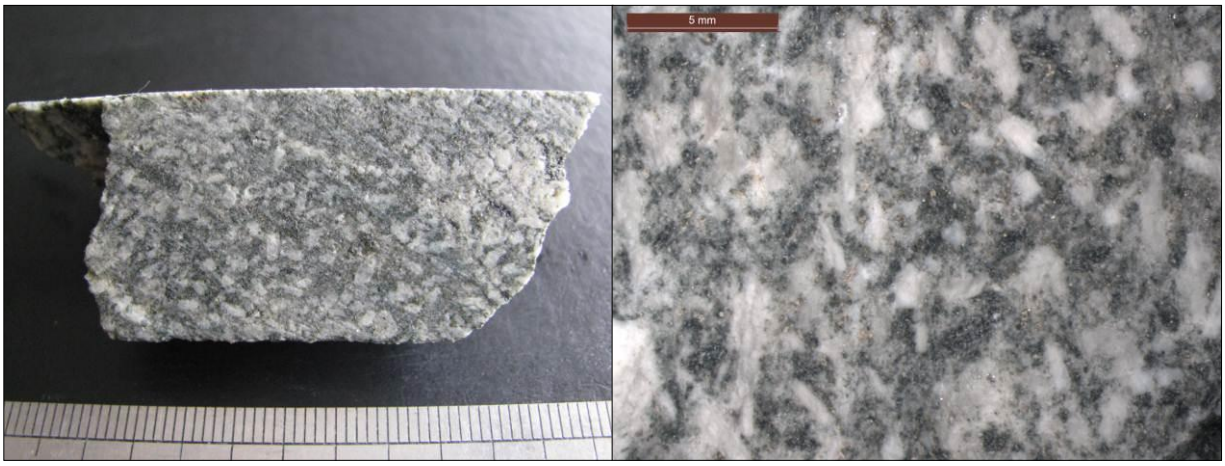

Figure 2: Sample A02 (TYHD004; 272.95 m) section offcut.

Texture & grainsize	Porphyritic texture with distinct large elongate feldspars in a groundmass of more rounded mixed quartz and feldspar along with sericite flakes. Feldspar phenocrysts are large, with average length 1-3 mm (up to 4 mm). Groundmass quartz/feldspars average ~ 10-50 μm length.
Primary mineralogy	Difficult to estimate the composition of feldspar phenocrysts due to sericitisation, however both complex (plagioclase) and Carlsbad (orthoclase) twins are observed (rare). The feldspar population has suffered severe albitisation. The groundmass appears more quartz rich than A1 (~25%). Quartz crystals are sub-rounded and interlocking with more prismatic to rounded feldspars. Relict igneous magnetite is present along with alteration magnetite. Prismatic to euhedral grain boundaries ~ 1 – 2 mm in length composed of alteration chlorite suggest that a ferromagnesian mineral was present initially (probably amphibole). Many zircons are observed throughout the sample, most within chlorite of ferromagnesian alteration aggregates, but also within feldspars, suggestive of a primary igneous presence.
Alteration minerals	Feldspar phenocrysts display intense sericitic alteration, with fine wispy flakes aligned over the entire surface of almost all large phenocrysts observed. These phenocrysts are likely albite (alteration), which is progressively being sericitised. Alignment generates a 'net like' appearance on many grains, which may be related to deformation rather than the initial alteration event. At high magnification, sericite flakes appear to be aligned in two primary directions, roughly 60° to one another. The groundmass has considerably less sericite; possibly due to its relatively high quartz content, however isolated flakes are larger in size. Pleochroic chlorite (yellow-green-brown to purple in XPL), magnetite, minor epidote and turbid-brown ?rutile/ilmenite occur throughout the section as aggregates often displaying a former prismatic to bladed grain boundary. Very minor calcite is observed in this sample.
Alt intensity	7.5/10
Veining	Magnetite vein trails with interstitial K-feldspar ± minor chlorite, hematite and pyrite crosscut the general foliation of the sample.
Deformation	Elongation and alignment of feldspars is evident, however no pressure shadows are observed. Sericite recrystallisation probably occurred synchronously with deformation due to alignment.
Other	Magnetite vein suggestive of early stage high temperature alteration.
Classification	Mineralisation related porphyry.

Sample: A07 (555.95 m – TYHD004)

Hand specimen: Intense pink-red coloured intrusive looking rock with blurred phenocrysts and darker interstitial minerals. Deformation fractures evident. From a dyke intersected by ~ 2m drill section. Image #: 411-415.

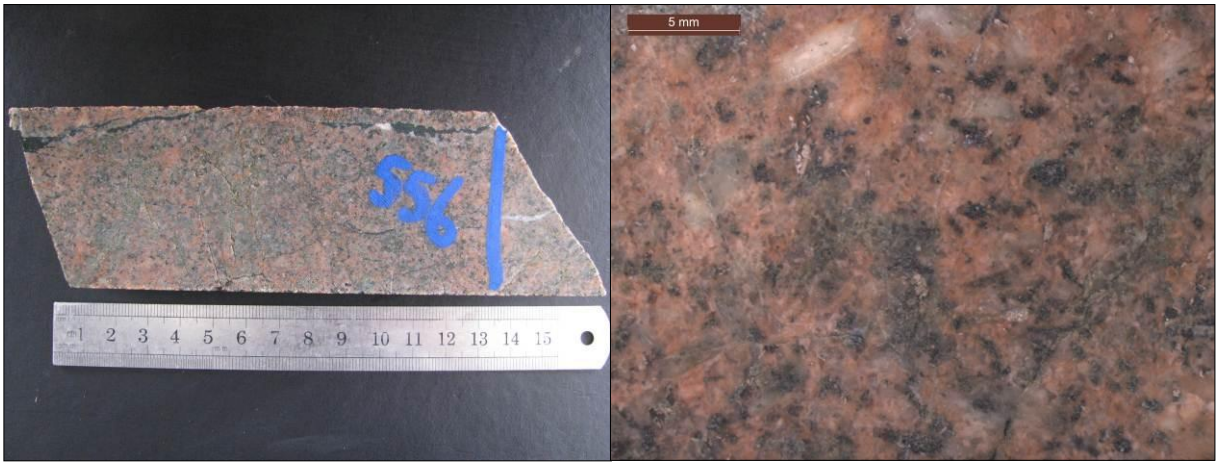

Figure 3: Sample A07 (TYHD004; 555.95 m) section offcut.

Texture & grainsize	Inequigranular texture consisting of randomly orientated feldspars and altered ferromagnesians (1-2 mm average length, up to 3mm), interlocking with a more rounded quartz/feldspar matrix of average grainsize 0.25-1 mm.
Primary mineralogy	Feldspars are dominant: plagioclase > orthoclase > microcline (70:20:10). Primary quartz is abundant particularly within finer grained 'matrix' (~25% of total), often diffuse margined and displaying undulose extinction. An obvious distinction between quartz and feldspars exists due to heavy hematite dusting of feldspars. Bladed to prismatic shaped alteration mineral aggregates (chlorite/magnetite) are likely to be representative of precursor ferromagnesians (amphibole inferred). Titanite, identified by its diamond shape has pseudomorphed to turbid rutile/leucoxene granular clusters (grains ~ 10 μm diameter). It may have been primary igneous or alternatively may have formed in an intermediate alteration stage. A moderate number of well-formed igneous zircons and apatite crystals are also observed.
Alteration minerals	Sericite is not abundant in this rock, occurring only in minor amounts as speckling on the surface of feldspars. The intense chlorite/magnetite alteration of ferromagnesians however suggests this was most likely a late regionally pervasive, or deformation related alteration event. Chlorite related to amphibole alteration is dark brown-purple (XPL), suggesting it is Fe-rich. Epidote is present throughout the rock as very fine grained aggregates, appearing to be particularly abundant around a central vein. This may be due to calcite introduction allowing for its formation. Alteration of titanate to semi-opaque rutile/ilmenite aggregates is relatively common. These clusters have also been shown to include fine grained hematite. Hematite is abundant throughout the section, mostly as vein fill to late deformation related tension gashes and intensely staining feldspars.
Alt intensity	4/10
Veining	Undulating fine-grained epidote veining predominates. A coarse calcite vein (~200 μm width) cross cuts all other minerals. Very late hematite and calcite fill in deformation cracks. A very late sericite vein also is evident associated with deformation (alignment of fibres).
Deformation	Evidence of considerable late brittle deformation includes fine transcrystalline fractures (filled with hematite and calcite). Quartz crystals display distressed undulose extinction and micro fractures.
Other	Intense red colour is attributed to the reasonably highly evolved nature of this finger dyke (high proportion of hematite dusted feldspars) and remobilisation/oxidation of iron into late fractures.
Classification	Dyke evolved off the Rain Hill Monzodiorite.

Sample: A08 (576.70 m – TYHD004)

Hand specimen: Pinkish red to pink-grey sub-equigranular plutonic looking rock. Alteration apparent due to blurred margins of feldspars and opaque yellow-cream grains. Irregular reddish hue suggests hematite staining likely. Thin, dark (chlorite) veins are also evident. Image #: 416-420.

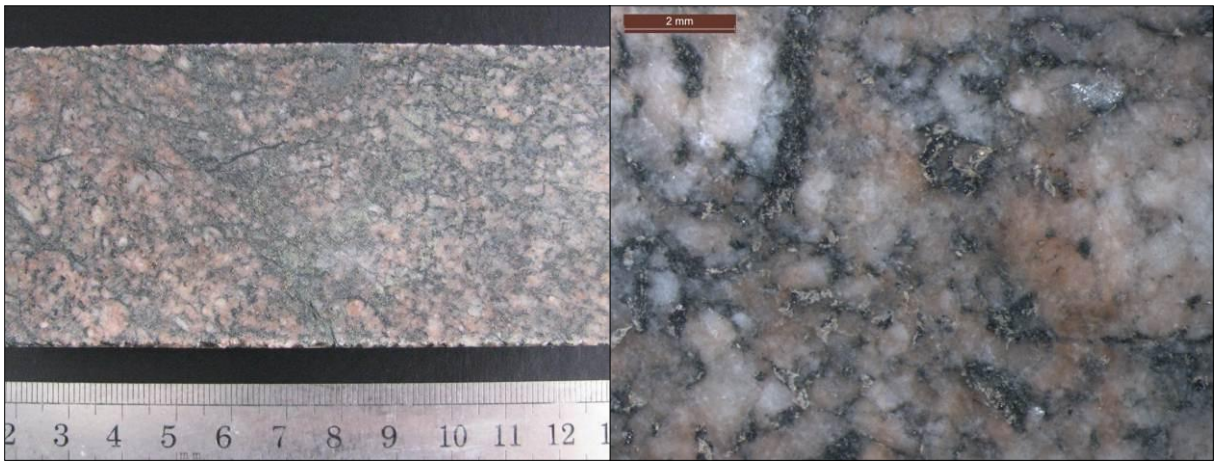

Figure 4: Sample A08 (TYHD004; 576.70 m) section offcut.

Texture & grainsize	Sub-equigranular and without a dominant foliation. Relatively large (average 0.25-2.5 mm, up to 4 mm) interlocking feldspars with 'interstitial' quartz grains (much of which is secondary) from fine to ~ 300 μm in addition to other minerals including diamond shaped (and more irregular) titanite (to 0.5 mm) and a former ferromagnesian, often elongate rectangular to ~ 4mm. Overall, the primary texture has been preserved very well.
Primary mineralogy	Original rock was relatively orthoclase rich as evidenced by Carlsbad and tartan twinning (~ 25% of feldspars appear to be orthoclase). Other primary minerals consist of plagioclase (mostly albite), quartz (10%, however most is likely secondary), primary titanite and opaques (magnetite and ilmenite). Opaques are distributed evenly and some show ragged textures. Accessory apatite to 50-100 μm is evident (1%) along with rounded to prismatic zircons averaging ~ 50 - 100 μm. Former ferromagnesian phase ~ 10% of total.
Alteration minerals	Many feldspars display partial recrystallisation effects, possibly K-feldspar alteration but more likely due to their being late stage fractionates (peritectic reactions). Former ferromagnesian crystals (probably hornblende due to prismatic shape) are completely altered to chlorite, secondary titanite and rutile/leucoxene. Minor alteration pyrite is present along with magnetite. Epidote is a minor constituent, present as aggregates to ~ 200 μm on feldspar surfaces. Minor flaky sericite is also present on feldspar surfaces.
Alt intensity	4/10
Veining	Late fine grained epidote/chlorite veins and chlorite dominated veins (~100-200 μm width) crosscut feldspars and other mineral phases. Latest chlorite-quartz also cross-cuts these veins. Other interstitial fill, which is likely to be vein sourced, consists of chlorite, epidote, quartz, sericite, K-feldspar, titanite and opaques. Red staining is attributed to hematite incorporated with secondary feldspars.
Deformation	Some offset of grains along fractures and deformed twinning on some plagioclase phenocrysts.
Classification	Rain Hill Monzodiorite/late stage RHM.

Sample: A11 (582.90 m – TYHD004)

Hand specimen: Green-grey to slightly pink tinged porphyritic rock with creamy to sub-translucent phenocrysts to ~ 3 mm diameter. Groundmass is relatively dark and generally indistinct. Late, cross-cutting epidote veining is evident. Image #: 435-439.

Figure 5: Sample A11 (TYHD004; 582.90 m) section offcut.

Texture & grainsize	Highly porphyritic, with sparse blocky feldspars to ~2 mm (1.0-1.5 mm average). Density of phenocrysts is ~ 25 % of total rock. Feldspars show a modest alignment. The groundmass consists of a fine-grained matrix of interlocking sub rounded feldspars (albite) and (lesser) quartz of ~ 50 μm diameter.
Primary mineralogy	Primary minerals consist of feldspar phenocrysts (complex twins suggest significant plagioclase although sericite alteration has obscured accurate classification), a quartz/feldspar groundmass, and a subsequently altered ferromagnesian component as suggested by high chlorite concentrations (~10% of rock). Small titanite crystals (to ~ 40 μm; diamond to irregular shaped) are relatively common, along with apatite (to 150 μm), zircons (20 – 75 μm) and relict primary magnetite (1.5%).
Alteration minerals	Sericite is the dominant alteration product in this sample, covering the entire surface of many feldspars, with flakes also occurring in the groundmass. Less sericitised feldspar phenocrysts display obvious recrystallisation textures, indicative of albitisation. Minor epidote is also common on feldspar crystal faces and throughout the rock. Chlorite is dispersed throughout the groundmass and is also associated with veins. Very few primary grain boundaries are preserved by chlorite as is the case in many other samples, which may be due to greater deformation in this sample. Quartz appears secondary or recrystallised, and occurs as a feldspar rim in one example. Very fine grained, intense cubic pyrite is present on the surface of some feldspars in addition to chlorite. This alteration does not always affect the entire feldspar crystal. Alteration magnetite and titanite/leucoxene aggregates are also evident. Hematite dusted.
Alt intensity	7/10
Veining	Coarse grained interlocking (infill) calcite vein to 1.5 mm width, with some quartz incorporated, cross-cuts fine grained epidote ± calcite/chlorite veins of ~ 100 μm up to 2 mm width.
Deformation	Aligned chlorite infills space between a deformed (optically continuous) feldspar. Some ductile deformation of plagioclase twins is also observed.
Other	This sample appears to be a late stage (poorly mineralised) monzodiorite porphyry which has suffered more severe alteration than those examples from TYHD005; mostly intense albitisation. The lack of quartz flooding (quartz not greater than 10%) suggests alteration was related more to regional deformation than porphyry related hydrothermal alteration.
Classification	Late post-mineralisation porphyry.

Sample: A12 (165.15 m – TYHD003)

Hand specimen: Grey to greenish-grey porphyritic rock with elongate to rounded ~ aligned phenocrysts to ~ 4 mm length. Creamy opaques on surface to ~ 200 μm length are rutile/leucoxene. Feldspar margins appear blurred, suggesting the rock has suffered alteration (albitisation). Image #: 492-498.

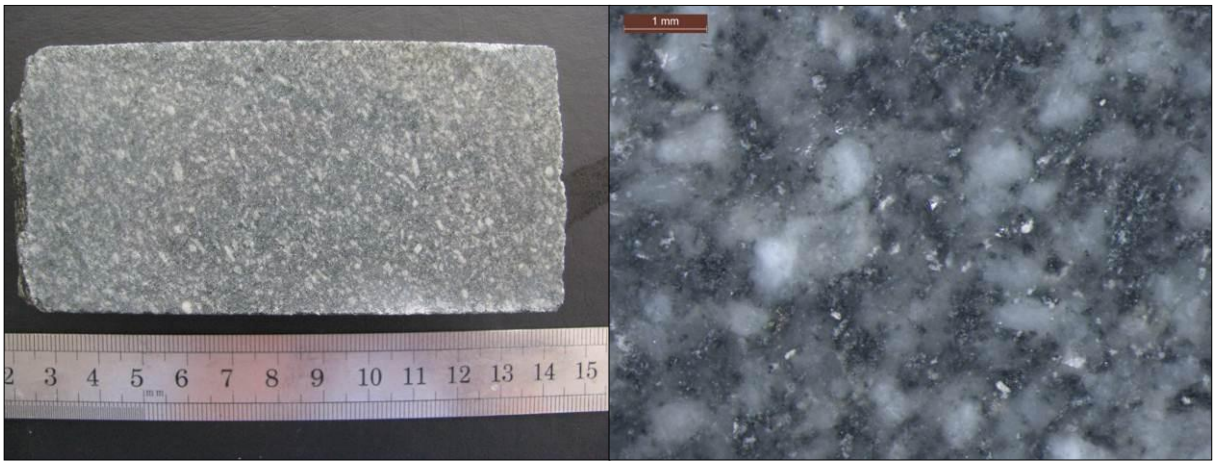

Figure 6: Sample A12 (TYHD003; 165.15 m) section offcut.

Texture & grainsize	Fairly densely packed porphyritic rock. Feldspar phenocrysts are mostly prismatic-elongate but some are more rounded. Average 1 mm, max 3 mm in this section. Groundmass consists of altered feldspar and some quartz, averaging 25 μm diameter. Sericite flakes ~ 20 μm. Stubby ferromagnesians ~ 0.5 – 1 mm length and those more elongate to ~ 4 mm. Foliation and elongation of feldspar phenocrysts deformation related; with those exhibiting a 'stretched' habit also generally intensely sericitised (increase of surface area exposure).
Primary mineralogy	Feldspar characterisation is difficult to establish due to extreme sericitisation, but plagioclase twinning is evident throughout the sample. Quartz is present in the groundmass, along with albitised feldspar. Minor titanite is observed, but a high prevalence of alteration rutile/leucoxene suggests it was probably a fairly significant component. Minor zircons are observed, along with significant primary magnetite, often rimmed with alteration rutile. Two or three primary hexagonal apatite cross sections to 300 μm diameter were observed, along with smaller stubby prismatic crystals.
Alteration minerals	Overall, the sample is intensely sericitised, with sheets/mats covering feldspar surfaces and speckled throughout the groundmass. Intense albitisation prior to sericitisation is also inferred. Chlorite alteration of ferromagnesians has been relatively strongly deformed, resulting in 'strung out' chlorite 'grains' of which many are sub-parallel to foliation. The purple colour (XPL) of some chlorite aggregates suggests it is iron-rich. Alteration magnetite is present, along with numerous rutile/leucoxene aggregates, often proximal to magnetite and in magnetite cleavage fractures (titanomagnetite). Titanite rutile/leucoxene pseudomorphs are also present. Minor calcite is present, mostly as vein fill.
Alt intensity	8.5/10
Veining	Quartz/carbonate veining occurs, not as distinct channels, but rather the whole rock appears 'flooded' along the foliation plane.
Deformation	Deformation of rock to foliated condition evident in ferromagnesian/chlorite alignment. No late fractures present, most likely due to altered state of rock prior to deformation resulting in ductile features.
Other	Hematite staining evident, as is the case in all units observed.
Classification	Mineralisation related porphyry.

Sample: A13 (185.05 m – TYHD003)

Hand specimen: Light grey to greenish grey sub-equigranular intrusive rock with visible pyrite and interstitial dark minerals. Image #: 516-518.

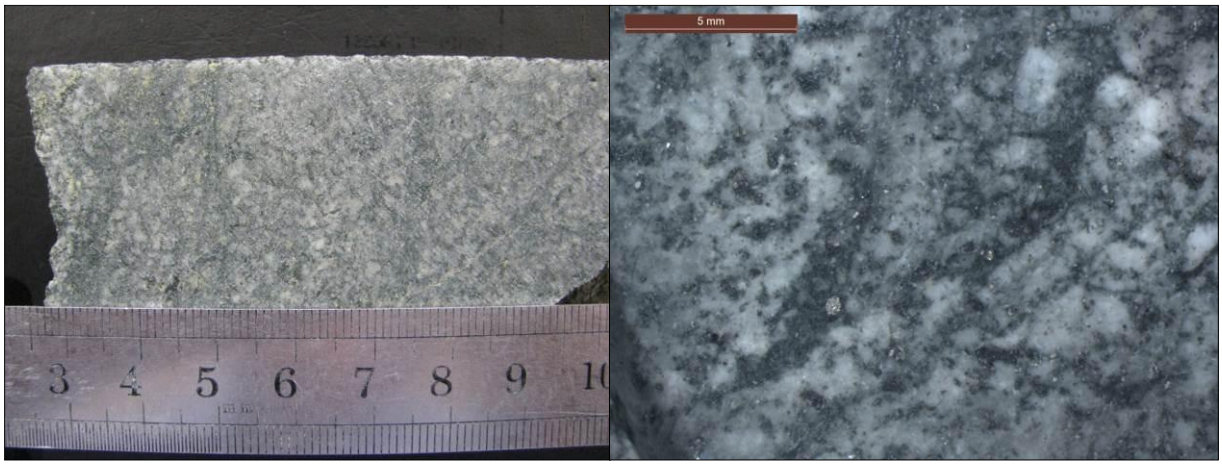

Figure 7: Sample A13 (TYHD003; 185.05 m) section offcut.

Texture & grainsize	Porphyritic, but relatively densely packed. Very altered, therefore difficult to distinguish between grains/groundmass in places. Phenocrysts are randomly orientated. Feldspars in this section range only to ~ 1 mm, while (former) ferromagnesians (fairly sparse) are to 2.5 mm. Groundmass crystals of feldspar/quartz are ~ 10 μm diameter.
Primary mineralogy	Feldspars (plagioclase present, otherwise difficult to distinguish due to sericitisation), a ferromagnesian component (chlorite preserved phenocryst outline rectangular to elongate), titanite, rare quartz, relict magnetite (very ragged), apatite, zircons (small, somewhat rounded ~ 20 μm, in alteration minerals and feldspars).
Alteration minerals	Sericite, in flakes over feldspar surfaces and as needles in veins and groundmass. Vein sericite is larger (to 200 μm growing into space), highly fibrous and associated with chlorite. Chlorite is additionally dispersed throughout the rock but particularly associated with former ferromagnesian minerals. Shades of up to Berlin blue (XPL) suggests chlorite is very iron rich. Pyrite occurs in blebs throughout the rock and as a vein. Epidote is relatively common, dispersed throughout the rock as highly birefringent granules and as anomalous blue/yellow (XPL) replacement minerals.
Alt intensity	8.5/10
Veining	Fine grained epidote veins (average 70 μm width) occur sub-parallel to one another. Space filling quartz-sericite-?kaolinite occur along with chlorite-sericite veins. One stringy pyrite vein is evident (50 μm width), cutting through all other minerals.
Deformation	Syn-kinematic veins of aligned fibrous sericite.
Other	Very similar to A12 despite textural difference in hand specimen. Appears that K originally contained in K-feldspars is now mostly contained in sericite; and feldspars are mostly albite (similar for A12).
Classification	Mineralisation related porphyry.

Sample: A15 (310.2 m – TYHD003)

Hand specimen: Indistinct textured, ~ subequigranular to porphyritic granitoid, of a grey to greenish grey hue. Small opaque rutile (/leucoxene) flecks are dispersed interstitially. Blurred margins of feldspars suggest the rock has been significantly altered. Image #: 523-526.

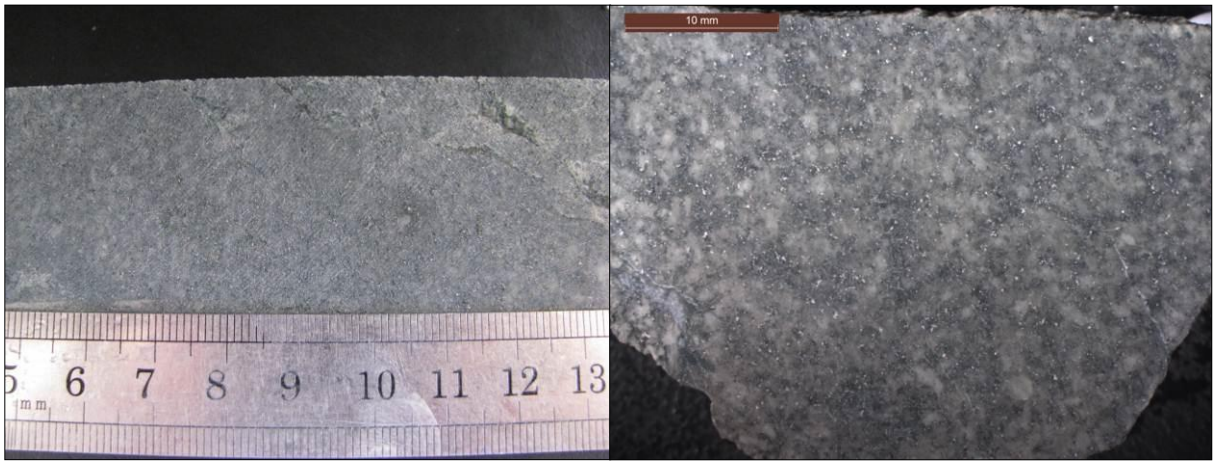

Figure 8: Sample A15 (TYHD003; 310.2m) section offcut.

Texture & grainsize	Porphyritic but densely packed. Feldspars are only ~1 mm on average, but some are up to 2 mm, and many are smaller (0.25-0.5 mm). The feldspars have a somewhat aligned nature which defines a moderate foliation. The groundmass consists of interlocking quartz/feldspar phenocrysts ~ 25 μm diameter and later sericite flakes. Elongate to blocky ferromagnesian minerals altered to chlorite, magnetite and rutile occur to 2.5 mm (most ~ 0.5 – 1.0 mm).
Primary mineralogy	Feldspars are dominant, with plagioclase twinning occasionally evident but difficult to distinguish due to sericitisation. Quartz, which has mostly been recrystallised, occurs throughout the groundmass but also as larger rounded patches ('globules') which may have been primary. Thin prismatic to blocky ferromagnesians (?amphiboles) are common. Minor titanite is evident, and the abundance of alteration rutile (/leucoxene) suggests it was a relatively major primary component. Zircon and apatite also are present in minor amounts.
Alteration minerals	Secondary recrystallised quartz 'globules' to 1 mm are the most unique feature of this sample. Sericite covers the surface of all feldspars, being the dominant alteration mineral. Chlorite in the configuration of former ferromagnesians is common. Epidote occurs mostly with chlorite as granular masses. Turbid rutile/leucoxene and magnetite is disseminated throughout the sample but is particularly associated with chlorite altered ferromagnesians. Some minor calcite and hematite dusting is also observed.
Alt intensity	9.5/10
Veining	No hydrothermal veining is evident in this section, however sericite has crystallised into tension gashes & along foliation. It is likely the intensity of deformation has led to wide scale recrystallisation of hydrous minerals and veins.
Deformation	Sericite is aligned parallel to phenocryst foliation, suggesting deformational rotation of phenocrysts and coeval (syn-kinematic) sericite crystallisation.
Classification	Mineralisation related porphyry.

Sample: A18 (426.6 m – TYHD003)

Hand specimen: Grey-green porphyritic intrusive rock with white/creamy feldspars ~ 2 mm length. Opaque specks of creamy yellow minerals (rutile/leucoxene) are present within the darker groundmass. Feldspar margins appear blurred and slightly pink. Image #: 499-504.

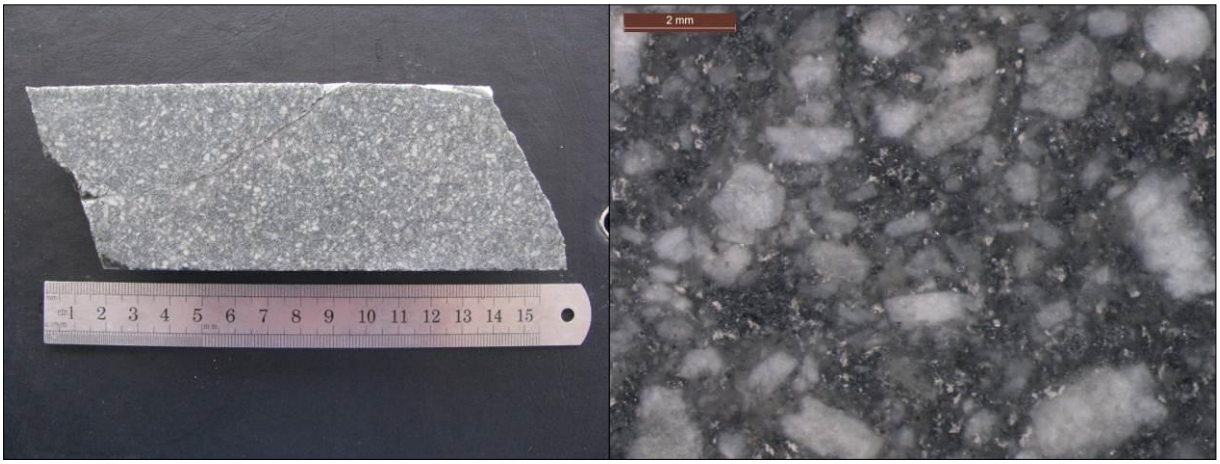

Figure 9: Sample A18 (TYHD003; 426.6m) section offcut.

Texture & grainsize	Strong porphyritic texture with a medium density of phenocrysts. Feldspars average ~ 1 mm, up to 3 mm. Ferromagnesians (altered to chlorite) to 3 mm. Groundmass is quartz/albite (grainsize ~ 50 μm) with sericite flakes, rutile clusters and magnetite.
Primary mineralogy	Feldspars are the dominant mineral, but are difficult to differentiate due to alteration. An elongate to prismatic shaped (chlorite relict grain margin) ferromagnesian mineral component was initially present. The grain shape is suggestive of amphibole. Chlorite throughout the sample is relatively green (XPL) suggesting it is not iron-rich. Ragged magnetite is dispersed evenly which is probably a primary feature. Quartz is dispersed in the groundmass, not representing > 10% of the rock. The rock does not appear quartz flooded or to contain significant recrystallised quartz.
Alteration minerals	Initial albitisation of feldspars was followed by intense sericitisation. Sericite flakes are present throughout the groundmass and over feldspar phenocrysts, where they occur as dense mats. Chloritisation of ferromagnesians was probably a later event, occurring alongside sericite alteration. Epidote alteration occurs as fine grained granules throughout and as larger clusters (~ 150 μm). Turbid rutile/leucoxene clusters are present throughout the sample. Late calcite is moderately prevalent.
Alt intensity	7/10
Veining	Veining consists of carbonate infill veins (1 mm) and a very straight, cross-cutting chlorite/calcite ± epidote vein (50 μm width). These veins are inferred to be related to deformation, with carbonate infill veins containing coarse, aligned crystals.
Deformation	This sample has been strongly albitised and moderately sericitised, however the lack of quartz flooding in the groundmass suggests that it did not undergo intense hydrothermal alteration; instead alteration has predominantly been due to later deformation.
Classification	Mineralisation related porphyry.

Sample: A19 (386.9 m – TYHD003)

Hand specimen: Equigranular to sub-equigranular plutonic looking rock with strong hematite staining resulting in deep red feldspar phenocrysts. Darker material is present in spaces between feldspar phenocrysts. Feldspars range to ~ 4mm, and display a slight foliation. Image #: 593-603.

Figure 10: Sample A19 (TYHD003; 386.9m) section offcut.

Texture & grainsize	Equigranular to sub-equigranular texture, with variably sized blocky feldspars to 2 mm length (averaging 0.5-1.5 mm). A very slight foliation is evident however phenocrysts are ~ randomly orientated. Former ferromagnesians (now altered to chlorite) are evident to at least 5 mm (average 1-2 mm). Around one in 20 phenocrysts are a former ferromagnesian (probably amphibole). Quartz infills interstitial space along with K-feldspar, smallish titanite (possibly some of which is secondary) and rare prismatic to hexagonal apatite (to ~ 500 μm).
Primary mineralogy	Feldspar phenocrysts appear to be predominantly plagioclase, although sericite alteration obscures identification somewhat (estimate of ~ 20/80 K-feldspar/plagioclase). Well preserved microcline is very prevalent interstitially, along with quartz (~10% of rock). The ferromagnesian component is most likely amphibole due to the blocky and elongate shapes. Hexagonal to prismatic apatite crystals to 0.5 mm (average 100 μm) occur sparsely throughout the sample (~1%). Titanite is prevalent, as both irregular and diamond shaped crystals, suggesting it may be both primary and alteration sourced. Both magnetite and ilmenite are also common throughout the section, in relatively good condition.
Alteration minerals	Sericitic alteration of feldspar surfaces ranges from flecks to dense mats. Hematite staining of feldspars is also intense. Titanite is often rimmed with granular rutile/leucoxene, while some crystals are completely altered to this product (but retain diamond shape). Many feldspar phenocrysts have siliceous rims, which may be related to late stage magmatic processes (resorbtion of feldspars with magma replenishment etc.). Ferromagnesians are altered to chlorite and magnetite, but generally retain prismatic shapes (some are cracked however). Some late stage carbonate/epidote/minor albite alteration appears related to regional deformation, as does possible perthitic recrystallisation of some microcline grains.
Alt intensity	5/10
Veining	Late, crosscutting ?hematite/iron oxide bearing veins cut all rocks in an undulating manner. Fine granular to coarser epidote veins (to 1 mm width) are evident. A coarse calcite-minor quartz vein to 3 mm diameter, rimmed with a chlorite selvedge is also present.
Deformation	Cross-cutting hematite (iron oxide) veins, propylitic/deformation-like products (cb/ep/alb).
Classification	Rain Hill Monzodiorite.

Sample: A21 (504.7 m – TYHD003)

Hand specimen: Pale creamy pink sub-equigranular plutonic rock with a dominance of feldspars to 4 mm length and dark needle shaped to prismatic amphiboles to 3 mm length. Image #: 610-615.

Figure 11: Sample A21 (TYHD003; 504.7m) section offcut.

Texture & grainsize	Blocky plagioclase phenocrysts (to 3 mm, averaging 0.5-1.5 mm) comprise ~ 70 % of feldspars, interstitial K-feldspar (mostly microcline) comprises ~ 30 %. Amphiboles are a major component (~15% of total) and are elongate to rectangular, sometimes diamond shaped averaging 1 mm, but up to 3 mm. K-feldspars mould to the shape of the plagioclase phenocrysts in interstitial areas which also contain quartz (~ 5 %); apatite (~ 1%), titanite (~ 2%) and titanomagnetite (~ 2%).
Primary mineralogy	Major: plagioclase, K-feldspar, amphibole, quartz. Accessory: titanite, apatite, titanomagnetite. Trace: prismatic zircons. Ampiboles have extinction symmetrical to their 60/120º cleavages which suggests most are hornblende. Amphiboles are strongly pleochroic (light forest green to yellow green, occasionally to light brown) elongate to fibrous, many with characteristic 60/120º cleavages, particularly where basal diamond shapes are cut. Simple twins are also common. Feldspars are hematite dusted. Titanite phenocrysts are euhedral, diamond shaped and in good condition. Apatite crystals can be quite large, up to 1 mm diameter. Zircons are mostly ~ 50 – 200 μm.
Alteration minerals	Some albitisation of feldspars and some sericitisation. Some microcline crystals which fill interstitial space appear to be recrystallising as perthite; giving these areas a fresh appearance (compared to sericitised feldspars). Some alteration of amphibole to chlorite is in its early stages, invading along cleavages in many cases. Primary magnetite has been somewhat altered to more ragged crystals, with proximal or adjoining leucoxene. Epidote is occasionally present on amphibole surfaces.
Alt intensity	2.5/10. Least altered sample examined.
Veining	Fine grained/granular epidote-chlorite vein ~ 300 μm thick. Slight selvedge of epidote in surrounding minerals. Faint (?early) quartz veining.
Deformation	Some deformation of plagioclase twins, bent crystals and some minor fractures are evident in hand specimen. Some recrystallised quartz in pressure shadows of (resistant) apatite crystals.
Other	Primary magnetite and titanite are supportive of an oxidised melt.
Classification	Rain Hill Monzodiorite.

Sample: A26 (469.1 m – TYHD005)

Hand specimen: Matrix-rich porphyritic appearing igneous rock with a light grey groundmass containing blurred margined creamy white rounded to elongate phenocrysts to 5 mm length. Cubic pyrite is also evident. Image #: 1325-1328.

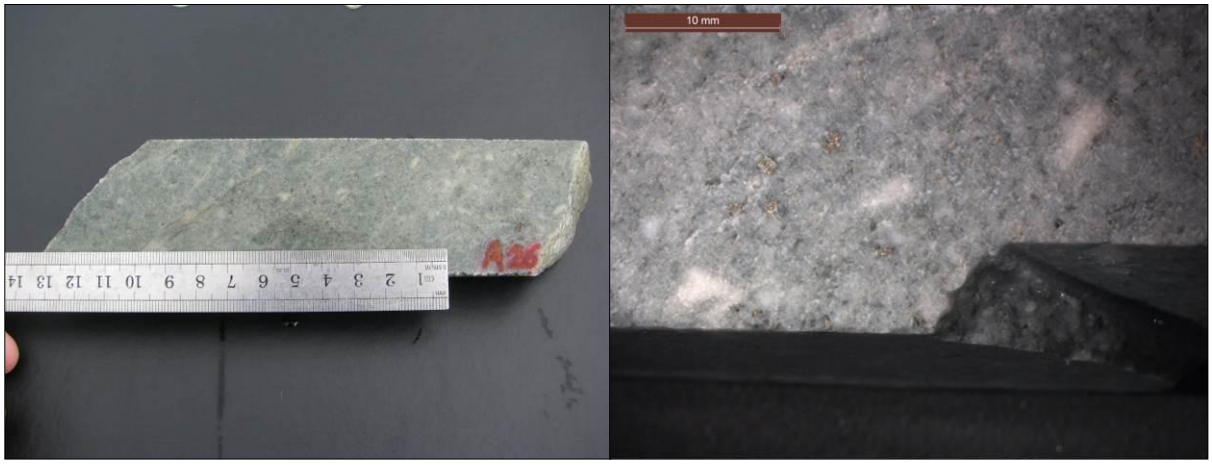

Figure 12: Sample A26 (TYHD005; 469.1m) section offcut.

Texture & grainsize	Very porphyritic, with sparse, large, randomly orientated plagioclase phenocrysts (most around 1 mm length but some up to 3 mm length), present as blocks or amalgamations of two or three phenocrysts. Elongate former ferromagnesian minerals, to 2.5 mm length (average 0.5 – 1.0 mm) are also present, but do not comprise as significant component as most other samples observed (~5%). Phenocrysts comprise only around 20% of the rock volume. The groundmass (80%) consists of moderately sorted interlocking ~ rounded feldspars/quartz to ~ 20 μm length.
Primary mineralogy	The groundmass consists of quartz and feldspars, which may have been orthoclase but have been subjected to albitisation. Titanite was probably present initially, with rutile/leucoxene replacement turbid-brown aggregates indicating it has suffered severe alteration. Euhedral prismatic zircons to 50 μm are observed. Apatite is present but rare. No relict magnetite is observed, the rock appears fairly felsic and siliceous (qz = ~25%) overall.
Alteration minerals	Sericite is abundant as 'vein-like' fibres throughout the sample. Calcite is especially prevalent replacing feldspars. Some chlorite is evident, but overall less is present than in the majority of other samples. Contrastingly, epidote is the dominant alteration product, occurring as fibrous aggregates/clumps and needles to 1 mm. Rutile is evident after ferromagnesians with epidote and pyrite. Alteration pyrite is relatively abundant, occurring in quite large blocks, up to 1.5 mm.
Alt intensity	8/10
Veining	Deformation has generated infill veins of relatively long fibrous bladed sericite precipitating into space along with chlorite. Some coarse grained calcite veining is evident.
Deformation	Aligned sericite and calcite in tension veins. Chlorite pressure shadows on opaques.
Other	The texture of this sample differs to other porphyry units observed, in that the phenocryst component is not as great (the rock is more matrix rich). It is also much more felsic, with lesser volumes of alteration chlorite.
Classification	Late stage, poorly mineralised porphyry intrusive.

Sample: A29 (365 m – TYHD005)

Hand specimen: Greenish-grey plutonic looking rock with visible feldspar phenocrysts to 3 mm and a dark mineral constituent of similar size which appears significantly altered. The texture appears sub-equigranular, with large feldspars evident and a possible finer grained groundmass or more severely altered phenocrysts. Image #: 1302-1307.

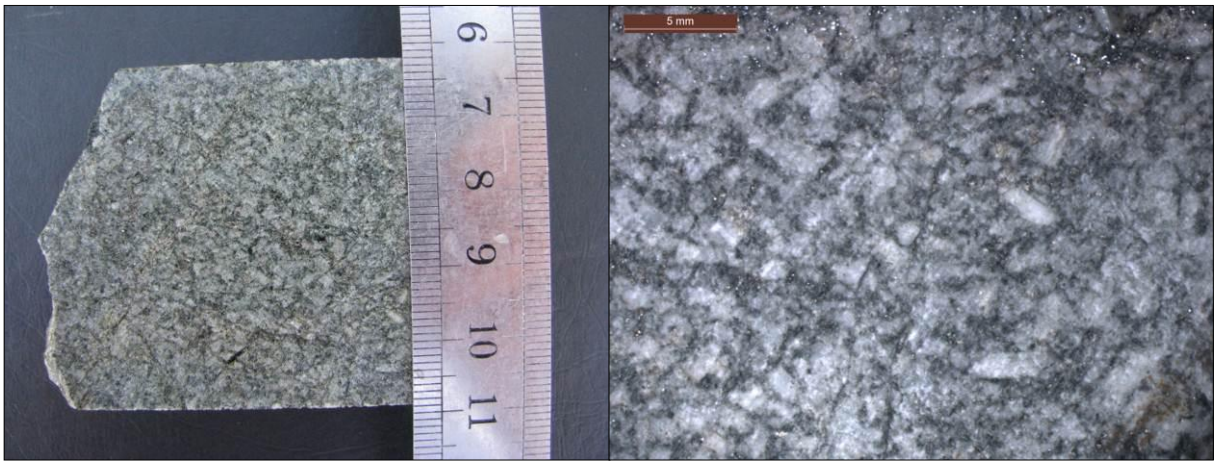

Figure 13: Sample A29 (TYHD005; 365.0 m) section offcut.

Texture & grainsize	Densely packed sub-porphyritic rock with feldspars to 2 mm, averaging 1.5 mm; chloritised former ferromagnesians to 2 mm, and a groundmass of feldspar/quartz from ~ 10 – 200 μm diameter. Sample appears quartz flooded.
Primary mineralogy	Common complex twinning suggests a high proportion of plagioclase which now appears to have been albitised. Former ferromagnesians are most likely an amphibole. Apatite observed to 1 mm. Euhedral prismatic zircons are also present.
Alteration minerals	Abundant fibres of late sericite (in a foliated nature 'wrapping' feldspars); brown – purple chlorite in veins and replacing ferromagnesians; secondary quartz both flooded and after primary quartz as rounded optically discontinuous masses; Epidote occurs as randomly distributed large granules to 1 mm; Pyrite is abundant and evenly dispersed; magnetite (not highly abundant); rutile occurs after titanite (not highly abundant) and also as acicular rutile needles, in chlorite (possibly after biotite or ?amphibole).
Alt intensity	7.5/10
Veining	Early coarse calcite/epidote vein crosscuts epidote/calcite-epidote/sericite veining. Latest veining consists of sericite and chlorite in net-like interstitial fibres. Magnetite trails are also observed (rare), with magnetite (titanomagnetite) rimmed by rutile.
Deformation	10 μm 'crack' with calcite in the centre and a hematite rim is suggestive of late deformation. Chlorite also exists on pyrite as pressure shadows.
Classification	Mineralisation related porphyry.

Sample: A30 (590.4 m – TYHD005)

Hand specimen: The hand specimen represents a porphyritic textured intrusive rock with randomly orientated ~ sub-rounded feldspars to 3 mm length. Relatively major alteration is suggested by the blurred margins of feldspar phenocrysts, specks of yellow-cream opaque rutile/leucoxene and epidote veining. Image #: 1331- 1332.

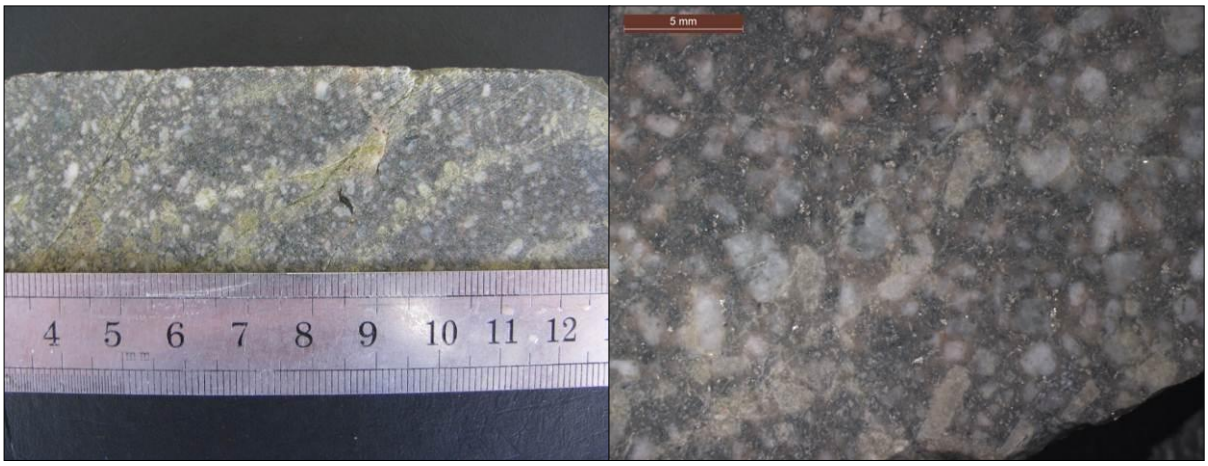

Figure 14: Sample A30 (TYHD005; 590.4 m) section offcut.

Texture & grainsize	Highly porphyritic textured intrusive with plagioclase phenocrysts to 4 mm (many ~ 2mm, many smaller ~ 0.5 mm) (variably sized). Most feldspars appear blurred (albitised) while some possess crisp complex twins. No clear K-feldspar is observed. The groundmass/matrix consists of feldspar (albite) grains (~50 μm diameter) with some quartz, which appears flooded (secondary). Small elongate former ferromagnesians (chlorite/epidote) averaging 1 mm are 'strung-out' between feldspar phenocrysts.
Primary mineralogy	Primary mineralogy consists of feldspars (plagioclase dominant); ?amphibole (chlorite altered); quartz (although much is probably secondary); moderately common apatite with blocky or hexagonal (basal cross-section) habit (~100 μm length average to 500 μm) and small (~100 μm) wedge shaped titanite. Zircons also are present as accessory minerals.
Alteration minerals	Albitised feldspars, chloritised ferromagnesians, moderately abundant pyrite, granular titanite, rutile/leucoxene aggregates approximately 300 μm in diameter and relatively abundant granular epidote are the most abundant alteration products. Epidote replaces whole feldspars in places (proximal to veins). Very little sericite is evident with its presence restricted chiefly to specks on feldspar surfaces.
Alt intensity	5.5/10
Veining	Sprawling, fine grained epidote veining to 150 μm thick along with fine grained epidote veins which have a significant selvedge effect on proximal feldspars. Late coarse calcite vein ~ 25 μm thick with neat edges. Some thinner calcite veins also observed with epidote selvedges.
Deformation	Deformation is not obvious in this sample; feldspars are not aligned and sericite is not abundant. There is however a late (infilling) calcite vein with sericite growing inward from the vein margins, inferred to be a brittle tension gash.
Other	Phenocrysts stained reddish, groundmass lighter pink (suggest iron oxides in the system).
Classification	This sample has a unique texture in that phenocrysts are not as dense as those observed in mineralised porphyry units. Unlike A26 however, it has a relatively high mafic component. The absence of sericite despite intense albitisation suggests that K-feldspar was probably not abundant in the original rock. This sample is therefore interpreted to be a pre-mineralisation porphyry, which experienced some later alteration related to hydrothermal fluids and also regional deformation whereby epidote was a major product.

Sample: A35 (488.6 m – TYHD005)

Hand specimen: Dark grey, strongly altered rock possessing a foliation of lighter ?phenocrysts, suggesting the rock is intrusive rather volcaniclastic (which develops a pervasive, whole rock cleavage). Possible relict titanite crystals (cream yellow specks). Image #: 1310-1312.

Figure 15: Sample A35 (TYHD005; 488.6 m) section offcut.

Texture & grainsize	Sheared porphyritic texture, with sub-rounded feldspars averaging 100-300 μm (ranging to 1 mm) within a felsic (highly sericitised) groundmass which also contains secondary quartz blebs. Quartz blebs are rounded, often composed of interlocking grains (individual grains ~75 μm average up to 300 μm). Overall sheared/foliated matrix (strong fabric) of chlorite (from ferromagnesians) and matted sericite.
Primary mineralogy	Intermediate composition of albitised feldspars (moderate rare plagioclase twinning observed or Carlsbad), former ferromagnesians to 2 mm (probably hornblende, squashed out along foliation), relict magnetite (ragged and associated with chlorite alteration products), rutile/ilmenite (suggestive of primary titanite, titanomagnetite) quartz (although all observed appears secondary), apatite (to 400 μm; resistant/well preserved) and zircon, mostly sub-rounded and ~ 50 μm.
Alteration minerals	Masses of sericite fibres, aligned and often intergrown with chlorite. Sericite occurs crystallising syn-kinematically behind apatite, quartz and between broken phenocrysts. Brown-purple chlorite occurs after ferromagnesians (Fe-rich), often also with magnetite and pyrite. Secondary quartz is prevalent, often in granules composed of many recrystallised, interlocking crystals. Rutile/?ilmenite is abundant, an alteration product of amphibole, titanate and titanomagnetite. Rutile also occurs as fine acicular needles, often radiating ('asterisks') in chlorite. Some feldspars are completely 'washed out'- inferred to have occurred during thin section preparation due to complete alteration of the mineral to sericite/kaolinite. Minor calcite, usually with sericite/chlorite is evident, along with minor epidote, generally associated with altered ferromagnesians.
Alt intensity	9/10
Veining	Sericite/chlorite 'channels' – formed during deformation. Coarse quartz vein 300 μm wide is late and related to deformation.
Deformation	Very strong foliation, consisting of chlorite/sericite aligned growth. Some crystals are cracked, with syn-kinematic chlorite/sericite infilling the space. Sericite/chlorite/quartz in pressure shadows.
Classification	Mineralisation related porphyry.

Sample: F01 (400-402 m – TYHD004) (zircon dated)

Hand specimen: Grey to green grey porphyritic textured rock with blurred margined phenocrysts to ~ 3 mm length. Alteration rutile/leucoxene grains are also evident (cream-yellow specks) along with some late carbonate veining. Image #: 252-260

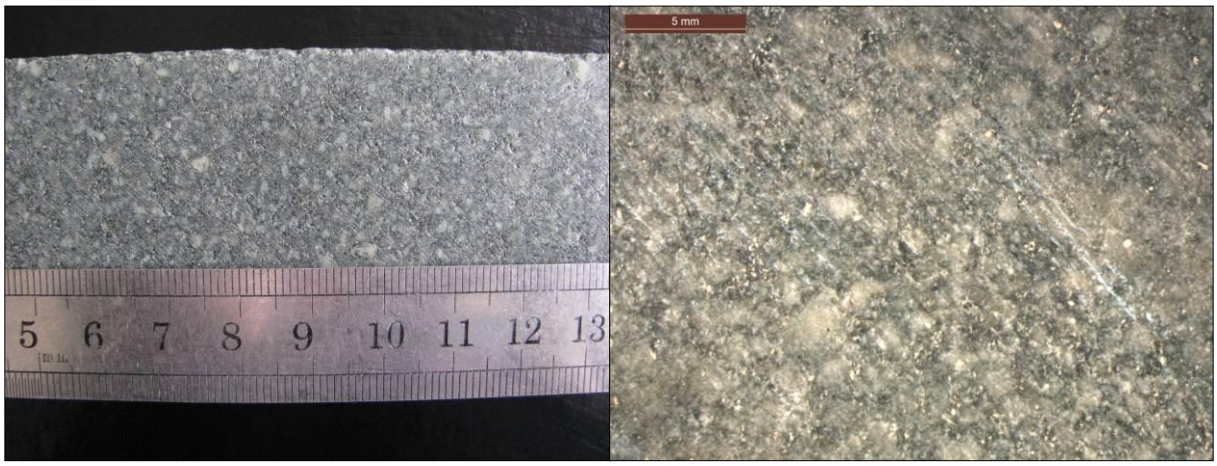

Figure 16: Sample F01 (TYHD004; 400-402 m) section offcut.

Texture& grainsize	Porphyritic textured with high ratio of phenocrysts to groundmass. Feldspars are randomly orientated, averaging ~ 2 mm length (most 0.5 – 1.5 mm). Many possess albite/complex twinning. Groundmass grainsize averages 20 μm diameter, consisting of blurred feldspars (minor quartz ~10%) with dense sericite fibres wrapping the feldspars to define a foliation.
Primary mineralogy	Feldspar phenocrysts consist of mostly variably sized rectangular plagioclase crystals (complex twinned), while rare Carlsbad twinning is also observed. Former ferromagnesians range from ~500 μm – 1.5 mm length, and are mostly 'strung-out' and not as abundant as in the Rain Hill Monzodiorite (<10% of total). Diamond shaped rutile/calcite clusters/pseudomorphs to 400 μm suggest titanite was a relatively significant primary component, whilst rutile is also associated with magnetite (titanomagnetite), which occurs as euhedral shaped, ragged crystals, to ~1 mm diameter. Zircons are also evident, averaging ~ 30 – 70 μm.
Alteration minerals	Sericite is speckled and aligned throughout the groundmass, with some feldspars possessing dense 'mats' of sericite. Epidote occurs as occasional crystals to ~200 μm long and on feldspar surfaces. Rutile is often proximal to magnetite, epidote and chlorite. Minor prehnite is associated with calcite. Secondary recrystallised quartz patches (to 500 μm) are evident, with the section containing a total estimate of ~ 15% quartz. Calcite is fairly abundant in large crystals (to 1 mm), suggesting a Ca-rich fluid passed through this rock. Chlorite is associated with ferromagnesians predominantly, which have been deformed significantly, to the point where they 'wrap' the phenocryst population.
Alt intensity	7.5/10
Veining	Syn-kinematic crystallisation of sericite and chlorite (to a lesser extent) along the foliation.
Deformation	Foliation in sample defined by wrapped textures. Bent twins in a calcite crystal. Deformational twinning of calcite.
Other	Less chlorite than many other samples observed suggests this sample is on the more magmatically evolved end of the spectra at Yiddah. Initial K-feldspar crystals have been severely albitised, with K^+ ions utilised in abundant sericite products.
Classification	Mineralisation related porphyry.

Sample: F02 (504.25-506.05 m – TYHD003) (zircon dated)

Hand specimen: Speckled cream to pink mesocratic medium to coarse grained plutonic rock with feldspars to 4 mm, no obvious quartz, and abundant dark material inferred to be amphibole, located somewhat interstitially. Some deformation related cracks cross-cut the surface of the sample, one appears to possess a slightly pink selvedge, probably related to iron oxides. Image #: 2048-2052

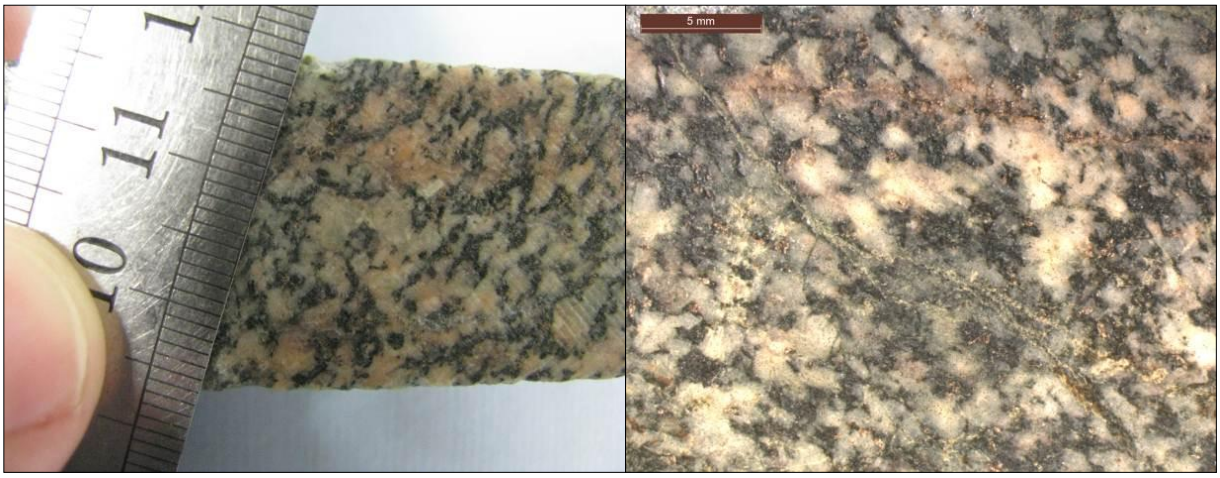

Figure 17: Sample F02 (504.25 -506.05 m – TYHD003) section offcut.

Texture & grainsize	This sample possesses a roughly equigranular texture, with plagioclase the dominant mineral, comprising ~ 60% of the rock volume and occurring as randomly orientated phenocrysts of variable size (most 0.5 – 1.5 m, up to 2 mm). Ferromagnesians (amphiboles) are the second major component (~15%), however most have been altered to chlorite and are subsequently 'strung-out' around other crystals. Those that are only partially altered to chlorite range in size from 0.5 – 1 mm, and in shape from prismatic to diamond (basal cross-sections). K-feldspar, mostly as microcline (15% of total) minor quartz (< 10%) and titanite are present interstitially. Microcline often poikilitically encloses plagioclase and amphibole. Zircons are randomly distributed throughout the thin-section, ranging from ~ 50-200 μm.
Primary mineralogy	Primary feldspars include plagioclase and K-feldspar (orthoclase and microcline). K-feldspar is late stage, infilling interstitial spaces along with quartz. Ferromagnesians are hornblende and/or actinolite, with both prismatic and basal cross-sections observed. Reasonably abundant titanite averages 200 μm – 1 mm, with some euhedral diamond shaped and some more granular. Minor allanite is also present. Apatite is relatively common, either as prismatic crystals to ~ 350 μm or hexagonal basal cross-sections to ~ 100 μm diameter (larger than in porphyries). Relict ragged magnetite (~ 1 mm) is fairly common (~ 2%).
Alteration minerals	Chlorite is abundant after amphibole, occurring within the cleavages of some semi-altered crystals. It also occurs surrounding ragged magnetite crystals. Sericite speckles are present throughout the sample at low density, mostly relating to feldspars. Some feldspars are 'cleaner' (without sericite coatings), and consist of microcline recrystallised to perthite, probably under deformational stress. Epidote and chlorite occur interstitially and also as veins. Some titanite appears to be alteration related, possessing a granular habit & associated with titanomagnetite. Some rutile is present, but its abundance is minor compared to other intrusive samples.
Alt intensity	4.5/10
Veining	An undulating fine-grained (~ 20 μm) epidote (+chlorite) vein of ~ 250 μm width, along with other sub parallel chlorite veins are cross-cut by a relatively coarse grained 'booklet' chlorite/calcite/K-feldspar(adularia)/quartz vein of ~ 300 μm width. The vein margins are straight and consistent, suggesting this is an infilled tension gash.
Deformation	Some 'snapping' (brittle deformation) of plagioclase, amphiboles and titanite; often with spaces filled by aligned (syn-kinematic) chlorite. Undulose extinction of quartz. Some bending of plagioclase twins. Perthitic recrystallisation of microcline.
Classification	Rain Hill Monzodiorite.

Sample: B01 (551.5 m – TYHD004)

Hand specimen: The hand specimen consists of a dark, well-sorted fine-grained unit, with extensive stringy sinuous epidote/carbonate veining in many orientations, crosscut by more consistently orientated coarser tension gashes filled with quartz/epidote/carbonate. Image #: 382-393.

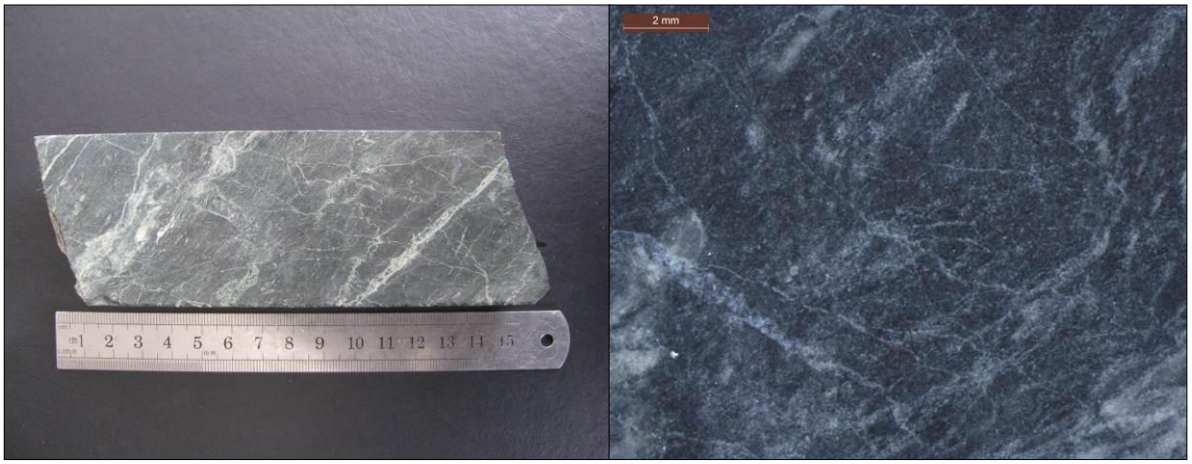

Figure 18: Sample B01 (TYHD004; 551.5 m) section offcut.

Texture & grainsize	Foliated/aligned amphiboles (actinolite) 10-50μm, with similar to smaller sized albite feldspars. Amphiboles stand out as jagged to blocky to elongate crystals of variable size, some interlocking in larger patches. Amphibole orientations are random to weakly foliated under highest resolution; however as a whole the section is strongly 'banded', defined by chlorite and plagioclase abundances.
Primary mineralogy	Primary mineralogy is difficult to distinguish but textures and alteration products suggest the original rock was highly mafic (~35% ferromagnesians) and quartz poor. It probably consisted of plagioclase-amphibole(?pyroxene). Ragged relict magnetite crystals are apparent.
Alteration minerals	Dominant products are amphibole and albite, probably the result of contact metamorphism (hornfelsing). Amphibole is dominantly yellow to brown (XPL) sometimes pink-blue and is occasionally twinned. Cordierite grains are observed rarely, however they are generally difficult to distinguish from plagioclase. Calcite and minor ankerite is also present throughout the matrix. Epidote is common as aggregates through and in veins, with possible tourmaline needles growing into epidote veins also. Epidote also occurs as granules and other replacement grains. Pyrite is a minor product, whilst magnetite trail veins and disseminated magnetite are fairly abundant. Titanite/allanite is also observed in rare abundance.
Alt intensity	7/10
Veining	Early (?primary) magnetite sometimes offset by epidote, which appears to be hydrothermally related, and associated with pyrite. Epidote and calcite veining to 200 μm (tension gash fill). Also some late sericite/chlorite veining.
Deformation	Late tension gash fractures. E.g. 20 μm vein with calcite and ankerite fill. Offset of epidote and early 'banding'.
Classification	Fine-grained basaltic volcaniclastic. (OR Amphibole-plagioclase metabasalt).

Sample: B03 (345.2 m – TYHD003)

Hand specimen: Intermediate grey coloured, fine grained rock with variable texture and mottled appearance at medium resolution. Image #: 649-653.

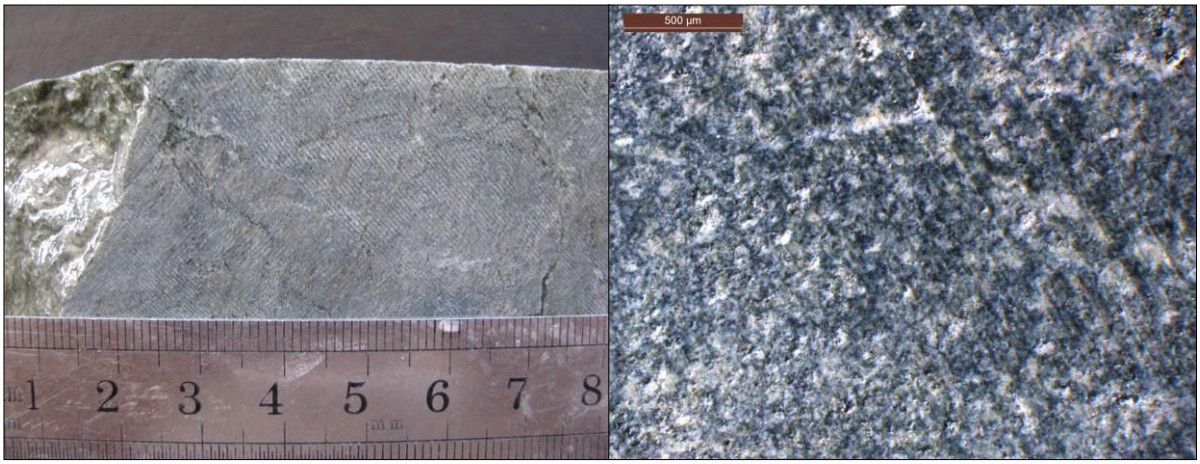

Figure 19: Sample B03 (TYHD003; 345.2 m) section offcut.

Texture & grainsize	Predominantly a fine grained matrix of feldspar (mostly albite) and quartz, with interstitial chlorite, sericite (~20μm diameter) and epidote. Some coarser grained material is variably present, such as larger quartz granules (recrystallised) and amphiboles (interlocking and inferred to be recrystallised). It is likely the intrusion of the Rain Hill Monzodiorite and hydrothermal alteration produced the interlocking textures observed, with the variability in grain size suggesting an original clastic nature.
Primary mineralogy	Albite and quartz are the dominant primary minerals, along with a ferromagnesian component which may be amphibole (as observed) or a precursor mineral to amphibole. This component is small however (~10%), with the rock possessing an overall relatively felsic character. Quartz probably comprises ~10% of the rock, much more than the fine-grained basaltic volcaniclastic unit. Trace zircons occur as 'stumpy,' small (20-50 μm) crystals. Titanite is mostly small (~50μm) and possibly secondary.
Alteration minerals	Fine grained chlorite and fine granular epidote define a significant microfoliation. Other alteration products include calcite, sericite (which occurs as flakes throughout), magnetite (dispersed throughout, often rimmed with ilmenite/rutile/leucoxene) and quartz. Pyrite is reasonably abundant, often in a considerably degraded condition.
Alt intensity	8/10
Veining	Coarse calcite veins, at times blocky and aligned with the foliation trend (syn-kinematic). Fine grained epidote veins (abundant). Quartz/pyrite plus lesser chlorite/epidote veins where quartz grains are ~ 50 μm, rounded and interlocking. One larger quartz vein (1 mm width)
Deformation	Variably orientated syn-kinematic aligned calcite and minor chlorite veins crosscut earlier pyrite, quartz, epidote veins parallel to 'foliation'.
Classification	Andesitic volcaniclastic.

Sample: B08 (624.8 m – TYHD005)

Hand specimen: Dark grey to black fine-grained rock with epidote/calcite veining and slight banding/?bedding. Some larger tension related veins possess quartz/epidote/carbonate assemblages. Image #: 1563-1565.

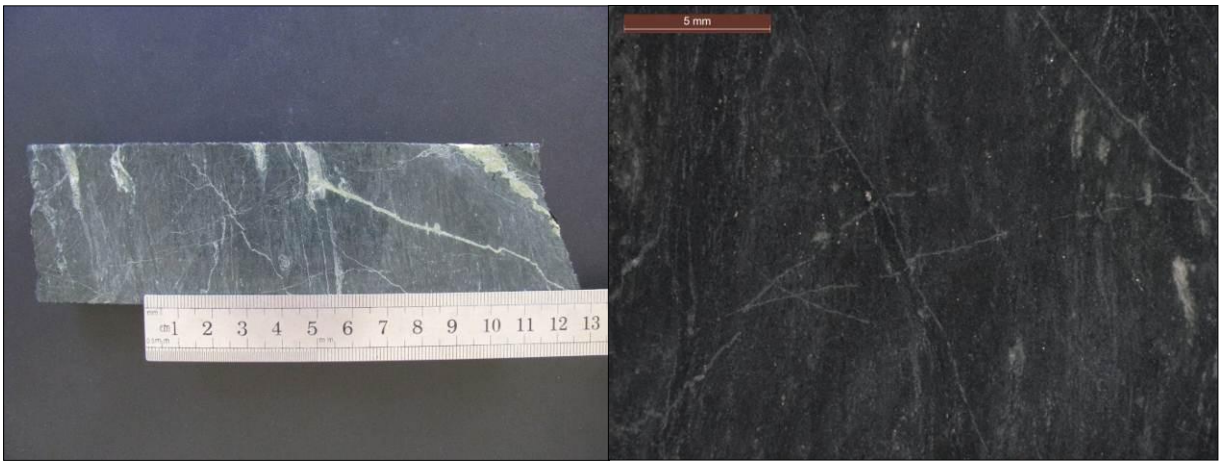

Figure 20: Sample B08 (TYHD005; 624.8 m) section offcut.

Texture & grainsize	Foliated matrix of elongated amphiboles (probably actinolite) intergrown/interspersed with more rounded albite (+ rare larger cordierite) and interstitial chlorite. Layered appearance, probably due to either invasion of fluids along bedding plane, variation of primary mineralogy in a bedded or banded configuration or later deformation and recrystallisation of chlorite along a foliation. Some lenses of slightly more coarse material (feldspars >100 μm) are possibly a primary feature, supporting a detrital primary nature of the metabasalt.
Primary mineralogy	Primary mineralogy is difficult to establish however it probably consisted of a mafic, silica poor assemblage; dominated by plagioclase (which has since been entirely albitised) and a ferromagnesian mineral, which was a precursor to amphibole. The occasional larger feldspar (to ~ 200 μm) suggests the rock was primarily volcaniclastic. Zircons are also evident, rounded to sub-euhedral; averaging ~30 μm. Disseminated magnetite may have also been a primary component.
Alteration minerals	Amphiboles dominate the rock, defining the foliation. Feldspars have suffered albitisation. Cordierite may also be a component of the groundmass. Epidote is present in veining and also dispersed through the entire section as very fine grains and occasional larger globules. Fine grained chlorite is disseminated throughout and is very predominant (25% of rock). Disseminated pyrite (20 μm, up to 200 μm average) is also prevalent.
Alt intensity	7/10
Veining	- Epidote veining containing needle-like actinolite or ?tourmaline to 500 μm width. - Fine grained/granular epidote veining containing pyrite crystals; averaging around 200 μm width. - Late, cross-cutting coarse grained epidote/calcite veins with fine grained chlorite selvedges.
Deformation	Deformation indicated by foliation of amphibole phenocrysts, groundmass; and offset/'kinking' of epidote veins.
Classification	Fine-grained basaltic volcaniclastic. (OR Amphibole-plagioclase metabasalt).

Sample: B10 (71.7 m – TYHD003)

Hand specimen: Intensely altered volcaniclastic rock with pervasive sericite/kaolinite matrix and larger contained pyrite crystals. A slight green tinge suggests that contained Cu is oxidising to malachite. Image #: 659-663.

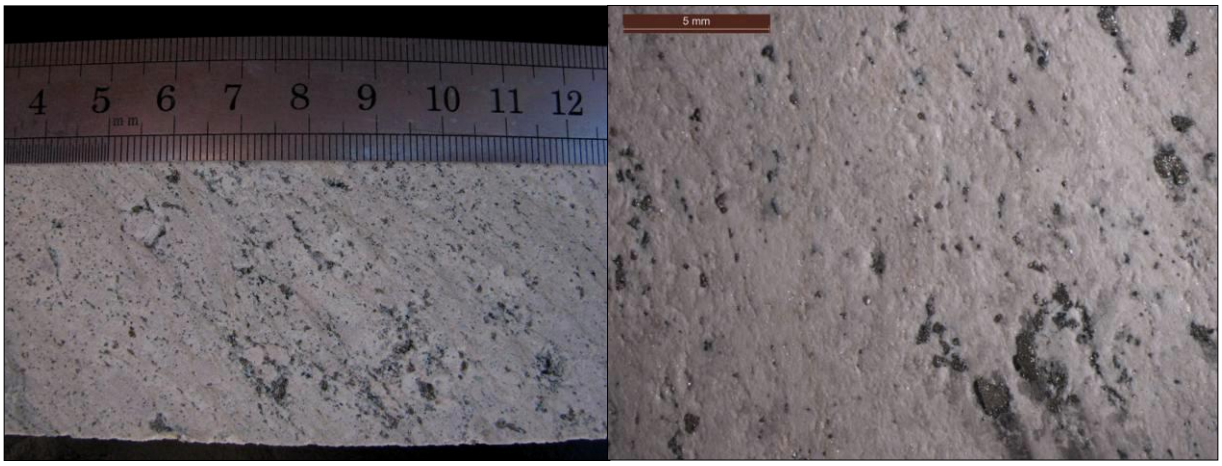

Figure 21: Sample B10 (TYHD003; 71.7 m) section offcut.

Texture & grainsize	Feldspars are completely altered to kaolinite (washed off slide), with gaps to ~1 mm diameter evident, surrounded by a fine matrix of quartz (~ 50 μm) and sericite (very fine elongate fibres up to ~50 μm). Overall texture is 'porphyryclastic'.
Primary mineralogy	Intense alteration has destroyed all primary minerals except infrequent zircons. Feldspars are inferred by rectangular gaps in the section.
Alteration minerals	Large pyrite cubes (average ~ 500 μm). Abundant sericite and kaolinite (much of which has been washed away). Secondary altered rutile needles and smudgy granular rutile patches. Silicification (all secondary quartz). Minor chlorite throughout but most was probably further altered to kaolinite, pyrite etc. Pyrite/magnetite trails - mostly pyrite but bit of magnetite (associated with one another)
Alt intensity	10/10
Veining	none preserved, probably quartz
Deformation	Alignment of deformation related sericite.
Classification	Intensely (shear-zone) altered andesitic volcaniclastic.

Sample: C03 (142.1 m – TYHD004)

Hand specimen: This sample consists of an intensely altered, foliated light coloured rock of unknown primary composition, inferred to consist of sericite, kaolinite and quartz (argillic alteration assemblage). Abundant disseminated pyrite is also evident, <1 mm diameter. No primary rock texture remains.

No thin section could be prepared for this sample due to its very soft nature.

Cu = ~ 500 ppm around this interval.

Classification: Late, shear related argillic.

Figure 22: Sample C03 (TYHD004; 142.10 m) section offcut.

Sample: C04 (208.95 m – TYHD004)

Hand specimen: Strongly altered rock of probable intrusive porphyry primary composition, with green to creamy grey groundmass and cream altered phenocrysts. The rock is friable and soft. Image #: 166-168.

Figure 23: Sample C04 (TYHD004; 208.95 m) section offcut.

Texture & grainsize	This rock consists of a strongly foliated groundmass of feldspar and alteration quartz, along with abundant aligned sericite and chlorite and larger feldspar phenocrysts (~ 200 μm). ~ 40% of the groundmass appears to be quartz, consisting of small recrystallised, interlocking crystals (10-100 μm). Feldspar phenocrysts are albitised and sericitised with rounded margins. Former ferromagnesians are also evident; with chlorite/sericite wrapping all larger crystals defining the foliation.
Primary mineralogy	Feldspars range from small (in the groundmass) to larger (~ 300 μm). No primary quartz is preserved, all appears secondary (silica flooded). Cross sections of former ferromagnesians suggests these were initially amphibole (now fine grained ?biotite, chlorite, some rutile). Some pseudomorphs are elongate to 1 mm, while some preserved diamond shaped basal sections are to 500 μm length. Most however are strung out within the foliation. Zircons average ~ 40 μm
Alteration minerals	Feldspars are entirely albitised, with blurred twins and margins. Ferromagnesians are altered to chlorite (possibly via biotite), along with granular to acicular rutile and titanite. The intermediate biotite phase is inferred by the presence of sagenitic rutile within chlorite patches, a feature associated with biotite. Sericite is very abundant in the groundmass, 'wrapping' feldspars along with chlorite, halloysite and kaolinite. These products suggest the host possessed a reasonably high content of K-feldspar or the rock has experienced K^+ ion addition during hydrothermal alteration (or both). Secondary quartz is very abundant, forming interlocking recrystallised grains throughout the whole sample (a product of conversion of feldspars to sericite, then kaolinite and amphiboles to chlorite; etc.).Abundant pyrite is disseminated throughout in blebs (not cubes), often ~200 μm to 1 mm.
Alt intensity	8/10
Veining	Foliation is pervasive throughout as moulded chlorite (pyrite/sericite/kaolinite) fibres/vein like features. Quartz 'channels' occur to ~ 100 μm width.
Deformation	Chlorite pressure shadows, intense foliation and syn-kinematic growth of sericite/chlorite.
Other	'Holes' in slide where kaolinite has washed out.
Mineralist'n	Disseminated chalcopyrite. Cu = 1000 – 2000 ppm around this interval.
Alt' class	Chlorite-sericite

Sample: C08 (349.5m – TYHD004)

Hand specimen: Grey to purple/green porphyritic textured rock with some feldspars evident in an overall washed, indistinct appearance. Epidote veining is also apparent with blurry selvedges. Image #: 303-304.

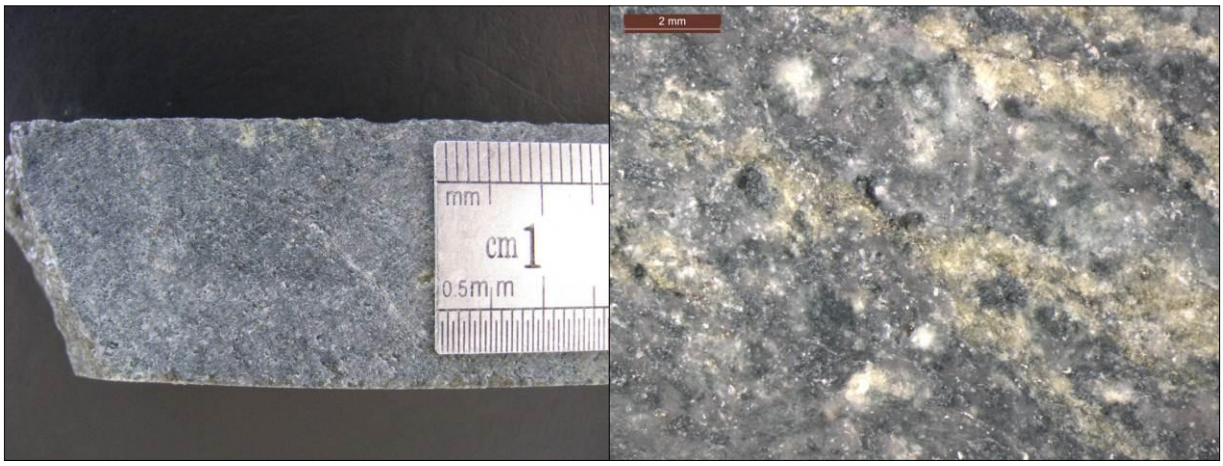

Figure 24: Sample C08 (TYHD004; 349.5 m) section offcut.

Texture & grainsize	Foliated porphyritic rock with feldspar and former ferromagnesian phenocrysts (grainsize averaging 0.5 – 1.5 mm, up to ~2 mm maximum). Groundmass consists of 10 – 50 μm sized feldspar/quartz crystals and alteration magnetite, sericite, pyrite, rutile, calcite and epidote (epidote more significant near veins).
Primary mineralogy	Feldspars are albitised, so it is difficult to determine primary mineralogy, however both complex and Carlsbad twins are observed. No primary quartz is preserved. Former ferromagnesians are evident through preserved prismatic to diamond shaped grain boundaries. No primary titanite is observed. Minor apatite is evident. Zircons average ~30-50 μm
Alteration minerals	Alteration products are dominantly albite, quartz, chlorite, sericite, epidote, magnetite, minor calcite, pyrite and rutile. Silicified secondary quartz comprises ~ 25% of the rock, often recrystallised and interlocking. Granular epidote is present as veins, with strong selvedges where it completely replaces feldspars with fine-grained granular crystals, along with calcite. Sericite and phengite are prevalent (~20% of total), 'wrapping' feldspars and also as net-like mats on feldspar surfaces. Magnetite is abundant from 10 μm – 200 μm, with alteration rutile in cleavages and surrounding grains (therefore probably titanomagnetite). While appreciable rutile is present, no fine grained radiating orientations are observed (more granular/globular habit). Pyrite and chalcopyrite are also present, generally larger than magnetite.
Alt intensity	6.5/10
Veining	Three main types - Epidote + pyrite ± sericite (+ more platy muscovite), undulating, completely destroying proximal feldspars, fairly pervasive. Likely associated with propylitic alteration (retrograde or deformation related) which overprints earlier chlorite-magnetite chalcopyrite bearing alteration. - Calcite veining - thick (1 mm), coarse grained (grains to 200 μm), cross cut by: - Quartz, width to 750 μm, coarse grained (grains to 500 μm) related to deformation.
Deformation	Ductile deformation has resulted in a strong foliation, defined by aligned sericite/chlorite fibres. Former ferromagnesians are also significantly smeared or 'strung out' along the foliation.
Mineralist'n	Disseminated chalcopyrite Cu = ~ 3000-5000 ppm around this interval.
Alt' class	Chlorite-magnetite (weak potassic overprinted by deformation related propylitic)

Sample: C09 (450.6 m – TYHD004)

Hand specimen: The sample resembles a greenish dark grey densely porphyritic intrusive rock, containing white to creamy opaque, blurry margined feldspars in a darker groundmass with specks of alteration rutile/leucoxene and abundant patches of alteration epidote to 10 mm diameter. Image #: 305-309.

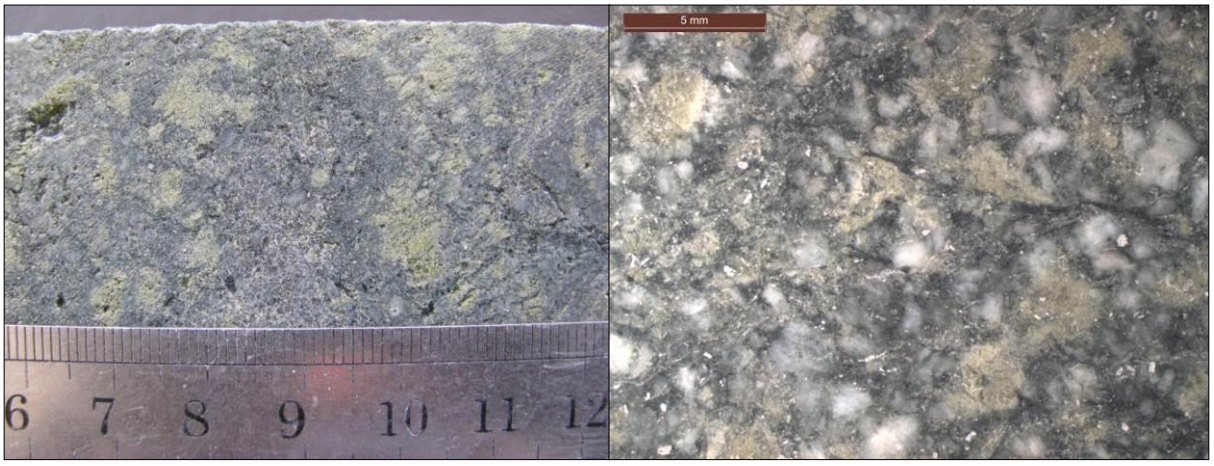

Figure 25: Sample C09 (TYHD004; 450.6 m) section offcut.

Microscopy	
Texture & grainsize	Porphyritic textured, with feldspars from ~200 μm to 3 mm. All ferromagnesian phenocrysts have been altered to epidote (predominantly) and (lesser so) chlorite, occurring throughout the groundmass of mostly feldspar and quartz; predominantly ~20-50 μm diameter.
Primary mineralogy	Predominant mineral constituent is plagioclase. Former ferromagnesian shapes are suggestive of amphibole. Quartz is secondary. Titanite (trace) and zircons.
Alteration minerals	Albite is the dominant alteration product, occurring after feldspar phenocrysts and groundmass feldspars. Chlorite is dispersed throughout the groundmass and also fills space in deformation fractures. Secondary quartz is relatively abundant (50 – 100 μm), some appearing 'flooded'. Epidote is very common, replacing ferromagnesians and some feldspars (close to epidote veins) with a fine grained, granular blocky habit. Sericite (phengite/muscovite) is apparent mostly in 'channels' rather than the general groundmass. Very fine grained (1 – 3 μm) kaolinite is evident in minor amounts. Altered titanomagnetite or ilmenite has associated stumpy fine alteration rutile. Rutile specks are also common throughout, mostly after titanomagnetite or primary magnetite (to 300 μm). Calcite is reasonably abundant – some fairly coarse. Magnetite appears primary, not alteration related.
Alt intensity	6.5/10
Veining	Epidote veining occurs throughout, with one 'channel-like' zone to 3 mm width. Sericite 'channel' 2 mm wide, with Ti mineral (rutile or titanate). Siliceous flooding evident by interlocking quartz grains ~ 25 μm. Some calcite veining with some secondary titanate.
Deformation	Deformation is evidenced by a slight foliation, sub parallel to some epidote/chlorite veining, deformed twins in plagioclase phenocrysts and the brittle fracture of some plagioclase crystals.
Other	
Mineralist'n	Low. 50 – 200 ppm Cu.
Alt' class	Propylitic (hydrothermal) with further propylitic (deformation)

Sample: C13 (559.25 m – TYHD004)

Hand specimen: This sample resembles an intensely altered plutonic rock, with pinkish cream (hematite stained) feldspars contained within indistinct pinkish dark grey minerals. Darker, reddish purple interstitial material is present in a net-like fashion. Relict specks of titanite (alteration rutile/leucoxene) are common. Image #: 440-442.

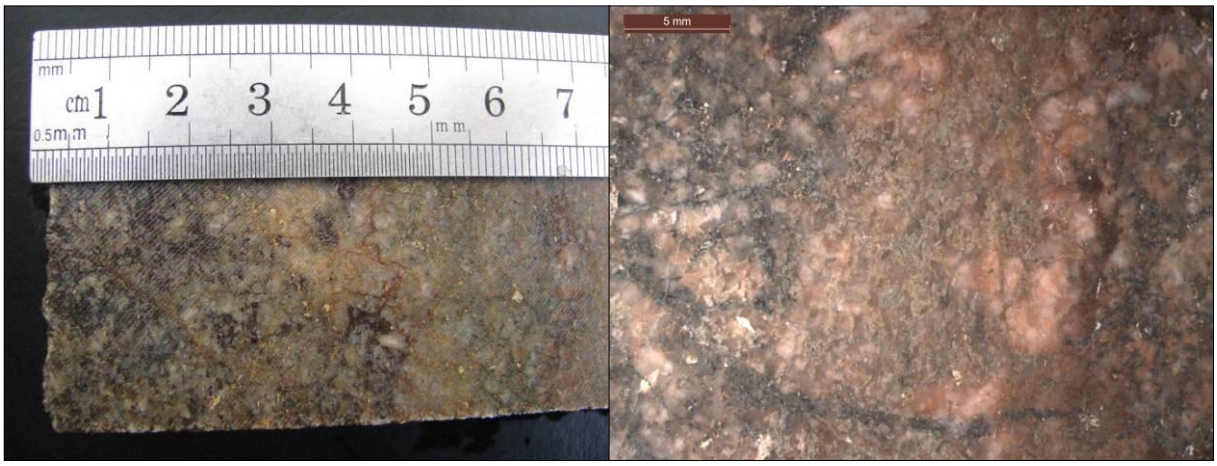

Figure 26: Sample C13 (TYHD004; 559.25 m) section offcut.

Microscopy	
Texture & grainsize	Feldspars range to 3 mm, most are between 0.5 – 1.5 mm. Grainsizes are variable (sub-equigranular; like A08). Foliation is mostly defined by epidote-chlorite veins however there is a slight foliation in phenocrysts. Where ferromagnesian shapes are preserved, they range to ~ 3 mm; however most are sheared out.
Primary mineralogy	Plagioclase is most common, followed by K-Feldspar; with albitisation affecting all feldspars. Yellowish to red staining affects many feldspars and quartz (hematite). Ferromagnesians are mostly altered to granular epidote, with chlorite and turbid stubby small rutile surrounding. Relict diamond titanate is observed to 400 μm length, altered to rutile. Zircons and apatite (v. rare and small) are also present.
Alteration minerals	Primary alteration mineral is albite. Quartz is also dominant, in a polycrystalline configuration following *in situ* production of silica from orthoclase/microcline and other silicates. Former ferromagnesians are largely replaced by epidote. Alteration occurs more intensely in selvedge areas. Chlorite is Fe rich (blue – purple colour). Sericite/phengite is present on K-feldspar surfaces and as speckles on plagioclase. No primary K-feldspar remains. Also evidence of kaolinite, paragonite and trace gypsum. Hematite has entered the rock via a fluid and floods the interstitial areas, along with staining of secondary feldspars. Altered rutile (leucoxene) and titanomagnetite (to > 1 mm) are also evident. Titanomagnetite is partially altered to rutile and hematite (leucoxene).
Alt intensity	6.5/10
Veining	Epidote veining throughout (initial). Selvedge with some quartz. Quartz veining follows epidote veining. Chlorite (Fe –rich) veining. Iron oxides.
Deformation	Strong deformation – may be near fault (source of oxidised fluids). Brittle fracture of phenocrysts, bedding of plagioclase twinning. Invasion of iron oxide rich or oxidising water with deformation brittle cracking.
Other:	Hematite fluid has infiltrated the whole sample (late stage – time of deformation), while propylitic Ca-rich fluid appears earlier. No acicular rutile needles observed.
Interpretation:	1st alteration - Epidote stage - Ca rich fluid, silicification, albitisation (propylitic, related to porphyry system). 2nd alteration - Fault related - more silica; oxidised fluid; iron bearing minerals, especially magnetite, converted to hematite; total conversion of Ti minerals to rutile; reprecipitation of chlorite/magnetite ferromagnesian clusters (purple chlorite) with a strong foliation. Minor sericitisation.
Mineralist'n	Low. 50 – 400 ppm Cu.
Alt' class	Propylitic (hydrothermal) with further deformation/fault related oxidation of minerals.

Sample: C18 (106.85 m – TYHD003)

Hand specimen: Strongly altered creamish green plutonic rock characterised by opaque white phenocrysts in an indistinct greenish groundmass, with minor pyrite and chlorite patches. Image #: 673-678.

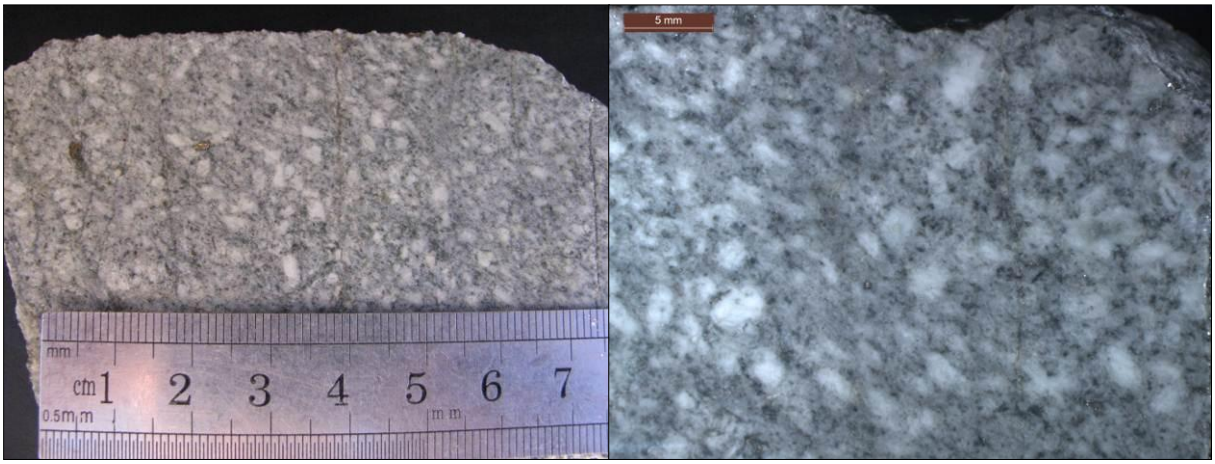

Figure 27: Sample C18 (TYHD003; 106.85 m) section offcut.

Microscopy	
Texture & grainsize	Porphyritic texture with phenocrysts ranging in size from ~ 0.5 to 1 mm, up to ~3 mm. Difficult to clearly identify due to intense sericitisation. Rounded secondary quartz. Groundmass completely covered with sericite flakes and lesser fine grained quartz.
Primary mineralogy	Plagioclase, now albitised and lesser sericitised. Former ferromagnesians to ~ 1 mm. Few grain boundaries are preserved, with those evident replaced by chlorite and minor epidote. Remnant titanite (diamond shaped rutile) fairly common. Zircons (minor)
Alteration minerals	Secondary quartz (recrystallised) is the dominant alteration mineral, consisting of rounded grains averaging ~ 200 – 400 μm diameter. Albite occurs after plagioclase. Fine grained sericite (muscovite and phengite) floods the entire sample in a net like fashion. Kaolinite alteration of feldspars is also observed, but appears mostly washed out of the thin section. Chlorite is strung-out throughout the groundmass and largely in pressure shadows, but also to a lesser degree after ferromagnesians. Minor granular epidote is observed after ferromagnesians. Significant granular rutile occurs throughout along with traces of pyrite.
Alt intensity	8.5/10
Veining	Pyrite trails containing blebby pyrite to 1 mm diameter (most ~ 100 μm). Sericite occurs in a flooded fashion, aligned around/over feldspars and quartz.
Deformation	Pressure shadows occur on pyrite. Chlorite and sericite have been recrystallised in low pressure zones. Kaolinite altered feldspars have coarser sericite-chlorite growing into them
Other:	All opaques identified are pyrite and (semi-opaque) rutile. No magnetite was observed. Biotite may be present as fine grains throughout difficult to identify. Possibly some chalcopyrite
Interpretation	Initial alteration has resulted in intense sericitisation and albitisation of feldspars and crystallised large secondary quartz grains (prior to regional deformation). Later deformation related alteration involved more sericite and chlorite which recrystallised into a flow alignment. Softer kaolinite altered phenocrysts were 'invaded' by coarser chlorite.
Mineralist'n	~ 1000 ppm Cu.
Alt' class	Sericitic

Sample: C22 (279.00 m – TYHD003)

Hand specimen: Fine-grained dark greenish grey volcaniclastic rock, with fine banding or bedding, minor pyrite, some larger sized particles. Image #: 698-701.

Figure 28: Sample C22 (TYHD003; 279.00 m) section offcut.

Microscopy	
Texture & grainsize	Fine grained strongly foliated chloritised matrix (10-20 μm) containing 'pods' (~200 μm-1.5 mm) of quartz/calcite, feldspar and epidote. Ferromagnesians ~200 μm – 1 mm (chlorite-epidote).
Primary mineralogy	Feldspar subsequently altered to albite, sericite, kaolinite, quartz. Ferromagnesians (smaller) altered to chlorite, rutile, titanite and quartz. Fine grained groundmass. Only chlorite – quartz – albite remains.
Alteration minerals	Chlorite dominant throughout matrix. Very abundant and fine grained with magnetite. Quartz in veining, some recrystallised. Albite in groundmass. Kaolinite in chlorite groundmass and altering feldspars. Epidote – in veins and as isolated granules. Sericite in quartz-calcite veins. Rutile is abundant and often associated with magnetite (inferred to be titanomagnetite), minor alteration titanate (rutile rimmed). Magnetite (very abundant) disseminated throughout and in veins, small (mostly 10-30 μm). Significant (but lesser) pyrite (larger ~ 100 μm).
Alt intensity	9.5/10
Veining	Siliceous flooding/veining (coarse grains to 0.5 mm) ± calcite, epidote, sericite. Siliceous phase has occurred prior to deformation. Areas not silicified are squashed/ intensely foliated. Pyrite trails in quartz/sericite/calcite/epidote veins. Magnetite veins (rutile altered) with later chlorite rich flooding and veining, crosscutting quartz veins.
Deformation	Strong foliation associated with chlorite-magnetite alteration and deformation shearing.
Other:	Overall very chlorite rich sample. Easily deformed due to soft nature, strong foliation.
Interpretation	This sample has suffered early siliceous veining associated with pyrite, epidote, calcite and sericite. Pyrite is associated with this early quartz stage. Pervasive chlorite/magnetite ± rutile/ epidote alteration also occurred early, with magnetite veins evident. Much of the magnetite has subsequently altered to rutile. Lastly, deformation induced further chloritisation of the groundmass, sericitisation and imparted a strong foliation. This resulted in the intense moulding of the chlorite-magnetite matrix around the more resistant quartz veins.
Mineralist'n	~ 500 - 1000 ppm Cu.
Alt' class	Chlorite – magnetite, propylitic overprint.

Sample: C24 (320.6 m – TYHD003)

Hand specimen: Medium grained plutonic rock with greyish blue to pink feldspars and darker amphibole components (~ 2 – 4 mm). Fine grained epidote veining cross-cuts the sample, with minor selvedges (~ 1 cm), along with fine grained chlorite veining. Image #: 710-718.

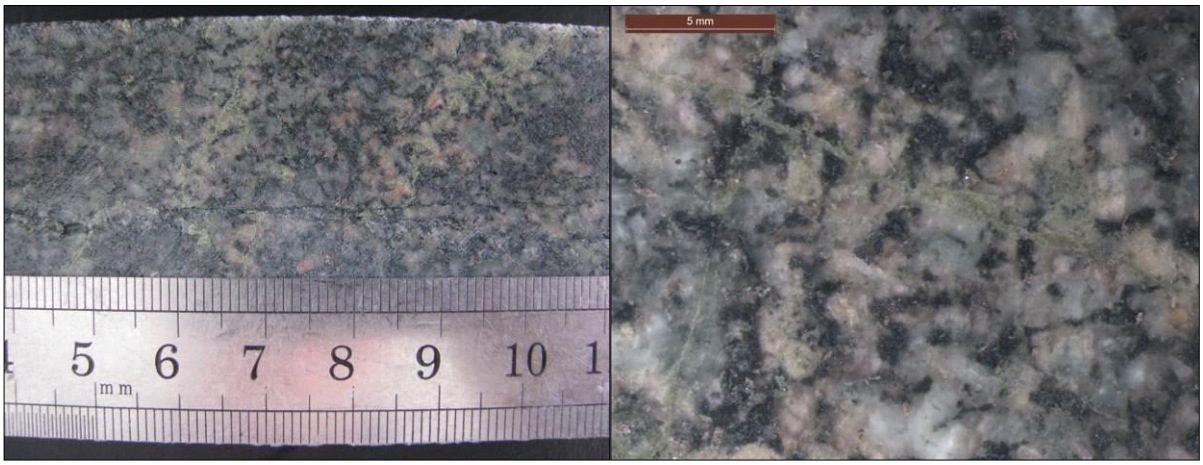

Figure 29: Sample C24 (TYHD003; 320.6 m) section offcut.

Microscopy	
Texture & grainsize	Feldspars variable in size (0.5 – 1 mm average, to 3 mm), randomly orientated. Elongate to stumpy former ferromagnesian grains to ~ 2.5 mm. Quartz and K-feldspar groundmass/interstitial/smaller grains.
Primary mineralogy	Larger phenocrysts of plagioclase (most appear primary) and ferromagnesians (elongate shape suggests amphiboles). Other lesser components include K-feldspar, some quartz, rare apatite, titanite (primary remnant and alteration- associated with magnetite). Large remnant magnetite (1 -2 mm), at least one being cracked with epidote infilling.
Alteration minerals	Quartz, some secondary. Calcite on feldspar/ferromagnesian surfaces. Chlorite occurs after ferromagnesians and is brown-purple suggesting it is Fe-rich. Slight albitisation of feldspars. Secondary recrystallised titanite is smaller and less euhedral. Rutile is present in small amounts on titanite margins, replacing titanite from titanomagnetite/?ilmenite Sericite specks on ferromagnesians and feldspar surfaces (not abundant). Epidote occurs on ferromagnesian surfaces and in granular, straight veins. Some minor alteration of magnetite around edges to rutile or titanite, epidote/chlorite. One allanite crystal observed 0.75 mm diameter.
Alt intensity	4/10
Veining	Epidote vein ~ 100 μm thick, very straight set of 3 that cross each other at right angles, appear contemporaneous (no consistent offset direction). Epidote vein also contains chlorite and pyrite; minor selvedges observed.
Deformation	Evidence of deformation includes cracks filled with chlorite, epidote, pyrite; stressed quartz (undulose extinction); and phenocrysts offset along cracks.
Other	Non-mineralised. Altered Rain Hill Monzodiorite granitoid.
Interpretation	Sample has not undergone intense alteration. Some albitisation of feldspars is evident along with chlorite-epidote alteration of ferromagnesians (amphiboles). Only very minor sericitisation has occurred. The sample shows both deformational features and propylitic style alteration.
Mineralist'n	Low. ~ 50 - 300 ppm Cu.
Alt' class	Propylitic.

Sample: C27 (413.85 m – TYHD003)

Hand specimen: Dark grey porphyritic textured rock containing pale green to pale pink variably sized feldspar phenocrysts (to 4 mm), with a minor flow foliation. Small opaque cream specks are rutile/leucoxene alteration products. Image #: 731-734

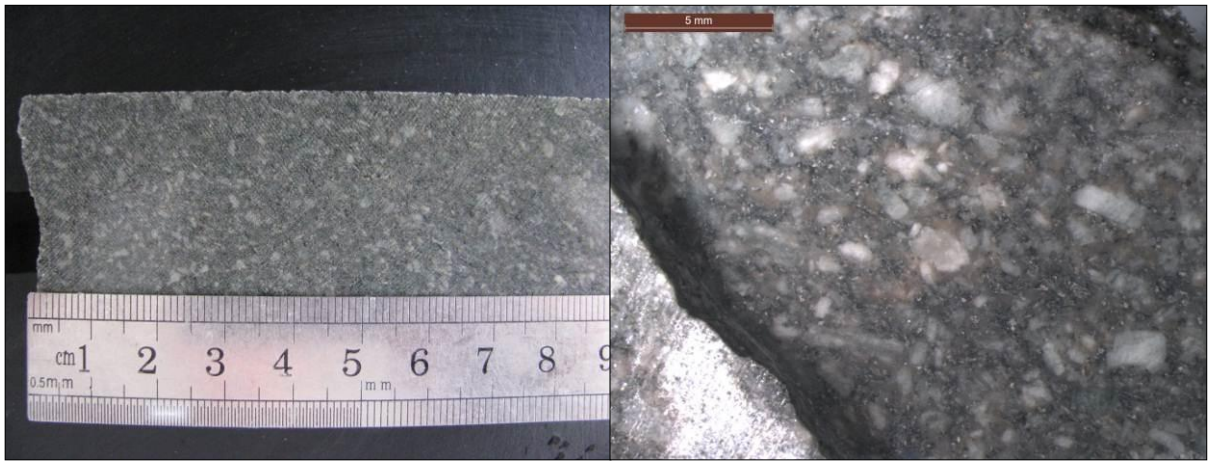

Figure 30: Sample C27 (TYHD003; 413.85m) section offcut.

Microscopy	
Texture & grainsize	Porphyritic texture, with major phenocrysts aligned (foliated). Phenocrysts consist of feldspars, which are blocky to elongate to 2 mm, and ferromagnesians to ~ 2 mm, some elongate, some diamond shaped. Fairly densely packed. Finer groundmass is totally altered to recrystallised interlocking quartz (~ 25 μm), albite, sericite flakes and minor calcite. Groundmass appears to engulf feldspars with no clear boundaries.
Primary mineralogy	Feldspars are dominantly albite (secondary), with some more calcic species also preserved, along with orthoclase. Amphiboles are suggested by elongate and diamond shaped chloritised/epidotised patches. Quartz concentrations would have initially been low (very few large qz patches, all secondary). Minor titanate is observed which is probably secondary, (primary destroyed). Zircons ~ 50 μm; apatite ~ 250 μm, Some relict ragged primary magnetite, however most appears secondary from ferromagnesians and fluids.
Alteration minerals	Dominant alteration mineral is albite- feldspar margins are blurred and indistinct. Significant chlorite is present after ferromagnesians and through groundmass (green in XPL). Phengite (sericite) occurs throughout the groundmass and on surface of grains (where it covers as dense mats). Blobs of secondary magnetite appear to be brought into the rock via fluids. Rutile present after magnetite, in chlorite after ferromagnesians, and as abundant small rutile needles with random orientation, some in clusters or single. Minor kaolinite and calcite in veining. Discrete crystals of epidote/allanite.
Alt intensity	9/10
Veining	Pervasive veining throughout (not really distinct veins), including calcite (vein to 1 mm), chlorite ~ 200 μm wide, sericite veining/flooding.
Deformation	Evidence of ductile deformation of plagioclase twins, possibly following weakening by sericite alteration. Chlorite-sericite pressure shadows also evident.
Other:	Albitisation seems to make feldspars much more susceptible to sericitisation.
Interpretation	Sample subject to severe alteration involving albitisation of feldspars (~ 40 % of rock, while ~ 10% of feldspar remains non-albitised); possible minor alteration biotite (chlorite habit mimics biotite); sericitisation over feldspar surfaces and also addition of quartz via these reactions. Allanite/epidote has grown to discrete large (0.5 mm) crystals. Magnetite has also been added. Foliation of phenocrysts suggests either alignment or deformation, which would promote further alteration due to higher surface areas. Milky appearance of feldspars (kind of opaque) is due to a covering of sericite, not due to albitisation.
Mineralist'n	Low. < 50 ppm.
Alt' class	Albite/sodic.

Sample: C29 (166.2 m – TYHD005)

Hand specimen: The hand specimen consists of a white to cream, strongly foliated rock of unknown primary composition, with visible pyrite and quartz. A large proportion of white mica is inferred from the shimmery lustre. Image #: 1202-1203.

Figure 31: Sample C29 (TYHD005; 166.2 m) section offcut.

Microscopy	
Texture & grainsize	Elongated highly foliated rock consisting mostly of 'sheets' of micas (sericite, kaolinite and fine grained biotite and chlorite) with interstitial quartz granules (fine grained to ~50 μm interlocking – recrystallised). Each sheet ~ 1 mm apart. Pyrite is dispersed throughout ~ 100 μm – 0.5 mm (max 2 mm). Pyrite has quartz/chlorite pressure shadows.
Primary mineralogy	Difficult to distinguish any primary mineralogy as everything has been destroyed by the deformational event that has imparted the strong foliation. It is also likely the rock was highly sericitised first (creating zones of weakness) leading to the intense nature of foliation. No feldspars are preserved.
Alteration minerals	Sericite is the major alteration product, occurring pervasively as very fine grains, with a few longer in pressure shadows. Secondary, interlocking quartz is the second major constituent. Appears to have been recrystallised with deformation. Traces of fine grained biotite. Chlorite is present mostly in pyrite pressure shadows and with some with sericite. Traces of rutile are probably remnant from titanite-magnetite alteration, caught in sericite bands and throughout.
Alt intensity	10/10
Veining	None preserved. Obvious highly pervasive alteration of whole rock resulting from lots of fluids, therefore vein like look to foliation.
Deformation	Ductile deformation as evidenced by the foliated, wavy texture observed.
Other:	Minor chalcopyrite in pyrite as contained blebs (some in ~ half pyrite observed).
Interpretation	This sample probably suffered intense initial sericitic style alteration with major sericitisation and silicification, and the addition of pyrite. This would have weakened the rock to the ductile deformation displayed here which also involved recrystallisation of mica and quartz (interlocking) during shearing. No primary mineralogy is preserved. The intensity of deformation has dissolved quartz, aligned micas in the vein like sheets (recrystallised) and further altered minerals to kaolinite and more sericite. It is possible that much of the originally contained chalcopyrite was removed in this event.
Mineralist'n	Low. ~ 300 ppm.
Alt' class	Sericitic.

Sample: C30 (111.6 m – TYHD005)

Hand specimen: Intensely altered pale green rock of unknown primary composition, with visible quartz, pyrite, chlorite and likely sericite and kaolinite. The sample possesses quartz and chlorite veining. Image #: 1204-1207

Figure 32: Sample C30 (TYHD005; 111.6 m) section offcut.

Microscopy	
Texture & grainsize	Strongly foliated. Consists of a groundmass/matrix of recrystallised alteration quartz (~ 50 μm), chlorite and sericite flakes. Relict ferromagnesians (altered chlorite ± rutile) to ~ 2 mm. Feldspars are completely altered to sericite and kaolinite, which are strung out to define a foliation. Pyrite is a major feature (to 1 mm grains) with quartz-chlorite pressure shadows.
Primary mineralogy	No primary feldspar is preserved. Significant abundance of chlorite suggests a considerable initial ferromagnesian component, with some outlines preserved as chlorite (rectangular to ~ 1.5 mm). These textures suggest the primary lithology was likely intrusive.
Alteration minerals	Most of the groundmass is secondary quartz; however some residual quartz phenocrysts are retained. Chlorite occurs following ferromagnesians and in pyrite pressure shadows. Also lesser amounts in groundmass. Sericite defines the foliation, appearing more intense in patches (feldspar sites). Traces of fine grained biotite and kaolinite are evident. Pyrite is dispersed throughout the sample as blocky cubes ~ 0.5 mm average which are altered/attacked at edges by sericite. Rutile occurs proximally to pyrite and also in ferromagnesian relics with chlorite.
Alt intensity	10/10
Veining	None preserved
Deformation	Quartz/chlorite pressure shadows on pyrite resulting from deformation
Other:	Sericitic-argillic alteration
Interpretation	This sample has suffered intense alteration which has destroyed all primary mineralogy. Relict ferromagnesians to 2 mm and possibly relict feldspars (intense sericite zones) suggest an original intrusive composition. Large pyrite cubes are suggestive of an early quartz/sericite/pyrite phyllic alteration with pressure shadows (chlorite/quartz) growing during a later deformation event in which quartz and sericite were recrystallised to the current foliation condition (pyrite was also attacked somewhat in the later deformation event).
Mineralist'n	Low. ~ 100 ppm.
Alt' class	Sericitic.

Sample: C34 (60.0 m – TYHD005)

Hand specimen: White to very pale green intensely altered rock of unknown primary composition, possessing high volumes of sericite and lesser chlorite, plus visible pyrite. Image #:1215-1217.

Figure 33: Sample C34 (TYHD005; 60.0 m) section offcut.

Microscopy	
Texture & grainsize	Foliated, largely texturally destroyed rock composed of aligned white micas, chlorite (pervasive), quartz (secondary, recrystallised to ~50 μm to 100 μm), disseminated kaolinite, flow aligned pyrite (fairly euhedral and intact) and rutile (granular, mostly disseminated).
Primary mineralogy	No primary mineralogy preserved. A few 'masses' of alteration products suggest original feldspars and ferromagnesians (as in C30). One feldspar outline (square) rimmed with aligned sericite. Preserved titanite grain outline (200 μm) may suggest plutonic precursor.
Alteration minerals	Sericite (muscovite, phengite, lepidolite) elongate fibres throughout which define foliation Significant secondary quartz. Chlorite, kaolinite. Possibly very fine grained biotite but may be rutile (similar brown hue). Pyrite is smaller than in C30, ~ 100-200 μm and aligned along foliation, some elongate, few pressure shadows observed in this section. Possibly much of pyrite coeval with deformation. Rutile dispersed as granules throughout. Some in ~ titanite configuration.
Alt intensity	10/10
Veining	No veining preserved
Deformation	Deformation has led to foliation of micas, recrystallisation of quartz, rare sericite pressure shadows on pyrite.
Other:	
Interpretation:	This sample has suffered intense alteration involving complete sericitisation of feldspars, chloritisation of ferromagnesian minerals, rutilisation of titanite and excessive production of quartz and pyrite. This was followed by intense deformation which produced a foliated rock with recrystallised quartz and sericite. Further sericite, pyrite and kaolinite production are likely to have occurred with deformation.
Mineralist'n	Low. < 50 ppm.
Alt' class	Sericitic – argillic.

Sample: C35 (359.5 m – TYHD005)

Hand specimen: In hand specimen, this rock is a dark grey/greenish grey colour, with dark chlorite predominating over a silicified appearing surface of primary intrusive nature that has been severely altered. Image #: 1341-1343.

Figure 34: Sample C35 (TYHD005; 359.5 m) section offcut.

Microscopy	
Texture & grainsize	Porphyritic rock with fairly densely packed feldspar phenocrysts (most ~ 1 mm up to 2.5 mm, albitised). Elongate ferromagnesians to 3 mm (most ~1.5 mm). Groundmass mostly recrystallised quartz (50 μm) with some sericite flecks and chlorite.
Primary mineralogy	Feldspars (mostly albitised). Alteration ranging from a few calcite/sericite specks to complete sericite/epidote mats (sericite dominant). Quartz former phenocrysts ~ 400μm. Little magnetite observed (pyrite dominates opaques). Zircon ~ 50μm (rounded/blocky)
Alteration minerals	Chlorite, after ferromagnesians, purple in places (XPL) suggesting the sample is iron-rich. Green in pressure shadows. Albitisation of most feldspar phenocrysts, lesser additional sericite/epidote alteration. Sericite is also in specks and fibres throughout the sample. Secondary recrystallised quartz, calcite- sometimes on feldspar surfaces (coarse). Trace rutile, epidote on some feldspar and ferromagnesian surfaces. Blebby pyrite disseminated throughout. Some pyrite is intergrown with rutile (altered titanomagnetite, ilmenite or hornblende?).
Alt intensity	7.5/10
Veining	Space filling sericite ± chlorite veins. Calcite veins, 200μm - 300μm ± epidote, even margined.
Deformation	Deformation evident by fine cracks in feldspar surfaces offsetting twinning; aligned sericite growing syn-kinematically between feldspars that have split apart and chlorite pressure shadows (brittle deformation).
Other:	Some rutile granules are in chlorite, but many are isolated (after titanite or titanomagnetite)
Interpretation:	This sample has suffered sericite (phyllic) alteration transitioning to chlorite –sericite alteration. This involved initial alteration causing albitisation, sericitisation and some kaolinite production contemporaneous to chlorite alteration of ferromagnesian minerals. The system was probably iron rich judging by the iron content of the ferromagnesian chlorites. Pyrite and minor chalcopyrite were added in this alteration stage. Later deformation was relatively brittle; indicating that feldspars had not been severely altered initially (still had some competency). Further sericitisation/kaolinite production was probably induced with deformation (e.g. growth of aligned sericite).
Mineralist'n	~ 1500 ppm.
Alt' class	Chlorite – sericite.

Sample: C39 (611.65 m – TYHD005)

Hand specimen: Medium grey to greenish grey fine grained volcaniclastic rock with intense epidote/pyrite veining. Image #: 1364-1368.

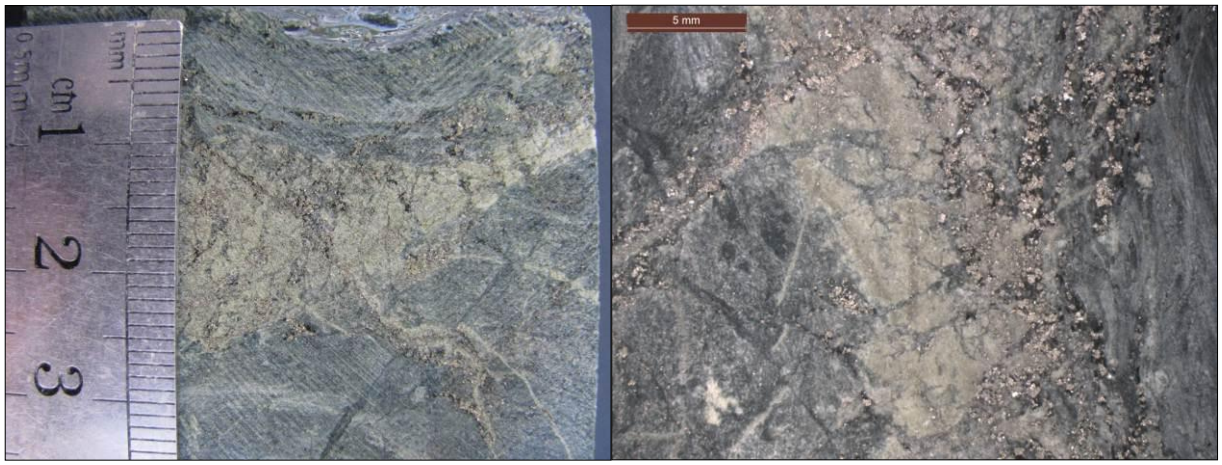

Figure 35: Sample C39 (TYHD005; 611.65 m) section offcut.

Microscopy	
Texture & grainsize	Fine grained (~ 20 μm grain size) foliated rock with intense pervasive chlorite alteration and early vein related epidote alteration (although epidote also invades groundmass pervasively). Groundmass of albitised feldspar, chlorite and epidote. Largest epidote pyrite vein = 1 cm in this section. Pyrite to 750 μm, most 50-500 μm.
Primary mineralogy	Very fine grained feldspars which have been albitised. Primary quartz originally low or absent (appears secondary in some veins and groundmass).
Alteration minerals	Chlorite alteration dominant (brightness suggests fair proportion of chamosite). Other alteration minerals include albite, quartz, kaolinite, titanite (through groundmass), phengite, epidote (small granular and large coarse veins), calcite, pyrite, cordierite and chalcopyrite.
Alt intensity	9/10
Veining	Early pervasive epidote-chlorite alteration caused thick (1cm) epidote vein, containing coarse epidote (150μm grains), lots of pyrite and production of some quartz. Late carbonate infill in cracks. Late chlorite veining (small, deformation related).
Deformation	Phengite and/or chlorite in pyrite pressure shadows.
Other:	Whole sample is covered in fine grained epidote which gives a brown 'dirty' look (due to higher relief grain boundaries).
Interpretation:	Early pervasive chlorite-epidote alteration characterised by fine granular epidote (~ 5 μm) and more fluent chlorite throughout the ground mass. This was sourced by thick epidote veins with coarser epidote (average ~ 150 μm grains) that contain abundant pyrite. Pyrite was also disseminated throughout the groundmass. This veining alteration stage is sometimes crosscut by quartz-rich flooding veins (fine grained) which appear approximately contemporaneous. A later stage of deformational related (infill) veining has produced calcite (coarse, to 300μm) which occurs in large cracks opening up in epidote veins. The later stage remobilised some quartz into these veins and reprecipitated chlorite/sericite in pyrite pressure shadows.
Mineralist'n	Low. ~ 100 ppm.
Alt' class	Propylitic (porphyry related and later deformation)

Sample: C42 (621.65 m – TYHD005)

Hand specimen: Dark grey to black coloured, fine-grained specimen displaying a somewhat banded texture crosscut by epidote/carbonate veining with lesser pyrite evident. Image #: 1379-1381.

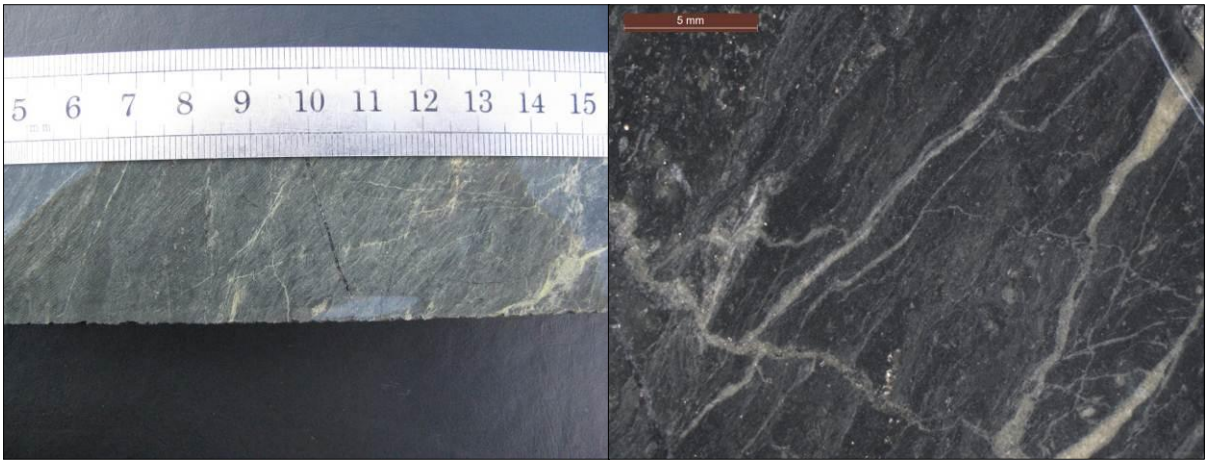

Figure 36: Sample C42 (TYHD005; 621.65 m) section offcut.

Microscopy	
Texture & grainsize	A fine grained (< 50 μm) matrix of chlorite, plagioclase and actinolite; which is broadly 'banded' (alternating light/dark bands ~ 1 cm apart). Banding is thought to be related to either variations in primary lithology or alteration induced variation of chlorite/calcite/plagioclase abundances.
Primary mineralogy	Some large relict feldspars are evident, which are likely strongly albitised. A significant mafic component was present, however no primary mineralogy is preserved. Possible relict magnetite.
Alteration minerals	Alteration minerals consist of pervasive chlorite throughout the groundmass, actinolite grains (~ 5-50 μm) ranging from interlocking to discrete biotite, kaolinite, pyrite and larger patches of cordierite, inferred to be the product of contact metamorphism. Calcite is also abundant, occurring throughout the groundmass and in tension veins along with green ferro-stilpnomelane fibres to ~200 μm.
Alt intensity	9/10
Veining	Early epidote dominated veins (0.5 mm) which are semi-sinuous and often normal to the foliation are cross cut by late calcite ± epidote ± stilpnomelane and minor quartz veins (0.4 mm, straight edged). Calcite in these veins possesses triple junctions, and ranges to 100-200 μm diameter.
Deformation	Kinking of earlier epidote veins and the banded texture. Tension gash/infill veins (calcite, epidote).
Mineralist'n	Low. ~ 100 – 200 ppm.
Alt' class	Propylitic (porphyry related and later deformation)

Sample: D15 (434.00 m – TYHD003)

Hand specimen: Mineralised (chalcopyrite + molybdenite) quartz seam vein ~ 1 cm wide, in Rain Hill Monzodiorite, no obvious selvedge. A few cross-cutting brittle fractures are also observed, infilled with calcite. Seam also contains grey material that may be alteration chlorite. Image #: 1087-1098

Figure 37: Sample D15 (TYHD003; 434.00m) section offcut.

Microscopy	
Description	Mineralised quartz seam vein in equigranular Rain Hill Monzodiorite. Chalcopyrite dominant in seam, also some molybdenite and calcite. Chalcopyrite and molybdenite also on margin and in country rocks + sericite, K-feldspar and magnetite. Host lithology resembles monzodiorite with interlocking altered feldspars (coarse grained, to 3 mm), scarce remnant amphiboles, (altered to chlorite/magnetite), and titanite, completely altered to rutile, some retaining original shape (to 2 mm length). Large apatite crystals are fairly abundant. A few zircons are observed. Deformation has resulted in scarce chlorite/sericite pressure shadows, cracked feldspars and some mineralisation sheared out in calcite (chalcopyrite). Quartz grains are relatively coarse (100 - 500 μm average) with chalcopyrite and molybdenite on peripherals. The central seam also contains calcite and magnetite (along with chalcopyrite). A strong sericite alteration selvedge of ~ 150 μm width is evident in thin section. Hydrothermal alteration associated with quartz veining has resulted in yellow-red staining (iron oxide) and silica rimmed feldspars. Sericite flooded. Orientated rutile needles in chlorite. Interstitial chlorite. Gangue minerals include quartz (vein), calcite (seam) and magnetite (minor vein). A significant amount of fine grained (~20 μm) magnetite is associated with the (sericitic) vein selvedge and throughout the ground mass. Some large magnetite occurs with chalcopyrite.

Sample: D16 (435.45 m – TYHD003)

Hand specimen: Late appearing vein containing a number of minerals. Quartz is prominent, along with a carbonate species and possibly a low temperature feldspar. Alteration chlorite and lesser magnetite is also apparent. Image #: 1099-1105

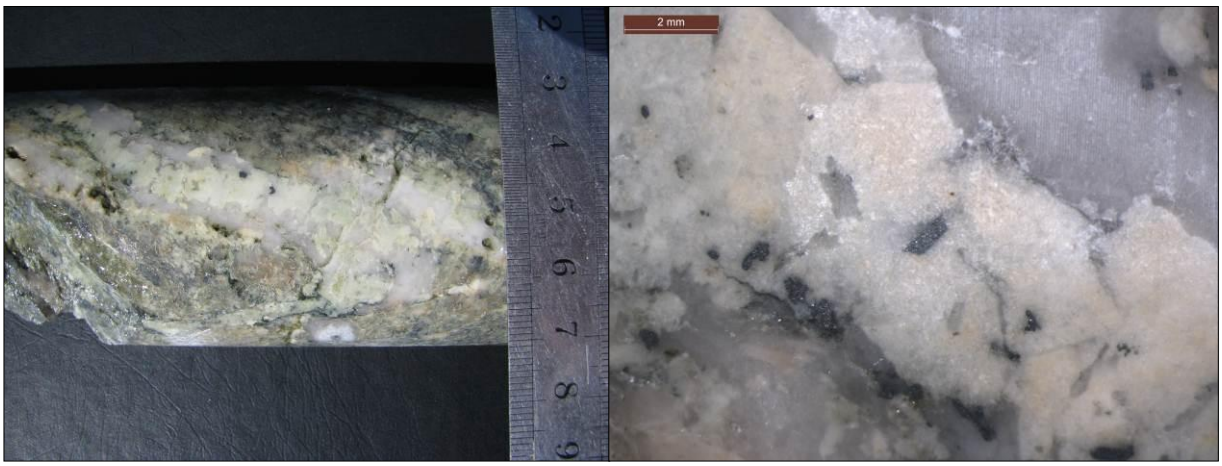

Figure 38: Sample D16 (435.45 m – TYHD003) section offcut.

Microscopy	
Description	Vein fill is dominated by quartz and dusty calcite, with calcite crystals ranging to quite coarse (> 2 mm), and quartz crystals mostly ~ 200 μm – 2 mm. Feldspars are also present to ~ 1 mm. These major constituents appear to have grown contemporaneously. Magnetite is relatively common, averaging ~ 1 mm diameter. Chalcopyrite is also observed although not common. Chlorite occurs interstitially in minor amounts, along with phengite/sericite (mostly phengite). Feldspars are hematite stained, along with calcite (reddish tinge). Quartz is relatively clean/clear. Deformation is evident by mechanical twinning and bending in calcite. Undulose (deformed) and cracked quartz crystals are also observed. Cracks are predominantly infilled by sericite). Other than this, the vein assemblage is fresh, particularly the feldspar components (contrasting those in the primary lithologies). This suggests this vein post-dates porphyry system hydrothermal alteration and is probably syn-kinematic tension gash infill.

Sample: D30 (571.9 m – TYHD005)

Hand specimen: The sample represents a thick (2 cm) vein displaying cocks-comb intergrown quartz and an opaque pink mineral; with stringy chlorite within and surrounding the vein margin. Quartz also invades the host rock in a blebby fashion, which displays epidote (propylitic) style alteration. Image #: 1508-1509.

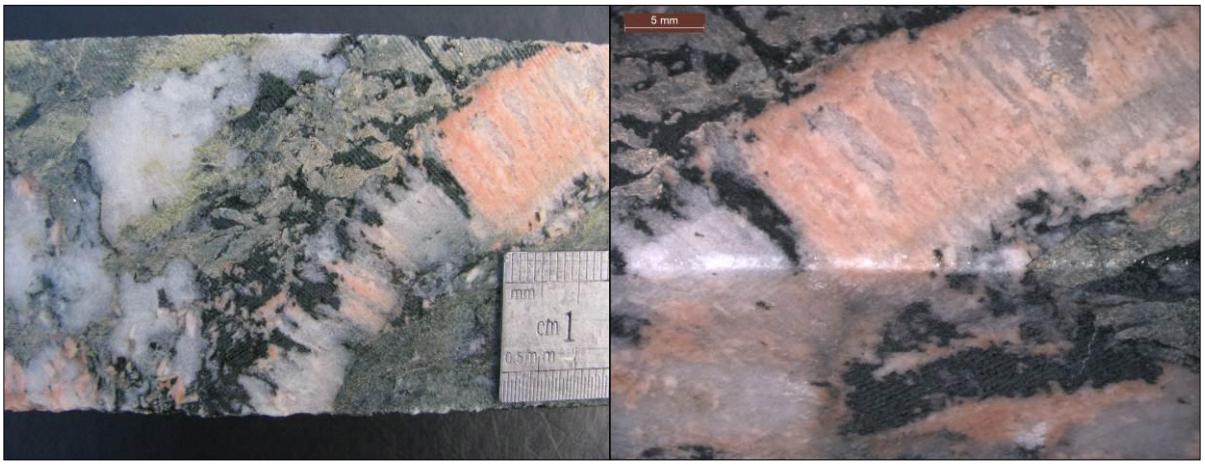

Figure 39: Sample D30 (571.9 m – TYHD005) section offcut.

Microscopy	
Description	This vein is composed of interlocking (contemporaneous) quartz, K-feldspar, chlorite and minor calcite. The most voluminous component is clear/clean quartz, which is variable in size from very small (< 50 μm) to large (> 2 mm). K-feldspar is the second major component, occurring as fine (< 50 μm) to larger (~ 2 mm) anhedral, non-twinned crystals. In plane polarised light, feldspars display a pink dusting (hematite), similar to calcite. In crossed polars, feldspars are first order greys. Calcite is rarer, however occurs interstitially to 2 mm grains; which are reddish cream in cross-polars and often mechanically twinned. Chlorite occurs in large aggregates of fine platy 'booklet' or 'pencil-shaving' interlocking shapes (~ 100 μm width average), indicating growth occurred into space. The cocks-comb texture, grain habits and interlocking crystals suggest this vein is syn-kinematic, occurring during deformation post-dating porphyry related alteration.

Sample: E05 (250.5 m – TYHD003)

Hand specimen: Blebby disseminated chalcopyrite contained within fine-grained volcaniclastic material, with quartz, pyrite and chlorite alteration products also evident.

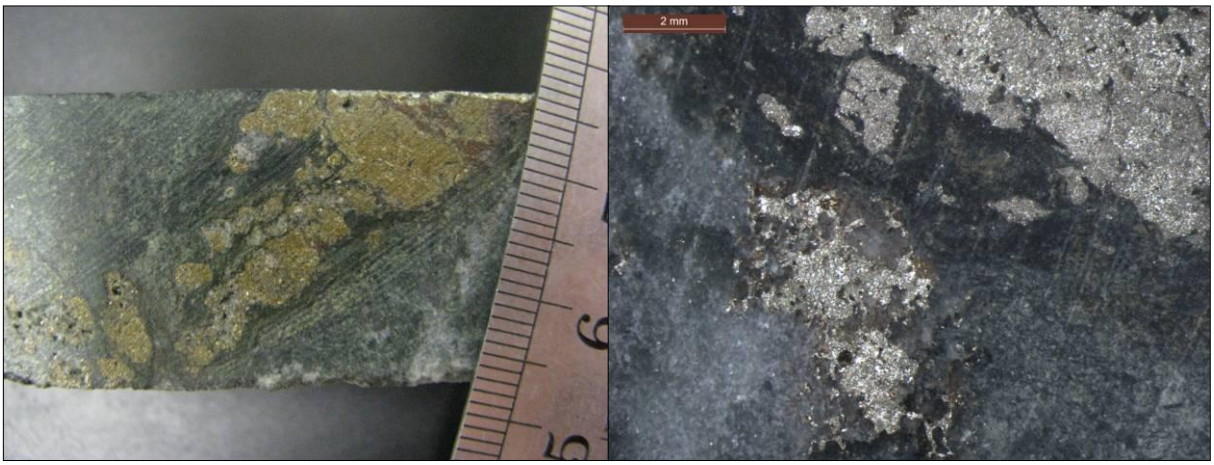

Figure 40: Sample E05 (TYHD003; 250.5m) section offcut.

Microscopy	
Description	Host rock is a fine grained (10 - 20μm) volcaniclastic rock (feldspar and quartz) suffering epidote veining (grains to 200μm), quartz flooding and banded pervasive chlorite alteration (foliated). Within the host rock is a pyrite-chalcopyrite vein approximately 1.5 cm in width, with a chlorite selvedge. Alteration appears to be related to mineralised veining but also appears to have an overprinted foliation, which probably contributed to much of the chlorite products. Rutile is also present throughout the host rock, along with mostly coarse grained calcite veining (~ 200μm grains). Minor magnetite appears which could be primary. Pyrite has precipitated first with some contained chalcopyrite, then chalcopyrite appears to mineralise around the cracks of the pyrite cubes. Chalcopyrite is stringy while pyrite is cubic. These minerals have probably been remobilised by the deformational event. No molybdenite is observed in the sample. The immediate selvedge is chlorite, with epidote surrounding. The main gangue constituent is quartz (fairly coarse grained ~ 100-300μm diameter) which occurs within and surrounding the pyrite and chalcopyrite veining. Relatively coarse grained calcite (~100-200 μm) is also present.

Sample: E06 (301.0 m – TYHD003)

Hand specimen: Quartz/carbonate/chlorite/chalcopyrite infill vein in weakly mineralised propylitic volcaniclastic.

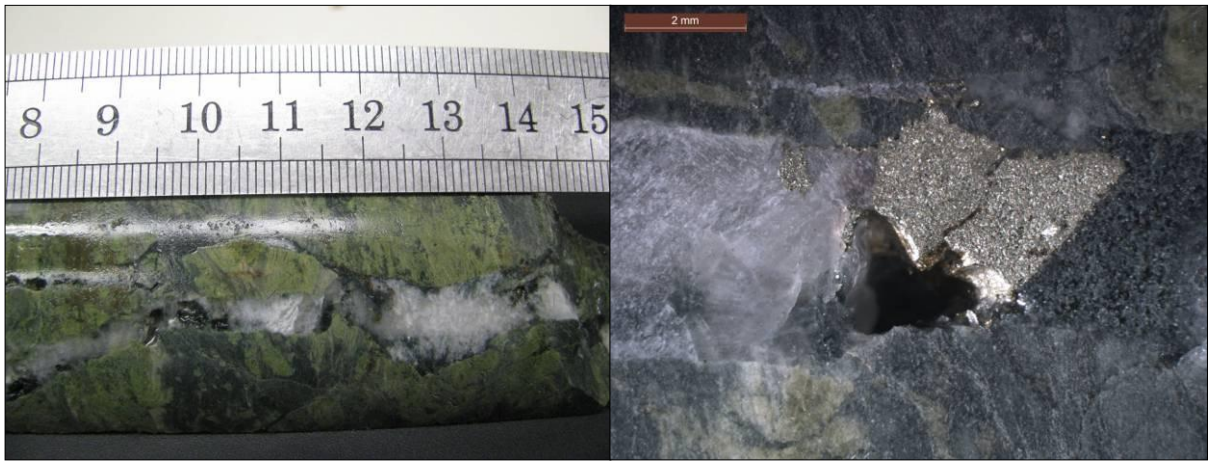

Figure 41: Sample E06 (301.0 m – TYHD003) section offcut.

Microscopy	
Description	Host rock is a feldspar/quartz fine to sand sized volcaniclastic. Feldspars are dominantly plagioclase, which are variably sized (20-40 μm), semi-aligned and mostly albitised. The interstitial areas are filled with pervasive chlorite, which is highly flow aligned. This flow alignment contains sub parallel epidote veins which contain some chalcopyrite mineralisation (ranging from ~ 200μm width to a broader flooding ~ 1.5 cm wide). Smaller veins contain epidote grains ~ 50-500μm, whilst larger flooded areas (where a few conduits are closely spaced) have larger (to1 mm) along with fine grained epidote and greater secondary silica and chalcopyrite. These vein areas, along with the groundmass, also have common fine grained rutile, which is abundant as an epidote vein selvedge. Observed mineralisation in epidote veins is usually fine chalcopyrite blebs (~100 μm diameter) but larger blebs in coarse epidote (~ 600x400 μm wide bleb maximum) also occur. Entirely crosscutting all these features is a large (4 mm wide) sharp margined vein, along with many fine infill veins (very late) which contain coarse grained quartz (to 2-4 mm) and calcite (to 3x4mm) grains, chalcopyrite (to 2x4 mm) and dense aggregations of booklet ('wormlike') chlorite, each typically ~ 30μm width and up to 300 μm lengths in clumps up to ~ 4 mm diameter. The primary platy chlorite texture suggests these minerals grew into space. Deformation is evident not only from infill veins but also as stressed quartz and *en echelon* textures. Very late fine (~ 20μm) chlorite ± quartz veins occur filing smaller tension cracks parallel to the main mineralised infill vein
Interpretation	This sample has had initial propylitic style alteration (chlorite, carbonate, epidote) with disseminated low grade chalcopyrite mineralisation. This has been followed by strong brittle deformation, which has produced infill veins of massive chalcopyrite (probably sourced from adjacent host), quartz, calcite, feldspar and booklet chlorite. The precipitated brittle infill veins show continued signs of deformation accommodated by the quartz/carbonate constituents (stressed, shadowy quartz and mechanically twinned calcite).

Sample: E08 (389.4 m – TYHD003)

Hand specimen: Large quartz seam vein (2 cm width) with molybdenite on vein margins and chalcopyrite in the seam. Contained within the Rain Hill Monzodiorite. Image #:

Figure 42: Sample E08 (389.4 m – TYHD003) section offcut.

Microscopy	
Description:	2 cm wide quartz seam vein with chalcopyrite in the centre (present as large blebs to 0.5 mm) and fine grained molybdenite on margins and outer quartz area (grain blebs to 400 μm and some strung out on vein rim). Chalcopyrite is also present in outer veins. The contact between the vein and the host rock is relatively sharp. The host lithology is an altered sub equigranular plutonic rock with feldspars to 1.5 mm. Initial plagioclase and K-feldspars appear to be subsequently altered (probably albitised). Chlorite occurs following former ferromagnesians. Overall texture resembles Rain Hill Monzodiorite. Rutile is evident probably from titanite. Sericite/chlorite/epidote alteration. Chalcopyrite is the dominant sulphide, occurring with a blebby habit along with minor pyrite in the centre of the vein. Molybdenite is present in random orientations in needle-like to more blebby habit. Molybdenite grains are smaller than chalcopyrite (most only ~100 μm in length), and most prevalent along the outer grain margin. Quartz is the dominant gangue mineral, occurring as interlocking grains (most 250 μm – 1.5 mm, but up to 2.5 mm). Fine grained quartz, chlorite and epidote are present in the vein centre. Deformed feldspars displaying undulose/bent extinction are evident in host rock along with stressed quartz in the seam vein (shadowy and undulose extinction).

Sample: E11 (469.05 m – TYHD003)

Hand specimen: Opaque white to slightly translucent vein containing blue-grey metallic fine grained clusters; cross-cutting fine grained volcaniclastic material.

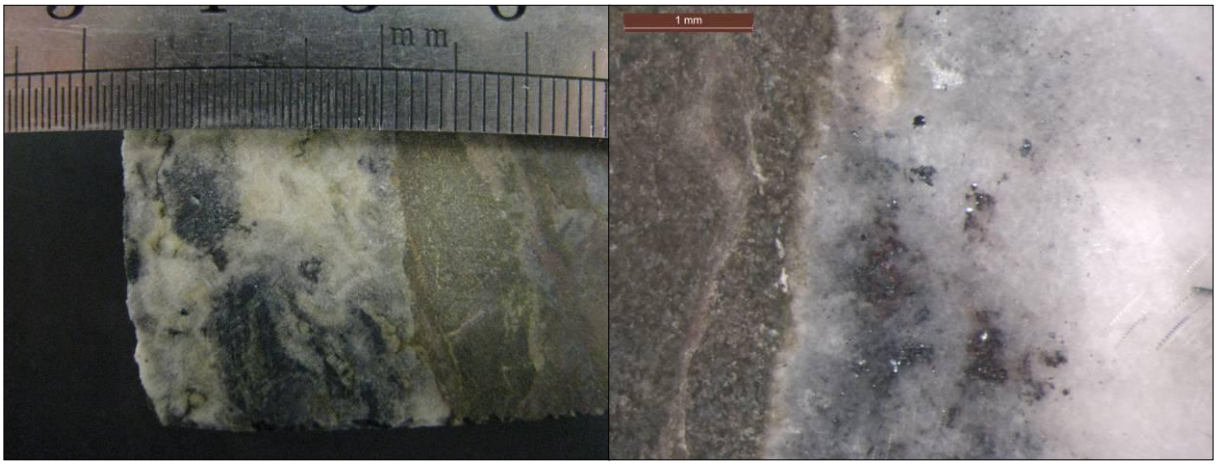

Figure 43: Sample E11 (469.05 m – TYHD003) section offcut.

Microscopy	
Description:	Highly altered volcaniclastic rock, with little preservation of primary mineralogy. Some titanomagnetite is evident which has altered to hematite and rutile. Remnant plagioclase is also apparent (~ 40 μm in diameter). Host rock is somewhat foliated. The host rock has suffered intense sericitisation giving it an overall light brown colour. Little chlorite is observed in this sample. Overall purple hue could be due to fine grained bladed anhydrite (~ 20μm). Within the volcaniclastic rock is a carbonate vein (at least 3 cm width in this offcut) containing hematite 'shards' (mostly ~ 20 – 300 μm in length). Carbonate grains are coarse (to 3 mm), while interlocking shards are in clusters, to 5 mm diameter. Hematite in carbonate is translucent bright red in non-reflected light if the grain is thin enough, otherwise they appear black. Some late fault surfaces contain reddish/purple anhydrite/hematite alteration, from late fluids
Interpretation:	Pervasive flooding by an oxidised carbonate fluid which has precipitated hematite. This could be due to later fracturing or shearing. The host rock has suffered alteration to hematite and also iron rich carbonates (e.g.: ankerite) and anhydrite which was possibly formerly alteration pyrite.

Sample: E12 (221.40 m – TYHD003)

Hand specimen: Large quartz/pyrite vein/flooded area, with pyrite cubes ranging to 4 mm.

Figure 44: Sample E12 (221.40 m – TYHD003) section offcut.

Microscopy	
Description:	Dense pyrite (~ 60% vol.) in quartz with minor sericite and some kaolinite which is mostly washed off the slide. Pyrite alteration is intense, occurring as cubes (~ 100μm – 4 mm diameter) which are fairly densely packed (~ 60% of sample is pyrite). Small chalcopyrite blebs (~ 10-30μm) are sometimes contained within pyrite cubes, but are relatively rare (< 10% of pyrite grains). Pyrite cubes occur in flood quartz, which is aligned in parts of the section. Pyrite grains display a uniform brittle deformation with grains cracked along a plane. Some appear ragged/somewhat dissolved on the edges. Sericite occurs in pyrite grains, pressure shadows or intergrown in cracks. The matrix/groundmass is almost completely quartz, which exhibits some flow alignment and is all secondary.

Sample: E16 (391.00 m – TYHD005)

Hand specimen: Dark grey to green intrusive rock containing cream opaque feldspars, alteration chlorite, more translucent quartz flooding and disseminated sulphides.

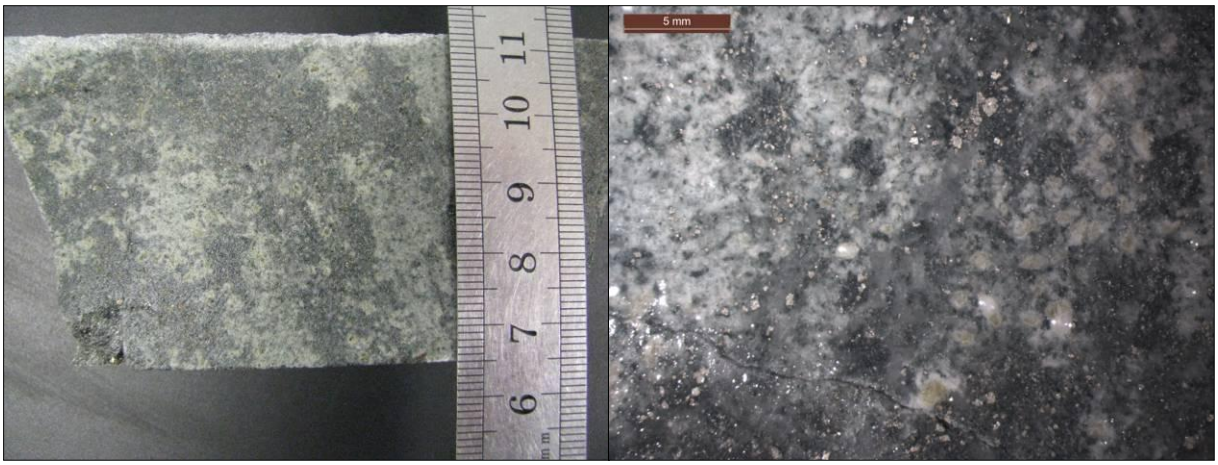

Figure 45: Sample E16 (391.00 m – TYHD005) section offcut.

Microscopy	
Description:	This sample consists of a pervasively sericitised porphyry intrusive containing disseminated sulphides. Complex twinned remnant plagioclase is evident in the host rock along with minor zircons (prismatic ~ 50μm length). Mafic components are altered to chlorite, sheared out and further altered to sericite. Sericite is a major alteration product, evident throughout the rock fabric as aligned fibrous grains generally no larger than 50μm. Apatite is more resistant and evident to 300μm. Alteration rutile/titanate granules are relatively common, whilst minor kaolinite is also observed throughout the groundmass. Pyrite is the dominant sulphide, although very minor chalcopyrite occurs in pyrite and in discrete blebs. Pyrite occurs as subhedral cubic grains (~ 100 - 300μm average), although some replacement pyrite is evident (after ferromagnesians, as evident by shape). Quartz flooding occurs throughout the sample, with all quartz being secondary and interlocking (to 1.5 mm, most ~100μm). Appears initial phase had minor chalcopyrite in quartz veins. Very minor chalcopyrite blebs appear related to quartz veining. Chlorite is a secondary major product, throughout the sample and in pyrite pressure shadows (probably after ferromagnesians). Minor glauconite.
Interpretation:	Initial alteration phase was probably chlorite-magnetite style, with rare chalcopyrite blebs within quartz veins which have introduced pervasive quartz to the sample. Phyllic/sericitic alteration overprints this assemblage and destroys almost all of the primary mineralogy (matted sericite, lesser chlorite). The final deformation phase has remobilised chlorite into pressure shadows, produced granular epidote, rutile/titanium and recrystallised sericite into a flow alignment.

Sample: E17 (413.00 m – TYHD005)

Hand specimen: Quartz seam vein, ~ 0.5 cm wide, contained within a porphyry intrusive host. Chalcopyrite is evident in the seam of the vein.

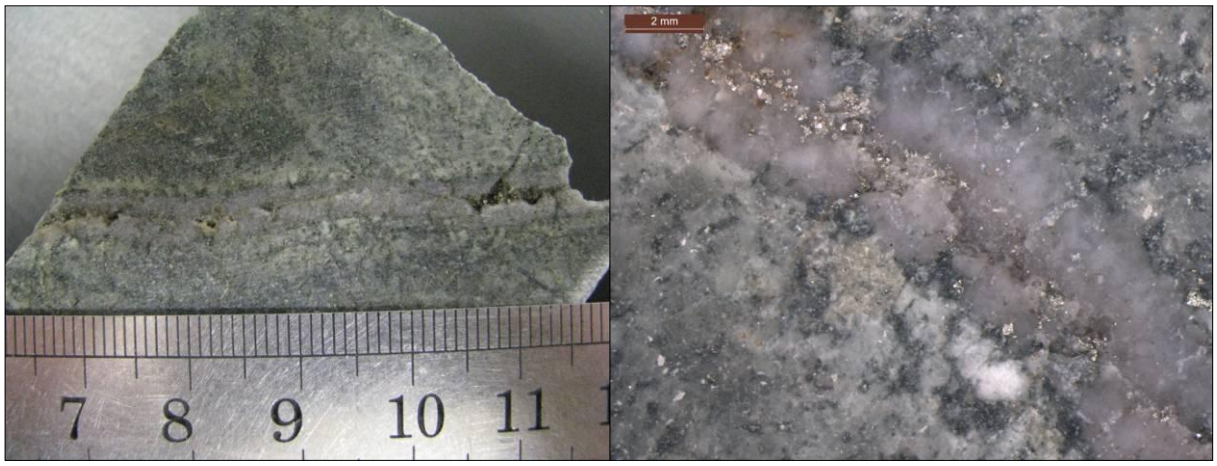

Figure 46: Sample E17 (413.00 m – TYHD005) section offcut.

Microscopy	
Description	Quartz seam vein (7 mm) in porphyritic plutonic rock (plagioclase, former titanate, magnetite, apatite, zircons identified of primary texture). Host rock is highly altered (mostly sericitised) with some epidote and rutile (after titanate and titanomagnetite). Host rock resembles a porphyry intrusive that has highly sericitised feldspars (plagioclase) to 2 mm, altered Fe-rich ferromagnesians (with small hydrothermal zircons), apatite to 1.5 mm (fairly common, resistant to sericitisation 0.5 – 1.5 mm). Although alteration is mostly sericitic there is also some secondary epidote and chlorite. Primary magnetite in host is remnant (to 200μm). Fine grained alteration magnetite (~10-20μm) is proximal to the seam vein. Alteration rutile from titanomagnetite or titanate. Groundmass has been completely altered to fine grained albite, sericite, quartz and minor carbonate. Mineralisation is contained predominantly within the seam as chalcopyrite, along with pyrite. The quartz seam is neat, ~ 7 mm in width with fairly sharp boundaries. At the petrographic scale there is no gradation to the selvedge. Symmetrical healing with pyrite (centre) and chalcopyrite (centre and throughout). Some carbonate is also contained within the seam, which appears late and infilling. These crystals are aligned and have an interstitial nature. Broader scale selvedge consists of magnetite, chalcopyrite (stringy and < 500μm length) and quartz in groundmass. Alteration appears early stage with a slight phyllic overprint, and regional propylitic overprint.
Interpretation	Early (resistant) quartz seam vein with associated alteration magnetite and mineralisation, subsequently overprinted by possibly retrograde phyllic and regional propylitic alteration.

Sample: E19 (410.75 m – TYHD005)

Hand specimen: Dark grey to greenish grey silicified plutonic rock containing visible chalcopyrite.

.

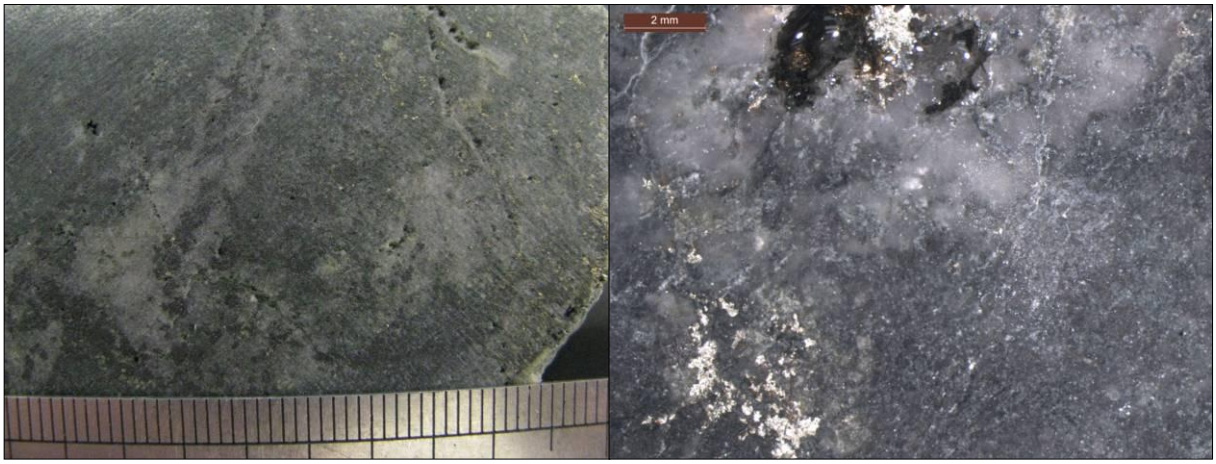

Figure 47: Sample E19 (TYHD005; 410.75 m) section offcut.

Microscopy	
Description:	The host rock consists of a highly chloritised (brown in XPL), epidotised and silica/magnetite flooded intrusive. Abundant alteration magnetite is granular, ranging from 20 - 400μm diameter. A 1 cm quartz vein with magnetite and minor chalcopyrite is captured in the section, also containing lesser carbonate and chlorite. Magnetite ranges to 3 mm and is blebby. Chalcopyrite is contained within magnetite in some instances, suggesting their deposition was contemporaneous. The quartz flooded area of the host rock has pyrite cubes and blebby chalcopyrite mineralisation although magnetite is more abundant closer to (and inside) the quarz vein with chalcopyrite/pyrite more abundant from about 2 cm out. The entire host rock is intensely chlorite altered, occurring in a stringy nature throughout (after ferromagnesians and in pressure shadows).
Interpretation:	It appears the quartz ± magnetite/chalcopyrite/carbonate/chlorite vein is the source of abundant silica/magnetite flooding observed throughout the host, along with chalcopyrite mineralisation. This mineralisation has probably been somewhat remobilised by later deformation events however remains associated with the initial conduit.

Sample: E21 (434.6 m – TYHD005)

Hand specimen: Foliated rock with molybdenite/chalcopyrite coating a fracture surface and chalcopyrite contained within the bulk of the rock. The host rock appears to be a dark coloured (?magnetite altered) intrusive unit with faint relict feldspars evident.

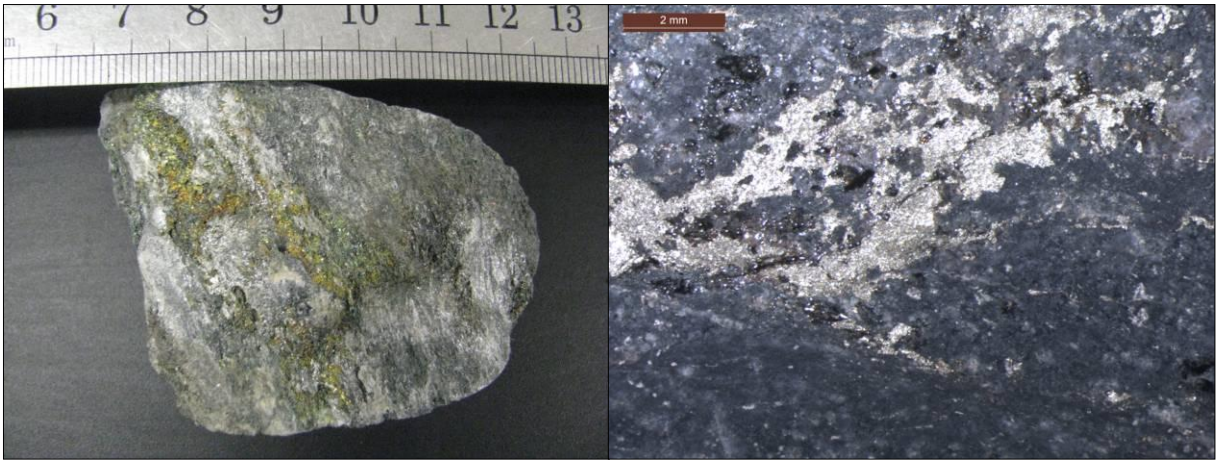

Figure 48: Sample E21 (TYHD005; 434.6 m) section offcut.

Microscopy	
Description	Mineralisation is contained within a foliated intrusive rock with original textures completely obscured by pervasive Fe-rich chlorite, sericite and quartz, containing large blebby chalcopyrite. Some original feldspar textures are evident. The groundmass is completely flooded with fine-grained replacement chlorite. The sample is quite Fe-rich (dark brown-purple chlorite colour in XPL). Rutile granules were likely originally titanate. Relict magnetite (euhedral, ~ 200μm, altered to rutile/hematite) suggests the rock was likely an intrusive porphyry stock (not volcaniclastic). The groundmass is flooded with fine grained Fe-rich chlorite, whilst chlorite-sericite 'veins' are more fibrous. Chalcopyrite is mineralised in disseminated blebs (to 4 mm length) associated with quartz/chlorite/sericite 'veins' along a foliation; suggesting chalcopyrite has been remobilised during deformational events and precipitated along the foliation plane. Chalcopyrite blebs are generally > 2 mm, intergrown with quartz and fibrous chlorite/white micas (grain sizes to 400 μm length). Some carbonate is also present in quartz veining, which occurs with the sheared out sericite/chlorite foliation/'veining'. In hand specimen, molybdenite coats the fracture surface, however none is observed in the cross-sectional thin section, suggesting this mineralisation is highly localised.
Interpretation	Fibrous sericite/chlorite with quartz is foliated/flowing parallel to chalcopyrite, suggesting deformational events have remobilised mineralisation and destroyed original ore textures.

Sample: E23 (444.00 – TYHD005)

Hand specimen: Very wide (45 cm intersection) quartz/carbonate/chalcopyrite/chlorite vein.

Figure 49: Sample E23 (TYHD005; 444.00 m) section offcut.

Microscopy	
Description	Coarse grained carbonate-quartz-(chlorite)-chalcopyrite vein. Neat interlocking mineralogy with coarse crystals; quartz to 5 mm (averaging 3-4 mm); carbonate to 4 mm (most ~ 2-3 mm; with an inner zone of smaller (~ 500μm) crystals. Chalcopyrite is stringy within a quartz/carbonate matrix, infilling between grain boundaries. Deformation has been absorbed mostly by chalcopyrite (has been bent). Quartz displays some cracking/buckling in some grains. No host rock was captured by the thin section.
Interpretation	This vein is in the same style as E06, on a large scale- being generated during later deformation of the ore-body.

Sample: E25 (458.1 m – TYHD005)

Hand specimen: In hand specimen, this sample consists of a strongly foliated intrusive rock, with chlorite and chalcopyrite alteration products both appearing to be aligned with the foliation trend. Remnant feldspars are evident, also appearing to be squashed within the foliation. The dark groundmass of the sample suggests a likely high magnetite component. On the fracture surface, molybdenite is evident as a thin slicken coating.

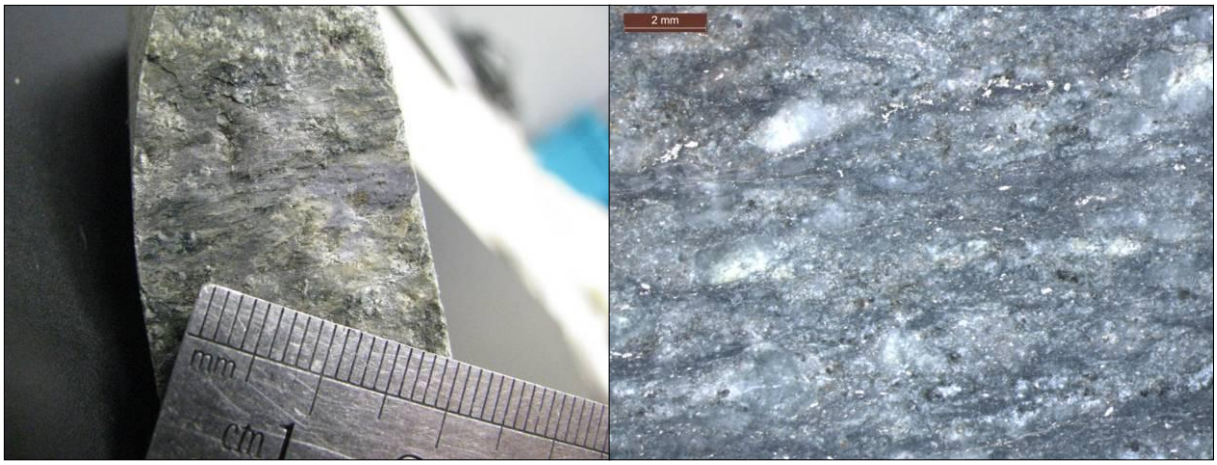

Figure 50: Sample E25 (TYHD005; 458.1 m) section offcut.

Microscopy	
Description	The host rock is porphyritic or porphyryclastic textured (with plagioclase to at least 1 mm). Plagioclase is evident to 2 mm, apatite to ~ 200 μm and K-feldspar, zircons and titanite (altered to rutile) also primary components. The entire fabric has been intensely deformed, with many phenocrysts rotated or flattened (including plagioclase, rutile and chalcopyrite) and sericite remobilised/introduced as very fine grained vein-like mats (possibly strung out altered phenocrysts). Relatively large grains of epidote (to 2 mm) are also strung out/grown along the foliation. Fibrous sericite/chlorite 'veining' and pervasive chlorite/sericite is evident along with alteration magnetite, which was coeval with chalcopyrite mineralisation (chalcopyrite inclusion in magnetite observed). Molybdenite occurs on the fracture plane this sample was taken from, not within the foliation, it therefore appears to either have been present in a fluid passing through the fracture plane or was the reason for the localisation of the fracture plane (Mo vein = lubricated surface). This rock appears to have suffered an early stage of alteration with related chalcopyrite-magnetite products (relatively high temperature), which may have been overprinted by sericite/phyllic assemblage (some mineralisation in the style of E21 (chl-ser)) but due to extreme deformation has suffered realignment and recrystallisation of alteration products.
Interpretation	Sequence: - early alteration magnetite, chalcopyrite - secondary, possibly retrograde chlorite-sericite alteration - strong deformation, recrystallisation of sericite particularly throughout the groundmass (strung out K-feldspar particularly), remobilisation of mineralisation, albitised plagioclase flattened; texture destroyed and foliated fabric created.

Sample: E26 (537.75 m – TYHD005)

Hand specimen: Dark greenish grey fine-grained basaltic volcaniclastic host rock containing visible stringy chalcopyrite mineralisation.

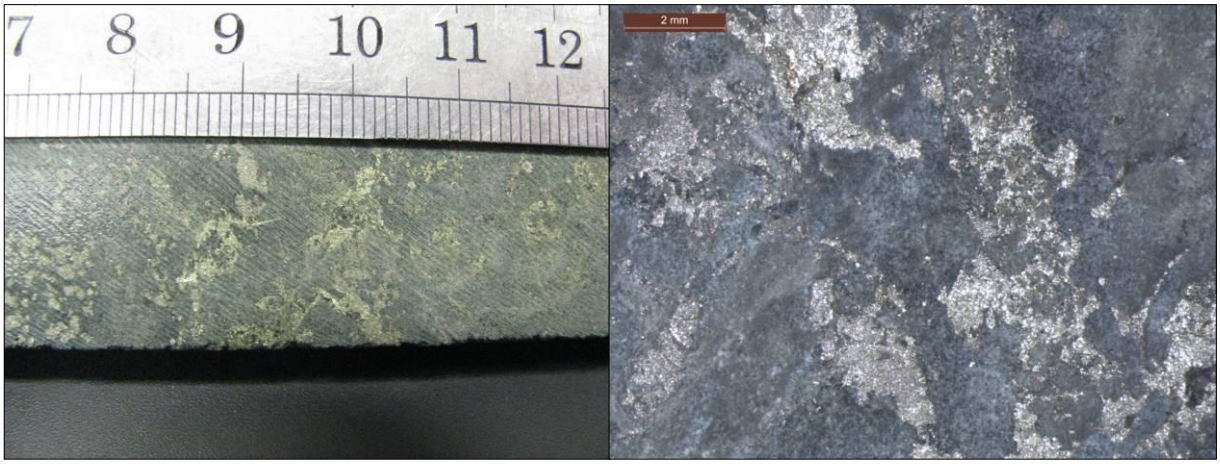

Figure 51: Sample E26 (TYHD005; 537.75 m) section offcut.

Microscopy	
Texture & grainsize	Host rock is intensely epidote/chlorite altered (granular to ~ 30μm). Primary mineralogy has been destroyed. Fine grained texture suggests the rock probably was a basaltic volcaniclastic. Very minor sericite, fibrous (deformation induced). Stringy chalcopyrite appears remobilised, occurring intergrown with chlorite. Chlorite remobilisation is evident by foliated chlorite and chlorite within pressure shadows. Mineralisation – initial mineralisation consisted of contemporaneous chalcopyrite and pyrite (from same ore fluid), with blebs of chalcopyrite commonly contained in pyrite, and sometimes the reverse. Chalcopyrite however appears further remobilised, often surrounding pyrite fluently or invading deformation related cracks in pyrite. Sulphide blebs occur to 2 cm, however are stringy and adjoining one another. Quartz gangue is associated with the sulphides.

APPENDIX D

X-RAY DIFFRACTION RESULTS

Sample	C3	C4	C8	C9	C13	C18	C22	C24	C27	C29	C30	C34	C35	C39	C42	D16	D30
Chi Squared	5.4	5.0	4.4	4.7	5.0	5.0	8.6	4.5	4.1	15.5	7.5	7.8	5.3	5.1	7.1	5.9	8.4
Primary lithology	?	PP	PP	RHM	RHM	PP	ANVC	RHM	PP	?	PP	PP	PP	BSVC	BSVC	vein	vein
Quartz																	
Albite																	
Bytownite																	
Anorthoclase																	
Anorthite																	
Orthoclase																	
Sanidine																	
Nepheline																	
Titanite																	
Actinolite																	
Cordierite																	
Epidote																	
Magnetite																	
Chlorite																	
Kaolinite																	
Sericite (musc)																	
Phengite																	
Biotite																	
Alunite																	
Halloysite																	
Calcite																	
Dolomite																	
Paragonite																	
Ankerite																	
Chalcopyrite																	
Pyrite																	
Rutile																	
Gypsum																	

Dominant > 30% Major > 10% Minor 2 - 10% Trace < 2%

APPENDIX E

ELECTRON MICROPROBE RESULTS

PART A: OXIDES (page 1)

Sample	Mineral	Association/setting	K2O (%)	CaO (%)	Na_2O (%)	FeO (%)	MgO (%)	SiO_2 (%)	MnO (%)	TiO_2 (%)	Cr_2O_3 (%)	F (%)	Al_2O_3 (%)	Total (%)	Elemental Formula	Calculated Formula
E05-01	Chlorite	py/chalcopy veining	0.03	0.03	0.02	18.12	20.10	28.10	0.41	0.01	1.04	0.16	19.09	87.10	$(Mg,Fe)_2Al(AlSi_3O_{10})(OH)_8$	$(Fe_{1.55}Mg_{3.07}Mn_{0.04}Al_{1.18})(Si_{2.88}Al_{1.12})O_{10}(OH)_8$
E05-02	Chlorite	py/chalcopy veining	0.05	0.01	0.06	18.39	20.07	27.88	0.39	0.02	0.59	0.08	20.07	87.61	$(Mg,Fe)_2Al(AlSi_3O_{10})(OH)_8$	$(Fe_{1.56}Mg_{3.04}Mn_{0.03}Al_{1.24})(Si_{2.83}Al_{1.17})O_{10}(OH)_8$
E05-03	Chlorite	py/chalcopy veining	0.01	0.02	0.01	18.44	20.24	27.79	0.45	0.01	0.70	0.04	20.26	87.96	$(Mg,Fe)_2Al(AlSi_3O_{10})(OH)_8$	$(Fe_{1.56}Mg_{3.06}Mn_{0.04}Al_{1.23})(Si_{2.81}Al_{1.19})O_{10}(OH)_8$
E05-04	Chlorite	groundmass	0.06	0.09	0.06	18.04	20.09	27.89	0.45	0.07	0.03	0.10	19.72	86.60	$(Mg,Fe)_2Al(AlSi_3O_{10})(OH)_8$	$(Fe_{1.55}Mg_{3.07}Mn_{0.04}Al_{1.25})(Si_{2.86}Al_{1.14})O_{10}(OH)_8$
E05-05	Chlorite	groundmass	0.01	0.02	0.00	17.55	21.08	28.89	0.43	0.02	0.38	0.15	19.01	87.55	$(Mg,Fe)_2Al(AlSi_3O_{10})(OH)_8$	$(Fe_{1.48}Mg_{3.18}Mn_{0.04}Al_{1.19})(Si_{2.92}Al_{1.08})O_{10}(OH)_8$
E05-06	Chlorite	groundmass	0.01	0.04	0.03	18.75	20.02	27.73	0.44	0.01	0.59	0.08	20.23	87.93	$(Mg,Fe)_2Al(AlSi_3O_{10})(OH)_8$	$(Fe_{1.59}Mg_{3.03}Mn_{0.04}Al_{1.24})(Si_{2.81}Al_{1.19})O_{10}(OH)_8$
E05-07	Epidote/Allanite	groundmass	0.04	23.10	0.02	13.51	0.41	37.81	0.26	0.07	1.61	0.01	19.99	96.82	$(Ca_2)(Al_2Fe^{3+})(Si_2O_7)(SiO_4)O(OH)$	$(Ca_{2.1})(Al_{1.97}Fe^{3+}_{0.94})(Si_{2.15}O_7)(SiO_4)O(OH)$
E05-08	Epidote	groundmass	0.02	23.10	0.01	12.54	0.33	37.91	0.23	0.11	0.16	0.00	22.02	96.42	$(Ca_2)(Al_2Fe^{3+})(Si_2O_7)(SiO_4)O(OH)$	$(Ca_{2.0})(Al_{2.15}Fe^{3+}_{0.87})(Si_{2.14}O_7)(SiO_4)O(OH)$
E05-09	Titanite	groundmass	0.03	27.27	0.03	0.98	0.38	30.17	0.02	35.67	0.00	1.22	4.00	99.77	CaTi(SiO4)O	$Ca_{0.96}Ti_{0.88}(Si_{0.99}O_4)O$
E05-10	Titanite	groundmass	0.01	24.23	0.02	0.74	0.00	25.60	0.03	44.18	0.03	0.96	3.28	99.06	CaTi(SiO4)O	$Ca_{0.86}Ti_{1.11}(Si_{0.85}O_4)O$
E06-01	Calcite	coarse qz/cl/cb/ep vn	0.01	64.81	0.03	0.07	0.01	0.00	0.46	0.02	0.00	0.03	0.02	65.46	$CaCO_3$	$Ca_{1.27}C_{0.86}O_3$
E06-02	Epidote	groundmass	0.02	23.66	0.03	14.83	0.02	38.09	0.15	0.00	0.00	0.00	20.50	97.30	$(Ca_2)(Al_2Fe^{3+})(Si_2O_7)(SiO_4)O(OH)$	$(Ca_{2.1})(Al_{2.01}Fe^{3+}_{1.03})(Si_{2.17}O_7)(SiO_4)O(OH)$
E06-03	Epidote	vein	0.00	23.88	0.01	13.49	0.16	38.59	0.30	0.00	0.00	0.03	21.12	97.59	$(Ca_2)(Al_2Fe^{3+})(Si_2O_7)(SiO_4)O(OH)$	$(Ca_{2.1})(Al_{2.05}Fe^{3+}_{0.93})(Si_{2.18}O_7)(SiO_4)O(OH)$
E06-04	Epidote	wall of crse cb vn	0.01	23.82	0.05	12.25	0.00	38.39	0.08	0.10	0.05	0.00	22.75	97.49	$(Ca_2)(Al_2Fe^{3+})(Si_2O_7)(SiO_4)O(OH)$	$(Ca_{2.1})(Al_{2.19}Fe^{3+}_{0.84})(Si_{2.13}O_7)(SiO_4)O(OH)$
E06-05	Rutile	groundmass	0.02	0.45	0.03	0.69	0.00	0.12	0.02	94.42	0.03	0.01	0.00	95.79	TiO_2	$Ti_{0.99}O_2$
E06-06	Chlorite	coarse qz/cl/cb/ep vn	0.01	0.02	0.02	19.66	19.64	28.28	0.73	0.00	0.02	0.05	19.36	87.79	$(Mg,Fe)_2Al(AlSi_3O_{10})(OH)_8$	$(Fe_{1.68}Mg_{2.99}Mn_{0.06}Al_{1.21})(Si_{2.89}Al_{1.11})O_{10}(OH)_8$
E06-07	Chlorite	altered amphibole	0.02	0.06	0.02	17.71	21.05	29.53	0.57	0.04	0.25	0.20	17.94	87.38	$(Mg,Fe)_2Al(AlSi_3O_{10})(OH)_8$	$(Fe_{1.50}Mg_{3.19}Mn_{0.05}Al_{1.14})(Si_{3.00}Al_{1.00})O_{10}(OH)_8$
E06-08	Chlorite	groundmass	0.01	0.06	0.02	18.93	19.85	28.09	0.64	0.05	0.06	0.10	19.56	87.37	$(Mg,Fe)_2Al(AlSi_3O_{10})(OH)_8$	$(Fe_{1.62}Mg_{3.02}Mn_{0.06}Al_{1.23})(Si_{2.87}Al_{1.13})O_{10}(OH)_8$
E06-09	Chlorite	coarse qz/cl/cb/ep vn	0.00	0.01	0.03	19.11	19.93	28.40	0.71	0.00	0.01	0.17	19.82	88.18	$(Mg,Fe)_2Al(AlSi_3O_{10})(OH)_8$	$(Fe_{1.62}Mg_{3.01}Mn_{0.06}Al_{1.24})(Si_{2.88}Al_{1.12})O_{10}(OH)_8$
E06-10	Chlorite	groundmass	0.04	0.03	0.12	19.00	19.50	28.09	0.67	0.04	0.05	0.13	19.93	87.60	$(Mg,Fe)_2Al(AlSi_3O_{10})(OH)_8$	$(Fe_{1.62}Mg_{2.97}Mn_{0.06}Al_{1.26})(Si_{2.87}Al_{1.13})O_{10}(OH)_8$
E06-11	Chlorite	coarse qz/cl/cb/ep vn	0.01	0.05	0.01	19.13	20.40	28.78	0.67	0.00	0.00	0.15	18.72	87.90	$(Mg,Fe)_2Al(AlSi_3O_{10})(OH)_8$	$(Fe_{1.63}Mg_{3.09}Mn_{0.06}Al_{1.17})(Si_{2.93}Al_{1.07})O_{10}(OH)_8$
E11-01	Calcite	vein	0.00	62.41	0.03	0.58	0.09	0.00	1.08	0.00	0.00	0.02	0.01	64.21	$CaCO_3$	$Ca_{1.21}C_{0.88}O_3$
E11-02	Ankerite	vein	0.00	34.49	0.01	10.34	11.06	0.01	0.82	0.02	0.00	0.00	0.09	56.85	$Ca(Fe,Mg,Mn)(CO_3)_2$	$Ca_{1.23}(Mg_{0.55}Fe_{0.29}Mn_{0.02})_{0.86}C_{1.95}O_6$
E17-01	Fluorapatite	groundmass	0.00	56.31	0.11	0.03	0.00	0.23	0.05	0.00	0.00	3.61	0.00	60.34	$Ca_5(PO_4)_3F$	$Ca_5P_{2.78}O_{12}F_{0.95}$
E17-02	Calcite	vein	0.01	58.05	0.04	0.40	0.16	0.01	1.81	0.00	0.03	0.02	0.01	60.53	$CaCO_3$	$Ca_{1.08}C_{0.94}O_3$
E17-03	Magnetite	qz seam vein	0.01	0.02	0.04	89.11	0.00	0.03	0.11	1.48	0.00	0.00	0.07	90.87	$FeO.Fe_2O_3$	$Fe^{2+}_{1.05}Fe^{3+}_{1.89}O_4$
E17-04	Magnetite	qz seam vein	0.00	0.01	0.00	89.72	0.00	0.02	0.06	0.96	0.01	0.00	0.04	90.82	$FeO.Fe_2O_3$	$Fe^{2+}_{1.06}Fe^{3+}_{1.91}O_4$
E17-05	Titanite	altered amphibole	0.01	30.80	0.02	0.96	0.04	24.86	0.27	34.04	0.00	0.57	2.04	93.62	CaTi(SiO4)O	$Ca_{1.19}Ti_{0.92}(Si_{0.90}O_4)O$
E17-06	Chlorite	altered amphibole	0.02	0.03	0.04	23.74	15.45	26.16	0.99	0.04	0.01	0.00	20.87	87.35	$(Mg,Fe)_2Al(AlSi_3O_{10})(OH)_8$	$(Fe_{2.09}Mg_{2.42}Mn_{0.09}Al_{1.34})(Si_{2.75}Al_{1.25})O_{10}(OH)_8$
E17-07	Chlorite	altered amphibole	0.06	0.04	0.08	23.28	15.29	26.18	1.02	0.04	0.02	0.08	20.80	86.90	$(Mg,Fe)_2Al(AlSi_3O_{10})(OH)_8$	$(Fe_{2.06}Mg_{2.41}Mn_{0.09}Al_{1.36})(Si_{2.77}Al_{1.23})O_{10}(OH)_8$
E17-08	Chlorite	altered amphibole	0.00	0.04	0.01	22.71	16.67	27.20	0.99	0.04	0.00	0.18	19.87	87.73	$(Mg,Fe)_2Al(AlSi_3O_{10})(OH)_8$	$(Fe_{1.98}Mg_{2.59}Mn_{0.09}Al_{1.27})(Si_{2.83}Al_{1.17})O_{10}(OH)_8$
E17-09	Chlorite	qz seam vein	0.01	0.03	0.00	23.21	15.64	24.39	0.87	0.05	0.02	0.01	20.86	85.08	$(Mg,Fe)_2Al(AlSi_3O_{10})(OH)_8$	$(Fe_{2.10}Mg_{2.53}Mn_{0.08}Al_{1.31})(Si_{2.64}Al_{1.36})O_{10}(OH)_8$
E17-10	Chlorite	altered amphibole	0.02	0.04	0.00	22.16	17.35	27.56	0.90	0.06	0.01	0.15	19.50	87.75	$(Mg,Fe)_2Al(AlSi_3O_{10})(OH)_8$	$(Fe_{1.92}Mg_{2.68}Mn_{0.08}Al_{1.25})(Si_{2.86}Al_{1.14})O_{10}(OH)_8$
E17-11	Chlorite	qz seam vein	0.02	0.02	0.01	23.44	15.91	26.66	0.85	0.03	0.02	0.00	21.22	88.19	$(Mg,Fe)_2Al(AlSi_3O_{10})(OH)_8$	$(Fe_{2.03}Mg_{2.46}Mn_{0.07}Al_{1.36})(Si_{2.76}Al_{1.24})O_{10}(OH)_8$

PART A: OXIDES (page 2)

Sample	Mineral	Association/setting	K2O (%)	CaO (%)	Na_2O (%)	FeO (%)	MgO (%)	SiO_2 (%)	MnO (%)	TiO_2 (%)	Cr_2O_3 (%)	F (%)	Al_2O_3 (%)	Total (%)	Elemental Formula	Calculated Formula
E19-01	Chlorite	amongst mg/cp/py	0.01	0.05	0.02	23.60	15.45	26.11	0.98	0.04	0.01	0.04	20.71	87.02	$(Mg,Fe)_2Al(AlSi_3O_{10})(OH)_8$	$(Fe_{2.08}Mg_{2.43}Mn_{0.09}Al_{1.33})(Si_{2.76}Al_{1.24})O_{10}(OH)_8$
E19-02	Chlorite	qz/mg seam vein	0.02	0.03	0.01	23.21	16.01	26.81	0.96	0.13	0.03	0.05	20.75	87.99	$(Mg,Fe)_2Al(AlSi_3O_{10})(OH)_8$	$(Fe_{2.02}Mg_{2.48}Mn_{0.08}Al_{1.33})(Si_{2.79}Al_{1.21})O_{10}(OH)_8$
E19-03	Chlorite	groundmass	0.02	0.05	0.03	23.67	15.76	26.47	0.97	0.06	0.05	0.07	21.01	88.15	$(Mg,Fe)_2Al(AlSi_3O_{10})(OH)_8$	$(Fe_{2.06}Mg_{2.45}Mn_{0.09}Al_{1.34})(Si_{2.76}Al_{1.24})O_{10}(OH)_8$
E19-04	Chlorite	qz/mg seam vein	0.01	0.01	0.02	24.15	15.69	26.06	0.99	0.01	0.02	0.04	21.01	88.01	$(Mg,Fe)_2Al(AlSi_3O_{10})(OH)_8$	$(Fe_{2.11}Mg_{2.45}Mn_{0.09}Al_{1.32})(Si_{2.73}Al_{1.27})O_{10}(OH)_8$
E19-05	Epidote	groundmass	0.02	23.42	0.02	12.51	0.02	38.24	0.35	0.03	0.00	0.00	22.83	97.44	$(Ca_2)(Al_2Fe^{3+})(Si_2O_7)(SiO_4)O(OH)$	$(Ca_{2.1})(Al_{2.02}Fe^{3+}_{0.86})(Si_{2.13}O_7)(SiO_4)O(OH)$
E19-06	Magnetite	quartz seam	0.01	0.01	0.00	89.92	0.01	0.04	0.10	0.64	0.02	0.00	0.07	90.83	$FeO.Fe_2O_3$	$Fe^{2+}_{1.07}Fe^{3+}_{1.92}O_4$
E19-07	Magnetite	quartz seam	0.01	0.03	0.03	89.10	0.01	0.02	0.10	1.61	0.02	0.00	0.09	91.00	$FeO.Fe_2O_3$	$Fe^{2+}_{1.05}Fe^{3+}_{1.89}O_4$
E21-01	Calcite	coarse qz/cl/cb/ep vn	0.00	61.93	0.00	0.61	0.33	0.00	2.60	0.00	0.00	0.00	0.02	65.51	$CaCO_3$	$Ca_{1.22}C_{0.86}O_3$
E21-02	Chlorite	cp veining	0.01	0.02	0.02	23.17	16.16	26.96	0.76	0.04	0.01	0.00	20.56	87.70	$(Mg,Fe)_2Al(AlSi_3O_{10})(OH)_8$	$(Fe_{2.02}Mg_{2.51}Mn_{0.07}Al_{1.33})(Si_{2.81}Al_{1.19})O_{10}(OH)_8$
E21-03	Chlorite	cp veining	0.00	0.00	0.00	23.55	16.06	26.69	0.82	0.03	0.00	0.09	20.75	88.01	$(Mg,Fe)_2Al(AlSi_3O_{10})(OH)_8$	$(Fe_{2.05}Mg_{2.49}Mn_{0.07}Al_{1.33})(Si_{2.78}Al_{1.22})O_{10}(OH)_8$
E21-04	Chlorite	qz/cp veining	0.01	0.01	0.03	23.76	16.00	26.08	0.80	0.05	0.01	0.01	20.86	87.63	$(Mg,Fe)_2Al(AlSi_3O_{10})(OH)_8$	$(Fe_{2.08}Mg_{2.50}Mn_{0.07}Al_{1.31})(Si_{2.73}Al_{1.27})O_{10}(OH)_8$
E21-05	Chlorite	fibrous/foliated assoc. w/ ser	0.00	0.04	0.00	23.37	15.57	25.59	0.72	0.02	0.01	0.07	20.68	86.07	$(Mg,Fe)_2Al(AlSi_3O_{10})(OH)_8$	$(Fe_{2.09}Mg_{2.48}Mn_{0.07}Al_{1.33})(Si_{2.73}Al_{1.27})O_{10}(OH)_8$
E21-06	Chlorite	fibrous/foliated assoc. w/ ser	0.01	0.01	0.00	23.29	16.26	26.58	0.72	0.05	0.02	0.14	20.38	87.45	$(Mg,Fe)_2Al(AlSi_3O_{10})(OH)_8$	$(Fe_{2.04}Mg_{2.54}Mn_{0.06}Al_{1.30})(Si_{2.78}Al_{1.22})O_{10}(OH)_8$
E21-07	Glauconite	fibrous/foliated assoc. w/ ser	11.70	0.00	0.24	4.23	1.37	46.90	0.02	0.32	0.03	0.08	30.30	95.19	$(K,Na)(Fe^{3+},Al,Mg)_2(Si,Al)_4O_{10}(OH)_2$	$K_{0.98}(Fe_{0.46}Al_{1.40}Mg_{0.13})_{2.00}(Si_{3.07}Al_{0.93})_4O(OH)_2$
E21-08	Glauconite	fibrous/foliated assoc. w/ ser	11.86	0.01	0.39	4.45	1.46	47.37	0.02	0.38	0.00	0.12	30.03	96.09	$(K,Na)(Fe^{3+},Al,Mg)_2(Si,Al)_4O_{10}(OH)_2$	$K_{0.98}(Fe_{0.48}Al_{1.36}Mg_{0.14})_{1.99}(Si_{3.07}Al_{0.93})_4O(OH)_2$
E21-09	Rutile	in chlorite	0.05	0.01	0.00	0.87	0.02	0.06	0.02	95.83	0.01	0.00	0.00	96.87	TiO_2	$Ti_{0.99}O_2$
E26-01	Epidote	in chlorite	0.01	23.36	0.00	14.37	0.06	38.29	0.42	0.21	0.01	0.01	20.77	97.51	$(Ca_2)(Al_2Fe^{3+})(Si_2O_7)(SiO_4)O(OH)$	$(Ca_{2.1})(Al_{2.02}Fe^{3+}_{0.99})(Si_{2.17}O_7)(SiO_4)O(OH)$
E26-02	Glauconite	fibrous/foliated assoc. w/ ser	11.76	0.01	0.20	4.18	1.69	47.87	0.00	0.09	0.00	0.06	30.58	96.45	$(K,Na)(Fe^{3+},Al,Mg)_2(Si,Al)_4O_{10}(OH)_2$	$K_{0.97}(Fe_{0.45}Al_{1.41}Mg_{0.16})_{2.02}(Si_{3.09}Al_{0.91})_4O(OH)_2$
E26-03	Chlorite	groundmass	0.00	0.04	0.00	23.87	15.57	25.76	0.95	0.05	0.01	0.02	20.97	87.24	$(Mg,Fe)_2Al(AlSi_3O_{10})(OH)_8$	$(Fe_{2.11}Mg_{2.45}Mn_{0.09}Al_{1.33})(Si_{2.93}Al_{1.07})O_{10}(OH)_8$
E26-04	Chlorite	chlorite in cp	0.00	0.04	0.03	23.46	15.81	26.31	0.92	0.02	0.02	0.01	20.26	86.87	$(Mg,Fe)_2Al(AlSi_3O_{10})(OH)_8$	$(Fe_{2.07}Mg_{2.49}Mn_{0.08}Al_{1.30})(Si_{2.78}Al_{1.22})O_{10}(OH)_8$
E26-05	Chlorite	pressure shadow of py	0.01	0.00	0.02	23.74	16.20	26.43	0.91	0.01	0.05	0.04	20.26	87.66	$(Mg,Fe)_2Al(AlSi_3O_{10})(OH)_8$	$(Fe_{2.08}Mg_{2.53}Mn_{0.08}Al_{1.27})(Si_{2.77}Al_{1.23})O_{10}(OH)_8$
E26-06	Chlorite	groundmass	0.01	0.03	0.00	23.88	15.62	25.90	0.98	0.03	0.00	0.00	20.74	87.19	$(Mg,Fe)_2Al(AlSi_3O_{10})(OH)_8$	$(Fe_{2.11}Mg_{2.46}Mn_{0.09}Al_{1.31})(Si_{2.73}Al_{1.27})O_{10}(OH)_8$
E26-07	Chlorite	py/cp mineralisation	0.02	0.02	0.00	23.48	16.08	26.29	0.92	0.03	0.00	0.00	20.44	87.28	$(Mg,Fe)_2Al(AlSi_3O_{10})(OH)_8$	$(Fe_{2.06}Mg_{2.52}Mn_{0.08}Al_{1.30})(Si_{2.76}Al_{1.24})O_{10}(OH)_8$

PART B: SULPHIDES

Sample	Mineral	S (%)	Al (%)	Fe (%)	Zn (%)	Cu (%)	Co (%)	Cr (%)	Ni (%)	As (%)	Pb (%)	Mo (%)	Ag (ppm)	Au (ppm)	Elemental Formula	Calculated Formula
E08-01	Molybdenite	37.90	0.02	0.06	0.03	0.03	0.01	0.00	0.06	0.00	0.00	54.43	-	-	MoS_2	$Mo_{0.96}S_2$
E08-02	Molybdenite	39.38	0.00	0.06	0.05	0.03	0.00	0.00	0.00	0.00	0.00	56.57	-	-	MoS_2	$Mo_{0.96}S_2$
E08-03	Chalcopyrite	35.10	0.00	30.77	0.00	34.58	0.00	0.00	0.00	0.00	0.82	0.00	-	-	$CuFeS_2$	$Cu_{0.994}Fe_{1.007}S_2$
E08-04	Pyrite	53.73	0.01	47.13	0.01	0.01	0.00	0.00	0.00	0.04	0.00	0.00	-	-	FeS_2	$Fe_{1.007}S_2$
E08-05	Chalcopyrite	35.14	0.00	30.53	0.00	34.16	0.00	0.00	0.00	0.00	0.02	0.00	-	-	$CuFeS_2$	$Cu_{0.981}Fe_{0.998}S_2$
E08-06	Chalcopyrite	34.78	0.00	30.68	0.00	34.49	0.00	0.00	0.00	0.03	0.00	0.00	-	-	$CuFeS_2$	$Cu_{1.001}Fe_{1.013}S_2$
E08-07	Chalcopyrite	34.83	0.02	30.50	0.06	34.40	0.00	0.03	0.02	0.00	0.96	0.00	-	-	$CuFeS_2$	$Cu_{0.997}Fe_{1.006}S_2$
E08-08	Pyrite	54.02	0.00	46.93	0.04	0.60	0.00	0.00	0.00	0.00	0.00	0.00	-	-	FeS_2	$Fe_{0.998}S_2$
E05-01	Chalcopyrite	35.08	0.02	31.05	0.00	34.70	0.00	0.02	0.00	0.00	0.00	0.00	-	-	$CuFeS_2$	$Cu_{0.998}Fe_{1.017}S_2$
E05-02	Chalcopyrite	34.91	0.00	30.81	0.00	34.85	0.00	0.00	0.01	0.08	0.39	0.00	-	-	$CuFeS_2$	$Cu_{1.007}Fe_{1.014}S_2$
E05-03	Chalcopyrite	34.92	0.00	30.48	0.00	34.99	0.00	0.01	0.00	0.00	0.60	0.00	-	-	$CuFeS_2$	$Cu_{1.011}Fe_{1.002}S_2$
E05-04	Chalcopyrite	35.00	0.01	30.75	0.00	34.64	0.00	0.04	0.01	0.00	0.00	0.00	-	-	$CuFeS_2$	$Cu_{0.999}Fe_{1.009}S_2$
E05-05	Chalcopyrite	34.64	0.01	30.86	0.04	34.62	0.00	0.01	0.01	0.06	1.58	0.00	-	-	$CuFeS_2$	$Cu_{1.009}Fe_{1.023}S_2$
E05-06	Chalcopyrite	34.82	0.01	30.75	0.01	34.88	0.00	0.00	0.00	0.05	1.17	0.00	-	-	$CuFeS_2$	$Cu_{1.011}Fe_{1.014}S_2$
E05-07	Chalcopyrite	34.76	0.00	30.62	0.00	34.87	0.01	0.00	0.00	0.04	0.09	0.00	-	-	$CuFeS_2$	$Cu_{1.013}Fe_{1.011}S_2$
E05-08	Chalcopyrite	34.72	0.00	30.65	0.07	34.98	0.00	0.00	0.03	0.02	0.05	0.00	-	-	$CuFeS_2$	$Cu_{1.017}Fe_{1.014}S_2$
E05-09	Pyrite	53.64	0.00	47.24	0.05	0.06	0.00	0.02	0.05	0.05	0.00	0.00	16	0	FeS_2	$Fe_{1.011}S_2$
E05-10	Chalcopyrite	35.02	0.00	30.83	0.06	34.89	0.00	0.00	0.00	0.03	0.00	0.00	0	0	$CuFeS_2$	$Cu_{1.005}Fe_{1.011}S_2$
E05-11	Chalcopyrite	35.27	0.00	30.88	0.00	34.68	0.00	0.00	0.00	0.00	0.00	0.00	96	0	$CuFeS_2$	$Cu_{0.992}Fe_{1.005}S_2$
E05-12	Chalcopyrite	35.06	0.01	30.90	0.03	34.45	0.00	0.01	0.03	0.06	0.68	0.00	29	0	$CuFeS_2$	$Cu_{0.992}Fe_{1.012}S_2$
E05-13	Pyrite	53.22	0.01	46.93	0.01	0.00	0.04	0.01	0.06	0.01	1.18	0.00	66	0	FeS_2	$Fe_{1.013}S_2$
E05-14	Pyrite	53.15	0.00	45.92	0.00	0.02	0.05	0.00	1.04	0.00	0.31	0.00	12	0	FeS_2	$Fe_{0.992}S_2$
E05-15	Pyrite	53.88	0.00	47.41	0.00	0.00	0.00	0.01	0.04	0.04	0.31	0.00	38	0	FeS_2	$Fe_{1.011}S_2$
E05-16	Pyrite	53.39	0.00	46.58	0.07	0.02	0.00	0.00	0.20	0.01	0.86	0.00	47	0	FeS_2	$Fe_{1.002}S_2$
E05-17	Pyrite	53.84	0.00	46.70	0.01	0.01	0.01	0.02	0.35	0.00	0.00	0.00	67	0	FeS_2	$Fe_{0.996}S_2$
E05-18	Pyrite	53.25	0.01	46.52	0.00	0.01	0.00	0.00	0.36	0.03	0.00	0.00	0	0	FeS_2	$Fe_{1.003}S_2$
E05-19	Pyrite	53.51	0.00	46.59	0.00	0.01	0.03	0.00	0.39	0.01	0.00	0.00	98	0	FeS_2	$Fe_{1.000}S_2$
E05-20	Pyrite	53.36	0.01	46.73	0.04	0.03	0.00	0.01	0.39	0.02	0.21	0.00	74	0	FeS_2	$Fe_{1.006}S_2$
E05-21	Chalcopyrite	34.79	0.00	30.55	0.02	34.96	0.00	0.01	0.00	0.01	1.09	0.00	0	0	$CuFeS_2$	$Cu_{1.014}Fe_{1.008}S_2$
E05-22	Chalcopyrite	35.02	0.00	30.66	0.00	35.43	0.00	0.01	0.00	0.00	0.00	0.00	5	0	$CuFeS_2$	$Cu_{1.021}Fe_{1.005}S_2$
E05-23	Chalcopyrite	34.74	0.00	30.72	0.00	35.00	0.00	0.00	0.01	0.00	0.00	0.00	0	0	$CuFeS_2$	$Cu_{1.017}Fe_{1.015}S_2$
E05-24	Chalcopyrite	35.21	0.00	30.53	0.03	34.87	0.00	0.00	0.03	0.02	0.27	0.00	124	0	$CuFeS_2$	$Cu_{0.999}Fe_{0.996}S_2$

APPENDIX F

GEOCHEMICAL RESULTS

Cat. No.	HONS527	HONS528	HONS529	HONS530	HONS531	HONS532	HONS533	HONS534	HONS535	HONS536
Rock type	Sth PP	Sth PP	Sth PP	Sth PP	Late dyke	Late dyke	Late dyke	Late dyke	Late dyke	Late dyke
Sample	A1	A2	A3	A4	A5	A6	A7	A8	A9	A10
XRF major elements (wt%)										
SiO2	61.17	64.19	62.18	62.36	62.40	70.20	68.88	61.92	65.42	63.50
TiO2	0.67	0.71	0.70	0.72	0.68	0.47	0.57	0.95	0.68	0.86
Al2O3	17.93	13.03	17.77	17.93	13.52	14.59	15.59	16.37	15.79	16.59
Fe2O3	4.85	6.43	5.02	5.08	3.54	2.87	3.69	6.15	4.35	5.00
MnO	0.15	0.05	0.12	0.12	0.13	0.07	0.07	0.08	0.07	0.11
MgO	1.91	1.88	1.78	1.90	1.50	0.90	1.02	1.96	1.56	1.94
CaO	4.31	0.74	4.14	3.51	8.10	2.72	3.00	2.60	3.30	3.33
Na2O	2.69	5.33	4.19	5.15	2.45	4.33	3.97	5.55	3.17	3.34
K2O	2.94	1.23	2.19	2.04	4.49	3.51	3.18	3.28	4.14	2.81
P2O5	0.31	0.37	0.30	0.30	0.31	0.68	0.22	0.29	0.23	0.28
S	< 0.01	1.54	< 0.01	< 0.01	0.06	0.19	0.02	< 0.01	< 0.01	0.01
O=S		-0.77			-0.03	-0.09	-0.01			-0.01
LOI	5.19	2.34	4.63	3.32	3.84	1.09	2.42	1.95	2.72	2.55
Total	**102.12**	**97.06**	**103.03**	**102.42**	**100.99**	**101.53**	**102.62**	**101.09**	**101.41**	**100.33**
XRF trace elements (ppm)										
V	98	62	85	87	57	32	58	122	95	148
Co	7	28	< 5	< 5	7	17	10	12	14	< 5
Cu	3	8453	5	31	72	145	225	26	5	3
Zn	83	143	95	97	48	65	122	65	44	64
Ga	17	19	18	16	10	16	17	18	18	17
As	1	< 1	1	1	5	5	2	2	1	2
Rb	50	22	35	29	32	35	34	25	42	29
Sr	299	334	907	691	328	375	371	519	778	1257
Y	18	24	20	20	14	12	15	24	19	21
Zr	135	172	139	139	131	125	131	187	134	144
Nb	14	18	14	15	13	10	15	22	18	16
Ba	1556	556	1219	1092	841	1061	887	1354	1977	4798
La	32	164	43	30	34	34	29	40	31	41
Ce	60	257	89	97	75	67	71	104	72	13
Hf	4	< 1	4	6	4	2	3	6	3	4
Pb	2	5	6	6	4	4	5	4	4	6
Th	6.3	10.3	7.0	7.0	7.7	13.4	17.8	17.3	17.0	10.9
U	4.1	4.4	3.6	4.3	6.0	8.2	6.5	7.0	9.9	6.9
ICP-MS trace and rare earth elements (ppm)										
Ba	1475	552	1180	1050	822	1030	869	1305	1905	4480
Ce	75.3	230.0	82.5	81.4	60.1	41.5	79.9	115.0	102.5	86.8
Co	7.8	16.6	8.8	8.9	9.5	10.5	6.8	10.4	9.0	9.9
Cr	60	210	60	70	110	200	170	80	100	80
Cs	0.36	0.22	0.29	0.25	0.07	0.27	0.61	0.12	0.59	0.30
Dy	3.38	4.73	3.41	3.78	2.82	1.95	2.80	4.72	3.55	3.56
Er	1.81	2.07	1.80	2.01	1.41	1.13	1.50	2.45	1.89	1.83
Eu	1.42	3.44	1.72	1.84	1.68	1.17	1.54	2.39	1.90	1.75
Ga	17.6	17.9	18.1	17.9	11.8	16.0	17.6	20.1	19.7	16.8
Gd	4.47	8.72	4.50	4.87	3.92	2.60	3.94	6.43	5.10	4.74
Hf	3.6	4.9	3.8	3.8	3.6	4.0	4.2	6.1	4.7	4.1
Ho	0.66	0.81	0.65	0.70	0.52	0.38	0.53	0.89	0.67	0.66
La	39.9	130.5	43.8	42.6	31.2	26.2	42.4	61.9	55.9	47.1
Lu	0.28	0.27	0.28	0.29	0.20	0.19	0.21	0.35	0.28	0.27
Mo	3	8	2	2	3	12	3	3	3	9
Nb	16.7	19.1	16.4	17.2	13.9	12.6	16.7	25.9	21.3	19.0
Nd	29.5	83.3	31.4	33.5	25.9	15.6	31.0	47.5	39.7	33.0
Pr	7.67	23.40	8.17	8.55	6.44	3.96	8.15	12.75	10.65	8.81
Rb	53.8	22.9	37.5	31.0	34.0	37.3	35.3	26.7	47.3	30.9
Sm	5.72	12.70	5.84	6.43	5.04	3.08	5.63	8.74	7.07	6.21
Sn	1	3	1	1	1	1	1	2	2	1
Sr	305	325	905	698	336	373	372	513	779	1240
Ta	1.1	1.2	1.1	1.2	0.7	0.9	1.1	1.9	1.5	1.3
Tb	0.76	1.09	0.76	0.81	0.65	0.47	0.69	1.02	0.82	0.78
Th	6.87	9.80	6.61	6.74	7.88	15.05	19.60	16.80	18.45	10.20
Tm	0.27	0.26	0.26	0.28	0.19	0.16	0.21	0.34	0.27	0.26
U	2.38	4.35	2.43	2.40	4.48	6.43	5.50	5.89	7.08	3.33
V	101	145	100	102	104	70	97	153	113	119
W	2	2	1	1	1	2	2	1	2	3
Y	18.4	22.0	18.1	19.3	14.2	10.7	14.1	23.7	18.8	18.4
Yb	1.76	1.60	1.76	1.85	1.29	1.12	1.36	2.22	1.77	1.69
Zr	152	216	157	162	163	141	165	235	179	173

Cat. No.	HONS537	HONS538	HONS539	HONS540	HONS541	HONS542	HONS543	HONS544	HONS545	HONS546
Rock type	Late PP	Sth PP	Sth PP	Late dyke	Sth PP	RHM	Sth PP	RHM	RHM	RHM
Sample	A11	A12	A13	A14	A15	A17	A18	A19	A20	A21
XRF major elements (wt%)										
SiO2	62.99	62.08	63.09	68.32	62.49	58.34	61.44	61.65	60.16	59.06
TiO2	0.61	0.82	0.81	0.52	0.78	1.19	0.75	1.05	1.11	1.08
Al2O3	17.26	16.87	16.04	15.40	16.65	16.93	16.51	17.70	18.19	16.36
Fe2O3	5.25	5.52	6.00	2.81	4.99	7.46	5.45	5.94	6.78	5.89
MnO	0.11	0.11	0.14	0.06	0.10	0.13	0.08	0.11	0.09	0.10
MgO	2.08	2.00	2.23	1.19	1.89	2.51	1.69	2.48	2.72	2.03
CaO	3.82	2.72	3.05	2.03	2.69	4.23	3.87	4.22	2.99	4.77
Na2O	5.07	4.54	4.75	3.36	3.60	3.87	5.26	4.17	3.44	5.63
K2O	2.01	1.46	1.48	4.11	2.52	2.28	2.00	2.55	2.64	3.16
P2O5	0.24	0.29	0.32	0.21	0.32	0.45	0.28	0.39	0.40	0.38
S	0.22	0.01	0.24	0.12	0.12	< 0.01	0.04	< 0.01	< 0.01	< 0.01
O=S	-0.11	0.00	-0.12	-0.06	-0.06		-0.02			
LOI	2.96	2.87	2.96	1.59	3.22	4.51	3.46	3.22	3.57	2.22
Total	**102.49**	**99.28**	**100.97**	**99.65**	**99.31**	**101.89**	**100.81**	**103.47**	**102.09**	**100.68**
XRF trace elements (ppm)										
V	131	113	123	49	126	116	119	62	152	69
Co	15	7	< 3	< 5	< 3	17	15	7	< 5	17
Cu	122	82	135	82	78	< 1	11	7	60	10
Zn	51	100	82	57	105	63	72	61	76	41
Ga	16	16	12	13	12	18	18	21	18	19
As	1	2	2	3	2	0	1	2	< 1	2
Rb	28	23	25	39	44	38	31	31	46	33
Sr	930	852	842	398	683	739	1197	1168	853	1006
Y	16	22	21	13	21	23	21	26	24	26
Zr	101	158	159	128	167	165	164	191	172	208
Nb	10	18	17	14	17	20	17	23	22	23
Ba	1461	1135	1798	1965	6051	1233	2892	1790	1929	1827
La	18	6	17	36	18	68	49	68	37	53
Ce	72	87	< 2	< 2	< 2	149	75	129	120	81
Hf	1	8	7	5	8	6	2	3	9	3
Pb	5	6	5	4	5	11	7	5	6	4
Th	6.6	10.5	11.0	13.4	11.8	11.1	13.3	10.9	10.5	9.8
U	5.6	3.6	4.9	7.0	7.0	6.4	6.4	5.8	6.1	5.3
ICP-MS trace and rare earth elements (ppm)										
Ba	1320	1360	1715	1820	5470	1165	2510	1665	1870	1320
Ce	62.4	89.0	78.9	63.8	88.6	123.0	91.0	110.0	120.0	62.4
Co	11.6	8.3	10.7	5.7	9.9	15.8	9.3	12.8	14.3	11.6
Cr	90	80	110	170	40	90	80	100	70	90
Cs	0.48	0.22	0.22	0.30	0.31	0.19	0.26	0.18	0.31	0.48
Dy	2.52	3.74	3.59	2.40	3.72	4.60	3.61	4.91	4.93	2.52
Er	1.43	1.95	1.87	1.20	1.95	2.12	1.86	2.44	2.43	1.43
Eu	1.23	1.96	1.90	1.17	1.95	2.38	1.86	2.55	2.54	1.23
Ga	16.3	18.5	17.2	16.0	16.3	22.4	18.2	21.2	22.5	16.3
Gd	3.25	5.10	4.84	3.30	5.32	7.15	4.76	6.80	7.12	3.25
Hf	2.7	4.5	4.1	3.8	4.4	5.2	4.4	5.5	5.9	2.7
Ho	0.48	0.69	0.68	0.45	0.69	0.80	0.68	0.91	0.90	0.48
La	35.8	47.0	41.3	35.1	46.7	65.1	48.7	59.4	63.3	35.8
Lu	0.23	0.28	0.27	0.19	0.28	0.27	0.27	0.33	0.33	0.23
Mo	2	4	5	7	2	3	3	3	4	2
Nb	10.7	20.3	19.4	15.6	18.6	23.6	19.1	25.9	25.9	10.7
Nd	23.3	35.2	33.5	24.3	36.0	56.6	35.1	49.2	52.1	23.3
Pr	6.14	9.30	8.48	6.41	9.51	14.50	9.56	12.70	13.85	6.14
Rb	28.7	25.6	26.2	41.5	46.6	42.3	32.9	32.1	49.2	28.7
Sm	4.39	6.54	6.37	4.42	6.60	10.35	6.61	9.16	9.65	4.39
Sn	1	2	1	1	1	2	1	2	2	1
Sr	902	864	843	394	667	755	1155	1130	842	902
Ta	0.7	1.3	1.3	1.0	1.3	1.4	1.3	1.6	1.6	0.7
Tb	0.58	0.79	0.80	0.59	0.87	1.06	0.79	1.04	1.05	0.58
Th	6.66	10.45	9.83	12.65	10.75	11.70	11.75	10.65	10.85	6.66
Tm	0.20	0.27	0.26	0.17	0.27	0.28	0.25	0.32	0.32	0.20
U	2.73	2.99	2.95	4.30	3.73	4.76	4.19	4.09	4.16	2.73
V	147	129	134	65	105	211	111	150	181	147
W	1	2	5	3	4	2	2	5	2	1
Y	13.7	20.0	19.2	12.1	18.6	23.2	18.6	24.7	24.4	13.7
Yb	1.39	1.80	1.73	1.16	1.81	1.84	1.78	2.16	2.16	1.39
Zr	114	196	174	148	180	234	187	237	253	114

Cat. No.	HONS547	HONS548	HONS549	HONS550	HONS551	HONS552	HONS553	HONS554	HONS555	HONS556
Rock type	RHM	Nth PP	Late PP	Late PP	Nth PP	Early PP	Nth PP	Early PP	Nth PP	Late dyke
Sample	A22	A24	A25	A26	A27	A28	A29	A30	A32	A33
XRF major elements (wt%)										
SiO2	57.13	63.70	67.42	66.91	63.01	61.54	63.05	58.53	61.83	61.71
TiO2	1.11	0.89	0.48	0.52	0.99	1.03	0.88	0.90	0.85	0.84
Al2O3	16.80	16.31	17.15	16.95	17.56	17.28	13.43	14.58	16.14	15.37
Fe2O3	7.56	7.00	3.34	2.86	5.67	5.33	6.86	5.66	5.81	5.16
MnO	0.11	0.09	0.11	0.09	0.14	0.14	0.10	0.13	0.12	0.12
MgO	2.79	1.20	< 0.01	1.24	4.01	2.94	1.64	0.91	3.02	1.73
CaO	5.06	2.01	3.42	3.56	1.84	4.29	1.25	4.69	2.73	4.13
Na2O	4.85	5.15	5.65	4.66	3.68	5.99	6.09	8.24	3.41	6.07
K2O	2.82	1.23	1.50	1.81	1.82	0.25	1.48	0.87	1.73	2.12
P2O5	0.42	0.28	0.19	0.19	0.38	0.46	0.27	0.36	0.35	0.30
S	< 0.01	0.05	0.03	0.55	< 0.01	0.24	1.64	1.90	0.61	0.44
O=S		-0.03	-0.01	-0.28		-0.12	-0.82	-0.95	-0.30	-0.22
LOI	2.68	2.47	2.37	3.25	3.47	2.11	3.44	3.39	5.04	3.70
Total	**101.32**	**100.35**	**101.63**	**102.31**	**102.56**	**101.49**	**99.30**	**99.21**	**101.34**	**101.47**
XRF trace elements (ppm)										
V	169	100	52	34	101	24	77	45	112	114
Co	25	< 3	< 5	< 3	14	16	17	< 3	< 5	14
Cu	35	340	50	57	112	49	5080	17	341	51
Zn	63	84	73	37	156	69	152	51	134	69
Ga	21	18	18	19	17	15	23	17	15	18
As	1	2	< 1	< 1	2	1	2	3	3	0
Rb	49	23	25	30	32	4	33	8	37	28
Sr	1170	617	1068	782	213	636	172	787	334	579
Y	27	18	18	18	16	30	14	28	20	21
Zr	180	215	188	197	204	258	172	241	197	180
Nb	20	22	19	20	23	28	20	26	22	20
Ba	1525	569	1252	1541	1260	91	421	598	555	1741
La	44	34	27	54	79	66	22	76	25	48
Ce	102	82	77	100	162	157	52	154	88	99
Hf	3	< 1	4	5	6	7	< 1	8	6	6
Pb	4	4	11	6	3	3	7	5	6	4
Th	10.0	10.7	11.8	12.1	11.6	11.6	8.3	12.1	9.7	15.5
U	6.3	2.5	6.9	5.9	4.3	5.8	1.8	6.3	3.1	9.2
ICP-MS trace and rare earth elements (ppm)										
Ba	1505	537	1140	1465	1245	103	388	573	528	1555
Ce	120.5	59.9	93.8	96.7	142.0	145.5	43.3	128.0	90.8	105.0
Co	14.5	3.1	2.9	4.7	16.5	16.4	16.1	12.0	7.1	8.6
Cr	90	80	80	90	140	150	100	110	80	70
Cs	0.53	0.17	0.20	0.30	0.25	0.02	0.27	0.05	0.27	0.62
Dy	5.34	2.96	2.87	3.08	3.71	5.64	2.56	5.05	3.82	4.14
Er	2.61	1.54	1.44	1.52	1.70	2.74	1.39	2.53	1.98	2.19
Eu	2.89	1.52	1.73	1.82	2.12	3.17	1.11	2.92	2.07	1.85
Ga	22.5	21.8	20.0	21.2	20.8	17.4	22.6	20.9	20.9	19.3
Gd	7.87	4.24	4.20	4.33	6.62	8.16	3.48	7.26	5.32	5.55
Hf	5.1	5.2	4.5	4.9	5.4	6.4	4.5	5.7	4.9	5.2
Ho	0.95	0.56	0.54	0.56	0.65	1.04	0.48	0.94	0.71	0.77
La	62.0	30.6	55.5	57.0	75.3	76.4	22.7	67.3	45.2	58.6
Lu	0.34	0.24	0.22	0.22	0.26	0.35	0.22	0.33	0.28	0.34
Mo	3	3	2	2	11	3	12	3	3	4
Nb	23.1	24.1	20.3	22.8	25.6	31.5	21.8	28.2	23.4	23.9
Nd	56.7	27.2	34.6	35.2	62.1	65.6	19.4	57.1	39.6	43.3
Pr	14.65	6.67	9.57	9.89	16.65	17.25	4.72	14.95	10.35	11.60
Rb	50.8	23.4	26.7	33.7	35.8	4.0	35.0	8.5	38.0	29.9
Sm	10.45	5.61	5.86	5.96	10.60	11.45	4.18	10.10	7.05	7.77
Sn	2	1	1	1	2	2	4	2	2	2
Sr	1155	593	1020	788	219	637	166	762	324	573
Ta	1.7	1.5	1.3	1.4	1.6	1.8	1.4	1.5	1.5	1.8
Tb	1.14	0.68	0.68	0.70	0.89	1.19	0.61	1.11	0.87	0.89
Th	9.36	9.99	11.20	11.50	11.85	11.55	9.03	10.50	9.86	18.70
Tm	0.35	0.22	0.20	0.20	0.23	0.37	0.19	0.33	0.27	0.32
U	3.72	1.87	3.65	3.75	3.62	4.51	2.23	4.12	2.82	6.39
V	193	146	63	71	177	137	123	149	152	134
W	2	2	2	3	6	2	2	3	1	2
Y	25.4	16.0	15.2	16.3	15.8	28.3	13.7	25.0	19.3	21.2
Yb	2.23	1.52	1.37	1.37	1.64	2.38	1.32	2.21	1.77	2.12
Zr	215	234	202	220	228	271	200	246	218	204

Cat. No.	HONS560	HONS557	HONS558	HONS561	HONS562	HONS563	HONS564	HONS631
Rock type	Nth PP	BSVC	ANVC	BSVC	ANVC	Sth PP	RHM	MHRC537
Sample	A35	B1	B3	B8	B10	F1	F2	RHM
XRF major elements (wt%)								
SiO2	61.61	48.06	58.17	51.21	54.28	62.42	57.15	
TiO2	1.00	1.71	0.97	1.80	0.67	0.70	1.27	
Al2O3	16.52	15.65	18.35	15.23	16.43	17.72	16.67	
Fe2O3	8.55	12.78	5.87	11.64	5.98	5.11	7.27	
MnO	0.21	0.26	0.09	0.25	0.00	0.12	0.10	
MgO	3.30	6.56	2.78	4.65	1.09	1.74	2.49	
CaO	1.71	8.70	4.23	7.97	0.12	3.81	4.20	
Na2O	2.62	3.73	3.19	5.18	5.17	4.91	6.55	
K2O	2.29	1.33	3.34	0.71	1.91	2.00	2.42	
P2O5	0.36	0.32	0.38	0.25	0.14	0.29	0.45	
S	0.20	0.13	0.55	0.10	5.42	< 0.01	< 0.01	
O=S	-0.10	-0.06	-0.27	-0.05	-2.71			
LOI	3.36	2.23	5.05	1.66	8.99	3.69	1.96	
Total	**101.62**	**101.40**	**102.71**	**100.60**	**97.48**	**102.51**	**100.51**	
XRF trace elements (ppm)								
V	138	240	134	216	134	76	116	171
Co	24	56	14	42	36	10	11	138
Cu	1086	148	126	92	3650	11	134	4
Zn	177	122	93	119	539	86	98	73
Ga	18	17	18	15	19	17	16	39
As	2	1	1	2	3	1	2	< 0.5
Rb	48	23	47	5	46	31	25	< 0.1
Sr	222	535	464	482	304	822	1228	55
Y	19	34	34	37	30	20	32	1063
Zr	190	125	178	145	165	133	246	21
Nb	23	12	8	10	11	15	26	149
Ba	1018	563	947	471	635	1161	1590	< 1.1
La	47	7	35	11	53	19	61	2479
Ce	132	< 2	75	42	128	67	134	35
Hf	< 1	4	7	6	< 1	5	9	73
Pb	4	4	3	2	8	6	4	1
Th	10.6	2.0	6.5	1.7	5.0	7.1	10.0	0.7
U	3.2	1.3	5.7	0.6	2.0	4.0	6.0	16.3
ICP-MS trace and rare earth elements (ppm)								
Ba	929	557	885	470	624	1135	1560	2440
Ce	89.8	32.7	83.2	31.3	113.5	77.8	132.0	113.5
Co	6.5	46.1	13.7	41.7	35.4	8.7	13.5	11.4
Cr	90	300	90	270	100	110	140	140
Cs	0.36	0.36	0.27	0.06	0.46	0.27	0.14	0.39
Dy	3.72	6.30	6.03	6.72	5.02	3.42	5.69	3.78
Er	1.92	3.64	3.46	4.08	2.76	1.75	2.80	1.89
Eu	1.75	1.98	2.49	1.77	2.74	1.70	2.91	2.14
Ga	22.2	20.3	20.3	20.1	16.0	18.2	20.1	19.1
Gd	5.48	5.88	7.43	6.17	7.14	4.38	7.82	5.62
Hf	5.1	3.4	4.4	3.8	4.3	4.1	6.8	4.6
Ho	0.69	1.29	1.19	1.40	0.96	0.61	1.03	0.67
La	43.8	16.1	42.0	14.7	55.5	41.3	69.8	65.4
Lu	0.27	0.50	0.51	0.57	0.41	0.28	0.37	0.26
Mo	3	3	3	3	41	5	4	9
Nb	24.3	14.6	8.6	12.2	11.8	16.7	29.4	16.4
Nd	40.3	18.0	40.6	18.0	56.8	31.3	59.6	46.0
Pr	10.05	3.88	9.98	3.91	14.35	8.51	15.50	12.30
Rb	49.2	24.4	49.7	6.1	47.5	33.7	28.1	62.1
Sm	7.63	5.11	8.74	5.19	10.45	5.90	10.85	8.14
Sn	2	2	2	1	4	1	2	2
Sr	219	576	462	503	293	818	1275	1090
Ta	1.5	0.9	0.5	0.8	0.8	1.1	1.9	1.0
Tb	0.86	1.17	1.17	1.18	1.21	0.94	1.32	1.01
Th	11.10	1.34	5.50	1.66	5.25	6.41	9.43	16.20
Tm	0.26	0.51	0.49	0.58	0.41	0.25	0.38	0.25
U	3.21	1.34	3.32	1.14	2.35	2.26	3.86	5.72
V	173	327	171	301	172	95	191	167
W	3	1	2	2	3	1	2	3
Y	18.7	34.2	33.4	37.3	27.8	18.6	30.2	20.1
Yb	1.69	3.28	3.35	3.79	2.64	1.78	2.50	1.70
Zr	220	146	186	168	179	167	286	189